# T Cell Proliferation in Lymphopenia Conditions: Modeling, Parameters Estimation and Mathematical Analysis

Houssein Ayoub

# THÈSE

Pour obtenir le grade de

## DOCTEUR DE L'UNIVERSITÉ DE BORDEAUX

École Doctorale de Mathématiques et Informatique

SPÉCIALITÉ: Mathématiques Appliquées et Calcul Scientifique

Présentée et soutenue par


## HOUSSEIN AYOUB


**Title: T Cell Proliferation in Lymphopenia Conditions: Modeling, Parameters Estimation and Mathematical Analysis**

**Titre: Prolifération des Cellules T dans des Conditions Lymphopénique: Modélisation, Estimation des Paramètres et Analyse Mathématique**

Sous la direction de: **Bedr'Eddine Ainseba, Professeur des Universités** et **Michel Langlais, Professeur des Universités**

le: 04/07/2014

Devant le jury composé de:

| | | |
|---|---|---|
| M. Bedr'Eddine Ainseba | Professeur, Université de Bordeaux ..... | Directeur |
| M. Jean Clairambault .. | Directeur de Recherche, INRIA Rocquencourt | Rapporteur |
| M. Michel Langlais ..... | Professeur Emérite, Université de Bordeaux .. | Co-Directeur |
| M. Mazen Saad ..... | Professeur, Ecole Centrale de Nantes ..... | Examinateur |
| M. Rodolphe Thiébaut . | Professeur , INSERM Bordeaux ..... | Examinateur |
| M. Vitaly Volpert ..... | Directeur de Recherche, CNRS Lyon ..... | Rapporteur |

*Université de Bordeaux - Les Sciences et les Technologies au service de l'Homme et de l'Environnement*

# *Acknowledgements*

***First and foremost, praises and thanks to the God, the Almighty, for His showers of blessings throughout my research work to complete the research successfully.***

***I would like to express my sincere gratitude to my advisors, Prof. Bedreddine Ainseba and Prof. Michel Langlais, for the continuous support of my Ph.D study and research, for their patience, motivation, enthusiasm, and immense knowledge. Their guidance helped me in all the time of research and writing of this thesis.***

***Besides my advisors, I would like to thank the rest of my thesis committee: Prof. Jean Clairambault, Prof. Vitaly Volpert, and Prof. Mazen Saad, for their participation.***

***I would like to thank Prof. Rodolphe Thiébaut for his collaboration. His vast knowledge, broaden horizons helped me get quick thinking and deep enlightenment. Many thanks also to Prof. Robin Callard and Prof. Benedict Seddon for all the great scientific discussions, helpful advice and encouragement with my work. Besides, I wish to express my gratitude to Professor Pierre Magal, Doctor Arnaud Ducrot, Doctor Mostafa Bendahmane and Doctor Jean-Baptiste Burie. I am benefited a lot from their profound knowledge. In addition, I would like to thank all my friends for their support.***

***Finally, it is difficult to overstate gratitude to my family, whose constant support, encouragement, teaching and love has guided and sheltered me all my life. I thank them for always believing in me, putting up with my complaints and for putting everything in perspective at the end of each day. This thesis would certainly not have existed without you all. I dedicate this thesis to the memory of my brother "ALI" who taught me the importance of truth and knowledge and without whose unconditional sacrifices and hard work I would not be where I am today.***

***To my father (Hassan) and my mother (Samira)***

***To my sisters: Soumaya, Samar, Rana and Rania***

***To my brothers: Ali and Ahmad***

***To all those who are dear to me...***

# Résumé Substantiel

Les lymphocytes T sont une composante essentielle du système immunitaire de l'organisme. Ils peuvent reconnaître et répondre à un antigène étranger en vertu de leur récepteur d'antigène. En effet, les cellules T qui n'ont pas encore rencontrées des antigènes, sont appelées "naïves". Lors d'un premier contact antigénique, l'expansion clonale des lymphocytes T spécifiques à un antigène augmente fortement leur fréquence, et déséquilibre transitoirement de façon plus ou moins intense le compartiment lymphocytaire T périphérique. Cet équilibre doit être rétabli pour ne pas menacer à terme le bon fonctionnement du système immunitaire. Outre le risque de réponse explosive lors d'une réexposition à l'antigène, l'accumulation de clones T de taille disproportionnée gênerait considérablement le recrutement de lymphocytes T spécifiques de nouveaux antigènes. Ainsi, après élimination de l'antigène ou son confinement dans l'organisme, différents mécanismes interviennent. Il faut en effet d'une part assurer le maintien d'un compartiment de cellules T naïves de taille suffisante pour faire face à de nouvelles stimulations antigéniques. D'autre part, la constitution d'un panel de cellules T mémoires est nécessaire pour permettre une réponse immunitaire plus rapide et plus efficace lors de réexpositions antigéniques. Donc les mécanismes d'homéostasie des cellules T sont essentielles pour maintenir le nombre de cellules T à un niveau à peu près constant en contrôlant la division cellulaire et la mortalité des cellules.

Dans le cas normal, le renouvellement des cellules T naïves est très faible et ces derniers restent approximativement dans un état de repos. Cependant, une perturbation de l'équilibre homéostatique peut résulter d'une grande variété de causes (infection virale, ou les traitements de chimiothérapie), et peut entraîner une lymphopénie (i.e. Une carence en lymphocytes T). Dans ces conditions lymphopéniques, les cellules T naïves subissent la division cellulaire avec un changement de l'expression de CD44 sur leur surface cellulaire. Ce processus est appelé "prolifération homéostatique" ou en anglais "lymphopenia induced proliferation" (LIP). Ainsi, le CD44 est un marqueur naturel qui caractérise la transition des cellules du phénotype naïf (CD44-) au phénotype mémoire (CD44+) durant LIP.

Les travaux de recherche dans les dernières décennies montrent que l'utilisation de modèles mathématiques en immunologie a abouti à de grands progrès, non seulement sur le plan théorique, mais aussi sur le plan de la gestion des politiques actuelles de santé publique. Dans la littérature, plusieurs études ont utilisé avec succès la modélisation mathématique pour décrire la réponse prolifférative des cellules T à

une lymphopénie [1–7, 7–10]. En outre, ces études n'ont pas pris en compte la transition des cellules du phénotype naïf au phénotype mémoire en utilisant le concept de CD44 au cours du processus homéostatique. L'objectif de cette thèse est donc de comprendre la relation complexe entre LIP [1] et le passage du phénotype naïf (CD44-) au phénotype mémoire (CD44+) en utilisant des modèles mathématiques et des données expérimentales. On s'intéresse en plus au comportement asymptotique des cellules T durant le processus d'homéostasie in vivo.

**Mots-clés:** Modélisation Mathématique, Analyse Numérique, Données Expérimentales, Identification des Paramètres, Comportement Asymptotique et Contrôle Optimal.

Ce travail est organisé sous la forme suivante:

**- La partie I** est divisée en deux chapitres:
• Le chapitre 1 est consacré à la définition des éléments biologiques utilisés dans cette thèse (Système immunitaire, Cycle cellulaire, Lymphocyte T, L'homéostasie, CD44, les Lymphopénies).
• Le chapitre 2 reprend les modèles mathématique souvent utilisés dans la littérature (Les modèles qui décrivent la réponse immunitaire et les données de CFSE, "Cyton model", Modèle de Smith-Martin).

**- La partie II** est divisée en deux chapitres:
• Dans le chapitre 4, on construit un modèle in vitro (noté $SM_{CD44}$) décrivant la dynamique des cellules T dans des conditions lymphopéniques, notamment la transition des cellules du phénotype naïf (CD44-) au phénotype mémoire (CD44+) durant le processus d'homéostasie. En effet, on introduit des nouveaux paramètres dans le modèle de Smith-Martin [3, 4, 7, 10] qui représentent l'évolution de la quantité de CD44 à la surface des cellules durant le processus d'homéostasie. Cette croissance de quantité de CD44 identifie la transition du phénotype naïf (CD44-) au phénotype mémoire (CD44+).
Comme dans le modèle de Smith-Martin, le modèle ($SM_{CD44}$) considère une phase A (phase de repos) et une phase B (phase de prolifération) où les cellules T subissent la division cellulaire sous forme d'un système en cascade (cf. Fig. 1). Le nombre de fois où les cellules sont divisées, est indexé par $i$. Le temps où les cellules restent dans la phase B, est mesurée par $\tau$. Ce qui reflète la maturité (i.e l'âge) des cellules

[1] lymphopenia induced proliferation

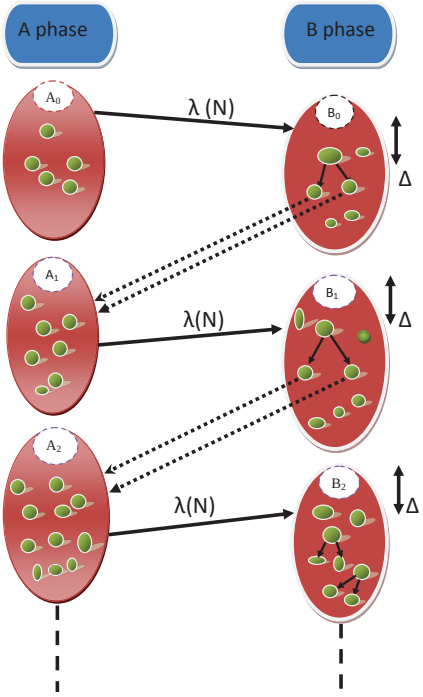


FIGURE 1: Modèle de prolifération des cellules T en conditions lymphopéniques. $A_i$ et $B_i$ sont le nombre des cellules T, qui ont subi $i$ divisions dans la phase A et B respectivement. $\Delta$ est la durée de la phase B (unité en heure). Le taux des cellules qui se divisent ($\lambda$), est une fonction qui dépend du nombre total des cellules ($N$) [10].

à ce stade. En plus, cette maturité $\tau$ a une valeur maximale $\Delta$. Les cellules dans la phase A et la phase B sont indexées encore par $s \in [0, m]$ qui représente l'intensité de CD44 sur la surface des cellules. La dynamique des cellules entre la phase A et la phase B est représentée par des EDOs et EDPs respectivement (cf. System (1-2)).

$$\begin{cases} \dfrac{dA_0(t,s)}{dt} = -\delta_A A_0(t,s) - \lambda(N) A_0(t,s), \\ \begin{cases} for \quad i = 1, ..., I \\ \dfrac{dA_i(t,s)}{dt} = 2\displaystyle\int_0^{\Delta} \mu(\tau) B_{i-1}(t,\tau,s)\, d\tau - \delta_A A_i(t,s) - \lambda(N) A_i(t,s), \end{cases} \\ \begin{cases} for \quad i = 0, ..., I \\ \dfrac{\partial}{\partial t} B_i(t,\tau,s) + \dfrac{\partial}{\partial \tau} B_i(t,\tau,s) + \dfrac{\partial}{\partial s}[v_i(s).B_i(t,\tau,s)] = -\left(\delta_B + \mu(\tau)\right) B_i(t,\tau,s), \end{cases} \end{cases} \tag{1}$$

où les variables $(t, \tau, s)$ appartiennent à $[0, T] \times [0, \Delta] \times [0, m]$.

**Les conditions au bord et les distributions initiales sont données par**

$$\begin{cases} B_i(t,0,s) = \lambda(N)A_i(t,s) \quad et \quad v_i(0)B_i(t,\tau,0) = 0 \quad pour \quad i = 0,...,I \\ \\ B_i(0,\tau,s) = 0, \quad for\ i = 0,...,I \quad et \quad A_i(0,s) = 0, \quad pour\ i = 1,...,I \\ \\ A_0(0,s) = A_{0,0}(s) \geqslant 0. \end{cases} \tag{2}$$

Les variables d'état $A_i$ et $B_i$ sont le nombre de cellules T ayant subi $i$ divisions dans la phase A et B respectivement. Pour $i = 0$, la croissance des cellules dans la phase $A_0$ vient du nombre initial $A_{0,0}(s)$. En outre, le recrutement stochastique de cellules de la phase A à la phase B se fait avec un taux $\lambda$ qui dépend du nombre total de cellules $N(t) = \sum_{i=0}^{I} \left( \int_0^m A_i(t,s)ds + \int_0^\Delta \int_0^m B_i(t,\tau,s)d\tau\ ds \right)$. Dans la phase B, les cellules régularisent leur niveau de CD44 par la vélocité $v_i(s)$. En complétant le processus (mitose) dans la phase B, les cellules se divisent avec un taux $\mu(\tau)$ qui dépend de l'âge des cellules en phase B. De plus les cellules filles héritent du même niveau d'expression de CD44 que leur cellule mère (cf. System (1-2) et Fig. 1).
Enfin dans ce chapitre 4, on dérive la solution implicite des équations $A_i$ et la formulation intégrale des équations $B_i$.

• Dans le chapitre 5, on développe un schéma numérique pour approcher la solution du modèle $SM_{CD44}$. Une analyse sur les propriétés du schéma est proposée.

**- La partie III** est divisée en quatre chapitres:
• Dans le chapitre 6, on décrit les données expérimentales générées par Hogan et al. [10]. De plus, on montre dans ce chapitre l'identifiabilité théorique de certains paramètres ($v_i$, $\lambda$, $\Delta$) dans le modèle $SM_{CD44}$.
• Dans le chapitre 7, on présente la dernière version de Smith-Martin utilisée dans la littérature et notre modèle $SM_{CD44}$ (sans la structuration de CD44). On s'intéresse dans ce chapitre à la comparaison de ces deux modèles. En effet, on décrit la méthode utilisée pour identifier numériquement plusieurs paramètres communs dans les deux modèles en utilisant les données de CFSE [10]. Enfin, on montre les paramètres et les simulations obtenues à partir de ces modèles. Puis on compare ces simulations aux données expérimentales.
• Dans le chapitre 8, on identifie la vélocité de CD44 $v_i$ (vitesse de croissance de CD44) en utilisant les données de CFSE et de CD44 [10]. Cette vélocité est le paramètre clé qui nous permet de savoir à partir de quelles divisions les cellules T

sont qualifiées comme naïves ou mémoires à partir du modèle $SM_{CD44}$.
La méthode utilisée pour identifier ce paramètre consiste à résoudre un problème d'identification de paramètres qui est bien détaillé dans ce chapitre. Dans la partie numérique, on montre les paramètres et les simulations obtenus à partir du modèle et on les compare aux données expérimentales. Les paramètres identifiés et les simulations numériques de $SM_{CD44}$ fournissent plusieurs interprétations biologiques sur la relation entre LIP et le passage du phénotype naïf au phénotype mémoire en utilisant le modèle $SM_{CD44}$.

• Dans le chapitre 9, on prend en compte la dépendance entre l'intensité de CD44 ($s$) et le taux d'entrée en division ($\lambda = \lambda(s, N(t))$) ou le taux de division ($\mu = \mu(\tau, s)$). Ici, on s'intéresse à identifier ces nouveaux paramètres qui dépendent du niveau de CD44 ($s$). Comme dans le chapitre précédent, les ingrédients pour résoudre les problèmes d'identification des paramètres sont donnés. Enfin, on présente les simulations et les paramètres identifiés, et on déduit biologiquement le lien entre le niveau de CD44 sur les cellules et leur taux d'entrée dans la phase de prolifération ou leur taux de division.

**- La partie IV** est divisée en trois chapitres:

• Dans le chapitre 10, on étend le modèle in vitro $SM_{CD44}$ à un modèle in vivo en introduisant un taux $\Lambda$ d'exportation de cellules du thymus. Dans ce modèle, on considère un grand nombre de divisions ($I >> 0$), et un taux d'entrée en division en fonction du nombre de division ($i$) et de nombre total de cellules ($N = N(t)$). En utilisant la méthode du point fixe, on démontre l'existence locale et l'unicité de la solution du système étendu. Enfin, on déduit l'existence globale en utilisant l'intervalle maximal d'existence.

• Dans le chapitre 11, on réécrit le modèle étendu comme un système structuré en âge et sans la structuration en CD44. Ici, on s'intéresse à investiguer l'étude asymptotique du modèle réduit. On trouve qu'il existe une ou trois solutions stationnaires quand les cellules subissent au moins cinq divisions, et seulement une seule quand les cellules subissent au plus trois divisions. Le cas limite de quatre divisions est numériquement traité. En appliquant la méthode de Lyapunov, on montre dans certains cas d'unicité que la solution stationnaire est globalement asymptotiquement stable.

• Dans le chapitre 12, on reformule le modèle in vivo proposé dans le chapitre 10 en une version plus réaliste avec une stratégie de vaccination. Le but de ce chapitre est de résoudre un problème de contrôle optimal qui renforce l'immunité durant

le processus d'homéostasie. Premièrement, on discute la fonction coût et on obtient les conditions d'optimalités. Deuxièmement, on exécute quelques simulations numériques pour calculer la vaccination optimale.

**- Enfin dans le chapitre 13**, on résume les principaux résultats de cette étude et on donne les perspectives et les nouveaux problèmes induits par ce projet de recherche.


Thèse préparée à
l'Institut de Mathématiques de Bordeaux
UMR CNRS 5251, Université de Bordeaux
33076 Bordeaux cedex, France

# Abstract

*T lymphocytes are a fundamental component of the immune system that can recognise and respond to foreign antigens by virtue of their clonally expressed T cell antigen receptor (TCR). T cells that have yet to encounter the antigen they recognise are termed 'naive' as they have not been activated to respond. Homeostatic mechanisms maintain the number of T cells at an approximately constant level by controling cell division and death. In normal replete hosts, cell turnover within the naive compartment is very low and naive cells are maintained in a resting state. However, disruption of the homeostatic balance can arise from a wide variety of causes (viral infection (e.g. HIV), or drugs used in peritransplant induction therapy or cancer chemotherapy) and can result in T cell deficiency or T lymphopenia. Under conditions of T lymphopenia, naive T cells undergo cell division with a subtle change in the cell surface phenotype (CD44 expression), termed homeostatic proliferation or lymphopenia induced proliferation (LIP). In this thesis, our purpose is to understand the process of T cell homeostatic through mathematical approach. At first, we build a new model that describes the proliferation of T cells in vitro under lymphopenic conditions. Our nonlinear model is composed of ordinary differential equations and partial differential equations structured by age (maturity of cell) and CD44 expression. To better understand the homeostasis of T cells, we identify the parameters that define T cell division by using experimental data. Next, we consider an age-structured model system describing the T cell homeostatic in vivo, and we investigate its asymptotic behaviour. Finally, an optimal strategy is applied in the in vivo model to rebuild immunity under conditions of T lympopenia.*

# Contents

# Part I

# General Introduction

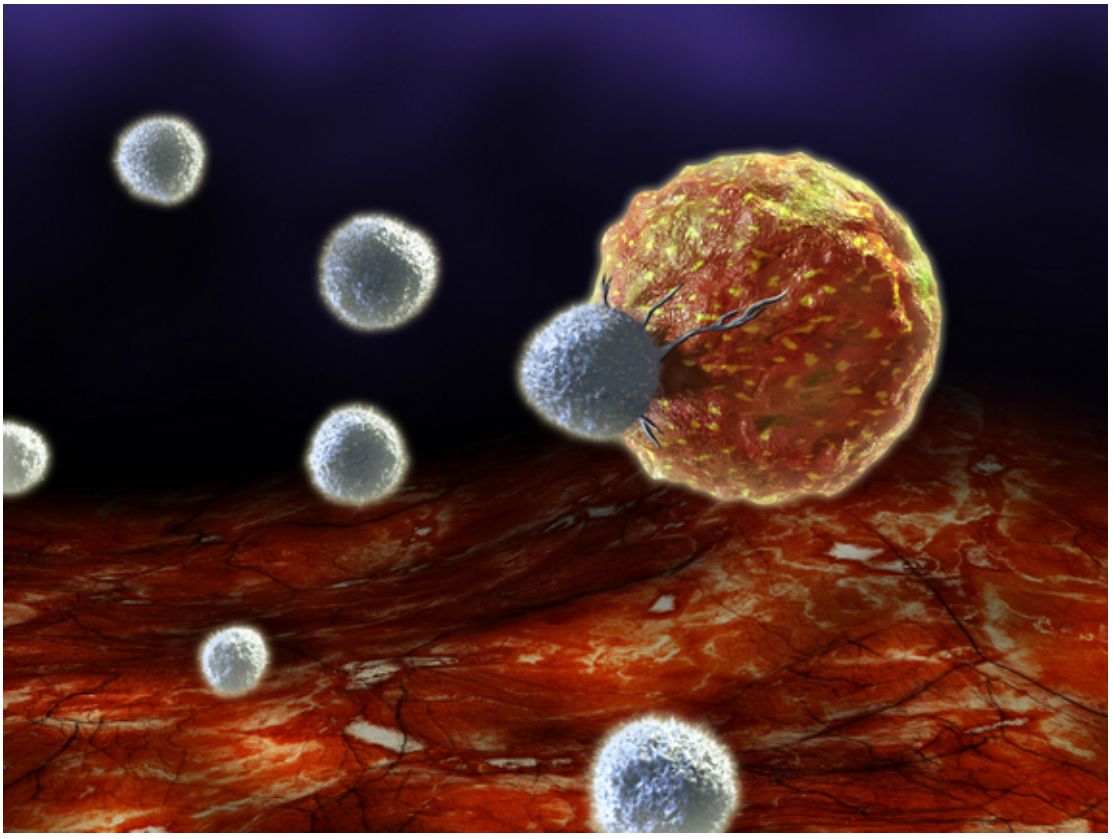

# Chapter 1

# Biological Background

## 1.1 Immune system

The immune system is a collection of organs, cells and tissues that work together to protect the body from disease caused mostly by pathogens (bacteria, viruses, parasites,...). The human body is protected by two main types of immunity.

- Innate immunity is the protection system present at birth which defends us against disease.
  - The skin and other tissues which cover the body (such as the lining of the nose and mouth), are a barrier which repels invaders.
  - The white blood cells respond to invaders such as bacteria and viruses, and expel or destroy them.
- Acquired immunity is the protection system which the body acquired, when it is exposed to certain diseases.
  - When the body makes contact with a bacterium, a virus or another antigen, it learns to recognize this antigen. When it is invaded again by this strange, the immune system remembers these organisms, and makes a stronger reaction against them, and can combat them faster.
  - The vaccines are based on acquired immunity. They contain small amounts of proteins (antigens) from an organism which can cause disease. If the organism invades the body again, the immune system will recognize and fight them even faster and better.

## 1.2 Structure of the immune system

The organs of the immune system (Fig. 1.1) are positioned throughout the body. They are called lymphoid organs because they are home to lymphocytes, small white blood cells that are the key players in the immune system. Bone marrow, the soft tissue in the hollow center of bones, is the ultimate source of all blood cells, including lymphocytes. The thymus is a lymphoid organ that lies behind the breastbone. Lymphocytes known as T lymphocytes or T cells (T stands for

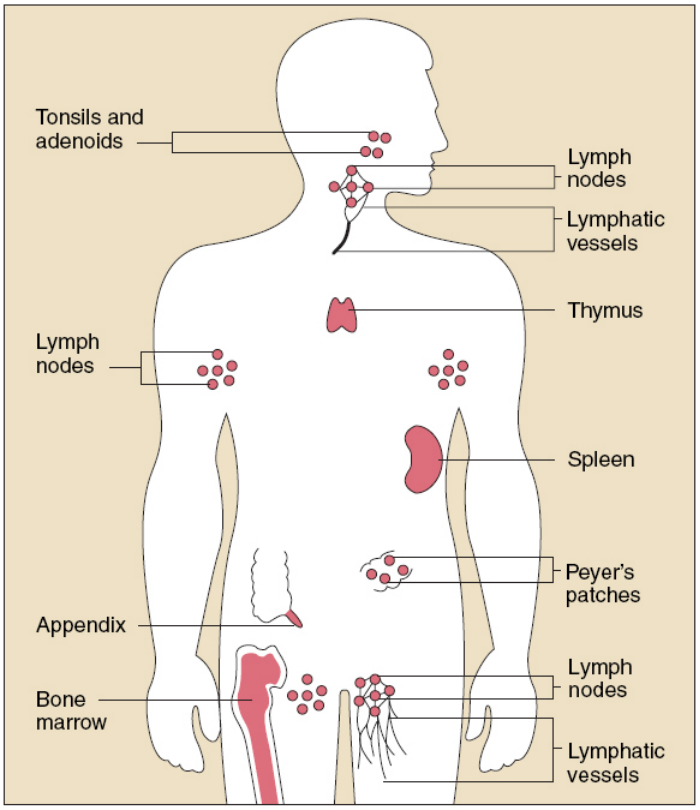


FIGURE 1.1: Organs of the immune system (www.niaid.nih.gov).

thymus) mature in the thymus and then migrate to other tissues. B lymphocytes, also known as B cells, become activated and mature into plasma cells, which make and release antibodies.
Lymph nodes (Fig. 1.2), which are located in many parts of the body, are lymphoid tissues that contain numerous specialized structures.

- T cells from the thymus concentrate in the paracortex.
- B cells develop in and around the germinal centers.

- Plasma cells occur in the medulla.

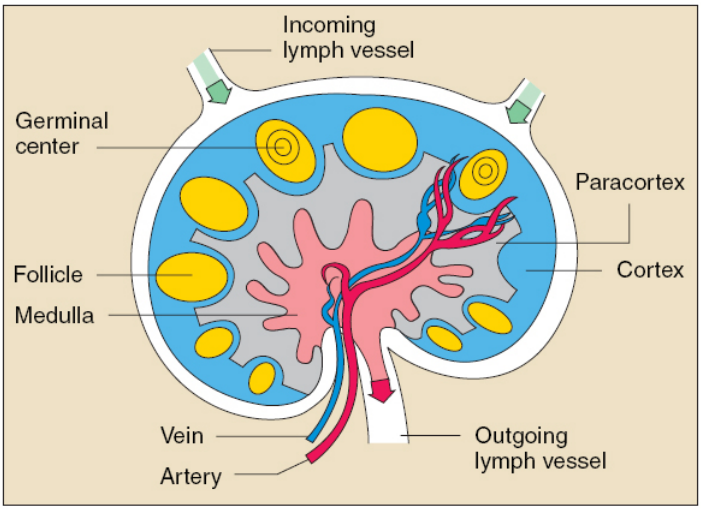


FIGURE 1.2: The lymph node contains numerous specialized structures. T cells concentrate in the paracortex, B cells in and around the germinal centers, and plasma cells in the medulla (www.niaid.nih.gov).

Lymphocytes can travel throughout the body using the blood vessels. The cells can also travel through a system of lymphatic vessels that closely parallels the bodys veins and arteries.

Cells and fluids are exchanged between blood and lymphatic vessels, enabling the lymphatic system to monitor the body for invading microbes. The lymphatic vessels carry lymph, a clear fluid that bathes the bodys tissues.

Small, bean-shaped lymph nodes are laced along the lymphatic vessels, with clusters in the neck, armpits, abdomen, and groin. Each lymph node contains specialized compartments where immune cells congregate, and where they can encounter antigens.

Immune cells, microbes, and foreign antigens enter the lymph nodes via incoming lymphatic vessels or the lymph nodes tiny blood vessels. All lymphocytes exit lymph nodes through outgoing lymphatic vessels. Once in the bloodstream, lymphocytes are transported to tissues throughout the body. They patrol everywhere for foreign antigens, then gradually drift back into the lymphatic system to begin the cycle all over again.

## 1.3 Cell cycle

The cell cycle, or cell-division cycle, is the series of events that take place in a cell leading to its division and duplication (replication) that produces two daughter cells. The biological cell cycle describes five distinct phases G0, G1, S, G2 and M grouping interphase and mitosis (see Fig. 1.3).

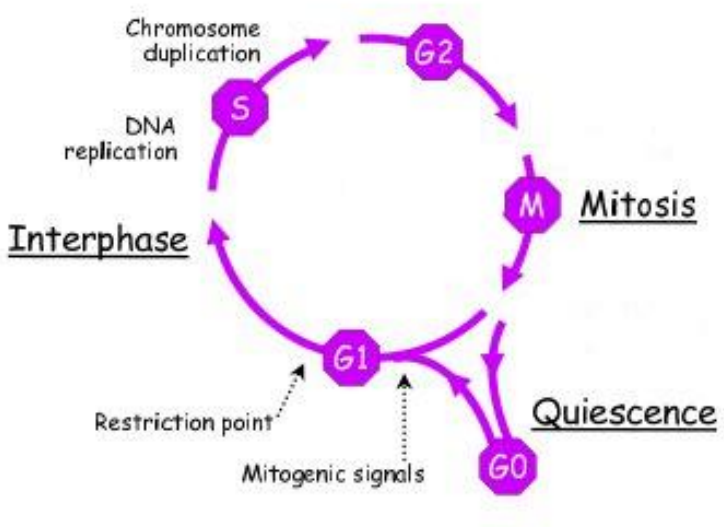


FIGURE 1.3: Schematic of the cell cycle [11].

**Quiescence**: Cells which are not proliferating are said to be quiescent or in "G0" phase. The metabolic demands of G0 phase varies according to the specialized functions being carried out by the quiescent cell, but there are often lower levels of gene expression, macromolecular biosynthesis and energy consumption compared with actively dividing cells.

**Interphase**: Before a cell can enter cell division, it needs to take in nutrients. All of the preparations are done during interphase. Interphase is a series of changes that takes place in a newly formed cell and its nucleus, before it becomes capable of division again. It is also called preparatory phase or intermitosis. Previously it was called resting stage because there is no apparent activity related to cell division. Typically interphase lasts for at least 90% of the total time required for the cell cycle. Interphase proceeds in three stages, G1, S, and G2, preceded by the previous cycle of mitosis and cytokinesis. The most significant event is the replication of genetic material (DNA) in S phase.

- **G1 phase**: The first phase within interphase, from the end of the previous M phase until the beginning of DNA synthesis, is called G1 (G indicating gap). It is also called the growth phase. During this phase, the cells passes through the restriction point. Here, the cell is irreversibly committed to the division, which no longer depends on the mitogenic factors.
- **S phase**: In this phase, the cell replicates their DNA and each chromosome is copied.
- **G2 phase**: This phase is a period of rapid cell growth and protein synthesis during which the cell makes itself ready for mitosis. Curiously, G2 phase is not a necessary part of the cell cycle, as some cell types (particularly young Xenopus embryos and some cancers [12]) proceed directly from DNA replication to mitosis.

**Mitosis or M phase**: Mitosis is the phase of the cell cycle in which cells physically divide into two separate daughter cells. In order to do so they first dissolve the nuclear membrane which will later reform once cell division is complete. The DNA-containing chromosomes then condense into structures so compact that they can seen with a light microscope. The chromosomes then precisely segregate to two sides of the cell, such that each half of the cell gets exactly one copy of each chromosome. At the completion of mitosis, cells undergo cytokinesis or separation into two halves. This occurs as a band forms around the circumference outer plasma membrane which gradual constricts like a belt until the cell pinches in two. The B-type cyclins remain active throughout M-phase, but their activity immediately ceases once cell division is complete and the two daughter cells once again enter G0 or G1.

## 1.4 T lymphocytes

T lymphocytes form an integral part of the adaptive immune system. The adaptive immune system allows the body to mount a response that is specific to invading pathogen and confers long-term protection to re-infection with the same antigen. Each T cell expresses a receptor on its surface that enables it to recognise specific antigen-peptides in association with major histocompatibility (MHC) molecules. Together, the receptors on all lymphocytes cover a broad repertoire of antigens.

### 1.4.1 The naive T cell pool

Naive T cells are the direct export product from the thymus. These cells have, by definition, not encountered antigen. Thus, these cells represent the naive repertoire present in the peripheral pool, that should allow a response to newly encountered antigens. In order to perform, these cells should be able to encounter the antigen, and it is then important that naive cells re-circulate, migrating continuously from one secondary lymphoid organ to another (reviewed in [13]). Importantly, these cells have been shown to express receptors for entry into the lymph nodes (CD62L) or for chemokines (CCR7), suggesting the type of signals responsible for the circulation pattern of naive T cells [13].
Accordingly, the phenotype of the naive T cells (CD4+ and CD8+ T cells) includes some of these molecules. In C57Bl6 mice (some markers vary depending on the mouse strain), naive T cells are typically defined as $CD44^{-}$ (this glycoprotein is detailed in Sec. 1.6), $CD62L^{high}$, $CD45RB^{high}$, $CD25^{-}$, $CD69^{-}$, small, resting cells. However, some of these markers can be shared with subsets of activated or memory cells, as is true for $CD62L^{high}$, described in a subset of human memory CD4+ and CD8+ T cells [14] and some cells can be activated as a result of homeostatic proliferation (homeostatic proliferation will be discussed later in this introduction) defying the definition of both naive and of effector T cells [15]. The result is a difficulty to define a naive T cell using a single cell surface marker. Thus, in most situations, combinations of the markers referred to above are used. When only a single marker is used the CD45RB marker for CD4+ T cells and the CD44 marker for CD8+ T cells are the ones most currently used.
The function of naive T cells depends on their activation which, in turn, depends on the encounter of these cells with antigen, processed and presented as MHC-peptide complexes at the surface of APCs (Antigen presenting cells). Together with signalling provided by co stimulatory molecules and cytokines, activation will result in proliferation and differentiation of T cells along the pathway to cytotoxic or helper cells (for CD8+ T cytotoxic killer and CD4+ helper T cells, respectively) [14].

### 1.4.2 The effector pool

Upon TCR (T cell receptor) mediated activation, T cells loose their naive status and integrate the effector compartment, differentiating into CD8+ T cytotoxic killer or CD4+ helper T cells.

The definition of the phenotype of effector cells is difficult, as it often coincides with that of the phenotype of memory cells. Effector T cells are large blastic cells, expressing activation markers, like CD25 or CD69 (often transitory for the first and short term for the second), express CD44 and have down-regulated CD45RB (some variations in this marker are dependent on the mouse strain used) and CD62-L expression [16]. This phenotype is shared with some memory cells and in part, with cells that are activated as a result of homeostatic proliferation [15, 17, 18]. For this reason, it is useful to consider in the peripheral T cell pool, naive versus activated/memory cells, thereby avoiding the difficulty in defining the line that phenotypically separates effector from memory cells.
The homing of effector cells also reflects their function and, here again, part of the phenotypic alterations observed, namely CD62L down-regulation are related to homing (reviewed in [13]). Thus, contrary to naive T cells, effector cells have the ability to circulate through extra-lymphoid immune effector sites [19], and as opposed to naive T cells, effector (and memory) T cells display great heterogeneity, with subsets often displaying a tissue-specific pattern of circulation [19].

### 1.4.3 The memory T cell pool

Immunological memory can be defined as an antigen-induced alteration in the reactive state of the immune system, occurring in such a way that the memory responses are more rapid on inset and more effective in antigen clearance [20]. Thus, it is important to consider the factors that are behind this faster and more efficient response. Two levels must be probed, namely the alterations in the frequency of antigen specific T cells and the qualitative differences that distinguish a memory T cell. By definition, a memory response is a secondary response. This means that a primary response occurred and thus, that responding T cell clones underwent considerable expansion (Fig. 1.4). This expansion is followed by a contraction phase, responsible for the death of $> 90\%$ of the effector cells (reviewed in [21]). After the contraction phase of an immune response, the memory phase follows (Fig. 1.4). By the end of the contraction phase, there are still enough cells from the responding T cell clone to increase the frequency of the T cell specificity in the order of 5 to 100 fold [21], it is thus a quantitative transformation. From this it can also be deduced that the repertoire of the memory compartment is less diverse than the repertoire of the naive compartment [23].

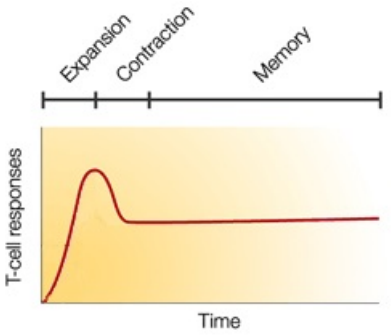


FIGURE 1.4: Immune responses. The Imuune response consists of three distinct phases. See text for the quantitative correspondence. (Modified from [22]).

### 1.4.4 T cell function and activation

The role of a T cell is to recognise foreign antigen expressed on antigen presenting cells (APCs) in association with the MHC complex and initiate an appropriate response. The initial interaction between a T cell and antigen-MHC complex will typically occur in the lymphoid organs. Each T cell has a different antigen-binding specificity and the number of T cells that can respond to a specific antigen is limited. As a result, the first stage of T lymphocyte activation involves clonal expansion of the relevant T cell receptor clone (Fig. 1.5).

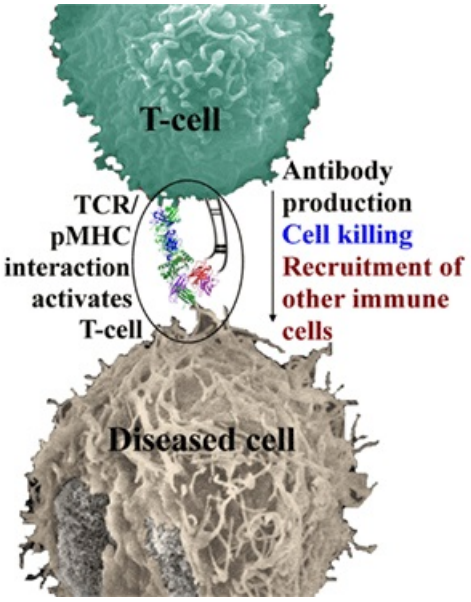


FIGURE 1.5: As a major part of the adaptive immune system, T-cells scan the intracellular environment in order to target and destroy infected cells. Small peptide fragments, representing the entire cellular content, are transported to the cell surface as pMHCs, allowing T-cell surface expressed antigen specific TCRs to scan for foreign signals. T-cells interact with a large number of different cell types and recognise a diverse array of pathogens. This diversity has lead to distinct antigen recognition pathways which generate the appropriate T-cell response. T-cell activation can lead to a number of immune responses such as antibody production, activation of phagocytic cells and direct cell killing. In this way, the appropriate immune response for different types of diseases is implemented. (www.tcells.org)

Activated naive T cells undergo extensive proliferation and differentiation producing effector and memory T cells (see Fig. 1.6).

The lineage relationship between naive, effector and memory T cells is not completely understood [24], however, it is widely accepted that antigen specific T cell populations can expand up to 1000 fold producing vast numbers of effector T cells that are able to destroy infected cells and release cytokines that stimulate B cells. Following the clearance of infection, the majority of effector T cells are thought to be lost to apoptosis, while a small fraction of antigen specific T cells will persist in the memory T cell pool [25]. The intensity of this response and the size and function of memory cells induced will depend upon the strength of TCR activation, duration of exposure to the MHC-peptide complex, the extent of binding, co-stimulation, inflammatory factors, intrinsic expression of signalling proteins, possibly the proximity of other cells and environmental stimuli.

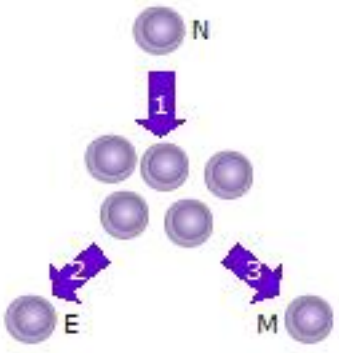


FIGURE 1.6: 1. After the naive T cell (N) encounters an antigen it becomes activated and begins to proliferate (divide) into many clones or daughter cells. 2. Some of the T cell clones will differentiate into effector T cells (E) that will perform the function of that cell (e.g. produce cytokines in the case of helper T cells or invoke cell killing in the case of cytotoxic T cells). 3. Some of the cells will form memory T cells (M) that will survive in an inactive state in the host for a long period of time until they re-encounter the same antigen and reactivate.

## 1.5 Homeostasis in the immune system

Homeostasis refers to the tendency of the body to preserve its internal steady state, allowing it to return to a normal set point following perturbation. The term was first used by the American physiologist Walter Canon in his seminal work, Wisdom of the Body, in 1932 [26]. He emphasized the dynamic nature of homeostasis, stating that while it ensures stability of the organism, homeostasis does not imply something set and immobile, a stagnation. This dynamism is evident in the homeostasis of

the adaptive immune system where rapid fluctuations in the number, diversity, and function of lymphocytes occur during immune responses. Yet, for the efficient function of the immune system, the population and activation states of T cells need to remain relatively stable in the long term [27]. The term lymphocyte homeostasis has been used to refer to the maintenance of lymphocyte numbers as well as the maintenance of lymphocyte diversity [28, 29]. Increasing evidence suggests that the homeostasis of both T cell number and diversity is regulated through competition for limiting resources, including self-peptide-MHC complexes (spMHC) and cytokines such as IL-7 and IL-15 [30].

## 1.6 Cluster of differentiation (CD44)

The CD44 antigen is a cell-surface glycoprotein involved in cell-cell interactions, cell adhesion and migration. In humans, the CD44 antigen is encoded by the CD44 gene on chromosome 11 [31].

### Multifunctionality of CD44

The CD44 expression is upregulated on naive T cells after activation via the T cell receptor (TCR) and high expression is maintained indefinitely on memory cells [32]. As a consequence, elevated expression of CD44 is generally used to identify antigen-experienced T cells. CD44 is associated with cell migration and together with HA (hyaluronic acid) has been implicated in numerous biological processes that are regulated by migrating cells [33]. The function of CD44 differs for different cell types and additional roles in the regulation of proliferation and apoptosis have been described [34]. Whereas CD44 has the potential to participate in several processes associated with immune responses, the physiological functions of CD44 in T cells in vivo remain ill defined. It has been established that T cells bind HA, and that either HA binding or TCR signaling can augment the adhesive function and expression of CD44 [35, 36]. CD44 can regulates T cell migration into sites of inflammation [37]. Therefore, CD44 is a multistructural and multifunctional cell surface molecule involved in cell proliferation, cell differentiation, cell migration, angiogenesis, presentation of cytokines, chemokines, and growth factors to the corresponding receptors, and docking of proteases at the cell membrane, as well as in

signaling for cell survival. All these biological properties are essential to the physiological activities of normal cells, but they are also associated with the pathologic activities of cancer cells [32].

## 1.7 Lymphopenia

Lymphopenia, or lymphocytopenia , is the condition of having an abnormally low level of lymphocytes in the blood. The quantity of circulating lymphocytes must be interpreted as a function of age: they are between 1500 and $4000/mm^3$ in adults and they can reach $6000/mm^3$ in children and $11000/mm^3$ in the new born. Lymphopenia is defined by a number of blood lymphocytes $< 1500/mm^3$ in adults and $4500/mm^3$ in children having an age less than 8 months [38].

### 1.7.1 Classification

In some cases, lymphopenia can be further classified according to which kind of lymphocytes are reduced. If all three kinds of lymphocytes are suppressed, then the term is used without further qualification.

- In T lymphopenia, there are too few T lymphocytes, but normal numbers of other lymphocytes. It causes, and manifests as, a T cell deficiency. This is usually caused by HIV infection (resulting in AIDS), but may be Idiopathic CD4+ lymphocytopenia (ICL), which is a very rare heterogeneous disorder defined by CD4+ T-cell counts below 300 cells/muL in the absence of any known immune deficiency condition, such as human immunodeficiency virus (HIV) infection or chemotherapy [39].
- In B lymphocytopenia, there are too few B lymphocytes, but possibly normal numbers of other lymphocytes. It causes, and manifests as, a humoral immune deficiency. This is usually caused by medications that suppress the immune system.
- In NK lymphocytopenia, there are too few natural killer cells, but normal numbers of other lymphocytes. This is very rare.

### 1.7.2 Causes

The most common cause of temporary lymphopenia is a recent infection. Lymphopenia is a frequent, temporary result of many types of chemotherapy, such as using cytotoxic agents or immunosuppressive drugs. Some malignancies that have spread to involve the bone marrow, such as leukemia or advanced Hodgkin's disease, also cause lymphopenia. In addition, large doses of radiation, such as those involved with nuclear accidents or medical whole body radiation, may cause lymphopenia.

### 1.7.3 T cell homeostasis

Homeostatic mechanisms maintain the number of T cells at an approximately constant level by controling cell division and death. In normal replete hosts, cell turnover within the naive compartment is very low and naive cells are maintained in a resting state [40]. However, disruption of the homeostatic balance can arise from a wide variety of causes and can result in T cell deficiency or T lymphopenia. Under conditions of T lymphopenia, naive T cells undergo cell division, termed homeostatic proliferation or lymphopenia induced proliferation (LIP).

### 1.7.4 Lymphopenia induced T cell proliferation

Slow turnover of naive CD8 T cells is essential for the maintenance of the naive T cell pool. Two types of proliferation have been described: the basal proliferation in lymphorepleted hosts and the homeostatic proliferation in lymphodepleted hosts [27, 41]. In fact, the basal proliferation of the naive T cell pool reflects the slow turnover of these cells and is minimal when we consider the $CD44^{low}$ population of CD8 T cells. On the other hand, the capacity of the naive CD8 T cells to replenish the peripheral pool in situations of severe lymphopenia allows for the return to homeostasis. Even though basal proliferation and lymphopenia induced proliferation (LIP) were often considered to be equivalent, they are not. In fact, the adoptive transfer of naive CD8 T cells in a lymphopenic environment leads to the acquisition of phenotypic and functional characteristics of memory T cells ($CD44^{high}$), which is distinctly different than the maintenance of a naive T cell pool.

# Chapter 2

# Mathematical models for the immune response of T cells

## 2.1 Introduction

Peripheral T cell populations are maintained by production of naive T cells in the thymus, clonal expansion of activated cells, homeostatic proliferation, and density dependent cell life spans. Despite great advances in immunological research during the last decades, relatively little is known about the quantitative characteristics of lymphocyte population kinetics [42]. There are widely divergent estimates of the growth rates, division rates, and life spans of mouse and human lymphocyte populations [43]. As a consequence, fundamental issues like the maintenance of a diverse naive lymphocyte repertoire, the maintenance of memory, and the nature of homeostatic mechanisms remain largely unresolved, and may be different in different species according to [42]. In fact, the mice are the most frequently studied experimental animal in immunology, but they may not provide information directly applying to humans [44].

Recently, several experimental techniques have been developed that have enabled the generation of quantitative data on lymphocyte dynamics. Some have made use of different lymphocyte labelling techniques, using agents such as the fluorescent dye carboxy-fluorescein diacetate succinimidyl ester(CFSE), the base analog 5-bromo-20-deoxyuridine (BrdU), deuterated glucose ($^2H_2$-glucose), or heavy water ($^2H_2O$). Although the techniques are used widely, the interpretation of kinetic data obtained using these labeling methods has turned out to be difficult [42]. In this chapter, we

review the various models in the literature that have given insights into the possibilities and limitations of the different experimental techniques, and have thereby helped the quantitative interpretation of immunological data. The reviewing of the literature in this chapter is inspired from the article of De Boer and Perelson [42].

## 2.2 General models for the immune response

The mathematical models used for describing the population of T lymphocytes are typically written as ordinary differential equations defining the rate at which the populations change over time. Most models that describe the immune response, resemble ecological predator-prey models where the immune effectors are the predators clearing a prey-like pathogen that is stimulating the effectors to grow [45–47]. The general predator-prey type model for the immune response to an exponentially growing pathogen B (for bacteria), can be written as

$$\frac{dB}{dt} = rB - kBA, \tag{2.1}$$

$$\frac{dN}{dt} = \sigma + r_N N - a_N F(B) N - d_N N, \tag{2.2}$$

$$\frac{dA}{dt} = F(B)\left[a_N N + a_M M + pA\right] - d_A A - (1 - F(B))mA, \tag{2.3}$$

$$\frac{dM}{dt} = (1 - F(B))mA + r_M M - a_M F(B) M - d_M M, \tag{2.4}$$

$$F(B) = \frac{B}{B + h}, \tag{2.5}$$

where $0 \leq F(B) \leq 1$ is a saturation function of the concentration of the pathogen, and h defines the pathogen concentration where the function is half-maximal; i.e, when $B = h$, $F(B) = \frac{1}{2}$. The variables $N$, $A$ and $M$ are the naive, activated, and memory T cells. It is assumed that naive T cells become activated by the pathogen at rate $a_N F(B)$, the activated cells then proliferate at rate $pF(B)$, and enter the memory pool at rate $(1-F(B))m$ [48]. Memory T cells are assumed to self-renew at rate $r_M$ and become activated at rate $a_M F(B)$. Naive , activated and memory cells die at rate, $d_N$, $d_A$, and $d_M$, respectively. The activation, $a$, and proliferation, $p$, rates were made proportional to $F(B)$ whereas the deactivation rate $m$, of activated cells into memory cells was made proportional to $(1 - F(B))$ [48]. The source of naive cells from the thymus, $\sigma$, is small, and it is treated as a stochastic variable. The pathogen is killed by the activated cells, which are supposed as immune effector

cells, according to a mass action term $kBA$, where $k$ is a killing rate [49]. The $r$ and $d$ parameters in this model are renewal rates, and death rates, respectively. This model forms a basis where De Boer et al. [42] have simplified this model in order to study a specific acute immune response, and to study the average turnover rates of naive and memory T cells with labeling techniques.
De Boer et al. [42] have assumed that the activation function is dependent on real time ($t$).

$$F(t) = \begin{cases} 1 & if \quad \tau_0 \leqslant t \leqslant \tau, \\ \\ 0 & else, \end{cases} \tag{2.6}$$

where the time point $\tau_0$, at which all naive T cells start to proliferate at the maximal rate [48] and $\tau$ is the time point at which the infections of all immune responses seem to shut down, which is called the peak of the response [42]. To fit the experimental data from acute immune responses to viruses and bacteria, De Boer et al. [42] have used Eq. (2.6) to reformulate Eqs. (2.2)-(2.4) of the general model into a piecewise linear model for the response to one specific epitope[1]

$$\begin{aligned} \frac{dA}{dt} &= F(t)pA - (1 - F(t))(d_A + m)A, \\ \frac{dM}{dt} &= (1 - F(t))(mA - d_M M), \end{aligned} \tag{2.7}$$

where $A$ is the number of activated cells, and $M$ is the number of memory cells of a population of T cells that are specific for the epitope of interest, and the total size of the immune response is defined by $T = A + M$. For a primary immune response, the initial number of cells can be defined as $M(0) = 0$ and $A(0) = A(\tau_0)$. Then, $A(\tau) = M(\tau)$ is the total number of cells at the peak of the response, since in this strict on/off model, memory cells only start to form after the peak [48]. Their results (De Boer et al. [42]) show that the experimental data provide typically the total number of T cells that are specific for one particular epitope, which in Eq. (2.7) corresponds to $A(t)$ when $t \leq \tau$ and $A(t) + M(t)$ after the peak.
Another approach for modeling the clonal expansion phase of an immune response is to explicitly write a cascade of equations that follow every division that the cells have completed [50]. Activation of naive or memory T cells recruits the cells into the first stage of the proliferation cascade, $P_0$, where the index denotes the number

[1] A localized region on the surface of an antigen that is capable of eliciting an immune response and of combining with a specific antibody to counter that response.

of completed divisions. For the closure of clonal expansion, it is assumed that after a certain number of divisions the cells differentiate into effector cells, $E$, that will leave the lymphoid tissue to clear antigen, and become memory cells.

$$\frac{dP_0}{dt} = F(.)\left[a_N N + a_M M\right] - (p + d_P)P_0, \tag{2.8}$$

$$\frac{dP_n}{dt} = 2pP_{n-1} - (p + d_p)P_n \quad for\, n = 1, ..., n_{max}, \tag{2.9}$$

$$\frac{dE}{dt} = 2pP_{n_{max}} - d_E E - (1 - F(.))mE, \tag{2.10}$$

where $F(.)$ can be either a function of time, or the concentration of antigen, and $n_{max}$ is the number of divisions cells complete during clonal expansion. Eq. (2.2) for the naive T cells in the general model ODEs can stay the same, but the first term in the memory cell equation, Eq. (2.4), has to become $(1 - F(.))mE$. Because the birth-death ODE model of Eq. (2.9) is linear, it implicitly assumes an exponential distribution of cell cycle times. This allows cells to rapidly proceed through the whole division cascade [51].

This model therefore does not allow for a strict time window of clonal expansion, it needs a strict time delay representing the minimal time to complete cell division [51]. Diekmann et al. [52] and later on Ganusov et al. [6] have formulated the previous model as a system of delay differential equations (DDEs). Indeed, the activated cells of Eq. (2.3) are divided here in proliferating activated cells, $P$, and effector cells, $E$. Then, their behaviour is described as follows

$$\begin{aligned}\frac{dP}{dt} = {} & F(t)\left[a_N N + a_M M\right] + pP - d_P P - a_N H(t - \tau_N)N(t - \tau_N)e^{(p-d_p)\tau_N} \\ & - a_M H(t - \tau_M)M(t - \tau_M)e^{(p-d_p)\tau_M}, \end{aligned} \tag{2.11}$$

$$\begin{aligned}\frac{dE}{dt} = {} & a_N H(t - \tau_N)N(t - \tau_N)e^{(p-d_p)\tau_N} + a_M H(t - \tau_M)M(t - \tau_M)e^{(p-d_p)\tau_M} \\ & - d_E E - (1 - F(t))mE. \end{aligned} \tag{2.12}$$

According to this model primed naive T cells, $N$, are involved in clonal expansion for a period of $\tau_N$ days during which time they divide at rate $p$ and die at rate $d_p$. At the end of this proliferative phase, they move into the effector population. The $e^{(p-d_p)\tau}$ terms are the net dimension less clonal expansion factors describing the expected clone size per primed cell given, the division rate $p$ and the death rate $d_p$ [42]. The $H(t - \tau)$ terms are Heaviside functions preventing the usage of negative time points, i.e, $H(t) = 0$ if $t < 0$ and $H(t) = 1$ otherwise. Memory cells, $M$, maintain themselves by division (i.e, self-renewal), at rate $r_M$, die at rate $d_M$

and may become primed by antigen at rate, $a_M$, to perform another round of clonal expansion for $\tau_M$ days.

Finally, division cascade models like Eq. (2.9) have been used many times for modeling immune responses and renewing cells in a homogeneous population [4, 51, 53–57]. Because self-renewal is in theory not bounded by a maximum number of divisions, unless cells run into the Hayflick limit [42]. De Boer et al. [42] have proposed an infinite cascade of random birth-death equations that keep track of the number of divisions cells have completed.

$$\frac{dP_0}{dt} = -(p+d)P_0, \tag{2.13}$$

$$\frac{dP_n}{dt} = 2pP_{n-1} - (p+d)P_n, \quad n = 1, ..., \infty, \tag{2.14}$$

where $n$ is the number of divisions cells have completed. Let $P(t)$ be the total number of cells at time $t$, then

$$\frac{dP}{dt} = \sum_n \frac{dP_n}{dt} = (p-d)P.$$

For the initial condition $P_0(0) = T(0)$ and $P_n(0) = 0$ for $n = 1, .., \infty$, where $T(0)$ is the initial number of undivided cells, the general solution is

$$P_n(t) = P(t) \times \frac{(2pt)^n}{n!} e^{-2pdt},$$

where $P(t) = \sum_n P_n(t) = T(0)e^{(p-d)t}$ is the total number of divided cells, and the second term of the right hand side of the above equation gives the distribution of the cells over the division numbers.

This simple models (2.13-2.14) is very general and has been used widely in the literature to describe several data like CFSE (it is detailed in the next section) or BRdU [4, 51, 53–57].

## 2.3 CFSE

Carboxyuorescein succinimidyl ester (CFSE) is an intracellular fluorescent dye that dilutes 2-fold when a cell divides [58]. Cells are typically labeled with CFSE in vitro, and labeled cells can be followed thereafter in vitro or in vivo. Harvesting the cells and sorting them by the CFSE intensity generates profiles with maximally 7 or 8

peaks, each reflecting the number of divisions the cells have undergone [42]. CFSE is currently the most informative technique for characterizing the division kinetics of cells in the immune system. A number of reviews address the experimental procedures [59, 60]. The interpretation of CFSE data has resulted in many different mathematical approaches. Here, we give some approaches from the literature.

Asquith et al. [56] wrote a random birth-death model like Eqs. (2.13-2.14), and estimated the number of divisions that were required for a $CFSE^+$ cell to become $CFSE^-$ from the ratio of the median fluorescence intensity (MFI) of all $CFSE^+$ cells over all $CFSE^-$ cells. Finding $2^5$-fold ratio, they truncated Eqs. (2.13-2.14) at the fifth division,

$$\begin{aligned} \frac{dP_0}{dt} &= -(p+d)P_0, \quad \frac{dP_n}{dt} = 2pP_{n-1} - (p+d)P_n, \\ \frac{dP_5}{dt} &= 2pP_4 + (p-d)P_5 + \sigma, \end{aligned}$$

for $n = 1, ..., 4$, and included a possible source, $\sigma$ of $CFSE^-$ cells for $P_5$ equation. This model predicts two observables, the fraction of $CFSE^+$ cells and the ration of the MFIs of $CFSE^+$ to $CFSE^-$ cells. These two observables were successfully fit to B cell data [56].

Luzyanina et al. [61] defined a model directly describing the kinetics of the CFSE intensity profile using a label-structured population model. Their models is comprised of a CFSE structured PDE allowing for cell death, for the 2-fold dilution per division, and for CFSE loss by normal catabolism. This has the immediate advantage of not having to classify CFSE profiles into individual peaks, which is particularly helpful when the data is not nicely fingered. Assuming that each CFSE peak represents a cohort of cells that entered their first division at approximately the same time. Luzyanina et al. [61] wrote a label structured population model for the density of cells with CFSE intensity $x$

$$\begin{aligned} \frac{\partial n(t,x)}{\partial t} + v(x)\frac{\partial n(t,x)}{\partial x} &= -\left[p(x)+d(x)\right]n(t,x) + 2\gamma p(\gamma x)n(t,\gamma x), \ x_{min} \le x \le x_{max}/\gamma, \\ \frac{\partial n(t,x)}{\partial t} + v(x)\frac{\partial n(t,x)}{\partial x} &= -\left[p(x)+d(x)\right]n(t,x), \ x_{max}/\gamma \le x \le x_{max}, \end{aligned} \tag{2.15}$$

where the $v(x)$ term describes the natural decay of the CFSE intensity, the proliferation $p(x)$ and death $d(x)$ rates depend on the CFSE expression of the cell, and $\gamma$ is the CFSE dilution factor. If cells divide into two daugther cells, then $\gamma = 2$. Fitting this PDE model directly to CFSE intensity profiles required smoothing of the data, and required non-trivial numerical integration methods for solving the

PDEs [61]. Two data sets obtained from in vitro proliferation of T cells following polyclonal activation were fit using this model. The loss rate of CFSE, $v(x)$, was not exponential. The death rate hardly depended on the CFSE intensity, whereas the division rate was found to be a bell-shaped function of the CFSE intensity x, with relatively slow maximum division rates of 0.55 $day^{-1}$ and 0.8 $day^{-1}$ at the third or fourth division. Finally, the dilution factor, $\gamma$, was less than two in both data sets [61].

The general label structured population approach of [61] has been extend by several authors [62–66]. For example, Schittler et al. [64] and Hasenauer et al. [65] extend Luzyanina et al. [61] model with discrete populations for each division, and this extension leads to the much more intuitive model.

$$\begin{aligned} \frac{\partial P_0(t,x)}{\partial t} + \frac{\partial \left(v(x)\, P_0(t,x)\right)}{\partial x} &= -\left[p_0(t) + d_0(t)\right] P_0(t,x), \\ \frac{\partial P_n(t,x)}{\partial t} + \frac{\partial \left(v(x)\, P_n(t,x)\right)}{\partial x} &= -\left[p_n(t) + d_n(t)\right] P_n(t,x) \\ &\quad +2\gamma p_{n-1}(t) P_{n-1}(t,\gamma x), \end{aligned} \tag{2.16}$$

for $n = 1, ..., n_{max}$, and where $x$ is the amount (or concentration) of CFSE in each cell, which decreases at a rate $v(x)$. The number of cells contained in the nth subpopulation is defined as $P_n(t) = \int_0^\infty P_n(t,x)dx$, and the number of cells having an amount $x$ of CFSE is given by $P(t,x) = \sum_{n=0}^{n_{max}} P_n(t,x)$. After adding the autofluorescence, the latter can be fitted directly by measured CFSE profiles, such that the total cell number in the data is predicted by $P(t) = \sum P_n(t)$ [65].

Furthermore, other models are proposed in the literature to analyse CFSE data, like the Cyton model and the Smith-Martin model. These two models are described briefly in the next sections.

## 2.4 Cyton model

Gett and Hodgkin [1] proposed a simple mathematical model for CFSE data analysis. This model was then compared with a relatively simple branching process model in Hyrien and Zand [67]. The key model assumption in Gett and Hodgkin [1] of a normal distribution of the time to first division turned out to be likely inappropriate [68]. The recent work of Hawakins et al. [59] extends the work of Gett and Hodgkin [1] by directly modeling the time to division and time to death of cell generations using independent single mode continuous distributions. This is called

Cyton model. Thus, the Cyton model does not require the assumption of a normal distribution and it is flexible enough to model different generations with different kinetic parameter values (e.g, different proliferation or death rates for different cell generations)[68]. In this section, the Cyton model is briefly reviewed and discussed. Let $n = 0, 1, ...$ denote the nth generation of cells. For the nth generation, a continuous distribution $\phi_n(t)$ is assigned to model the distribution of the time to divide, and $\psi_n(t)$ is assigned to model the distribution of time to die. To calculate the cell number in each generation at time $t$, this model consists in starting with the first generation. Given $N(0)$ cells of age zero at time zero, then, at time $t$, the rates of cell division or death in the first generation are given by

$$\begin{aligned} r_0^{div}(t) &= f_0\, N(0) \left(1 - \int_0^t \psi_0(\tau) d\tau\right) \phi_0(t), \\ r_0^{die}(t) &= N(0) \left(1 - f_0 \int_0^t \phi_0(\tau) d\tau\right) \psi_0(t), \end{aligned}$$

where $f_0$ represents the probability that a cell will divide in response to the given stimulus. Then for later generations, the rates of cell division and death are given by

$$\begin{aligned} r_n^{div}(t) &= 2 f_n \int_0^t \left[ r_{n_1}^{div}(\tau) \left(1 - \int_0^{t-\tau} \psi_n(\zeta) d\zeta\right) \phi_n(t-\tau) \right] d\tau, \\ r_n^{die}(t) &= 2 \int_0^t \left[ r_{n-1}^{die}(\tau) \left(1 - f_n \int_0^{t-\tau} \phi_n(\zeta) d\zeta\right) \psi_n(t-\tau) \right] d\tau. \end{aligned}$$

Thus the number of cells in each generation can be calculated as follows

$$\begin{aligned} N_0(t) &= N(0) - \int_0^t \left( r_0^{div}(\tau) + r_0^{die}(\tau) \right) d\tau, \\ N_n(t) &= \int_0^t \left( 2 r_{n-1}^{div}(\tau) - r_n^{div}(\tau) - r_n^{die}(\tau) \right), \quad n = 1, 2... \end{aligned}$$

The construction of the model above is straightforward. See Hawakins et al. [59] for more details. Note that, $\phi_n(t)$ and $\psi_n(t)$ in the Cyton model are the probability density functions of some continuous distributions.

## 2.5 Smith-Martin model

The model for the cell cycle developed by Smith and Martin [69] has been successfully used for analyzing the population dynamics of dividing cells as it prevents too rapid progression through the cell cycle by introducing the equivalent of a time delay, i.e, a fixed length for the S, G2 and M phases of the cell cycle [42].
The Smith-Martin model allows for two phases of the cell cycle: cells in the "A" state, which approximately corresponds to the G0 or G1 phase of the cell cycle, are randomly activated to divide, and dividing cells in the "B" phase remain in this phase for a fixed time $\Delta$. Later on, they yield two daughter cells in the A-state.
Based on the Smith-Martin model, several investigations have developed mathematical models for the purpose of CFSE data analysis [3, 8, 51, 70], including deterministic models as well as stochastic models. However, the Smith-Martin model has been criticized for its simplicity and inaccuracy [67, 71–73] and more complicated cell cycle models have been proposed [74–76]. The recent work of Lee and Perelson [8] greatly extended the Smith-Martin model by introducing the gamma distribution for the A phase generation, generation dependent death rates, and variables length of the B phase. Three models were developed in Lee and Perelson [8], including the time to first division (TFD) model, generalized Smith-Martin (GSM) model and the heterogeneous generalized Smith-Martin (HGSM) model. Although the GSM and HGSM models are more flexible to accommodate variations from generation to generation, some assumptions in Lee and Perelson [8] have been made to simplify the analysis of models, which may not hold in practice. For example, it was assumed that after the first division, cells of different ages have the same average A and B phase lengths. Also, more complex Smith-Martin models were shown to be comparable to the Cyton model [9]. The Smith-Martin model in [8], is written as follows

$$\begin{aligned}
\frac{dA_0(t)}{dt} &= -(\lambda+\delta_A)A_0(t), \\
\frac{dA_i(t)}{dt} &= 2\lambda e^{-\delta_B\Delta}A_{i-1}(t-\Delta) - (\lambda+\delta_A)A_i(t),\ i \geqslant 1, \\
\frac{dB_i(t)}{dt} &= \lambda A_i(t) - \lambda e^{-\delta_B\Delta}A_i(t-\Delta) - \delta_B B_i(t),\ i \geqslant 0,
\end{aligned}$$

where $A_i(t)$ and $B_i(t)$ $(i = 0, 1, 2, ...)$ denote the number of cells in the A-state and the B-phase in the ith generation, respectively. The cells in the A-state and B-phase have death rates $\delta_A$ and $\delta_B$ respectively. Cells in the A-state are triggered

to enter the B-phase at a rate $\lambda$ and divide when they complete the process in B phase. This Smith-Martin model has four parameters, with the length of the cell cycle defined as $p^{-1}+\Delta$, and two different death rates. According to [42], the death rates $\delta_A$ and $\delta_B$, cause a problem of identifiability by using CFSE data. This version of Smith-Martin model will give unique fits to CFSE data if the model is simplified to three parameters, e.g, by assuming that $\delta_A = \delta_B$, $\delta_A = 0$ or $\delta_B = 0$ [4, 70]. Note that the similar problems with the uniqueness of fits exist in the Cyton model [59], and that one needs more information, like the number of dead cells per division, to resolve these parameter identification problems.

Luzyanina et al. [77] compare fits obtained with a classical Smith-Martin model, with fits obtained with a heterogeneous random birth-death model, i.e, Eqs. (2.13-2.14) extended division and death rates, $p_n$ and $d_n$, that depend on the division number $n$. They find that the random birth-death models fits their data better. This is not a fair comparison, however, because the heterogeneous model has many parameters, that could compensate for the absence of the time delay, $\Delta$, of the Smith-Martin model [42].

De Boer et al. [5], Ganusov et al. [6] and Lee et al. [8] have shown that the quiescent cells are in the G0 state of the cell cycle, and need more time to enter the G1 state of the cell cycle, and their first B-phase could take longer than subsequent B phases. Then, the Smith-Martin can be extended with a longer first division by implementing a recruitment function $R(t)$, defining the distribution of times to complete the first division.

$$\begin{aligned}
\frac{dA_1(t)}{dt} &= R(t) - (\lambda_1 + \delta_1)A_1(t), \\
\frac{dA_i(t)}{dt} &= 2\lambda_{i-1}e^{-\delta_{i-1}\Delta}A_{i-1}(t-\Delta) - (\lambda_i + \delta_i)A_i(t),\ i > 1, \\
\frac{dB_i(t)}{dt} &= \lambda_i A_i(t) - \lambda_n e^{-\delta_i \Delta}A_i(t-\Delta) - \delta_i B_i(t),\ i \geqslant 1,
\end{aligned}$$

where $\lambda_i$ and $\delta_i$ are the division and death rates at the ith division, respectively. Fitting either a time-shifted log-normal [6] or a gamma distribution [6, 8] for $R(t)$ to experiments explicitly measuring the time to first division, this heterogeneous Smith-Martin model was successfully fitted to CFSE data from T cells stimulated in vitro with various concentrations of the cytokine IL-2 [78].

Furthermore, Bernard et al. [3] and Ganusov et al. [4] have formulated the Smith-Martin model in terms of PDEs to take into account the continuous age of cells in

B-phase. The latter is written as follows

$$(SM)\quad \begin{cases} \frac{dA_0}{dt} = -(\lambda + \delta_A)A_0(t), \quad \{A_0(0) > 0\} \\ \\ \frac{dA_i}{dt} = 2B_{i-1}(t,\Delta) - (\lambda + \delta_A)A_i(t), \quad \{A_i(0) = 0\},\ i = 1, ..., I \\ \\ \begin{cases} \frac{\partial}{\partial t}B_i(t,\tau) + \frac{\partial}{\partial \tau}B_i(t,\tau) = -\delta_B B_i(t,\tau),\ i = 0, ..., I \\ \\ B_i(t,0) = \lambda A_i(t),\ B_i(0,\tau) = 0 \end{cases} \end{cases}$$

where $\Delta$ is the duration of cells in B-phase, $\lambda$ is the rate of entry into division, and, $\delta_A$, $\delta_B$ are the death rate in A-state and B-phase respectively. Ganusov et al. [4] have shown that no general robust method exists to estimate all parameters of the $SM$ model by using CFSE data alone. It is, however possible to estimate the duration of division $\Delta$, probability of cell death during the cell cycle $\delta$ (by assuming $\delta = \delta_A = \delta_B$), and in some cases the average division time $T$. In addition, measuring an additional parameter, like the fraction of cells in division (i.e, fraction of cells that are in the $S + G_2 + M$ phase of the cell cycle), may allow estimation of all parameters of the $SM$ model [4].

## Models of T cell homeostatic proliferation

The homeostatic proliferation (or lymphopenia induced proliferation) that naive T cells undergo following adoptive transfer into an environment with low T cell number was studied by Yates et al. [7] and Hogan et al. [10].
In [7], they labeled F5 TCR transgenic naive CD8+ T cells, which are specific for an influenza peptide, with CFSE and transferred these cells into Rag1 knockout mice that have no endogenous T cells. At different time points, lymph nodes were recovered from the recipient mice to record the CFSE profiles and expression of CD44 were assessed by flow cytometry. In the presence of cognate antigen, i.e, the influenza virus, CFSE dilution was rapid due to the vigorous clonal expansion of the F5 T cells. In its absence, the F5 cells started to grow exponentially after a few days. The mean division number increased linearly with time, with some evidence for a slowing-down after about two weeks. Furthermore, using the CFSE profile to calculate the precursor frequency (see Materials and Methods in [7]) revealed that the $CD44^{high}$ population arise from only 17% of the precursor population.

The remaining 83% pool remained $CD44^{low}$ and divided more slowly or not at all. Therefore, their data in [7] suggest that F5 TCR transgenic CD8+ T cells divided slowly, or not at all, without up-regulating activation markers like CD44.
To analyse the regulation of LIP, Yates et al. [7] fitted a series of mathematical models of cell division to their data. At first, they compared the time course of cell division predicted by Cyton model to the response observed experimentally, the model appeared to provide a very poor description of the data [7]. The second class of model used in their study, is the $SM$ model, in which cells spend exponentially distributed times in a quiescent A-state (corresponding approximately to the $G_0/G_1$ states of the cell cycle) and then progress through a B-phase ($S$, $G_2$ and $M$) before dividing and returning to the A-state. The B-phase was taken to be of fixed duration $\Delta$. The rate of transition from A-state to B-phase is represented by a constant term $\lambda$. This assumption of a constant mean rate of entry into division ($\lambda$) gave a reasonable fit to the data [7]. The third class of model is a modified $SM$ model where they extend the $SM$ model. Indeed, they considered that the rate of entry into division depends on the time $t$ ($\lambda = \lambda_0 e^{-\eta t}$). This improved the fit significantly.

Furthermore, Hogan et al. [10] analysed two TCR transgenic of T cells (OT-1 cells and F5 cells). Their data allow to conclude that the undivided OT-1 cells expressed a similar level of CD44 to naive CD8+ T cells, and began to upregulate expression of this marker after the 4th-6th division in response to lymphopenia. However, F5 T cells retained a low level of CD44 expression throughout division. The expression of CD44 by OT-1 T cells at approximately 4-6 divisions in response to lymphopenia, indicates the acquisition of a memory like phenotype, which is not observed for F5 T cells under the same conditions. This result is consistent with the result of F5 T cells deduced by Yates et al. [7]. In addition, Hogan et al. [10] extended the modified $SM$ model proposed by Yates et al. [7] (it is denoted by $SM_1$ model). This new version of Smith-Martin consists to take into account the competition between cells to enter B-phase, then the rate of entry into division is considered as a function of the cell number ($\lambda = \lambda_0 e^{-\eta N(t)}$ where $N(t)$ is the total cell number in A-state and B-phase). In their work, they compared this new version of Smith-Martin model ($SM_1$ model) to Cyton model for OT-1. They concluded that LIP by OT-1 was much better modeled with the $SM_1$ model than the Cyton model, as reflected in the lower CrV for the $SM_1$ model fit, which is a measure of goodness of fit.

## 2.6 Discussion and Motivation

Throughout adult life, the size and composition of the peripheral lymphocyte pool is tightly regulated and, in the absence of disease, is maintained at relatively constant levels [40, 79]. The correct representation of the T-cell pool is essential to maintain adequate immune competence against pathogens, since it has to maintain a sufficiently diverse repertoire of naive T cells to recognize a broad range of antigens, while efficient immune responses against previously encountered pathogens depend on the memory T-cell pool. For these demanding tasks, homeostatic mechanisms have evolved to maintain distinct populations of naive and memory cells and to retain an appropriate mixture of CD4+ helper T cells and CD8+ cytotoxic T cells. A few general principles govern the physiologic response to perturbations of the balance between T cells. For example, viral infections (HIV, Tuberculosis,...), or drugs used in peritransplant induction therapy or cancer chemotherapy, are the main factors that disrupt the balance of T cells. This perturbation results in Lymphocytopenia or lymphopenia (i.e. the condition of having an abnormally low level of lymphocytes in the blood) which induces a rapid in vivo proliferation of T cells with a recruitment of naive T cells from the thymus.
As proved in the last decades, the use of mathematical models in immunology has allowed great advances, not only on the theoretical side, but also on the side of the management of actual public health policies. As summarized in this chapter, several studies have successfully used mathematical modeling to describe the proliferative response of T cells to lymphopenia [7, 10] and greatly facilitated our understanding of the cell cycle control involved. However, these studies have not taken into account the transition from naive to memory status by using the concept of a relevant phenotype as structuring during the homeostatic process. This transition can be assessed phenotypically by measuring expression levels of several surface markers such as CD44.
In this thesis, our research objectives are to elaborate some answers to the following immunological subjects:

- **Understanding the complex relationship between LIP[2] and the switch from a naive to memory phenotype through mathematical models.**
- **Studying the asymptotic behaviour of T cells during the homeostatic process in vivo.**

[2]Lymphopenia Induced Proliferation

The key tools used in this work are: **Mathematical Modeling, Numerical Analysis, Experimental Data, Parameter Identification Problem, Asymptotic Behaviour and Optimal Control.**

# Chapter 3

# Publications and Plan of Thesis

**Journal:**

- Ayoub, H., Ainseba, B. E., Langlais, M., Hogan, T., Callard, R., Seddon, B., Thibaut, R. (2014). Parameter identification for model of T cell proliferation in Lymphopenia conditions. *Mathematical Biosciences*, 251, 63-71.
- Ainseba, B. E., Ayoub, H., Langlais, M., An age-structured model for T cell homeostasis in vivo. *SIAM Applied Mathematics* (Accepted).
- Ayoub, H., Ainseba, B. E., Langlais, M., Thiébaut, R., Parameters identification for a model of T cell homeostasis (submitted).
- Ayoub, H., Ainseba, B. E., Langlais, M., An optimal strategy of rebuilding immunity in conditions of T Lympopenia (in progress).

**Proceeding:**

- Ayoub, H., Ainseba, B. E., Langlais, M., Global dynamics of a model of T cell proliferation in lymphopenia conditions, LAAS 20 International Science Conference, pp. 265-286, 27-29 March 2014.

# Plan of Thesis

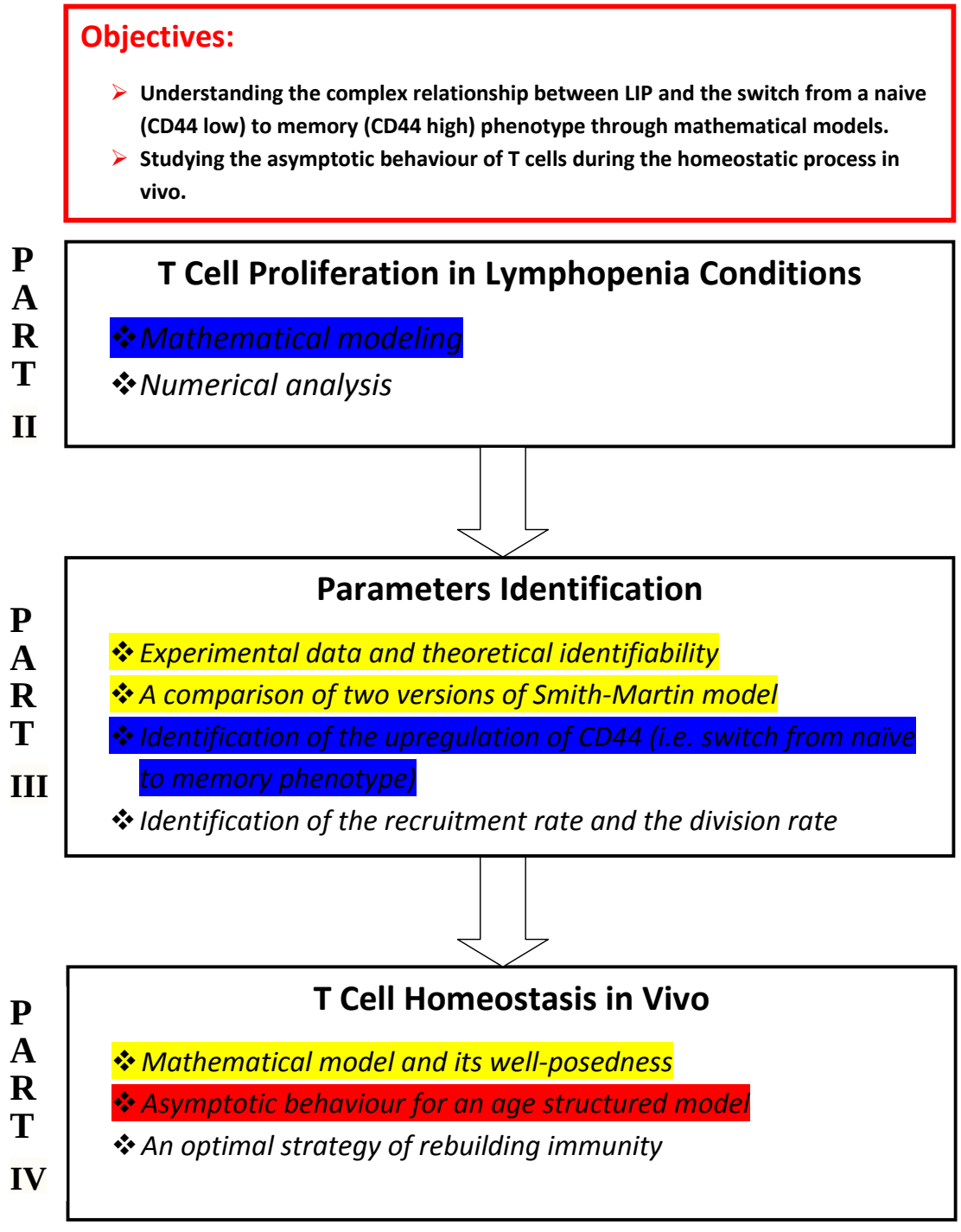


Flowchart of thesis. Items in blue, red and yellow resume the articles [80] (Published), [81] (Accepted), [82] (Submitted) issues from this thesis respectively.

This work is organised as follows.

**- Part II** is divided in two chapters:

- In Chapter 4, we build a new in vitro model (noted $SM_{CD44}$) to include the transition from naive (CD44 low) to memory (CD44 high) cells. By including in the Smith-Martin model [3, 4, 7, 10] new parameters which link the phenotypic (i.e. gradual upregulation of CD44 expression) and functional conversion of cells with their number and/or rate of division, we explore the nature of the LIP response that generate CD44 phenotype expression in T cells.
  As in the Smith-Martin model, the $SM_{CD44}$ model includes an A-state (resting phase) and a B-phase (proliferative phase) where cells undergo division such as a cascade system. The number of times cells transfer between the A-state to the B-phase is indexed by $i$, which is the number of times a cell has undergone division. The time since entering the B-phase (either the first time or any subsequent time) is measured by $\tau$ which reflects the maturity of the cells at this stage and has a maximum value $\Delta$. Both the cells in A-state and B-phase are also indexed by $s \in [0, m]$, the intensity of CD44 expression. The A-state and B-phase are described by ODEs and PDEs respectively. The different A-state and B-phase components are given by $A_i(t, s)$ and $B_i(t, \tau, s)$ respectively for $i = 0, 1, ..., I$ (depending on how many times the cells have undergone division). For $i = 0$ the growth of the $A_0$ component in this in vitro model comes from the initial number of cells in $A_0$ phase. Furthermore, the stochastic recruitment of cells from A-state into B-phase is done with a rate $\lambda$ that depends on the total cell number $N(t)$. In B-phase, the cells are up-regulating their level of CD44 with a velocity $v_i(s)$. After completing the process (mitosis) in B-phase, the cells divide with rate $\mu(\tau)$ which depends on the age of cells in B-phase, and the daughter cells inherit the same level of CD44 of their mother cells (See (4.2-4.3) and Fig. 4.1 in Chapter 4). For this structured system, we derive an implicit solution of the $A_i$ equation and the integral formulation of the $B_i$ equation.

- In Chapter 5, we build a numerical scheme to approximate the solution of $SM_{CD44}$ model. Furthermore, an analysis of properties of the scheme is proposed. Indeed, the proofs of stability, consistency and convergence of the scheme to an analytical solution of the model, are established in this chapter.

**- Part III** is divided in four chapters:

- In Chapter 6, we describe the data generated by Hogan et al. [10]. Next, we prove the identifiability of some parameters ($v_i$, $\lambda$, $\Delta$) in $SM_{CD44}$ model.

- In Chapter 7, we present the latest version of Smith-Martin in the literature and our reduced $SM_{CD44}$ model (i.e without the CD44 structure). In addition, we describe the method used to identify numerically several common parameters in both models by using the CFSE data [10]. Finally, we show the parameters and the simulations that we obtain from the models, and compare them to experimental data.

- In Chapter 8, we interest to identify the velocity of CD44 up-regulation during lymphopenia induced proliferation. This velocity is the key parameter that distinguishes from which divisions, T cells can be considered as naive or memory through the mathematical model $SM_{CD44}$.
  The methodology used to identify this parameter consists to solve a parameter identification problem where it is well detailed in this chapter. In the numerical results, we show the parameters and the simulations that we obtain from the model and compare them to experimental data. Finally, the identified parameters and the simulations of $SM_{CD44}$ provide several biological interpretations of the complex relationship between LIP and the switch from a naive to memory phenotype through $SM_{CD44}$ model.

- In Chapter 9, we connect the intensity of CD44 with the rate of entry into division ($\lambda$) and the rate of division ($\mu$). Here, we interest to identify these new parameters which depend on the level of CD44 ($s$). As in the previous chapter, the ingredients to solve the parameters identification problems are given. Finally, we present the simulations and the identified parameters, and we conclude by biological interpretations about the link between the level of CD44 on the cells and their rate of entry into the proliferative phase or their division rate.

**- Part IV** is divided in three chapters:

- In Chapter 10, we extend the $SM_{CD44}$ model to an in vivo model by implementing a rate $\Lambda$ of export of cells from the thymus. In addition, we consider

a large number of division ($I >> 0$) with a rate of entry into division depending on the number of division ($i$) and the total cell number ($N$). By using the fixed point method, we prove the local existence and uniqueness of the solution of the extended model system. Finally, we conclude on the global existence of solutions by using the maximal interval of existence.

- In Chapter 11, we rewrite the extended model system as an age-structured model system without the CD44 structure, and we investigate its asymptotic behaviour. We find that there exists one or three stationary solutions when cells undergo at least five divisions and only one stationary solution when cells undergo at most three divisions, the limiting case with four divisions is numerically handled. By applying the Lyapunov method, we prove in some cases of uniqueness that the stationary solution is globally asymptotically stable.

- In Chapter 12, we reformulate the in vivo model proposed in Chapter 10 into a more realistic version with vaccination strategy. The purpose of this chapter is to address the problem of determining an optimal strategy that lead to enhanced immunity during the homeostatic process. Firstly, we discuss the cost function and we derive the optimality conditions. Secondly, we perform some simulations to compute the optimal vaccination.

**- Finally in Chapter 13**, we summarize the main results of this study and we give perspectives and new problems induced from this research project.

# Part II

# T Cell Proliferation in Lymphopenia Conditions: Mathematical Modeling and Numerical Analysis

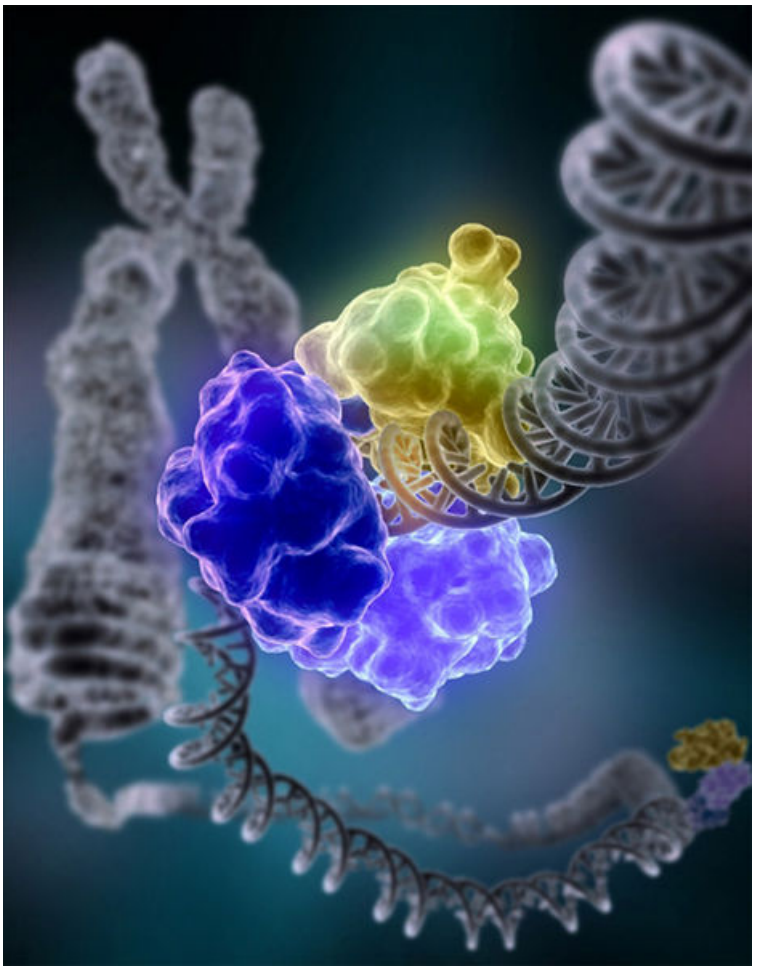

# Chapter 4

# Mathematical modeling of Lymphopenia induced proliferation

## 4.1 Introduction.

T lymphocytes are a fundamental component of the immune system that can recognise and respond to a foreign antigen by virtue of their clonally expressed T cell antigen receptor (TCR). T cells that have yet to encounter the antigen they recognise are termed 'naive' as they have not been activated to respond.
Homeostatic mechanisms maintain the number of T cells at an approximately constant level by controling cell division and death. In normal replete hosts, cell turnover within the naive compartment is very low and naive cells are maintained in a resting state [40]. However, disruption of the homeostatic balance can arise from a wide variety of causes and can result in T cell deficiency i.e T lymphopenia. Under conditions of T lymphopenia, naive T cells undergo cell division, termed homeostatic proliferation or lymphopenia induced proliferation (LIP).
The homeostatic proliferative response of naive T cells is complex and depends on the affinity of the TCR for self antigens. Studies on TCR transgenic mouse models reveal a spectrum of responses. T cells expressing some TCR transgenes fail to proliferate in lymphopenia [28]. T cells expressing other transgenic TCR undergo cell divisions at a slow rate [83] whereas some others undergo more rapid divisions accompanied by changes in the cell surface phenotype including increased CD44

expression, which is commonly associated with a "memory like" phenotype [84–86]. This transition can be assessed phenotypically by measuring expression levels of several surface markers such as CD44 on which this thesis is focused. Understanding the complex relationship between LIP and the switch from a naive to memory phenotype is an important question to address. There have been several studies modelling the cell cycle in lymphopenia conditions [7, 10]. However these studies did not take into account the changes in phenotype.

An important step in using the mathematical approach is the estimation of model parameters using experimental data. Several types of data have been used in this context. Using cell dyes, such as Carboxy Fluorescein diacetate Succinimidyl Ester (CFSE), is currently one of the most informative methods to characterize the dynamics of cell division in the immune system. Following each division, CFSE divides equally between daughter cells, resulting in a two-fold decrease in the intensity of cellular fluorescence in each successive generation. This property of CFSE allows accurate tracking of the number of divisions that a given cell has undergone either in vitro or following transfer in vivo [87].

Several authors have tried to understand T cells homeostasis by using mathematical models with CFSE data and employing many methods for the estimation of model parameters [1, 4, 5, 8–10, 51, 59, 78].

Gett and Hodgkin [1] used a different class of model (GH model) in which heterogeneity in proliferation stems from variable times to first division, with quasi-deterministic division from then onwards. This has been used successfully to describe antigen-driven 'programmed' cell division [1, 78, 88].

The Smith-Martin model (Smith and Martin [69]) is another standard mathematical model for analysing the kinetics of the cell cycle, which allows two phases of the cell cycle. Cells in "A-state" are in rest and are recruited stochastically to divide in the proliferative "B-phase". This phase has a fixed total duration.

The Smith-Martin model has been applied widely to CFSE data [2–9], and the duration of deterministic phase (B-phase) and the probability of cell death has been estimated from experimental data mainly based on CFSE cell division profiles. Hogan et al [10] improved the technique and accuracy of the parameters estimations from the Smith-Martin model. The DNA binding dye, 7-Aminoactinomycin D (7AAD), was used with CFSE to distinguish the proliferating and non-proliferating cells, therefore enabling estimations of the rate of recruitment of cells from A-state into B-phase.

In this chapter, we build a new model for including the transition from naive (CD44

low) to memory (CD44 high) cells. By including new parameters to the Smith-Martin model which link the phenotypic (i.e. gradual upregulation of CD44 expression) and functional conversion of cells to their number and/or rate of division, we explore the nature of the LIP response that generate CD44 expression phenotype cells.

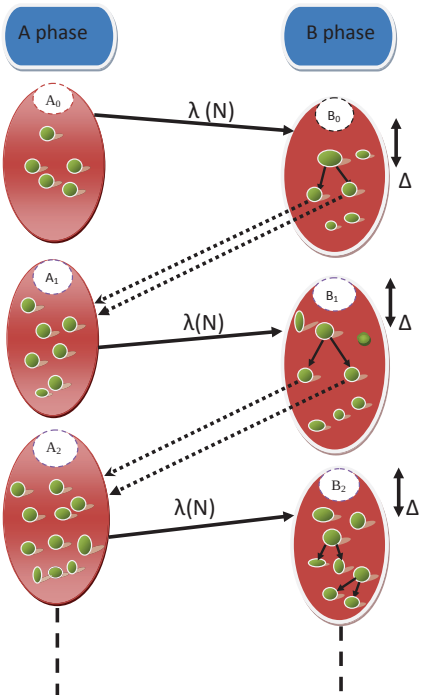


FIGURE 4.1: Model of T cell proliferation in lymphopenia conditions. $A_i$ and $B_i$ are the number of T cells, having undergone $i$ divisions in A-state and B-phase respectively. $\Delta$ is the duration of B-phase (unit in hour). The rate of entry into division ($\lambda$) is described by a function of the total cell number ($N$), which is linked to all phases and all divisions [10].

## 4.2 The model (noted $SM_{CD44}$)

The biological cell cycle describes five distinct phases G0, G1, S, G2 and M grouping interphase and mitosis. Phase G0 is a quiescent phase as cells are in a non dividing state and require a specific extrinsic signal to enter the cell cycle. In G1, cells grow in size and make the cytoplasmic proteins necessary for cell division. The phases S, G2 and M are the proliferative phases where a cell duplicates its genome and divides in two daughter cells.

In the case of T cell division, a mother cell gives rise to two new cells called daughter cells. This process can be modeled by two phases, proliferative phase and resting

phase. The proliferative phase is the active phase of DNA synthesis and cell division. A cell cannot stay indefinitely in the proliferative phase, it divides when it completes the process of mitosis. After cell division, daughter cells re-enter the resting phase. In contrast to the proliferation phase, cells in the resting phase may remain stable and viable indefinitely.
In lymphopenic conditions (Fig. 4.1), the progression of cells through the cell cycle involves a stochastic recruitment of cells from A-state (corresponding approximately to the G0/G1 phase of the cell cycle) into the dividing B-phase (approximately equivalent to the S, G2, and M phases of the cell cycle) [5, 7]. The B-phase has a fixed duration $\Delta$. It is assumed that a cell in B-phase has an age $\tau \in [0, \Delta]$. After completing the deterministic B-phase, a cell delivers two daughter cells into the stochastic A-state from which the cells may be recruited for another round of division. Cells in the A-state and B-phase have death rates $\delta_A$ and $\delta_B$ respectively.

To better understand the dynamics of memory T cell generation in lymphopenic conditions, we model the transition of cells from a naive (CD44 low) to a memory-like (CD44 high) phenotype as a consequence of LIP. The dynamics of this transition has been measured by the phenotypic (CD44) change on the surface of T cells. For this reason, we take into account the CD44 expression in the Smith-Martin model. We suppose that cells have an expression of CD44, $s \in [0, m]$, where $m$ is the maximum CD44 expression.

We denote by

- $A_i(t, s)$ is the number of cells at time t having undergone $i$ divisions in A-state and having an intensity $s$ of CD44 expression.
- $B_i(t, \tau, s)$ is the number of cells at time t having undergone $i$ divisions, having spent time $\tau$ in B-phase and having an intensity $s$ of CD44 expression.

Subscripts $i = 0, ..., I$ refer to division or generation number, $I$ is the maximum number of divisions that can be performed (8 - 9 with CFSE labelling) [7, 10].

**The total number of cells is given at time $t$ by**

$$N = N(t) = \sum_{i=0}^{I} \left( \int_0^m \int_0^\Delta B_i(t, \tau, s) ds \, d\tau + \int_0^m A_i(t, s) ds \right). \tag{4.1}$$

**Rate of entry into division**

Recruitment of cells from A-state into the B-phase occurs at a rate $\lambda$. As the cellular population increases, the amount of resources per cell decreases and the recruitment rate is reduced. A smaller division rate corresponds to the smaller transfer rate $\lambda$ of the model [10]. Therefore, $\lambda$ depends on the total number of cells $N = N(t)$.

**Division rate**

In the Smith-Martin model, cells are triggered from A-state to enter the proliferative B-phase. They spend some time, indexed by $\tau \in [0, \Delta]$ to divide in B-phase. A proliferative cell divides into two daughter cells only when it has completed the process of mitosis ($\Delta$ is approximately the time to finish the process). More specifically, when a cell divides, it disappears from the B-phase.
In this study, we introduce a function $\mu$ in order to remove the cells that have divided. Therefore, $\mu(\tau)$ represents the rate of cells which divided at age $\tau$ and have given rise to two daughter cells in the resting phase.

The cumulative probability that a cell is still in B-phase at time $\tau$, having not divided ($\mu$) nor been killed ($\delta_B$) until this time point, is

$$\Pi(\tau) \quad = \quad e^{-\int_0^\tau (\delta_B + \mu(a))da},$$

and the cumulative probability that a cell has divided until time point $\tau$, is

$$d(\tau) \quad = \quad 1 - e^{-\int_0^\tau \mu(a)da}.$$

**Velocity of CD44 up-regulation**

To describe the CD44 expression and its accumulation on the surface of T cells, a velocity ($v_i$) was introduced in the model which depends on the CD44 expression ($s$) and the number of divisions ($i$). This velocity is used to represent the extent of up-regulation of CD44 expression in the proliferation process. Indeed, we assume that cells are up-regulating CD44 during the proliferating phase [89]. This velocity can take into account the level of receptors that have been already presented on the surface of cells at the beginning of the phase.

**Then, the dynamics of T cells in lymphopenia conditions is given in**

**the following model**

$$\begin{cases} \dfrac{dA_0(t,s)}{dt} = -\delta_A A_0(t,s) - \lambda(N)A_0(t,s), \\ \begin{cases} for \quad i = 1,...,I \\ \dfrac{dA_i(t,s)}{dt} = 2\displaystyle\int_0^{\Delta} \mu(\tau)B_{i-1}(t,\tau,s)\ d\tau - \delta_A A_i(t,s) - \lambda(N)A_i(t,s), \end{cases} \\ \begin{cases} for \quad i = 0,...,I \\ \frac{\partial}{\partial t}B_i(t,\tau,s) + \frac{\partial}{\partial \tau}B_i(t,\tau,s) + \frac{\partial}{\partial s}[v_i(s).B_i(t,\tau,s)] = -\left(\delta_B + \mu(\tau)\right)B_i(t,\tau,s), \end{cases} \end{cases} \tag{4.2}$$

where the variables $(t,\tau,s)$ lie in $[0,T]\times[0,\Delta]\times[0,m]$.

**The boundary and initial distributions are**

$$\begin{cases} B_i(t,0,s) = \lambda(N)A_i(t,s) \quad and \quad v_i(0)B_i(t,\tau,0) = 0 \quad for \quad i = 0,...,I \\ B_i(0,\tau,s) = 0, \quad for\ i = 0,...,I \quad and \quad A_i(0,s) = 0, \quad for\ i = 1,...,I \\ A_0(0,s) = A_{0,0}(s) \geqslant 0. \end{cases} \tag{4.3}$$

We denote (4.2-4.3) by $SM_{CD44}$ model.

## 4.3 Integral formulation

In this section, one derives an integral formulation of the solution of System (4.2-4.3).

By using the Lagrange method, one obtains implicit solutions of the ordinary differential equations that are in System (4.2-4.3)

$$\begin{aligned} A_0(t,s) &= A_{0,0}(s)\ e^{-\int_0^t(\delta_A+\lambda(N(u)))du}, \\ A_i(t,s) &= 2\int_0^t\int_0^{\Delta} e^{-\int_r^t(\delta_A+\lambda(N(q)))dq}\mu(\tau)B_{i-1}(r,\tau,s)d\tau\ dr, \quad i = 1,...,I. \end{aligned} \tag{4.4}$$

In addition, consider the following ordinary differential equations

$$\begin{cases} \frac{ds_i^1(t)}{dt} = v_i(s_i^1(t)) \\ \\ s_i^1(t_0) = s_{i,0}^1 \geqslant 0, \end{cases} \qquad \begin{cases} \frac{ds_i^2(\tau)}{d\tau} = v_i(s_i^2(\tau)) \\ \\ s_i^2(\tau_0) = s_{i,0}^2 \geqslant 0. \end{cases} \tag{4.5}$$

$s_i^1(t; t_0; s_i^1(t_0))$ and $s_i^2(\tau; \tau_0; s_i^2(\tau_0))$ are the curves which go through $(t_0, s_i^1(t_0))$ and $(\tau_0, s_i^2(\tau_0))$ respectively. The curves, $Z_i^1(t) := s_i^1(t; 0; 0)$ and $Z_i^2(\tau) := s_i^2(\tau; 0; 0)$ are the characteristic through the origin. The solutions of (4.5) are given by the following equations

$$s_i^1(t) = s_i^1(t_0) + \int_{t_0}^{t} v_i(s_i^1(z))dz, \quad s_i^2(\tau) = s_i^2(\tau_0) + \int_{\tau_0}^{\tau} v_i(s_i^2(r))dr.$$

*Assumption* 4.3.1.

- Natural mortalities rates $\delta_A$ and $\delta_B$ are non-negative constants.

- Function $\mu(.)$ is bounded, non-negative and satisfies the following inequality

$$0 \leq \underline{\mu} \leq \mu(\tau) \leq \bar{\mu}, \quad \forall\ \tau \in [0, \Delta].$$

- Function $\lambda(N)$ is non-negative, bounded and Lipschitz continuous with constant $k$

$$|\lambda(N) - \lambda(N^*)| \leqslant k|N - N^*|, \qquad N \geqslant 0, \quad N^* \geqslant 0.$$

- Function $v_i$ is bounded, non-negative for all $i \in \mathbb{N}_I := \{0, ..., I\}$, satisfies the condition

$$v_i(0) = 0, \quad and \quad 0 < \underline{v_i} \leq v_i(s) \leq \bar{v_i}, \ \forall s \in ]0, m],$$

and continuously differentiable with respect to the variable $s$. In addition, there exists a positive constant $d_{v_i}$, $\forall\ i \in \mathbb{N}_I$, such that

$$|\frac{\partial v_i}{\partial s}| \leqslant d_{v_i}, \quad \forall \ \ s \in [0, m].$$

- Initial condition $A_{0,0}(.)$ is non-negative and belongs to $L_+^1((0, m))$.

Let Assumption 4.3.1 be satisfied. By using the method of characteristics, one has:

1-) Let $u_i(t) := B_i(t, t+c, s_i^1(t))$, where $c \geqslant 0$. Using the PDEs in System (4.2-4.3), one obtains

$$\frac{du_i(t)}{dt} = -\left[\delta_B + \mu(t+c) + \frac{\partial v_i(s_i^1(t))}{\partial s_i^1(t)}\right] u_i(t).$$

Using $u_i(0) = B_i(0, c, s_i^1(0)) = 0$, then $B_i(t, \tau, s) = 0$ for all $t \leq \tau$ and $Z_i^1(t) < s$.

2-) Let $w_i(\tau) := B_i(\tau + c, \tau, s_i^2(\tau))$, where $c \geqslant 0$. Using the PDEs in System (4.2-4.3), one obtains

$$\frac{dw_i}{d\tau} = -\left[\delta_B + \mu(\tau) + \frac{\partial v_i(s_i^2(\tau))}{\partial s_i^2(\tau)}\right] w_i(\tau),$$

which implies $B_i(\tau + c, \tau, s_i^2(\tau)) = B_i(c, 0, s_i^2(0))\, e^{-\int_0^\tau (\delta_B + \mu(r))dr}\, e^{-\int_0^\tau \frac{\partial v_i(s_i^2(r))}{\partial s_i^2(r)} dr}$. Performing the change of variable $\sigma = s_i^2(r)$, one gets

$$\begin{aligned} B_i(\tau + c, \tau, s_i^2(\tau)) &= B_i(c, 0, s_i^2(0))\, e^{-\int_0^\tau (\delta_B + \mu(r))dr}\, e^{-\int_{s_i^2(0)}^{s_i^2(\tau)} \frac{\partial v_i(\sigma)}{\partial \sigma} \frac{1}{v_i(\sigma)} d\sigma} \\ &= \frac{B_i(c, 0, s_i^2(0))\, v_i(s_i^2(0))}{v_i(s_i^2(\tau))}\, e^{-\int_0^\tau (\delta_B + \mu(r))dr}. \end{aligned}$$

For $t := \tau + c$ and $s := s_i^2(\tau)$, one obtains

$$B_i(t, \tau, s) = \frac{\lambda(N(t-\tau)) A_i(t-\tau, \zeta_i)\, v_i(\zeta_i)}{v_i(s)}\, e^{-\int_0^\tau (\delta_B + \mu(r))dr}, \quad \forall\ 0 \leq \tau < t,\ Z_i^2(\tau) < s$$

where $\zeta_i := s_i^2(0) = s - Z_i^2(\tau)$.

3-) Let $\varpi_i(s) := B_i(t(s), \tau(s), s)$, where $t(s)$ and $\tau(s)$ are the inverse functions of $s_i^1(t)$ and $s_i^2(\tau)$ respectively. Using the PDEs in System (4.2-4.3), one obtains

$$B_i(t, \tau, s) = 0, \quad \forall\ s \leq Z_i^1(t),\ s \leq Z_i^2(\tau).$$

Then, the integral formulation of $B_i$, $\forall\ i = 0, ..., I$, is

$$B_i(t,\tau,s) = \begin{cases} 0 & t \leq \tau,\ Z_i^1(t) < s \\ \frac{\lambda(N(t-\tau))A_i(t-\tau,\zeta_i)\,v_i(\zeta_i)}{v_i(s)}\, f(\tau) & 0 \leq \tau < t,\ Z_i^2(\tau) < s \\ 0 & s \leq Z_i^1(t),\ s \leq Z_i^2(\tau) \end{cases} \tag{4.6}$$

where $\zeta_i = s - Z_i^2(\tau)$ and $f(\tau) := e^{-\int_0^\tau (\delta_B + \mu(r))dr}$.

Assuming that the solution $(A_i(t,.), B_i(t,.,.))$ of System (4.4-4.6) belongs to $L^1(0,m)\times L^1((0,\Delta),(0,m))$ for all $t > 0$.

**Definition 4.1.** Let $T > 0$ and $i \in \mathbb{N}_I := \{0, ..., I\}$, the norms of $A_i$ and $B_i$ in the Banach spaces,

$$\begin{aligned} H_T^1 &:= L^\infty((0,T); L^1(0,m)) \\ L_T^1 &:= L^\infty((0,T); L^1((0,\Delta),(0,m))) \end{aligned}$$

are defined respectively by

$$\begin{aligned} \|A_i\|_{H_T^1} &= \sup_{0\leqslant t\leqslant T} \|A_i(t,.)\|_{L^1(0,m)}, \\ \|B_i\|_{L_T^1} &= \sup_{0\leqslant t\leqslant T} \|B_i(t,.,.)\|_{L^1((0,\Delta),(0,m))}. \end{aligned}$$

**Definition 4.2.** For all $T > 0$. $(A_i, B_i)$, $\forall\ i \in \mathbb{N}_I := \{0, ..., I\}$ is called a global solution of (4.2-4.3) (in the sense of the expressions (4.4)-(4.6)), if it belongs to $L^\infty(0,T,L^1(0,m))$ and $L^\infty(0,T,L^1((0,\Delta)\times(0,m)))$ respectively and it satisfies System (4.4)-(4.6).

**Theorem 4.3.** *Let Assumption 4.3.1 be satisfied. Then, there exists a unique solution of System (4.4)-(4.6) for all $t \in (0,\infty)$.*

*Proof.* The existence of global solution of System (4.4)-(4.6) is deduced from the general result in Part IV - Chapter 10. □

*Remark* 4.4. Using (4.4), (4.6) and Assumption 4.3.1, one may check by induction over $i$ the positivity of $(A_i, B_i)$ for all $i \in \mathbb{N}_I$.

# Chapter 5

# Numerical analysis of the $SM_{CD44}$ model

## 5.1 Introduction

In this chapter, we build a numerical scheme to approximate the solution of $SM_{CD44}$ model. Furthermore, an analysis of properties of the scheme is proposed.

In the literature, the numerical schemes of the structured models are constructed from the equations or the solution calculated by the characteristic method. Douglas and Milner [90] have developed a finite difference scheme (FD) of the equation of McKendrick-Von Forster, with a mortality function that depends on the total population. Know et al. [91] have improved this scheme to a second order accuracy. Later on, Sulky [92] has applied this approximation method to the model of Sinko and Streifer [93]. The non-linear structured models of the populations dynamics have been studied by Angulo et al. [94, 95] and Kostova [96] for example. The accuracy of these schemes has order 2 for Angulo et al. [94, 95] and 3 for Kostova [96].
In this chapter, we provide a finite difference method to approximate the equations of our $SM_{CD44}$ model. This method is used widely in case of hyperbolic equations, such as the PDEs that constitute our model. The proofs of stability, consistency and convergence of scheme to an analytical solution of the model, are established in this chapter.

## 5.2 Numerical approximation scheme

In this section, we build an approximate solution of System (4.2-4.3). To establish our scheme, we define a mesh in $[0,T]\times[0,\Delta]\times[0,m]$. Let $\Delta t$, $\Delta\tau$ and $\Delta s$ be the time, age and CD44 expression mesh sizes respectively. We subdivide the intervals $[0,T]$, $[0,\Delta]$ and $[0,m]$ in $N_T+1$ points $t^n$, $N_\tau+1$ points $\tau^j$ and $N_s+1$ points $s^k$ respectively. Such that for $n=0$, $j=0$, $k=0$ one has $t^0=0$, $\tau^0=0$, $s^0=0$ and for $n=N_T$, $j=N_\tau$, $k=N_s$ one has $t^{N_T}=T$, $\tau^{N_\tau}=\Delta$, $s^{N_s}=m$. The grid points are defined by

$$\begin{aligned} t^n &= n\Delta t, \quad n=0,...,N_T,\\ \tau^j &= j\Delta\tau, \quad j=0,...,N_\tau,\\ s^k &= k\Delta s, \quad k=0,...,N_s. \end{aligned}$$

We introduce the following approximations for all $i\in\mathbb{N}_I:=\{0,...,I\}$, $0\leqslant n\leqslant N_T$, $0\leqslant j\leqslant N_\tau$ and $0\leqslant k\leqslant N_s$

$$A_k^{i,n}=A_i(t^n,s^k),\ B_{j,k}^{i,n}=B_i(t^n,\tau^j,s^k),\ \mu^j=\mu(\tau^j),\ \lambda^n=\lambda(N(t^n)).$$

Let $v_{N_s}=(v_{0,N_s},...,v_{I,N_s})$ be the approximate function $v=(v_0,...,v_I)$. It belongs to the space $K_{N_s}=(C_+^{\bar u,N_s})^I$ where

$$C_+^{\bar u,N_s}=\{u(s^k)=u^k,\quad u^0=0,\quad 0<u^k\leqslant\bar u,\quad k=1,..,N_s\}.$$

The equations of System (4.2-4.3) are approximated by

$$\begin{cases} B_{j+1,k}^{i,n+1}=\dfrac{(1-\frac{\Delta t}{\Delta s}v_i^k)B_{j,k}^{i,n}+\frac{\Delta t}{\Delta s}v_i^{k-1}B_{j,k-1}^{i,n}}{1+\Delta t\delta_B+\Delta t\mu^j}, \quad k=1,...,N_s,\quad i=0,...,I,\\ v_i^0B_{j,0}^{i,n}=0,\\ B_{0,k}^{i,n+1}=\lambda^nA_k^{i,n}. \end{cases} \tag{5.1}$$

$$\begin{cases} A_k^{0,n+1}=\dfrac{A_k^{0,n}}{1+\Delta t\delta_A+\Delta t\lambda^n},\\ A_k^{i,n+1}=\dfrac{A_k^{i,n}+2\Delta t\Delta\tau\sum_j\mu^jB_{j,k}^{i-1,n}}{1+\Delta t\delta_A+\Delta t\lambda^n}, \quad i=1,...,I. \end{cases} \tag{5.2}$$

for $n$ from 0 to $N_T - 1$ and $j$ from 0 to $N_\tau - 1$.
The CFL condition is

$$0 < \frac{\Delta t}{\Delta s}\|v_{i,N_s}\|_\infty \leqslant 1 \quad for \;\; i = 0, ..., I. \tag{5.3}$$

The initial condition $A_{0,0}$ is approximated by its mean value on each mesh $k$, for all $k = 1, ..., N_s$.

$$A^k_{0,0} = \int_{s_{k-1}}^{s_k} A_{0,0}(s)ds. \tag{5.4}$$

For all $n = 0, ..., N_T - 1$, $j = 0, ..., N_\tau - 1$ and $i = 0, ..., I$ fixed, the first equation of System (5.1) can be written in the following matrix form

$$\begin{pmatrix} B^{i,n+1}_{j+1,1} \\ : \\ : \\ : \\ : \\ B^{i,n+1}_{j+1,N_s} \end{pmatrix} = \begin{pmatrix} \frac{(1-\frac{\Delta t}{\Delta s}v_i^1)}{1+\Delta t\delta_B+\mu^j} & 0 & \dots & 0 \\ \frac{\frac{\Delta t}{\Delta s}v_i^1}{1+\Delta t\delta_B+\mu^j} & \frac{(1-\frac{\Delta t}{\Delta s}v_i^2)}{1+\Delta t\delta_B+\mu^j} & \dots & 0 \\ \vdots & & \ddots & 0 \\ 0 & ..... & \frac{\frac{\Delta t}{\Delta s}v_i^{N_s-1}}{1+\Delta t\delta_B+\mu^j} & \frac{(1-\frac{\Delta t}{\Delta s}v_i^{N_s})}{1+\Delta t\delta_B+\mu^j} \end{pmatrix} \begin{pmatrix} B^{i,n}_{j,1} \\ : \\ : \\ : \\ : \\ B^{i,n}_{j,N_s} \end{pmatrix}$$

where the above matrix is defined positive under condition (5.3).

## 5.3 Numerical analysis of scheme

In this section, we study the positivity and the stability of our scheme. These proprieties will be used to proof the convergence of the discrete solution of our scheme to the continuous solution of $SM_{CD44}$ model.

Let us define the following discrete norms

$$\|B^{i,n}\|_1 = \sum_{j=0}^{N_\tau}\sum_{k=1}^{N_s}|B^{i,n}_{j,k}|, \qquad \|A^{i,n}\|_1 = \sum_{k=1}^{N_s}|A^{i,n}_k|,$$
$$\|B^{i,n}\|_\infty = \sup_{0\leqslant j\leqslant N_\tau}\sup_{1\leqslant k\leqslant N_s}|B^{i,n}_{j,k}|, \qquad \|A^{i,n}\|_\infty = \sup_{1\leqslant k\leqslant N_s}|A^{i,n}_k|,$$

and for all $i \in \mathbb{N}_I$, $n \geqslant 0$, $j \geqslant 0$

$$B^{i,n}_j \in BV([0,m]) \Leftrightarrow \sum_{k=0}^{N_s-1}|B^{i,n}_{j,k+1} - B^{i,n}_{j,k}| \leqslant c, \quad c > 0.$$

In what follows, we will make use the following assumption.

*Assumption* 5.3.1.
- $0 < \|A_{0,0}\|_\infty, \|A_{0,0}\|_1 < \infty, \;\; A_{0,0} \in BV([0,m])$.
- Parameter $\mu^j$, for all $j = 0, ..., N_\tau$, is bounded, non-negative and satisfies the following inequality

$$0 \leq \underline{\mu} \leq \mu^j \leqslant \bar{\mu}.$$

- Parameter $\lambda^n := \lambda(N^n)$, for all $n = 0, ..., N_T$, is non-negative, bounded and satisfies the following inequality

$$0 < \lambda^n \leqslant \lambda_0.$$

- Parameter $v_i^k$, for all $i \in \mathbb{N}_I$ and $k = 1, ..., N_s$ belongs to $C_+^{\bar{u},N_s}$ such that $0 \leq \|v_{i,N_s}\|_\infty \leq \tilde{v}_i$ and $\frac{|v_i^{k+1} - v_i^k|}{\Delta s} \leq v_i^\infty$ for all $k = 0, .., N_s - 1$.

The following lemma is devoted to proof the positivity.

**Lemma 5.1.** *Let Assumption 5.3.1 be satisfied. The numerical scheme (5.1 - 5.2) preserves the positivity of the solution under condition (5.3). For all $i \in \mathbb{N}_I$, $n = 0, ..., N_T$ , $j = 0, ..., N_\tau$ and $k = 1, ..., N_s$, one has*

$$(A_k^{i,n}, B_{j,k}^{i,n}) \geqslant 0 \Longrightarrow (A_k^{i,n+1}, B_{j+1,k}^{i,n+1}) \geqslant 0.$$

*Proof.* Let $(A_k^{i,n+1}, B_{j+1,k}^{i,n+1})$ be the numerical solution of (5.1 - 5.2). The absolute value of this solution, is equal to

$$|B_{j+1,k}^{i,n+1}| \;\; = \;\; |\frac{(1 - \frac{\Delta t}{\Delta s} v_i^k) B_{j,k}^{i,n} + \frac{\Delta t}{\Delta s} v_i^{k-1} B_{j,k-1}^{i,n}}{1 + \Delta t \delta_B + \Delta t \mu^j}|, \tag{5.5}$$

$$|A_k^{0,n+1}| = |\frac{A_k^{0,n}}{1 + \Delta t \delta_A + \Delta t \lambda^n}| \;\; and \;\; |A_k^{i,n+1}| = |\frac{A_k^{i,n} + 2\Delta t \Delta\tau \sum_j \mu^j B_{j,k}^{i-1,n}}{1 + \Delta t \delta_A + \Delta t \lambda^n}|. \tag{5.6}$$

Under Assumption 5.3.1 , the denominator of (5.5) is strictly positive. Using condition (5.3), one obtains

$$0 < \frac{\Delta t}{\Delta s} v_i^k \leqslant 1 \quad for \;\; i \in \mathbb{N}_I \;\; and \;\; k = 1, ..., N_s.$$

Then, one deduces the positivity of the numerator of equation (5.5). Therefore, by induction over $i$, one concludes the positivity of $(A^i, B^i)$ for all $i \in \mathbb{N}_I$. □

In what follows, we shall use the following convention

$$\sum_{j}^{i} = 0 \quad , \quad \prod_{j}^{i} = 1 \quad and \quad B^{i-j} = 0 \qquad if\, j > i.$$

**Lemma 5.2.** *Let Assumption 5.3.1 be satisfied. Under condition (5.3), the numerical scheme (5.1 - 5.2) is stable with respect to the discrete norm $L^1$. Furthermore, for all $i \in \mathbb{N}_I$ and $n = 0, ..., N_T$, one has*

$$\|B^{i,n}\|_1 \leqslant M_1^i \|A_{0,0}\|_1, \qquad \|A^{i,n}\|_1 \leqslant N_1^i \|A_{0,0}\|_1,$$

*where $M_1^i$ and $N_1^i$ are positive constants.*

*Proof.* The numerical solution of (5.1 - 5.2) can be written as following $\forall\ i \in \mathbb{N}_I$

$$B_{j+1,k}^{i,n+1} = B_{j,k}^{i,n} - \frac{\Delta t}{\Delta s}(v_i^k B_{j,k}^{i,n} - v_i^{k-1} B_{j,k-1}^{i,n}) - (\Delta t \delta_A + \Delta t \mu^j) B_{j+1,k}^{i,n+1}, \tag{5.7}$$

and,

$$\begin{aligned} A_k^{0,n+1} &= A_k^{0,n} - (\Delta t \delta_B + \Delta t \lambda^n) A_k^{0,n+1}, \\ A_k^{i,n+1} &= A_k^{i,n} + 2\Delta t \Delta \tau \sum_{j=1}^{N_\tau} \mu^j B_{j,k}^{i-1,n} - (\Delta t \delta_B + \Delta t \lambda^n) A_k^{i,n+1} \quad \forall\ i \in \mathbb{N}_I^*. \end{aligned} \tag{5.8}$$

Using Lemma 5.1, taking the absolute value of equation (5.7) and then summing over all mesh $(j, k)$, one deduces

$$\begin{aligned} \sum_{j=0}^{N_\tau - 1} \sum_{k=1}^{N_s} |B_{j+1,k}^{i,n+1}| &= \sum_{j=1}^{N_\tau} \sum_{k=1}^{N_s} B_{j,k}^{i,n} - \frac{\Delta t}{\Delta s} \sum_{j=0}^{N_\tau} \sum_{k=1}^{N_s} (v_i^k B_{j,k}^{i,n} - v_i^{k-1} B_{j,k-1}^{i,n}) \\ &\quad - \sum_{j=0}^{N_\tau - 1} \sum_{k=1}^{N_s} (\Delta t \delta_A + \Delta t \mu^j) B_{j+1,k}^{i,n+1}. \end{aligned}$$

The boundary condition in (5.1) can used to reduce the second term of the above equation. It becomes $\left(-\frac{\Delta t}{\Delta s} \sum_{j=0}^{N_\tau} v_i^{N_s} B_{j,N_s}^{i,n}\right)$, then it can be bounded by 0. By induction over $j$ and from Assumption 5.3.1, one has

$$\sum_{j=0}^{N_\tau - 1} \sum_{k=1}^{N_s} |B_{j+1,k}^{i,n+1}| \leqslant \sum_{k=1}^{N_s} B_{0,k}^{i,n-N_\tau} \leqslant \lambda_0 \sum_{k=1}^{N_s} A_k^{i,n-N_\tau}.$$

By taking the absolute value of equations (5.8) and then summing over all mesh $k$, one obtains

$$\begin{aligned}\sum_{k=1}^{N_s}|A_k^{0,n+1}| &\leqslant \sum_{k=1}^{N_s}|A_k^{0,n}| \\ \sum_{k=1}^{N_s}|A_k^{i,n+1}| &\leqslant \sum_{k=1}^{N_s}|A_k^{i,n}| + 2\Delta t\Delta\tau\bar{\mu}\sum_{j=0}^{N_\tau}\sum_{k=1}^{N_s}B_{j,k}^{i-1,n} \quad for \quad i\in\mathbb{N}_I^*\end{aligned}$$

Finally, by induction over $i$ and $n$, one deduces

$$\|A^{i,n}\|_1 \leqslant 2^i\lambda_0^i\bar{\mu}^i\Delta\tau^iT^i\|A_{0,0}\|_1 \quad and \quad \|B^{i,n}\|_1 \leqslant 2^i\lambda_0^{i+1}\bar{\mu}^i\Delta\tau^iT^i\|A_{0,0}\|_1.$$

Therefore, the numerical scheme is stable with respect to the discrete norm $L^1$ where $\forall\ i\in\mathbb{N}_I$

$$M_1^i = 2^i\lambda_0^{i+1}\bar{\mu}^iT^i \quad and \quad N_1^i = 2^i\lambda_0^i\bar{\mu}^iT^i.$$

This ends the proof of Lemma 5.2. □

**Lemma 5.3.** *Let Assumption 5.3.1 be satisfied. Under condition (5.3), the numerical scheme (5.1 - 5.2) is stable with respect to the discrete norm $L^\infty$. Furthermore, for all $i\in\mathbb{N}_I$ and $n=0,...,N_T$, one has*

$$\|B^{i,n}\|_\infty \leqslant M_2^i\|A_{0,0}\|_\infty, \qquad \|A^{i,n}\|_\infty \leqslant N_2^i\|A_{0,0}\|_\infty,$$

*where $M_2^i$ and $N_2^i$ are positive constants.*

*Proof.* By using Lemme 5.1 and Assumption 5.3.1, the upper bound of equation (5.7) over all meshes $j$ and $k$, can be estimated by

$$\sup_{k,j}|B_{j+1,k}^{i,n+1}| \leqslant (1+\frac{\Delta t}{\Delta s}\|v_{i,N_s}\|_\infty)\sup_{k,j}|B_{j,k}^{i,n}|.$$

By induction over $j$, one obtains

$$\sup_{k,j}|B_{j+1,k}^{i,n+1}| \leqslant \lambda_0(1+\frac{\Delta t}{\Delta s}\|v_{i,N_s}\|_\infty)^{N_\tau+1}\sup_{k}|A_k^{i,n-N_\tau}|. \tag{5.9}$$

From Lemma 5.1, the induction over $n$ allows to estimate the equations (5.8) by

$$\begin{aligned} |A_k^{0,n}| &\leqslant |A_{0,0}^k| \\ |A_k^{i,n+1}| &\leqslant 2\Delta t\Delta\tau\bar{\mu}\sum_{m=0}^{n-1}\sum_{j=0}^{N_\tau} B_{j,k}^{i-1,n-m}, \quad \forall\ i \in \mathbb{N}_I^* \end{aligned} \tag{5.10}$$

Finally by induction over $i$, the inequalities (5.9) and (5.10) are estimated by

$$\begin{aligned} \|B^{i,n}\|_\infty &\leqslant (2T\Delta)^i\lambda_0^{i+1}\prod_{l=0}^{i}(1+\frac{\Delta t}{\Delta s}\|v_l\|_\infty)^{N_\tau+1}\|A_{0,0}\|_\infty, \\ \|A^{i,n}\|_\infty &\leqslant (2T\Delta\lambda_0)^i\prod_{l=0}^{i-1}(1+\frac{\Delta t}{\Delta s}\|v_l\|_\infty)^{N_\tau+1}\|A_{0,0}\|_\infty, \end{aligned}$$

for all $i \in \mathbb{N}_I$ and $n = 0, ..., N_T$.
Then, one has $\forall\ i \in \mathbb{N}_I$

$$\begin{aligned} M_2^i &= (2T\Delta)^i\lambda_0^{i+1}\prod_{l=0}^{i}(1+\frac{\|v_l\|_\infty}{\|v_{i,N_s}\|_\infty})^{N_\tau+1}, \\ N_2^i &= (2T\Delta\lambda_0)^i\prod_{l=0}^{i-1}(1+\frac{\|v_l\|_\infty}{\|v_{i,N_s}\|_\infty})^{N_\tau+1}. \end{aligned}$$

This ends the proof of Lemma 5.3. □

These two lemmas 5.2 and 5.3 ensure that the scheme does not explode even in large time. Now, we give a lemma that will be used to prove the convergence of the solution of System (5.1 - 5.2) to the solution of System (4.2 - 4.3).

**Lemma 5.4.** *Let Assumption 5.3.1 be satisfied. Under condition (5.3), one has for all $n > 0$ and $j > 0$,*

$$\max_{i\in\mathbb{N}_I}\left(\sum_{k=0}^{N_s-1}|B_{j,k+1}^{i,n}-B_{j,k}^{i,n}|\right) \leqslant \alpha\left(\sum_{k=0}^{N_s-1}|A_{0,0}^{k+1}-A_{0,0}^k|\right)+\beta\|A_{0,0}\|_1,$$

*where $\alpha$ and $\beta$ are positive constants which are independent on $n$.*

*Proof.* For all $i \in \mathbb{N}_I$, one considers the solution of the numerical scheme (5.2) in the following form

$$A_k^{i,n+1} = A_k^{i,n} + 2\Delta t\Delta\tau\sum_{j=0}^{N_\tau}\mu^j B_{j,k}^{i-1,n} - E_n A_k^{i,n+1}, \tag{5.11}$$

where $E_n = \delta_B + \lambda^n$.
Let calculate the difference of the previous solutions (5.11) between two consecutive meshes $k$ and $k+1$ by fixing $i$, $n+1$ and $j+1$,

$$\gamma_{k+1}^{i,n+1} = \gamma_{k+1}^{i,n} + 2\Delta t\Delta\tau \sum_{j=0}^{N_\tau} \mu^j \left(B_{j,k+1}^{i-1,n} - B_{j,k}^{i-1,n}\right) - E_n \gamma_{k+1}^{i,n+1},$$

where $|\gamma_{k+1}^{i,n+1}| := |A_{k+1}^{i,n+1} - A_k^{i,n+1}|$.

By multiplying each term of the above equation by $\bar{\varsigma}_k^{i,n+1}$ which is the sign of $\gamma_k^{i,n+1}$, one obtains

$$|\gamma_{k+1}^{i,n+1}| \leqslant |\gamma_{k+1}^{i,n}| + 2\Delta t\Delta\tau \sum_{j=0}^{N_\tau} \mu^j |B_{j,k+1}^{i-1,n} - B_{j,k}^{i-1,n}|. \tag{5.12}$$

Now, one considers the solution of the numerical scheme (5.1) in the following form

$$B_{j+1,k}^{i,n+1} = B_{j,k}^{i,n} - \frac{\Delta t}{\Delta s}(v_i^k B_{j,k}^{i,n} - v_i^{k-1} B_{j,k-1}^{i,n}) - \Delta t h_j B_{j+1,k}^{i,n+1}, \tag{5.13}$$

where $h_j := \delta_B + \mu^j$.
Next, one calculates the difference of the previous solutions between two consecutive meshes $k$ and $k+1$ by fixing $i$, $n+1$ and $j+1$

$$\begin{aligned} B_{j+1,k+1}^{i,n+1} - B_{j+1,k}^{i,n+1} &= (B_{j,k+1}^{i,n} - B_{j,k+1}^{i,n}) - \frac{\Delta t}{\Delta s}(v_i^{k+1} B_{j,k+1}^{i,n} - v_i^k B_{j,k}^{i,n}) \\ &\quad + \frac{\Delta t}{\Delta s}(v_i^k B_{j,k}^{i,n} - v_i^{k-1} B_{j,k-1}^{i,n}) - \Delta t h_j (B_{j+1,k+1}^{i,n+1} - B_{j+1,k}^{i,n+1}). \end{aligned}$$

One notes $\delta_{j+1,k+1}^{i,n+1} := B_{j+1,k+1}^{i,n+1} - B_{j+1,k}^{i,n+1}$. The above equation becomes

$$\begin{aligned} \delta_{j+1,k+1}^{i,n+1} &= \delta_{j,k+1}^{i,n} - \frac{\Delta t}{\Delta s} v_i^{k+1} \delta_{j,k+1}^{i,n} + \frac{\Delta t}{\Delta s} v_i^k \delta_{j,k}^{i,n} - \frac{\Delta t}{\Delta s}(v_i^{k+1} - v_i^k)\delta_{j,k+1}^{i,n} \\ &- \frac{\Delta t}{\Delta s}(v_i^{k+1} - 2v_i^k + v_i^{k-1}) B_{j,k-1}^{i,n} - \Delta t h_j \delta_{j+1,k+1}^{i,n+1}. \end{aligned}$$

One multiplies each term of the above equation by $\varsigma_{j+1,k}^{i,n+1}$ which is the sign of $\delta_{j+1,k}^{i,n+1}$, and then one sums with respect to $k = 1, ..., N_s - 1$

$$\begin{aligned}\sum_{k=1}^{N_s-1} \varsigma_{j+1,k}^{i,n+1}\delta_{j+1,k+1}^{i,n+1} &= \sum_{k=1}^{N_s-1} \varsigma_{j,k+1}^{i,n}\delta_{j,k+1}^{i,n} - \frac{\Delta t}{\Delta s}\sum_{k=1}^{N_s-1} v_i^{k+1}\varsigma_{j,k+1}^{i,n}\delta_{j,k+1}^{i,n} + \frac{\Delta t}{\Delta s}\sum_{k=1}^{N_s-1} v_i^{k}\varsigma_{j,k}^{i,n}\delta_{j,k}^{i,n} \\ &+ \frac{\Delta t}{\Delta s}\sum_{k=1}^{N_s-1} |v_i^{k+1} - v_i^k|\varsigma_{j,k}^{i,n}\delta_{j,k}^{i,n} + \frac{\Delta t}{\Delta s}\sum_{k=1}^{N_s-1} |v_i^{k+1} - 2v_i^k + v_i^{k-1}|B_{j,k-1}^{i,n} \\ &- \Delta t\sum_{k=1}^{N_s-1} h_j\varsigma_{j+1,k+1}^{i,n+1}\delta_{j+1,k+1}^{i,n+1}.\end{aligned}$$

By adding the second and the third term and using Assumption 5.3.1, one gets

$$\begin{aligned}\sum_{k=1}^{N_s-1} \varsigma_{j+1,k}^{i,n+1}\delta_{j+1,k+1}^{i,n+1} &\leqslant \sum_{k=1}^{N_s-1} \varsigma_{j,k+1}^{i,n}\delta_{j,k+1}^{i,n} - \frac{\Delta t}{\Delta s}v_i^{N_s}\varsigma_{j,N_s}^{i,n}\delta_{j,N_s}^{i,n} + \frac{\Delta t}{\Delta s}v_i^1\varsigma_{j,1}^{i,n}\delta_{j,1}^{i,n} \\ &+ \Delta t v_i^\infty\sum_{k=1}^{N_s-1} \varsigma_{j,k}^{i,n}\delta_{j,k}^{i,n} + \Delta t\epsilon_i\|B^{i,n}\|_1,\end{aligned}$$

where $\epsilon_i$ is given by

$$|v_i^{k+1} - 2v_i^k + v_i^{k-1}| \leqslant \epsilon_i\Delta s.$$

The second term of the previous inequality can be estimated by 0. Since $v_i^0 = 0$, the third term is estimated by

$$\frac{\Delta t}{\Delta s}v_i^1\varsigma_{j,1}^{i,n}\delta_{j,1}^{i,n} \leq \Delta t\frac{(v_i^1 - v_i^0)}{\Delta s}\varsigma_{j,1}^{i,n}\delta_{j,1}^{i,n} \leq \Delta t v_i^\infty\sum_{k=1}^{N_s-1} \varsigma_{j,k}^{i,n}\delta_{j,k}^{i,n}.$$

By definition, one has

$$\sum_{k=1}^{N_s-1} \varsigma_{j+1,k+1}^{i,n+1}\delta_{j+1,k+1}^{i,n+1} = \sum_{k=1}^{N_s-1} |\delta_{j+1,k+1}^{i,n+1}|.$$

Then using the boundary conditions of (5.1), one obtains an estimation of the bounded variation

$$\begin{aligned}\sum_{k=0}^{N_s-1} |\delta_{j+1,k+1}^{i,n+1}| &\leqslant \sum_{k=1}^{N_s-1} |\delta_{j,k+1}^{i,n}| + (1 + 2\Delta t v_i^\infty)\sum_{k=1}^{N_s-1} |\delta_{j,k}^{i,n}| \\ &+ \Delta t\epsilon_i\|B^{i,n}\|_1,\end{aligned}$$

We assume the following notations

$$\begin{aligned} F_j^{i,n} &= \sum_{k=0}^{N_s-1} \delta_{j,k}^{i,n},\ G^{i,n} = \sum_{k=0}^{N_s-1} \gamma_k^{i,n},\ F_j^n = \max_i BV\ F_j^{i,n},\ G^n = \max_i BV\ G^{i,n}, \\ \bar{v} &= \max_i v_i^\infty,\ \epsilon = \max_i \epsilon_i,\ u = 2(1+\Delta t\bar{v}),\ q = \Delta t\epsilon \max_i \|B^{i,n}\|_1. \end{aligned}$$

Then, the above inequality becomes

$$\max_{0\leqslant i\leqslant I} F_{j+1}^{i,n+1} \leqslant u \max_{0\leqslant i\leqslant I} F_j^{i,n} + q.$$

By induction over $n$ and $j$, one obtains

$$\max_{0\leqslant i\leqslant I} F_{j+1}^{i,n+1} \leqslant u^{N_\tau+1}\lambda_0 \max_{0\leqslant i\leqslant I} G^{i,n-N_\tau} + q\sum_{p=0}^{N_\tau} u^p. \tag{5.14}$$

Using (5.12), the above inequality becomes

$$\begin{aligned} \max_{0\leqslant i\leqslant I} F_{j+1}^{i,n+1} &\leqslant ru^{N_\tau+1} \max_{1\leqslant i\leqslant I} \sum_{m_1=N_\tau}^{N_T}\sum_{j=1}^{N_\tau} F_j^{i-1,n-m_1} + q\sum_{p=0}^{N_\tau} u^p \\ &\leqslant ru^{N_\tau+1} \max_{1\leqslant i\leqslant I} \sum_{l_1=1}^{N_T}\sum_{m_1=N_\tau}^{N_T} (u^l F_0^{i-1,n-m_1-l_1} + q\sum_{p=0}^{l_1-1} u^p) + q\sum_{p=0}^{N_\tau} u^p \\ &\leqslant ru^{N_\tau+1} \max_{1\leqslant i\leqslant I} \sum_{l_1=1}^{N_T}\sum_{m_1=N_\tau}^{N_T} (u^l F_0^{i-1,n-m_1-l_1}) + rN_Tqu^{N_\tau+1}\sum_{l_1=1}^{N_T}\sum_{p=0}^{l_1-1} u^p + q\sum_{p=0}^{N_\tau} u^p \end{aligned}$$

where $r = 2\Delta t\Delta\tau\bar{\mu}\lambda_0$.

Using the boundary condition of System (5.1) and inequality (5.12), the backward induction over $i$, allows to estimate the above inequality in terms of $i = 0$. Elementary but lengthy calculus yields

$$F_{j+1}^{n+1} \leqslant \alpha G^0 + \beta \max_i \|B^{i,n}\|_1,$$

where

$$\begin{aligned} \alpha &= (2\bar{\mu})^I \lambda_0^{I+1} u^{N_\tau+1} \sum_{l_1,\ldots,l_I} u^{\sum_{i=1}^I l_i}, \\ \beta &= Eu^{N_\tau+1} \sum_{i=1}^{I} \left[ (2\bar{\mu}\lambda_0 T)^i \sum_{l_1,\ldots,l_I}\sum_{p=0}^{l_i-1} u^{p+\sum_{j=1}^{i-1} l_j} \right] + E\sum_{p=0}^{N_\tau} u^p, \end{aligned} \tag{5.15}$$

and $l_i$ from 1 to $N_T$.
Then from Lemma 5.2, one deduces

$$F_{j+1}^{n+1} \leqslant \alpha G^0 + \beta(\max_i M_1^i)\|A_{0,0}\|_1.$$

This ends the proof of Lemma 5.4. □

The following lemma allows to obtain the bounded variation in time and age of the approximate solution $(A^i, B^i)$. This is necessary to prove the convergence.

**Lemma 5.5.** *Let Assumption 5.3.1 be satisfied. Under condition (5.3), one has for all $n > 0$ and $j > 0$*

$$\begin{aligned}
\max_i \left( \sum_{k=0}^{N_s} |B_{j+1,k}^{i,n+1} - B_{j,k}^{i,n}| \right) &\leqslant \alpha_1 \left( \sum_{k=1}^{N_s} |A_{0,0}^k - A_{0,0}^{k-1}| \right) + \beta_1 \|A_{0,0}\|_1, \\
\max_i \left( \sum_{k=0}^{N_s} |A_k^{i,n+1} - A_k^{i,n}| \right) &\leqslant \beta_2 \|A_{0,0}\|_1,
\end{aligned}$$

*where $\alpha_1$, $\beta_1$ and $\beta_2$ are positive constants independent on $n$.*

*Proof.* let fix $i$ and $k$. From equations (5.11) and (5.13), the difference of the solutions between two points $(n+1,\, j+1)$ and $(n,\, j)$, is

$$\begin{aligned}
B_{j+1,k}^{i,n+1} - B_{j,k}^{i,n} &= -\frac{\Delta t}{\Delta s} v_i^k (B_{j,k}^{i,n} - B_{j,k-1}^{i,n}) - \Delta t \left(\frac{v_i^k - v_i^{k-1}}{\Delta s}\right) B_{j,k-1}^{i,n} - \Delta t h_j B_{j+1,k}^{i,n+1}, \\
A_k^{i,n+1} - A_k^{i,n} &= 2\Delta t \Delta \tau \sum_{j=0}^{N_\tau} \mu^j B_{j,k}^{i-1,n} - \Delta t E_n A_k^{i,n+1}.
\end{aligned}$$

By taking the absolute value of these equations and then summing over $k$, one gets

$$\begin{aligned}
\sum_{k=0}^{N_s} |B_{j+1,k}^{i,n+1} - B_{j,k}^{i,n}| &\leqslant \frac{\Delta t}{\Delta s} v_i^\infty \sum_{k=1}^{N_s} |B_{j,k}^{i,n} - B_{j,k-1}^{i,n}| + \Delta t v_i^\infty \|B^{i,n}\|_1 \\
&\quad + \Delta t \lambda_0 \|B^{i,n+1}\|_1, \\
\sum_{k=0}^{N_s} |A_k^{i,n+1} - A_k^{i,n}| &\leqslant 2\Delta t \Delta \tau \bar{\mu} \|B^{i-1,n}\|_1 + \Delta t (\delta_B + \bar{\mu}) \|A^{i,n+1}\|_1.
\end{aligned}$$

Using Lemmas 5.2, 5.4 and condition 5.3, one obtains

$$\begin{aligned}\max_i \sum_{k=0}^{N_s} |B_{j+1,k}^{i,n+1} - B_{j,k}^{i,n}| &\leqslant \alpha \left( \sum_{k=1}^{N_s} |A_{0,0}^{k} - A_{0,0}^{k-1}| \right) + \beta_1 \|A_{0,0}\|_1, \\ \max_i \sum_{k=0}^{N_s} |A_{k}^{i,n+1} - A_{k}^{i,n}| &\leqslant \beta_2 \|A_{0,0}\|_1,\end{aligned}$$

where

$$\alpha_1 = \alpha, \qquad \beta_1 = (\beta + \Delta t \bar{v} + \Delta t \lambda_0) \max_i M_1^i,$$

and

$$\beta_2 = \left( 2\Delta\tau\bar{\mu} \max_i M_1^i + (\delta_B + \bar{\mu}) \max_i N_1^i \right) \Delta t.$$

□

## 5.4 Convergence of the scheme in $L^1$

In this section, we use Helly's Theorem (see Book Brézis [97]) in order to obtain the convergence of the solution of (5.1-5.2).

**Theorem 5.6.** *Let Assumption 5.3.1 be satisfied. Under condition (5.3), the solution $(A_\Delta^i, B_\Delta^i)$ is calculated from (5.1-5.2) for all $i \in \mathbb{N}_I$. Therefore, when the mesh sizes tend to zeros, we can extract a subsequence which converges to $(A_i, B_i)$. This limit is a weak solution of System (4.2-4.3) for all $i \in \mathbb{N}_I$.*

*Proof.* **In the first step**, we show the convergence of scheme to a limit which is bounded and its derivative is also bounded. Next, we prove that this limit verifies

$$\int_0^T \int_0^m \left( \frac{dA_\Delta^0}{dt} + E(t) A_\Delta^0(t,s) \right) \Phi_0(t,s) ds dt = 0 \tag{5.16}$$

$$\begin{aligned}\int_0^T \int_0^m \Big( \frac{dA_\Delta^i}{dt} - 2 \int_0^\Delta \mu(\tau) B_\Delta^{i-1}(t,\tau,s) d\tau \\ + E(t) A_\Delta^i(t,s) \Big) \Phi_i(t,s) ds dt = 0\end{aligned} \tag{5.17}$$

$$\begin{aligned}\int_0^T \int_0^\Delta \int_0^m \big( \partial_t B_\Delta^i + \partial_\tau B_\Delta^i + \partial_s(v_i B_\Delta^i) \\ + h(\tau) B_\Delta^i \big) \Psi_i(t,\tau,s) ds d\tau dt = 0\end{aligned} \tag{5.18}$$

For all test functions $\Phi_i \in D((0,T)\times(0,m))$ and $\Psi_i \in D((0,T)\times(0,\Delta)\times(0,m))$, $\forall$, $i \in \mathbb{N}_I$. In addition, we denote $h(\tau) := \delta_B + \mu(\tau)$ and $E(t) := \delta_A + \lambda(N(t))$.

From Lemma 5.3, the functions $A^i_\Delta, B^i_\Delta$ are uniformly bounded in $L^\infty(0,m)$, $L^\infty((0,\Delta)\times(0,m))$ respectively for all $i \in \mathbb{N}_I$. Then, the set of functions $(A^i_\Delta, B^i_\Delta)$ contain an subsequence $(A^i_{\Delta_j}, B^i_{\Delta_j})$ which weak* converges to $(A^i, B^i)$ in $L^\infty(0,m) \times L^\infty((0,\Delta)\times(0,m))$.

Let $\Pi A^i_\Delta$ and $\Pi B^i_\Delta$ be the interpolation polynomials of degree 1 for the functions $A^i_\Delta$ and $B^i_\Delta$ respectively. They are defined in the domains $(0,T)\times(0,m)$ and $(0,T)\times(0,\Delta)\times(0,m)$ respectively by

$$\begin{aligned}
\Pi A^i_\Delta(t,s) &= A^{i,n}_k + (A^{i,n+1}_k - A^{i,n}_k)\frac{(t-t_n)}{\Delta t},\\
\Pi B^i_\Delta(t,\tau,s) &= B^{i,n}_{j,k} + (B^{i,n}_{j,k+1} - B^{i,n}_{j,k})\frac{s-s_k}{\Delta s} + (B^{i,n+1}_{j+1,k} - B^{i,n}_{j,k})\frac{t-t_n}{\Delta t}\\
&\quad +(B^{i,n+1}_{j+1,k+1} - B^{i,n+1}_{j+1,k} - B^{i,n}_{j,k+1} + B^{i,n}_{j,k})\frac{(s-s_k)(t-t_n)}{\Delta t\Delta s},
\end{aligned}$$

where the mesh size $\Delta t$ is equal to $\Delta\tau$ from the scheme (5.1-5.2).

These functions are bounded and continuous differentiable. From their expressions and Lemmas 5.4 and 5.5, the total variations are also bounded

$$\begin{aligned}
TV(\Pi A^i_\Delta) &= \|\frac{dA^i_\Delta}{dt}\|_{L^1} = \frac{1}{\Delta t\Delta s}\sum_{n,k}\int_{t_n}^{t_{n+1}}\int_{s_{k-1}}^{s_k}|\frac{dA^i_\Delta}{dt}|dsdt,\\
TV(\Pi B^i_\Delta) &= \|(\partial_t+\partial_\tau)B^i_\Delta\|_{L^1} + \|\partial_s \Pi B^i_\Delta\|_{L^1}\\
&= \frac{1}{\Delta t\Delta_\tau\Delta s}\sum_{n,j,k}\int_{t_n}^{t_{n+1}}\int_{\tau_j}^{\tau_{j+1}}\int_{s_{k-1}}^{s_k}|\partial_t B^i_\Delta + \partial_\tau B^i_\Delta|dsdt\\
&\quad +\frac{1}{\Delta t\Delta_\tau\Delta s}\sum_{n,j,k}\int_{t_n}^{t_{n+1}}\int_{\tau_j}^{\tau_{j+1}}\int_{s_{k-1}}^{s_k}|\partial_s B^i_\Delta|dsdt.
\end{aligned}$$

According to Helly's Theorem [97], there exits a subsequence of $(\Pi A^i_\Delta, \Pi B^i_\Delta)$ noted $(A^i_{\Delta_j}, B^i_{\Delta_j})$ which converges in $L^1_{loc}((0,T)\times(0,m)) \times L^1_{loc}((0,T)\times(0,\Delta)\times(0,m))$. Since the subsequence associated weak* converges also in $L^\infty$, then one obtains the convergence of $(A^i_\Delta, B^i_\Delta)$ to $(A^i, B^i)$ in $L^1_{loc}((0,T)\times(0,m)) \times L^1_{loc}((0,T)\times(0,\Delta)\times(0,m))$.

**In the second step**, we prove that the limit obtained is a weak solution. Let

$\Phi_i$ and $\Psi_i$ be the test function in the spaces $C^1((0,T)\times(0,\Delta)\times(0,m))$ and $C^1((0,T)\times(0,m))$ respectively with compact support. We define for all $(t,\tau,s)\in [t_n,t_{n+1}[\times[\tau_j,\tau_{j+1}[\times[s_{k-1},s_k[$

$$\begin{aligned}\Phi_k^{i,n+1} &\sim \int_{t_n}^{t_{n+1}}\int_{s_{k-1}}^{s_k}\frac{\Phi_i(t,s)}{\Delta s\Delta t}dsdt,\\ \Psi_{j+1,k}^{i,n+1} &\sim \int_{t_n}^{t_{n+1}}\int_{\tau_j}^{\tau_{j+1}}\int_{s_{k-1}}^{s_k}\frac{\Psi_i(t,\tau,s)}{\Delta s\Delta\tau\Delta t}dsd\tau dt.\end{aligned}$$

We multiply (5.13) by $\Delta t\Delta s\Psi_{j+1,k}^{i,n+1}$ and we sum over $n$, $j$, $k$. For all $i\in\mathbb{N}_I$, we have

$$\begin{aligned}&\sum_{n=0}^{N_T-1}\sum_{j=0}^{N_\tau-1}\sum_{k=1}^{N_s}\left[\Delta t\Delta s(B_{j+1,k}^{i,n+1}-B_{j,k}^{i,n})\Psi_{j+1,k}^{i,n+1}+(\Delta t)^2(v_i^kB_{j,k}^{i,n}-v_i^{k-1}B_{j,k-1}^{i,n})\Psi_{j+1,k}^{i,n+1}\right]\\ &=-(\Delta t)^2\Delta s h_jB_{j+1,k}^{i,n+1}\Psi_{j+1,k}^{i,n+1}.\end{aligned}\tag{5.19}$$

The first term of this sum is equal to

$$\begin{aligned}\sum_{n,j,k}\Delta t\Delta s(B_{j+1,k}^{i,n+1}-B_{j,k}^{i,n})\Psi_{j+1,k}^{i,n+1} &= \sum_{n,j,k}-B_{j+1,k}^{i,n}\Delta t\Delta s(\Psi_{j+1,k}^{i,n+1}-\Psi_{j+1,k}^{i,n})\\ &\quad+\Delta t\Delta s\sum_{j,k}(B_{j+1,k}^{i,N_T}\Psi_{j+1,k}^{i,N_T}-B_{j+1,k}^{i,0}\Psi_{j+1,k}^{i,0})\\ &\quad+\sum_{n,j,k}-B_{j,k}^{i,n}\Delta t\Delta s(\Psi_{j+1,k}^{i,n+1}-\Psi_{j,k}^{i,n+1})\\ &\quad+\Delta t\Delta s\sum_{n,k}(B_{N_\tau,k}^{i,n}\Psi_{N_\tau,k}^{i,n+1}-B_{0,k}^{i,n}\Psi_{0,k}^{i,n+1})\end{aligned}$$

Using the definitions of the approximations, one obtains

$$\begin{aligned}&\sum_{n,j,k}\Delta t\Delta s(B_{j+1,k}^{i,n+1}-B_{j,k}^{i,n})\Psi_{j+1,k}^{i,n+1}=\\ &-\int_0^{T-\Delta t}\int_0^{\Delta-\Delta\tau}\int_0^m B_\Delta^i\left[\frac{\Psi_i(t,\tau,s)-\Psi_i(t-\Delta t,\tau,s)}{\Delta t}\right.\\ &\qquad\left.+\frac{\Psi_i(t,\tau,s)-\Psi_i(t,\tau-\Delta\tau,s)}{\Delta\tau}\right]dsd\tau dt\\ &+\int_0^{\Delta-\Delta\tau}\int_0^m\left[B_\Delta^i(T,\tau,s)\Psi_i(T,\tau,s)-B_\Delta^i(0,\tau,s)\Psi_i(0,\tau,s)\right]d\tau ds\\ &+\int_0^{T-\Delta t}\int_0^m\left[B_\Delta^i(t,\Delta,s)\Psi_i(t,\Delta,s)-B_\Delta^i(t,0,s)\Psi_i(t,0,s)\right]dtds.\end{aligned}$$

Similarly, the second term of equation (5.19) can be written in the following form

$$
\begin{aligned}
&(\Delta t)^2 \sum_{n,j,k} (v_i^k B_{j,k}^{i,n} - v_i^{k-1} B_{j,k-1}^{i,n}) \Psi_{j+1,k}^{i,n+1} \\
&= - \int_0^{T-\Delta t} \int_0^{\Delta-\Delta\tau} \int_0^{m} v_i(s-\Delta s) B_\Delta^i(t,\tau,s-\Delta s) \left( \frac{\Psi_i(t,\tau,s) - \Psi_i(t,\tau,s-\Delta s)}{\Delta s} \right) dt d\tau ds \\
&+ \int_0^{T-\Delta t} \int_0^{\Delta-\Delta\tau} \left[ v_i(N_s) B_\Delta^i(t,\tau,N_s) \Psi_i(t,\tau,N_s) - v_i(0) B_\Delta^i(t,\tau,0) \Psi_i(t,\tau,0) \right] dt d\tau.
\end{aligned}
$$

Finally, the last term of this sum is equal to

$$
\begin{aligned}
&- \sum_{n,j,k} (\Delta t)^2 h_j B_{j+1,k}^{i,n+1} \Psi_{j+1,k}^{i,n+1} \\
&= - \int_0^{T-\Delta t} \int_0^{\Delta-\Delta\tau} \int_0^{m} h(\tau+\Delta\tau) B_\Delta^i(t+\Delta t, \tau+\Delta\tau, s) \Psi_i(t,\tau,s) ds d\tau dt.
\end{aligned}
$$

Using an integration by parts, equation (5.19) is equal to

$$
\int_0^T \int_0^\Delta \int_0^m \left( \partial_t B_\Delta^i + \partial_\tau B_\Delta^i + \partial_s v_i B_\Delta^i + h(\tau) B_\Delta^i(t,\tau,s) \right) \Psi_i(t,\tau,s) ds d\tau dt = 0,
$$

when the mesh sizes tend to zeros.

Obviously by the same method, we prove that the solution of (5.2) converges to the weak solution of (4.2-4.3) for all $i \in \mathbb{N}_I$. □

## 5.5 Continuity of scheme with respect to parameters

In this section, we prove some properties of System (5.1 - 5.2) that will be useful in estimating the parameters.

**Lemma 5.7.** *Let Assumption 5.3.1 be satisfied. Under condition (5.3), there exists positive constants $C_{A^i}$, $C_{B^i}$ independent on $N_s$, $N_\tau$ and $N_T$ such that*

$$
\begin{aligned}
\|B^{i,n+1} - \tilde{B}^{i,n+1}\|_\infty &\leqslant C_{B^i} \|v_{i,N_s} - \tilde{v}_{i,N_s}\|_\infty \quad \forall \ i \in \mathbb{N}_I, \\
\|A^{i,n+1} - \tilde{A}^{i,n+1}\|_\infty &\leqslant C_{A^i} \|v_{i-1} - \tilde{v}_{i-1}\|_\infty \quad \forall \ i \in \mathbb{N}_I^*,
\end{aligned}
$$

*where* $A^{i,n} = A^{i,n}(v_{i,N_s})$, $B^{i,n} = B^{i,n}(v_{i,N_s})$ *and* $\tilde{A}^{i,n} = \tilde{A}^{i,n}(\tilde{v}_{i,N_s})$, $\tilde{B}^{i,n} = \tilde{B}^{i,n}(\tilde{v}_{i,N_s})$ *are the solutions of System (5.1 - 5.2).*

*Proof.* We proceed the proof by induction. The first step consists to estimate in $L^\infty$ the difference between $B^{i,n}_{j,k}$, $\tilde{B}^{i,n}_{j,k}$ and the difference between $A^{i,n}_k$, $\tilde{A}^{i,n}_k$ for all $i$ and $n$. Let

$$\begin{aligned}\zeta^{i,n} &= \sup_{j,k}|\zeta^{i,n}_{j,k}| = \sup_{j,k}|B^{i,n}_{j,k} - \tilde{B}^{i,n}_{j,k}|,\\ \gamma^{i,n} &= \sup_{k}|\gamma^{i,n}_{j,k}| = \sup_{k}|A^{i,n}_{k} - \tilde{A}^{i,n}_{k}|.\end{aligned}$$

From the equations in (5.1-5.2), one calculates the variable $\zeta^{i,n}$ and $\gamma^{i,n}$

$$\begin{aligned}\zeta^{i,n+1}_{j+1,k} &= (1-\frac{\Delta t}{\Delta s}v^k_i)\zeta^{i,n}_{j,k} - \frac{\Delta t}{\Delta s}\tilde{B}^{i,n}_{j,k}(v^k_i - \tilde{v}^k_i) + \frac{\Delta t}{\Delta s}v^{k-1}_i\zeta^{i,n}_{j,k-1}\\ &\quad + \frac{\Delta t}{\Delta s}\tilde{B}^{i,n}_{j,k-1}(v^{k-1}_i - \tilde{v}^{k-1}_i) - \Delta t(\delta_B + \mu^j)\zeta^{i,n+1}_{j+1,k} \qquad (5.20)\end{aligned}$$

$$\begin{aligned}\gamma^{i,n+1}_k &= \gamma^{i,n}_k + 2\Delta t\Delta\tau\sum_{j=0}^{N_\tau}\mu^j\zeta^{i-1,n}_{j,k} - \Delta t(\delta_A + \lambda^n)\gamma^{i,n+1}_k \quad \textit{pour} \quad i \in \mathbb{N}^*_I\\ \gamma^{0,n+1}_k &= \gamma^{0,n}_k - \Delta t(\delta_A + \lambda^n)\gamma^{0,n+1}_k. \qquad (5.21)\end{aligned}$$

Using Lemma 5.3 and condition (5.3), the upper bound of equation (5.20) is

$$\zeta^{i,n+1} \leqslant \zeta^{i,n} + \Delta t(\delta_B + \bar{\mu})\zeta^{i,n+1} + \frac{\Delta t}{\Delta s}M_i^2\|A_{0,0}\|_\infty\|v_{i,N_s} - \tilde{v}_{i,N_s}\|_\infty.$$

By induction over $n$ for all $i \in \mathbb{N}_I$, one obtains

$$\zeta^{i,n+1} = \|B^{i,n} - \tilde{B}^{i,n}\|_\infty \leqslant TM_2^i\|A_{0,0}\|_\infty e^{T(\delta_B+\bar{\mu})}\|v_{i,N_s} - \tilde{v}_{i,N_s}\|_\infty.$$

Then, $C_{B^i}$ is equal to $TM_2^i\|A_{0,0}\|_\infty e^{T(\delta_B+\bar{\mu})}$.

Similarly, by taking the upper bound of equation (5.21) and by induction, one obtains for all $n$ and $i \in \mathbb{N}^*_I$

$$\gamma^{i,n+1} = \|A^{i,n+1} - \tilde{A}^{i,n+1}\|_\infty \leqslant 2\Delta T\bar{\mu}N_2^i\|A_{0,0}\|_\infty e^{T(\delta_A+\lambda_0)}\|v_{i-1,N_s} - \tilde{v}_{i-1,N_s}\|_\infty.$$

Therefore, $C_{A^i}$ is equal to $2\Delta\bar{\mu}TN_2^i\|A_{0,0}\|_\infty e^{T(\delta_A+\lambda_0)}$. □

**Lemma 5.8.** *Let Assumption 5.3.1 be satisfied. Under condition (5.3), there exists positive constants $C^1_{A^i}$, $C^1_{B^i}$ independent on $N_s$, $N_\tau$ and $N_T$ such that*

$$\begin{aligned} \|B^{i,n+1} - \tilde{B}^{i,n+1}\|_\infty &\leqslant C^1_{B^i}\|\mu - \tilde{\mu}\|_\infty \quad \forall \ i \in \mathbb{N}_I, \\ \|A^{i,n+1} - \tilde{A}^{i,n+1}\|_\infty &\leqslant C^1_{A^i}\|\mu - \tilde{\mu}\|_\infty \quad \forall \ i \in \mathbb{N}^*_I, \end{aligned}$$

*where $A^{i,n} = A^{i,n}(\mu)$, $B^{i,n} = B^{i,n}(\mu)$ and $\tilde{A}^{i,n} = \tilde{A}^{i,n}(\tilde{\mu})$, $\tilde{B}^{i,n} = \tilde{B}^{i,n}(\tilde{\mu})$ are the solutions of System (5.1 - 5.2).*

**Lemma 5.9.** *Let Assumption 5.3.1 be satisfied. Under condition (5.3), there exists positive constants $C^2_{A^i}$, $\bar{C}^2_{A^i}$, $C^2_{B^i}$ and $\bar{C}^2_{B^i}$ independent on $N_s$, $N_\tau$ and $N_T$ such that*

$$\begin{aligned} \|B^{i,n+1} - \tilde{B}^{i,n+1}\|_\infty &\leqslant C^2_{B^i}\|v_{i,N_s} - \tilde{v}_{i,N_s}\|_\infty + \bar{C}^2_{B^i}\|\lambda - \tilde{\lambda}\|_\infty \quad \forall \ i \in \mathbb{N}_I, \\ \|A^{i,n+1} - \tilde{A}^{i,n+1}\|_\infty &\leqslant C^2_{A^i}\|v_{i,N_s} - \tilde{v}_{i,N_s}\|_\infty + \bar{C}^2_{A^i}\|\lambda - \tilde{\lambda}\|_\infty \quad \forall \ i \in \mathbb{N}_I, \end{aligned}$$

*where $A^{i,n} = A^{i,n}(v_{i,N_s}, \lambda)$, $B^{i,n} = B^{i,n}(v_{i,N_s}, \lambda)$ and $\tilde{A}^{i,n} = \tilde{A}^{i,n}(\tilde{v}_{i,N_s}, \tilde{\lambda})$, $\tilde{B}^{i,n} = \tilde{B}^{i,n}(\tilde{v}_{i,N_s}, \tilde{\lambda})$ are the solutions of System (5.1 - 5.2).*

The proofs of these two lemmas are similar to the proof of Lemma 5.7.

# Part III

# Models of T Cell Proliferation in Lymphopenia Conditions: Identification of Parameters

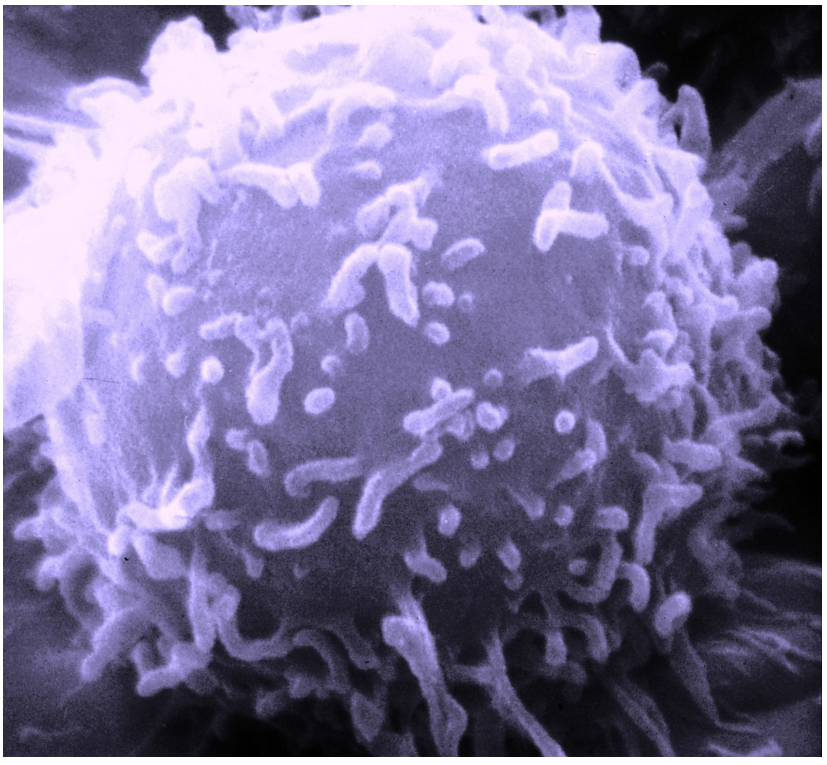

# Chapter 6

# Experimental data and theoretical identifiability

## 6.1 Introduction

The dynamic nature of immune responses requires the development of appropriate experimental tools to quantitatively understand the division and death processes which determine the turnover of immune cells. In the literature, several types of data have been explored and used in the context of T cell proliferation induced by LIP (Lymphopenia Induced Proliferation). Using cell dyes, such as Carboxy Fluorescein diacetate Succinimidyl Ester (CFSE), is currently one of the most informative methods for characterizing the dynamics of cell division in the immune system. Following each division, CFSE divides equally between daughter cells, resulting in a two-fold decrease in the intensity of cellular fluorescence in each successive generation. This property of CFSE allows accurate tracking of the number of divisions that a given cell has undergone either in vitro or following transfer in vivo [87].
The Smith-Martin model has been applied widely to CFSE data [2–9], and the duration of deterministic phase (B-phase), the division rate and the probability of cell death have been estimated from experimental data mainly based on CFSE cell division profiles [4–6]. Hogan et al. [10] improved the technique and accuracy of the parameter estimations from the Smith-Martin model. The DNA binding dye, 7-Aminoactinomycin D (7AAD), was used with CFSE to distinguish the proliferating and non-proliferating cells, therefore enabling estimations of the rate of recruitment of cells from A-state into B-phase.

In this chapter, we describe the data generated by Hogan et al. [10]. Next, we prove the identifiability of some parameters in $SM_{CD44}$ model by using the data of Hogan et al. [10].

## 6.2 Experimental data

Data were collected during a previously published study [10]. The behavior of two different T cell clonotypes was studied in lymphopenic Rag1-/- mice by using CFSE, 7AAD dyes and CD44 expression measured by flow cytometry. Following adoptive transfer of T cells, cohorts of between three and five host mice were analysed at different days. At each date, the number of T cells, the proportion of cells actively replicating their DNA as determined by 7AAD staining, and the intensity of expression of CD44 on the cell surface were measured in each host and separated according to the number of divisions performed as assessed by CFSE labeling. Note that the intensity of CD44 is the MFI (median fluorescence intensity) normalised to CD44 expression on NK cells. In other word, it represents the weight of CD44 expression (without unit) on the surface of cells in each division.

## 6.3 Identifiability

In this section, we are interested in the identifiability of the parameters $v_i$, $\forall$ $i = 0, ..., I$, $\lambda$ and $\Delta$ by using the data stated in Section 6.2.

Let us denote the experimental data by

$$N_i^{exp}(t, s) := \int_0^{\Delta} B_i(t, \tau, s)d\tau + A_i(t, s),$$

where $i \in \mathbb{N}_I := \{0, ..., I\}$, $t \in [0, T]$, $s \in [0, m]$ and $(A_i, B_i)$ is the solution of $SM_{CD44}$ model.

*Assumption* 6.3.1.
- Functions $(v_0, ..., v_I)$ are defined in the space $K = (C_+^{\bar{u}})^I$ where

$$C_+^{\bar{u}} = \{u \in C^0([0, m]),\ u(0) = 0,\ 0 < u(s) \leqslant \bar{u}\ ,\ \forall\ s \in (0, m]\}.$$

- Initial condition $A_{0,0}(s) > 0$ for all $s \in (0, m]$.

**Lemma 6.1.** *Let Assumptions 4.3.1 and 6.3.1 be satisfied. The velocity $v_i$ is identifiable for all $i \in \mathbb{N}_I := \{0, ..., I\}$.*

*Proof.* Let us fix $(v_0, ..., v_I) \in K$ and consider a second parameter $(\bar{v}_0, ..., \bar{v}_I) \in K$ wherein

$$N_i^{exp}(t, s; v_i) = N_i^{exp}(t, s; \bar{v}_i), \quad \forall\ i \in \mathbb{N}_I, \tag{6.1}$$

and $(\bar{A}_i(t, s), \bar{B}_i(t, \tau, s))$ is the solution relative to $\bar{v}_i$.
By integrating and summing (6.1) over $s$ and $i$ respectively, one gets

$$N(t) = \bar{N}(t). \tag{6.2}$$

By using the implicit solution (4.4), one obtains

$$A_0(t, s) = \bar{A}_0(t, s) \quad \forall\ s \in [0, m]. \tag{6.3}$$

From (6.1), one gets $\int_0^\Delta B_0(t, \tau, s)d\tau = \int_0^\Delta \bar{B}_0(t, \tau, s)d\tau$.

Furthermore by induction, if we prove $v_{i-1}(s) = \bar{v}_{i-1}(s)$, $\forall\ \ i \in \mathbb{N}_I^*$ and $s \in [0, m]$, one obtains $A_i(t, s) = \bar{A}_i(t, s)$ and then from (6.1), one gets $\int_0^\Delta B_i(t, \tau, s)d\tau = \int_0^\Delta \bar{B}_i(t, \tau, s)d\tau$. Therefore, the problem reverts to proving the identifiability of $v_i$ through the following system

$$\begin{cases} \frac{\partial}{\partial t}B_i(t, \tau, s) + \frac{\partial}{\partial \tau}B_i(t, \tau, s) + \frac{\partial}{\partial s}\left[v_i(s)B_i(t, \tau, s)\right] = -\left(\delta_B + \mu(\tau)\right)B_i(t, \tau, s), \\ \\ B_i(0, \tau, s) = 0; \quad B_i(t, 0, s) = \lambda(N(t))A_i(t, s); \quad v_i(0)B_i(t, \tau, 0) = 0. \end{cases} \tag{6.4}$$

Let $\tilde{B}_i := B_i - \bar{B}_i$ and $\tilde{v}_i := v_i - \bar{v}_i$. $B_i$ and $\bar{B}_i$ are the solutions given by (6.4) relative to $v_i$ and $\bar{v}_i$ respectively. Then, one has

$$\begin{cases} \frac{\partial}{\partial t}\tilde{B}_i(t, \tau, s) + \frac{\partial}{\partial \tau}\tilde{B}_i(t, \tau, s) + \frac{\partial}{\partial s}\left[\tilde{v}_i(s)B_i(t, \tau, s) + \bar{v}_i(s)\tilde{B}_i(t, \tau, s)\right] = -f(\tau)\tilde{B}_i(t, \tau, s), \\ \\ \tilde{B}_i(0, \tau, s) = 0; \quad \tilde{B}_i(t, 0, s) = 0; \quad \tilde{v}_i(0)B_i(t, \tau, 0) = 0, \\ \\ \textit{Observation}: \quad \int_0^\Delta \tilde{B}_i(t, \tau, s)d\tau = 0, \end{cases} \tag{6.5}$$

where $f(\tau) := \delta_B + \mu(\tau)$.
Now, we define the following Lagrangian formulation related to System (6.5).

$$\begin{aligned}\mathscr{L}(\tilde{B}_i, \tilde{v}_i, \tilde{q}_i) \;=\; & \int_\Omega [\frac{\partial}{\partial t}\tilde{B}_i(t,\tau,s) + \frac{\partial}{\partial \tau}\tilde{B}_i(t,\tau,s) + \frac{\partial}{\partial s}\left[\tilde{v}_i(s)B_i(t,\tau,s) + \bar{v}_i(s)\tilde{B}_i(t,\tau,s)\right] \\ & + f(\tau)\tilde{B}_i(t,\tau,s)]\tilde{q}_i(t,\tau,s)d\Omega + \int_\Omega \tilde{B}_i(t,\tau,s)d\Omega,\end{aligned}$$

where $\Omega = [0,T]\times[0,\Delta]\times[0,m]$, $d\Omega = dt\,d\tau\,ds$ and $\tilde{q}_i$ corresponds to the dual variable. The first derivative of the Lagrangian $\mathscr{L}$ with respect to $\tilde{B}_i$, gives us the adjoint equation.

$$\begin{cases} \frac{\partial}{\partial t}\tilde{q}_i(t\tau,s) + \frac{\partial}{\partial \tau}\tilde{q}_i(t,\tau,s) + \frac{\partial}{\partial s}\left[\bar{v}_i\tilde{q}_i(t\tau,s)\right] = F(\tau)\tilde{q}_i(t\tau,s) + 1, \\ \\ \tilde{q}_i(T,\tau,s) = \tilde{q}_i(t,\Delta,s) = \tilde{q}_i(t,\tau,m) = 0. \end{cases} \tag{6.6}$$

Multiplying (6.6) by $\tilde{B}_i(t,\tau,s)$ and integrating over $\Omega$, one obtains

$$\int_\Omega \left(\tilde{B}_i(t,\tau,s) - \left[\frac{\partial \tilde{v}_i(s)B_i(t,\tau,s)}{\partial s}\right]\tilde{q}_i(t,\tau,s)\right)d\Omega = 0.$$

Using the observation in (6.5), one gets

$$\frac{\partial}{\partial s}\left[\tilde{v}_i(s)B_i(t,\tau,s)\right] = 0.$$

Replacing the above equality in (6.5), one has

$$\begin{cases} \frac{\partial}{\partial t}\tilde{B}_i(t,\tau,s) + \frac{\partial}{\partial \tau}\tilde{B}_i(t,\tau,s) + \frac{\partial}{\partial s}\left[\bar{v}_i(s)\tilde{B}_i(t,\tau,s)\right] = -f(\tau)\tilde{B}_i(t,\tau,s), \\ \\ \tilde{B}_i(0,\tau,s) = 0; \quad \tilde{B}_i(t,0,s) = 0; \quad \bar{v}_i(0)B_i(t,\tau,0) = 0. \end{cases} \tag{6.7}$$

Integrating along the characteristic curve the PDE of the above system, one obtains $\forall\ (t,\tau,s)\in\Omega$ and $i\in\mathbb{N}_I$

$$\tilde{B}_i(t,\tau,s) = 0, \quad \textit{and then} \quad B_i(t,\tau,s) = \bar{B}_i(t,\tau,s). \tag{6.8}$$

Let $\bar{Z}_i^2(\tau) = Z_i^2(\tau) + c_i(\tau)$, where $c_i(\tau) > 0$ for all $\tau\in(0,\Delta]$ and $i\in\mathbb{N}_I$. Then for a fixed $i_0\in\mathbb{N}_I$ and $s = \bar{Z}_{i_0}^2(\tau)$, one obtains from (6.8) and (4.6)

$$B_{i_0}(t,\tau,s) = A_{i_0}(t-\tau, c_{i_0}(\tau))v_{i_0}(c_{i_0}(\tau)) = 0 \quad \forall\ \ 0<\tau<t \ \ \textit{and} \ \ c_{i_0}(\tau) > 0.$$

Using (4.4), one remarks that the previous equality leads to a contradiction with Assumptions 4.3.1 and 6.3.1 (specifically $A_{0,0}(s) > 0$ and $v_{i_0}(s) > 0$ for all $s \in (0, m]$). Therefore, one deduces

$$Z_i^2(\tau) = \bar{Z}_i^2(\tau) \quad \forall\, 0 \leq \tau < t \;\; \textit{and} \;\; i \in \mathbb{N}_I.$$

Using (6.8) and (4.6), one gets for all $s > Z_i^2(\tau)$ and $0 < \tau < t$

$$\frac{v_i(s - Z_i^2(\tau))}{v_i(s)} = \frac{\bar{v}_i(s - Z_i^2(\tau))}{\bar{v}_i(s)}. \tag{6.9}$$

Using (6.9) and the definition of $Z_i^2(\tau)$ and $\bar{Z}_i^2(\tau)$ , one obtains

$$\int_0^\tau v_i(s(r)) \left[\frac{\bar{v}_i(s(r) - Z_i^2(r))}{v_i(s(r) - Z_i^2(r))} - 1\right] dr = 0.$$

By deriving the above equation with respect to $\tau$, one gets

$$v_i(s) \left[\frac{\bar{v}_i(s - Z_i^2(\tau))}{v_i(s - Z_i^2(\tau))} - 1\right] = 0,$$

where $s := s(\tau)$. Therefore, one concludes $v_i(s) = \bar{v}_i(s)$, $\forall\, s \in [0, m]$ and $i \in \mathbb{N}_I$. □

**Theorem 6.2.** *Let Assumptions 4.3.1 and 6.3.1 be satisfied. The parameters $v_i(s)$, $\lambda(N(t))$ and $\Delta$ are identifiable for all $i \in \mathbb{N}_I$, $s \in [0, m]$ and $t \in (0, T]$.*

*Proof.* Let fix $\theta = [(v_0, ..., v_I) \in K, \lambda, \Delta]$ and consider a second parameters $\bar{\theta} = \left[(\bar{v}_0, ..., \bar{v}_I) \in K, \bar{\lambda}, \bar{\Delta}\right]$ wherein $\forall\, t \in [0, T]$ and $s \in [0, m]$,

$$A_i(t, s; \theta) + \int_0^\Delta B_i(t, \tau, s; \theta) d\tau = \bar{A}_i(t, s; \bar{\theta}) + \int_0^{\bar{\Delta}} \bar{B}_i(t, \tau, s; \bar{\theta}) d\tau, \quad \forall\, i \in \mathbb{N}_I\,, \tag{6.10}$$

where $(A_i(., .; \theta), B_i(., ., .; \theta))$ and $\left(\bar{A}_i(., .; \bar{\theta}), \bar{B}_i(., ., .; \bar{\theta})\right)$ are the solutions of $SM_{CD44}$ model, and are related to the parameters $\theta$ and $\bar{\theta}$ respectively.

If $\bar{\Delta} \leq \Delta$, we consider

$$\bar{B}_i^*(t, \tau, s) := \begin{cases} \bar{B}_i(t, \tau, s) & if \quad \tau \in [0, \bar{\Delta}], \\ \\ 0 & if \quad \tau \in (\bar{\Delta}, \Delta]. \end{cases}$$

Using the integral formulation of (4.6), one gets for all $\tau \in (0, \Delta]$

$$B_0(t, \tau, s) = \bar{B}_0^*(t, \tau, s) = 0 \quad \forall\ s \leq \min(Z_0^2(\tau), \bar{Z}_0^2(\tau)).$$

Replacing the previous equality in (6.10), one obtains for all $\tau \in (0, \Delta]$

$$A_0(t, s) = \bar{A}_0(t, s) \quad \forall\ s \leq \min(Z_0^2(\tau), \bar{Z}_0^2(\tau)).$$

Using the implicit solution (4.4), one obtains

$$\int_0^t \left(\lambda(N(u)) - \bar{\lambda}(\bar{N}(u))\right) du = 0. \tag{6.11}$$

Deriving the previous equality with respect to $t$,

$$\lambda(N(t)) = \bar{\lambda}(\bar{N}(t)).$$

By integrating and summing (6.10) over $s$ and $i$ respectively, one gets

$$N(t) = \bar{N}(t). \tag{6.12}$$

Then, one deduces $\lambda(N(t)) = \bar{\lambda}(N(t))$ for all $t \in (0, T]$.

Using Lemma 6.1, one deduces $v_i(s) = \bar{v}_i(s)$ for all $s \in [0, m]$ and $i \in \mathbb{N}_I$. Therefore, one has

$$\int_0^{\Delta} B_0(t, \tau, s) d\tau = \int_0^{\bar{\Delta}} B_0(t, \tau, s) d\tau.$$

Since $\bar{\Delta} \leq \Delta$, then the previous equality can be written as

$$\int_{\bar{\Delta}}^{\Delta} B_0(t, \tau, s) d\tau = 0.$$

Under Assumptions 4.3.1 and 6.3.1, one has $B_0(t, \tau, s) > 0$ for all $s > Z_0^2(\tau)$, $\tau \in [\bar{\Delta}, \Delta]$ and $t$ large enough ($t > \Delta$). Therefore, one deduces $\bar{\Delta} = \Delta$ from the previous equality. □

### 6.3.1 Generalisation

In this subsection, we consider the following cases:

1-) The recruitment rate ($\lambda$) depends on the division number $i$ undergone by cells and the total cell number $N := N(t)$ (noted $\lambda^i(N)$).

2-) The duration of B-phase ($\Delta$) depends on the division number $i$ undergone by cells (noted $\Delta^i$).

Then $SM_{CD44}$ model becomes

$$
(SM^i_{CD44})\begin{cases}
\dfrac{dA_0(t,s)}{dt} = -\delta_A A_0(t,s) - \lambda^0(N)A_0(t,s), \\
\begin{cases} for \quad i \in \mathbb{N}_I^*, \\ \dfrac{dA_i(t,s)}{dt} = 2\displaystyle\int_0^{\Delta_{i-1}} \mu(\tau)B_{i-1}(t,\tau,s)\ d\tau - \delta_A A_i(t,s) - \lambda^i(N)A_i(t,s), \end{cases} \\
\begin{cases} for \quad i \in \mathbb{N}_I, \\ \frac{\partial}{\partial t}B_i(t,\tau,s) + \frac{\partial}{\partial \tau}B_i(t,\tau,s) + \frac{\partial}{\partial s}[v_i(s).B_i(t,\tau,s)] = -\left(\delta_B + \mu(\tau)\right)B_i(t,\tau,s), \end{cases} \\
\begin{cases} B_i(t,0,s) = \lambda^i(N)A_i(t,s) \quad and \quad v_i(0)B_i(t,\tau,0) = 0 \quad for \quad i \in \mathbb{N}_I, \\ B_i(0,\tau,s) = 0, \quad for\ i = 0,...,I \quad and \quad A_i(0,s) = 0, \quad for\ i \in \mathbb{N}_I^*, \\ A_0(0,s) = A_{0,0}(s) \geqslant 0. \end{cases}
\end{cases}
$$

**Theorem 6.3.** *Let Assumptions 4.3.1 and 6.3.1 be satisfied. The parameters $v_i(s)$, $\lambda^i(N(t))$ and $\Delta^i$ are identifiable for all $i \in \mathbb{N}_I$, $s \in [0,m]$ and $t \in (0,T]$.*

*Proof.* Here, we use the same techniques as in the previous proof. Let us fix $\theta_i = [v_i, \lambda^i, \Delta_i]$ and consider a second parameter $\bar{\theta}_i = \left[\bar{v}_i, \bar{\lambda}^i, \bar{\Delta}_i\right]$ wherein $\forall\ t \in [0,T]$ and $s \in [0,m]$,

$$
A_i(t,s;\theta_i) + \int_0^{\Delta_i} B_i(t,\tau,s;\theta_i)d\tau = \bar{A}_i(t,s;\bar{\theta}_i) + \int_0^{\bar{\Delta}_i} \bar{B}_i(t,\tau,s;\bar{\theta}_i)d\tau, \quad \forall\ i \in \mathbb{N}_I\,, \tag{6.13}
$$

where $(A_i(.,.;\theta_i), B_i(.,.,.;\theta_i))$ and $\left(\bar{A}_i(.,.;\bar{\theta}_i), \bar{B}_i(.,.,.;\bar{\theta}_i)\right)$ are the solutions of $SM^i_{CD44}$ model, and are related to the parameters $\theta_i$ and $\bar{\theta}_i$ respectively.

By integrating and summing (6.13) over $s$ and $i$ respectively, one gets

$$N(t) = \bar{N}(t). \tag{6.14}$$

If $\bar{\Delta}_i \leq \Delta_i$, we consider

$$\bar{B}_i^*(t,\tau,s) := \begin{cases} \bar{B}_i(t,\tau,s) & if \quad \tau \in [0, \bar{\Delta}_i], \\ \\ 0 & if \quad \tau \in (\bar{\Delta}_i, \Delta_i]. \end{cases}$$

Using the integral formulation of (4.6), one gets for all $\tau \in (0, \Delta_i]$

$$B_i(t,\tau,s) = \bar{B}_i^*(t,\tau,s) = 0 \quad \forall\ s \leq \min(Z_i^2(\tau), \bar{Z}_i^2(\tau)). \tag{6.15}$$

Now, we proceed by induction.
For $i = 0$: one has for all $\tau \in (0, \Delta_0]$

$$A_0(t,s) = \bar{A}_0(t,s) \quad \forall\ s \leq \min(Z_0^2(\tau), \bar{Z}_0^2(\tau)).$$

Using the implicit solution (4.4), one obtains for all $t \in (0, T]$

$$\int_0^t \left(\lambda^0(N(u)) - \bar{\lambda}^0(\bar{N}(u))\right) du = 0. \tag{6.16}$$

Deriving the previous equality with respect to $t$ and using (6.14), one deduces

$$\lambda^0(N(t)) = \bar{\lambda}^0(\bar{N}(t)) \quad \forall\, t \in (0, T].$$

Using Theorem 6.1, one deduces $v_0(s) = \bar{v}_0(s)$ for all $s \in [0, m]$. Therefore, equation (6.13) becomes

$$\int_{\bar{\Delta}_0}^{\Delta_0} B_0(t,\tau,s) d\tau = 0.$$

Under Assumptions 4.3.1 and 6.3.1, one has $B_0(t,\tau,s) > 0$ for all $s > Z_0^2(\tau)$, $\tau \in [\bar{\Delta}_0, \Delta_0]$ and $t$ large enough ($t > \Delta_0$). Therefore, one deduces $\bar{\Delta}_0 = \Delta_0$.

For $i \in \mathbb{N}_I^*$:

Assuming that the following equalities are satisfied

$$\lambda^{i-1}(N(t)) = \bar{\lambda}^{i-1}(N(t)), \quad v_{i-1}(s) = \bar{v}_{i-1}(s) \ \ and \ \ \Delta^{i-1} = \bar{\Delta}^{i-1},$$

for all $i \in \mathbb{N}_I^*$, $t \in (0, T]$ and $s \in [0, m]$. Then $B_{i-1}(t, \tau, s) = \bar{B}_{i-1}(t, \tau, s)$, $\forall$ $\tau \in [0, \Delta_{i-1}]$ and $s \in [0, m]$. Let us show that the previous equalities still hold for $i$.

Using (6.15), equation (6.13) becomes

$$A_i(t, s) = \bar{A}_i(t, s) \quad \forall\ s \leq \min(Z_i^2(\tau), \bar{Z}_i^2(\tau)).$$

By deriving the previous equality with respect to $t$ and by using the ODEs in $SM_{CD44}^i$ model, one gets

$$\begin{aligned} &2\int_0^{\Delta_{i-1}} \mu(\tau) B_{i-1}(t, \tau, s)\ d\tau - \delta_A A_i(t, s) - \lambda^i(N) A_i(t, s) \\ &= 2\int_0^{\bar{\Delta}_{i-1}} \mu(\tau) \bar{B}_{i-1}(t, \tau, s)\ d\tau - \delta_A \bar{A}_i(t, s) - \bar{\lambda}^i(\bar{N}) \bar{A}_i(t, s). \end{aligned}$$

Using the induction hypothesis and (6.14), one deduces for all $t \in (0, T]$

$$\lambda^i(N(t)) = \bar{\lambda}^i(N(t)).$$

Using Theorem 6.1, one deduces $v_i(s) = \bar{v}_i(s)$ for all $s \in [0, m]$. Therefore, equation (6.13) becomes

$$\int_{\bar{\Delta}_i}^{\Delta_i} B_i(t, \tau, s) d\tau = 0.$$

As in the case $i = 0$, for $t$ large enough ($t > \Delta_i$), one has $B_i(t, \tau, s) > 0$ for all $s > Z_i^2(\tau)$ and $\tau \in [\bar{\Delta}_i, \Delta_i]$. Therefore, one deduces $\bar{\Delta}_i = \Delta_i$. □

# Chapter 7

# A comparison of two versions of the Smith-Martin model

## 7.1 Introduction

A biologically reasonable specific model of cell division is given by the Smith-Martin model [69]. Based on their quantitative study of the FLM (fraction of labelled mitoses) curves of dividing cell populations in vitro, Smith and Martin (1973) formulated a simple quantitative description for the process of cell division. In fact, this description is similar to the model proposed by Burns and Tannock (1970) [98]. The Smith-Martin model divides the complete division cycle into an A-state and a B-phase. The A-state corresponds to the G0 or G1 phase where the cells are randomly activated to enter and divide in B-phase (S, G2, M phase). This model has successfully been used for analysing the population dynamics of dividing cells as it prevents too rapid progression through the cell cycle by introducing the equivalent of a time delay (i.e a fixed length for the S, G2 and M phases of the cell cycle) [42]. Several authors have developed mathematical models based on the Smith-Martin model in order to analyse CFSE data [2–9]. Specially, Bernard et al [3] and Ganusov et al [4] have formulated the Smith-Martin model in terms of PDEs (termed by $SM$ model). Later on, several studies have been made to improve the prediction of this model to CFSE data. For example, Yates et al. [7] and Hogan et al. [10] have modified the $SM$ model by considering that the rate of entry in B-phase depends on the time evolution [7] or on the total cell number [10]. Their results show that the modified $SM$ models provides the best description of the observed response by F5

and OT-1 T cells to lymphopenia.
This chapter is organised as follows. At first, we present the modified $SM$ model [10] (previously latest version of Smith-Martin model in the literature) and our reduced $SM_{CD44}$ model (i.e without the CD44 structure). Next, we describe the method used to identify numerically several common parameters in both models by using the CFSE data of OT-1 T cells [10]. Finally, we show the parameters and the simulations that we obtain from the models, and compare them with experimental data.

## 7.2 Materials and methods

### 7.2.1 Mathematical modeling

In the model of proliferation presented in [7, 10], the authors assume that cells undergo simple stochastic divisions. As with the Smith Martin model, in their model, cells are in one of two compartments that imprecise to resting (A-state) or dividing (B-phase) cells. Cells in A-state are considered to be non dividing cells in G0 state. These cells can then receive a stochastic trigger to enter the cell cycle (B-phase) at a rate captured by the parameter, $\lambda$. A reduction in $\lambda$ dependent on the number of cells (competition for resources) was achieved by making $\lambda = \lambda_0 \exp(-\eta N)$, with the parameter $\eta$ determining the size of the reduction caused by increasing the number of competing cells ($N$). In addition, $\lambda_0$ is considered to represent the ability of each clonotype to respond to an unlimited resource, $\eta$ can be considered to be proportional to the reciprocal of the resource availability, and N the total number of cells. The B-phase, the duration of which is described by the parameter $\Delta$, represents cells in G1, S, G2, and M stages of the cycle, before returning to G0 (A-state). The time spent in the A-state is exponentially distributed, such that each cell can make the $A \rightarrow B$ transition at a rate $\lambda$ (the

mean time for cells residing in A-state is $\frac{1}{\lambda}$). Then, the model is

$$(SM_1)\quad \begin{cases} \frac{dA_0}{dt} = -(\lambda(N)+\delta_A)A_0(t), \quad \{A_0(0)>0\} \\ \\ \frac{dA_i}{dt} = 2B_{i-1}(t,\Delta) - (\lambda(N)+\delta_A)A_i(t), \quad \{A_i(0)=0\},\ i=1,...,I \\ \\ \begin{cases} \frac{\partial}{\partial t}B_i(t,\tau) + \frac{\partial}{\partial \tau}B_i(t,\tau) = -\delta_B B_i(t,\tau),\ i=0,...,I \\ \\ B_i(t,0) = \lambda(N)A_i(t),\ B_i(0,\tau)=0 \end{cases} \end{cases}$$

where $(t,\tau)\in[0,T]\times[0,\Delta]$ and

$$N = N(t) := \sum_{i=0}^{I} N_i(t) := \sum_{i=0}^{I}\left(A_i(t) + \int_0^{\Delta} B_i(t,\tau)d\tau\right).$$

In the general case, cells are triggered from the A-state, to enter the proliferative phase, they spend in B-phase a time $\tau\in[0,\Delta]$ to divide. Proliferative cell divides into two daughter cells only when it completes the process of mitosis ($\Delta$ is approximately the time to finish the process). More specifically, when a cell divides, it disappears from the B-phase.
In $SM_1$ model, the Smith-Martin model describes the dynamics of cells that we have discussed in the previous paragraph, but the mother cells are not removed from the B-phase after dividing (see the right side of the PDE in $SM_1$ model) that is because their age become larger than $\Delta$. Indeed, since the age ($\tau$) is defined between 0 and $\Delta$, the mother cells with an age more than $\Delta$, are not counted in the dynamics, but in fact, they stay in B-phase. This means that $\Delta$ is not really the maximum age of cells in B-phase, as it is defined in $SM_1$ model.

On the other side, by integrating our $SM_{CD44}$ model with respect to variable $s$ (CD44 expression), we derive an age-structured system as $SM_1$ model but with

additional parameter $\mu(.)$. It reads

$$(SM_2)\quad \begin{cases} \frac{dA_0}{dt} = -(\lambda(N)+\delta_A)A_0(t), \quad \{A_0(0)>0\} \\ \\ \frac{dA_i}{dt} = 2\int_0^{\Delta}\mu(\tau)B_{i-1}(t,\tau)d\tau - (\lambda+\delta_A)A_i(t), \quad \{A_i(0)=0\},\ i=1,...,I \\ \\ \begin{cases} \frac{\partial}{\partial t}B_i(t,\tau)+\frac{\partial}{\partial \tau}B_i(t,\tau) = -(\delta_B+\mu(\tau))B_i(t,\tau),\ i=0,...,I \\ \\ B_i(t,0)=\lambda(N)A_i(t),\ B_i(0,\tau)=0 \end{cases} \end{cases}$$

where $A_i(t) := \int_0^m \tilde{A}_i(t,s)ds$, $B_i(t,\tau) := \int_0^m \tilde{B}_i(t,\tau,s)ds$ and $(\tilde{A}_i, \tilde{B}_i)$, $\forall\ i \in \mathbb{N}_I$ are the state variable of System (4.2-4.3).

In this $SM_2$ model, a function $\mu(.)$ is introduced in order to remove the mother cells from B-phase after dividing. Therefore, $\mu(\tau)$ represents the rate of cells which divided at age $\tau$ and have given rise to two daughter cells in the resting phase (A-state).

Note that if a cell divides only when its age is close to $\Delta$, the function $\mu$ can be approximated by a non-negative rectangular function with a mean value 1

$$\mu(\tau) = \begin{cases} \frac{1}{h} & \text{if } \Delta - h \leqslant \tau \leqslant \Delta, \\ \\ 0 & \text{else,} \end{cases}$$

where $0 < h << \Delta$.

Furthermore, the cumulative probability that a cell is still in B-phase at time $\tau$, having not divided ($\mu$) nor been killed ($\delta_B$) until this time point, is

$$\Pi(\tau) \quad = \quad e^{-\int_0^\tau(\delta_B+\mu(a))da},$$

and the cumulative probability that a cell has divided until time point $\tau$, is

$$d(\tau) \quad = \quad 1 - e^{-\int_0^\tau \mu(a)da}.$$

As in [10], the recruitment rate of cells from A-state into the B-phase is expressed in the following form for $SM_2$ and $SM_1$ models,

$$\lambda = \lambda(N(t)) = \lambda_0\, e^{-\eta\, N(t)}, \tag{7.1}$$

where $\lambda_0 > 0$ represents the ability of each clonotype to respond to an unlimited resource, and $\eta > 0$ determines the size of the reduction caused by increasing number of competing cells ($N$) [10].
In contrast to the $SM_1$ model, the model with the removal rate $\mu$ ($SM_2$ model) provides an overview of the incoming and outcoming fluxes of cells in A-state and B-phase. Then, the purpose here is to estimate numerically the parameters ($\Delta$, $\lambda_0$, $\eta$) of each models ($SM_1$ and $SM_2$) in order to evaluate the difference between $SM_1$ and $SM_2$ models caused by the function $\mu(.)$, and to identify which model fits better the data of Hogan et al. [10].

### 7.2.2 Parameter estimation

An important step in using the mathematical approach is the estimation of model parameters using experimental data. Let $N_{i,m}^{exp}(t_k)$ be the data set given in (Sec. 6.2) that represents the total cell number having undergone $i$ divisions at time $t_k$ in each mouse $m$. The parameters to estimate in $SM_1$ and $SM_2$ models are: $\vec{\theta} = (\lambda_0, \Delta, \eta)$. We used weighted sums of squared residuals ($SSRs$) for optimization with variance over observed cells with given $i$ at given day as the measurement error function.

### 7.2.3 Comparison of the models

Comparison of the different models ($SM_1$ and $SM_2$) was done using a cross validation approach. The whole data set (Sec. 6.2) was separated into two parts each day of the experiment: a validation set with data for one given mouse, $m$, and a training set with the remaining data ($M-1$) ($M$ is the total number of mice).
Parameter value were obtained by minimizing the $SSR$ with the training set.

$$SSR^{-m} = \sum_{i=0}^{I} \sum_{k=1}^{K} \sum_{\substack{j=1 \\ j \neq m}}^{M} \frac{\left(N_i(\vec{\theta}, t_k) - N_{i,j}^{exp}(t_k)\right)^2}{\sigma_i^2(t_k)} \tag{7.2}$$

where

$$N_i(\vec{\theta}, t_k) = \Delta t \left( A_i(t_k) + \Delta\tau \sum_{s=1}^{N_\tau} B_i(t_k, \tau^s) \right)$$

are calculated from $SM_1$ and $SM_2$ models. $\sigma_i^2(t)$, $\Delta t$ and $\Delta\tau$ are the variance and the mesh size of time and age respectively. Here, $i$ stands for the number of divisions

(total number $I = 8$), $k$ is the number of sampling day (with total number $K = 5$), $j$ is the number of mouse, $M$ is the total number of mice in the experiment ($M = 20$ for OT1 cells).
Indeed, we use an optimization algorithm (BCONF [99]) based on the quasi-Newton method to solve (7.2). Let us explain briefly this algorithm.

### Optimization algorithm

From a given starting point (vector) $\vec{\theta^c}$, an active set $IA$, which contains the indices of the variables at their bounds, is built. A variable is called a " free variable " if it is not in the active set. The routine then computes the search direction for the free variables according to the formula

$$d = -B^{-1}g^c$$

where $B$ is a positive definite approximation of the Hessian and $g^c$ is the gradient evaluated at $\vec{\theta^c}$; both are computed with respect to the free variables. The search direction for the variables in IA is set to zero. A line search is used to find a new point $\vec{\theta^n}$,

$$\vec{\theta^n} = \vec{\theta^c} + \lambda d$$

where $\lambda \in ]0, 1]$, such that

$$SSR^{-m}_{SM_j}(\vec{\theta^n}) \leq SSR^{-m}_{SM_j}(\vec{\theta^c}) + \alpha g^T d, \qquad \alpha \in (0, 0.5) \;\; and \;\; j = 1, 2$$

Finally, the optimality condition

$$\|g(\vec{\theta^n})\| \leq \epsilon, \quad \vec{Lower} < \vec{\theta^n} < \vec{Upper}$$

is checked, where $\epsilon$ is a gradient tolerance. When optimality is not achieved, B is updated according to the BFGS formula

$$B \longleftarrow B - \frac{Bss^TB}{s^TBs} + \frac{yy^T}{y^Ts}$$

where $s = \vec{\theta^n} - \vec{\theta^c}$ and $y = g^n - g^c$. Another search direction is then computed to begin next iteration.
The active set is changed only when a free variable hits its bounds during an iteration or the optimality condition is met for the free variables but not for all variables

in IA, the active set. In the latter case, a variable that violates the optimality condition will be dropped out of $IA$. For more details on the quasi-Newton method and line search, see Dennis and Schnabel [100].

At the next step, for each mouse $m$, the comparison reference value ($CrV$) criterion is calculated by using the estimated parameter values $\vec{\theta}^*$ using the validation set

$$CrV_m = \sum_{i=0}^{I} \sum_{k=1}^{K} \frac{\left(N_i(\vec{\theta}, t_k) - N_{i,m}^{exp}(t_k)\right)^2}{\sigma_i^2(t_k)}$$

The $CrV_m$ was calculated for each experimental mouse $m$ in the validation set. The final estimate of the cross validation was

$$CrV = \frac{1}{M} \sum_{m=1}^{M} CrV_m.$$

The lower value of $CrV$ indicates the better model.

## 7.3 Results

In the experiment, CFSE-labeled OT-1 T cells was transferred to $Rag1^{-/-}$ recipients by injection $1.5 \times 10^6$ cells mouse at the initial date (i.e $A_0(0) \simeq 1.5 \times 10^6$) and the rate of cell death ($\delta_A$ or $\delta_B$) observed was very close to zeros for OT-1 T cells [10]. We therefore omitted $\delta_A$ and $\delta_B$ from $SM_1$ and $SM_2$ models. In addition, the time division ($h$) is supposed here small ($h = 0.5$ hour) with respect to the age of cells in B-phase ($\Delta$ is estimated in hours [10]).
Best-fit parameters for $SM_1$ and $SM_2$ models were determined by minimizing weighted $SSR$ for LIP by OT-1 cells (Table 7.1).

| Model | $\eta$ | $\Delta$(hour) | $\lambda_0$ (/cell/hour) | $CrV$ |
|---|---|---|---|---|
| $SM_1$ | 1.00000E-06 | 8.51000 | 3.764693E-02 | 109.902 |
| $SM_2$ | 1.97568E-06 | 7.17858 | 3.768979E-02 | 48.0315 |

TABLE 7.1: Best-fit parameter estimations for $SM_1$ and $SM_2$ models.

Despite the constraining data sets, the parametrization in Table 7.1 ($\Delta$, $\eta$ and $\lambda_0$) of $SM_1$ model is close to those of the previous studies ([7, 10]). From Fig 7.1, the

$SM_1$ and $SM_2$ models were successful in describing LIP by OT-1 T cells as apparent in the predicted division profiles. Also despite the differences between the parameterization of $SM_1$ and $SM_2$ model, specific estimates of $\eta$ and $\lambda_0$ ($1.0E-06$ and $3.764693E-02$, respectively) of $SM_1$ were in close agreement with those of $SM_2$ ( $1.97568E-06$ and $3.768979E-02$, respectively).

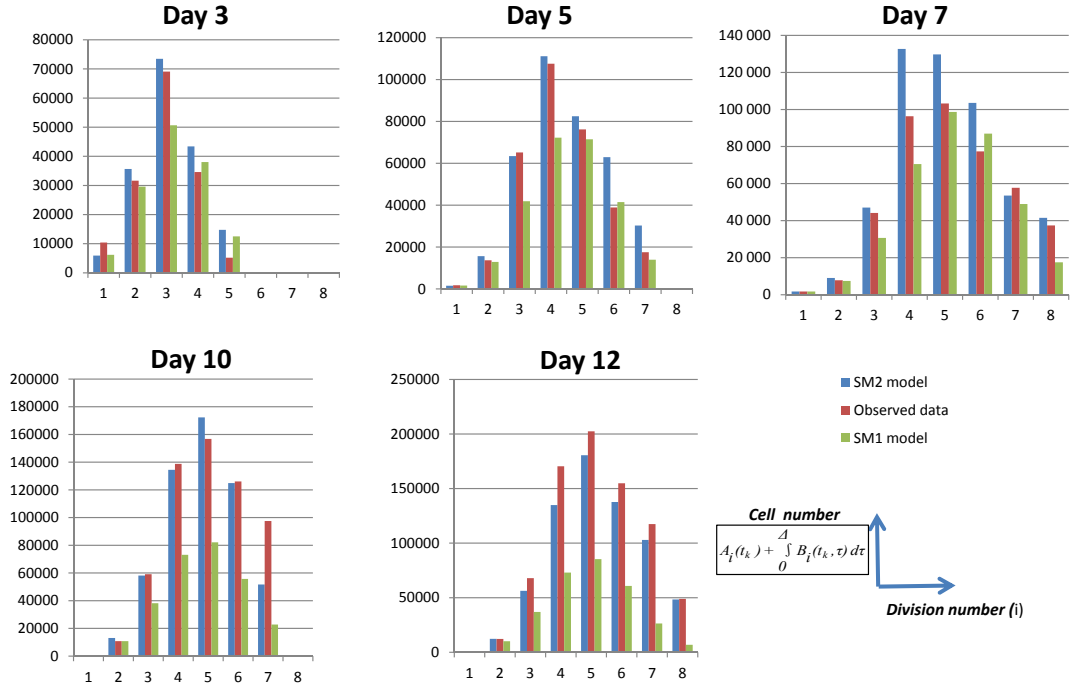


FIGURE 7.1: $SM_2$ model fits more the proliferation of OT-1 T cells than $SM_1$ model. Best-fit parameter estimates from $SM_1$ and $SM_2$ models (see Table 7.1) were used to predict the cell number in each division. At the indicated time points after transfer, data predicted by $SM_1$ (green) and $SM_2$ (blue) models were compared with experimental data for OT-1 cells (red).

In contrast, the small difference in the parametrizations of $SM_1$ and $SM_2$ was captured with distinct values for the parameter $\Delta$ (the duration of B-phase). The estimated value of $\Delta$ was higher for $SM_1$ (8.51 $h$) than $SM_2$ (7.17858 $h$). Then, the key parameter $\Delta$ is affected by taking into account the dynamic of the dividing cells. Therefore, it was important to compare $SM_2$ with $SM_1$ model. However, it was clear that LIP by OT-1 was better modeled with the $SM_2$ than $SM_1$ model, as reflected in the lower $CrV$ for $SM_2$ model fit (Table 7.1), which is a measure of goodness of fit (low is better).

## 7.4 Conclusion

In the literature, the most mathematical models based on Smith-Martin model assume that the cells divide in B-phase exactly at age $\Delta$. In contrast, the $SM_2$ model takes into account the small variability in the time of division of cells in B-phase, and eliminates the assumption of an immediate switch at time $\Delta$. In this chapter, we interest to compare these two types of modeling by fitting $SM_1$ and $SM_2$ models to the data of OT-1 T cells. By taking into account the small variability in the time of division, we remark that the duration of B-phase related to $SM_2$ model becomes shorter than this related to $SM_1$. In contrast, the rate of entry into division is approximately the same in these two models. Finally, we find that $SM_2$ model fits better the experimental data (CrV for $SM_2$ is much less than $SM_1$).

# Chapter 8

# Identification of the velocity of CD44 expression

**This chapter is based on the article [80].**

***Abstract.*** *The number of T Lymphocytes (T cells) in the body is under homeostatic control. At equilibrium, the majority of naive T cells are non-dividing and express low levels of the surface protein CD44. In conditions of T cell deficiency (lymphopenia), naive T cells enter into a proliferative phase, undergoing cell division accompanied by a subtle change in their surface expression of CD44. In this study, we use a mathematical modeling approach to analyse the proliferative response of transgenic T cells in lymphopenic conditions. Our nonlinear model is composed of ordinary differential equations and partial differential equations structured by age (maturity of cell) and CD44 expression. To better understand the evolution of CD44 expression on the surface of T cells during cell division, we present a numerical analysis to solve a parameter identification problem. Finally, we show the parameters and the simulations that we obtain from the model and compare them with experimental data.*

## 8.1 Introduction

Regulation by homeostatic mechanisms ensures that the number and functional diversity of peripheral T cells is maintained at an approximately constant level. However, under conditions of lymphopenia, disruption of the homeostatic balance

can induce naive T cells to undergo cell division. This lymphopenia induced proliferation (LIP) of naive T cells requires signal from cytokines such as IL-7 (Interleukine 7), and stimulation of the T cell receptor via interaction with self peptide [41]. Under the experimental conditions used in [7], it has been shown that the dividing F5 T cells retained a naive phenotype. However, for some T cells, LIP is accompanied by a transition to a memory-like phenotype [41] which is indicated by having a strong CD44 expression on their surface [32, 89].

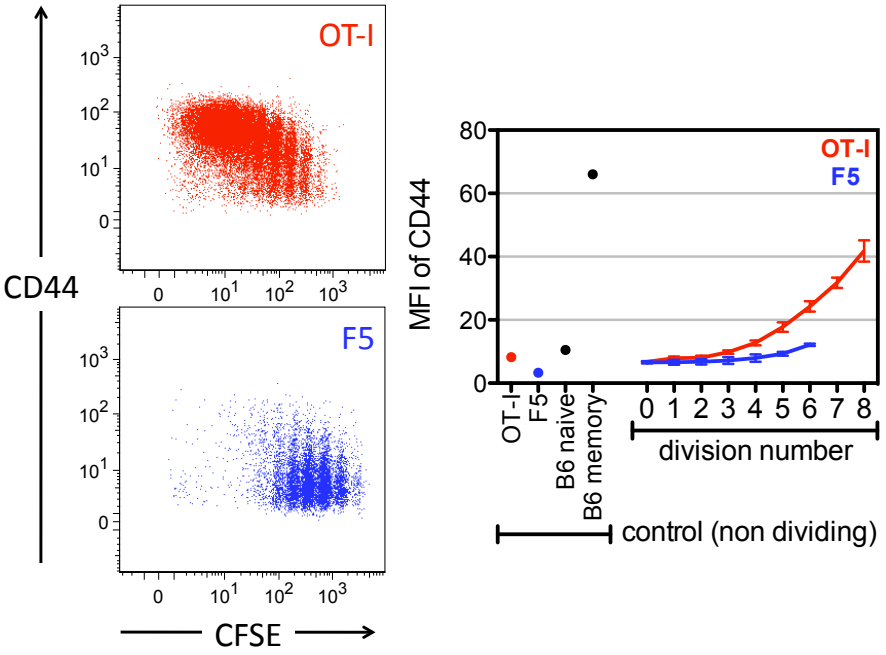


FIGURE 8.1: . Representative dot plots gated on $CD8$ lymphocytes show $CD44$ expression versus CFSE labeling in the lymph nodes of mice that received either OT-1 and F5 T cells (left panel). In the right panel, the evolution of CD44 expression versus division number for both OT-1 and F5 is presented here. Note that these figures make reference to the experimental data obtained and reported in [10].

Moreover, Hogan et al [10] have shown that the undivided OT-1 T cells expressed a similar level of CD44 to naive $CD8^+$ T cells, and began to upregulate expression of this marker after the$4^{th} - 5^{th}$ division in response to lymphopenia. F5 T cells, however, retained a low level of CD44 expression throughout division (see Fig 8.1). In addition, the experiment reported in [10] shows that the expression of CD44 by OT-1 T cells at approximately $5-6$ divisions in response to lymphopenia indicates the acquisition of a memory-like phenotype, which is not observed for F5 T cells under the same conditions.

In the present study, the velocity of CD44 up-regulation is the key parameter that distinguishes from which divisions OT-1 T cells can be considered as naive or memory through the mathematical model $SM_{CD44}$. The purpose of this chapter is then to

identify numerically this velocity in order to evaluate the prediction of our $SM_{CD44}$ model with respect to the observation of CD44 expression of OT-1 T cells stated in the previous paragraphs.

## 8.2 Parameter identification problem

In this section, we present our methodology for estimating the velocity $v_i(.)$ in $SM_{CD44}$ model that represents the extent of CD44 expression on the surface of cells during their divisions.

Note that this velocity depends on each level of CD44 that can be presented on the cells ($s$). So, it is much more relevant to interpret the average growth of CD44 per division (or implicitly per $\Delta$, since $\Delta$ is the duration of each division), which allows to compare the up-regulation of CD44 between the division number. Furthermore, according to [32, 89], memory cells are characterized by having a strong CD44 expression on their surface. Then, by estimating the parameters $v_i(s)$, we derive the mean growth of CD44 (average velocity) per division which allows us to distinguish from which division, the cells can be considered as memory cells.

*Remark* 8.1. In the experiment of Hogan et al. [10], several mice were sacrificed at each time point. Working with different mice at different time points generated additional variability making the identifiability of parameters more difficult. Therefore, we decided to work on a given time point. We chose 7 days because it was a good compromise between early days where there were too few divisions and later time points where CFSE is too much diluted to be very easily measured.

Let $N_{i,s}^{exp}$ be the total number of cells given by the experimental data set at day $T = 7$. In addition we denote by

$$D = \{s, \text{ where } N_{i,s}^{exp} \text{ is given by the experimental data } \}.$$

Furthermore, by integrating our model with respect to the variable $s$ (CD44 expression), one gets the $SM_2$ model. Therefore, we can use the estimated parameters $(\Delta, \lambda_0, \eta)$ from the previous chapter and then estimate the velocity $v_i(s)$, $i = 0..., I$.

Thus we want to minimize the cost function

$$[P] \quad \left\{ \min_{v\in K} \sum_{i=0}^{I} \sum_{s\in D} \left[ \Delta s \left( \int_0^{\Delta} B_i(T,\tau,s)d\tau + A_i(T,s) \right) - N_{i,s}^{exp} \right]^2 ,$$

where the constant $\Delta s$ is the mesh size of the CD44 expression, $B_i(T,\tau,s)$, $A_i(T,s)$ are given by (10.1-4.3) and $\{N_{i,s}^{exp}\}$ are the observed data. The parameters $(v_0,...,v_I)$ belong to the space $K = (\tilde{C}_+^{\bar{u}})^I$ where

$$\tilde{C}_+^{\bar{u}} = \{u \in C^0([0,m]),\ u(0) = 0,\ 0 \leq u(s) \leqslant \bar{u}\ ,\ \forall\ s \in ]0,m]\}.$$

### 8.2.1 The discrete parameter identification problem

Now, we define the parameter identification scheme and the algorithm to identify the velocity of CD44 up-regulation. The approximate problem of $[P]$ is defined by

$$[P_d] \quad \left\{ \min_{v_{N_s}\in K_{N_s}} J(v_{N_s}) := \min_{v_{N_s}\in K_{N_s}} \sum_{i=0}^{I} \sum_{k\in D} \left[ \Delta s \left( \Delta\tau \sum_{j=0}^{N_\tau} B_{j,k}^{i,N_T} + A_k^{i,N_T} \right) - N_{i,k}^{exp} \right]^2 .$$

The discrete vector $v_{N_s} \in K_{N_s}$ is the set of unknown parameters defined by $v_{N_s} = (v_{0,N_s},...,v_{I,N_s})$. It belongs to the space $K_{N_s} = (\tilde{C}_+^{\bar{u},N_s})^I$ where

$$\tilde{C}_+^{\bar{u},N_s} = \{u(s^k) = u^k,\quad u^0 = 0,\quad 0 \leq u^k \leqslant \bar{u},\quad k = 1,..,N_s\}.$$

That is an approximate finite dimensional compact set of $K$. Hence, one obtains the following result.

**Theorem 8.2.** *Under Assumption 5.3.1 and condition (5.3), the problem $[P_d]$ admits at least one optimum.*

*Proof.* Let $d < \infty$ be the lower bound of the cost function $J(v_{N_s})$. Let $\{v_{N_s}^h\}_{h\geqslant 0}$, be a minimizing sequence on the space $K_{N_s}$, such that

$$d < J(v_{N_s}^h) \leqslant d + \frac{1}{h}.$$

The value of the cost function at the point $v^h_{N_s} = (v^h_{0,N_s}, ..., v^h_{I,N_s})$ is given by

$$J(v^h_{N_s}) = \sum_{i=0}^{I} \sum_{k\in D} \left[ \Delta s \left( \Delta\tau \sum_{j=0}^{N_\tau} B^{i,N_T}_{j,k}(v^h_{i,N_s}) + A^{i,N_T}_{k}(v^h_{i,N_s}) \right) - N^{exp}_{i,k} \right]^2,$$

where $B^{i,N_T}_{j,k}(v^h_{i,N_s})$ and $A^{i,N_T}_{k}(v^h_{i,N_s})$ are the solution of (5.2)-(5.1).
The sequence $\{v^h_{N_s}\}_h$ is bounded. According to the Bolzano-Weierstrass theorem, one can extract a subsequence, termed $\{v^{h_r}_{N_s} = (v^{h_r}_{0,N_s}, ..., v^{h_r}_{I,N_s})\}_{r\geqslant 0}$, which converges to $v^*_{N_s} = (v^*_{0,N_s}, ..., v^*_{I,N_s})$ on the space $K_{N_s}$. Then by using Lemma 5.7, one obtains

$$\begin{aligned} |B^{i,n}_{j,k}(v^h_{i,N_s}) - B^{i,n}_{j,k}(v^*_{i,N_s})| &\leqslant C_{B^i} |v^h_{i,N_s} - v^*_{i,N_s}| \underset{h\to+\infty}{\longrightarrow} 0, \quad \forall \ \ i \in \mathbb{N}_I := \{0, ..., I\}, \\ |A^{i,n}_{k}(v^h_{i-1,N_s}) - A^{i,n}_{k}(v^*_{i-1,N_s})| &\leqslant C_{A^i} |v^h_{i-1,N_s} - v^*_{i-1,N_s}| \underset{h\to+\infty}{\longrightarrow} 0, \quad \forall \ \ i \in \mathbb{N}^*_I := \{1, ..., I\}. \end{aligned}$$

Therefore, one deduces

$$\begin{aligned} J(v^h_{N_s}) &= \sum_{i=0}^{I} \sum_{k\in D} \left[ \Delta s \left( \Delta\tau \sum_{j=0}^{N_\tau} B^{i,N_T}_{j,k}(v^h_{i,N_s}) + A^{i,N_T}_{k}(v^h_{i,N_s}) \right) - N^{exp}_{i,k} \right]^2 \\ &= \sum_{i=0}^{I} \sum_{k\in D} \left[ \Delta s \left( \Delta\tau \sum_{j=0}^{N_\tau} \left[ \left( B^{i,N_T}_{j,k}(v^h_{i,N_s}) - B^{i,N_T}_{j,k}(v^*_{i,N_s}) \right) + B^{i,N_T}_{j,k}(v^*_{i,N_s}) \right] \right. \right. \\ &\quad \left. \left. + \left( A^{i,N_T}_{k}(v^h_{i,N_s}) - A^{i,N_T}_{k}(v^*_{i,N_s}) \right) + A^{i,N_T}_{k}(v^*_{i,N_s}) \right) - N^{exp}_{i,k} \right]^2 \\ &\underset{h\to+\infty}{\longrightarrow} \sum_{i=0}^{I} \sum_{k\in D} \left[ \Delta s \left( \Delta\tau \sum_{j=0}^{N_\tau} B^{i,N_T}_{j,k}(v^*_{i,N_s}) + A^{i,N_T}_{k}(v^*_{i,N_s}) \right) - N^{exp}_{i,k} \right]^2 = J(v^*_{N_s}) = d. \end{aligned}$$

□

To numerically solve problem $[P_d]$, we use an optimization algorithm based on the Quasi-Newton method (see [101]). This algorithm needs to compute the adjoint variables and the gradient of the cost function.

In the following, we consider the Lagrangian formulation of $[P_d]$ that is

$$\begin{aligned}
L(W) \quad &= \sum_{i=0}^{I}\sum_{k=0}^{N_s}\gamma_D^k\left[\Delta s\left(\Delta\tau\sum_{j=0}^{N_\tau}B_{j,k}^{i,N_T}+A_k^{i,N_T}\right)-N_{i,k}^{exp}\right]^2\\
&+\sum_{n=1}^{N_T}\sum_{k=0}^{N_s}\left[A_k^{0,n}-\frac{A_k^{0,n-1}}{1+\Delta t\delta_A+\Delta t\lambda^n}\right]P_k^{0,n}\\
&+\sum_{i=1}^{I}\sum_{n=1}^{N_T}\sum_{k=0}^{N_s}\left[A_k^{i,n}-\frac{A_k^{i,n-1}+2\Delta t\Delta\tau\sum_{j=1}^{N_\tau}\mu^{j-1}B_{j-1,k}^{i-1,n-1}}{1+\Delta t\delta_A+\Delta t\lambda^n}\right]P_k^{i,n}\\
&+\sum_{i=0}^{I}\sum_{n=1}^{N_T}\sum_{j=1}^{N_\tau}\sum_{k=1}^{N_s}\left[B_{j,k}^{i,n}-\frac{(1-\frac{\Delta t}{\Delta s}v_i^k)B_{j-1,k}^{i,n-1}+\frac{\Delta t}{\Delta s}v_i^{k-1}B_{j-1,k-1}^{i,n-1}}{1+\Delta t\delta_B+\Delta t\mu^j}\right]Q_{j,k}^{i,n}\\
&+\sum_{i=0}^{I}\sum_{n=1}^{N_T}\sum_{k=0}^{N_s}\left[B_{0,k}^{i,n}-\lambda^{n-1}A_k^{i,n-1}\right]Q_{0,k}^{i,n},
\end{aligned}$$

where the vector $W=(W_0,...,W_I)$, with $W_i=(v_i,A^i,B^i,P^i,Q^i)$ for all $i=0,...,I$. The variable $(P^i,Q^i)$ corresponds to the dual variables. $\gamma_D^k$ is a function in the following form

$$\gamma_D^k=\begin{cases}1 & \text{if } k\in D\\ \\ 0 & \text{else}\end{cases}$$

The first derivative of the Lagrangian with respect to $A_k^{i,n}$ and $B_{j,k}^{i,n}$ gives us the adjoint equations.

For $i=I,...,0$; $n=N_T-1,...,0$; $j=N_\tau-1,...,0$ and $k=0,...,N_s-1$, one has

$$\begin{cases}
Q_{j,k}^{i,n}=\frac{(1-\frac{\Delta t}{\Delta s}v_i^k)Q_{j+1,k}^{i,n+1}+\frac{\Delta t}{\Delta s}v_i^kQ_{j+1,k+1}^{i,n+1}}{1+\Delta t\delta_B+\Delta t\mu^{j+1}}+\gamma_{[0,I-1]}^i\frac{2\Delta t\Delta\tau\mu^jP_k^{i+1,n+1}}{1+\Delta t\delta_A+\Delta t\lambda^{n+1}}\\
P_k^{i,n}=\frac{P_k^{i,n+1}}{1+\Delta t\delta_A+\Delta t\lambda^{n+1}}+\lambda^nQ_{0,k}^{i,n+1}\\
Q_{j,k}^{i,N_T}=2\gamma_D^k\Delta s\Delta\tau\left[N_{i,k}^{exp}-\Delta sA_k^{i,N_T}-\Delta s\Delta\tau\sum_{j=0}^{N_\tau}B_{j,k}^{i,N_T}\right]\\
P_k^{i,N_T}=2\gamma_D^k\Delta s\left[N_{i,k}^{exp}-\Delta sA_k^{i,N_T}-\Delta s\Delta\tau\sum_{j=0}^{N_\tau}B_{j,k}^{i,N_T}\right]\\
Q_{N_\tau,k}^{i,n}=Q_{j,N_s}^{i,n}=0
\end{cases}\tag{8.1}$$

where $[0, I-1] := \{0, ..., I-1\}$.

The first derivative of the Lagrangian with respect to $v_{i_0}^{k_0}$ are : $\forall\ k_0 = 0, ..., N_s - 1$ and $i_0 = 0, ..., I$.

$$\frac{\partial L}{\partial v_{i_0}^{k_0}} = \sum_{n=1}^{N_T} \sum_{j=1}^{N_\tau} \frac{\frac{\Delta t}{\Delta s} B_{j-1,k_0}^{i_0,n-1} \left[ Q_{j,k_0}^{i_0,n} - Q_{j,k_0+1}^{i_0,n} \right]}{1 + \Delta t \delta_B + \Delta t \mu^{j-1}} \tag{8.2}$$

and

$$\frac{\partial L}{\partial v_{i_0}^{N_s}} = \sum_{n=1}^{N_T} \sum_{j=1}^{N_\tau} \frac{\frac{\Delta t}{\Delta s} B_{j-1,N_s}^{i_0,n-1} Q_{j,N_s}^{i_0,n}}{1 + \Delta t \delta_B + \Delta t \mu^{j-1}} \tag{8.3}$$

The (BCONG/BCONF) routine of IMSL minimizes a function of $n$ variables subject to bounds on the variables using the BFGS quasi-Newton method [99]. To numerically solve problem $[P_d]$, we use this routine. The strategy can be summarized in the following algorithm

#### 8.2.1.1 Algorithm

1- ***Input*** $I$, $N_T$, $N_\tau$, $N_s$, $\lambda_0$, $\eta$, $\Delta t = \Delta\tau, \Delta s$.

2- *Set initial guess* $v^{g_0} = (v_0^{g_0}, ..., v_I^{g_0})$ *for the velocity* $v_0 = (v_{0,0}, ..., v_{0,I})$.

3- *Build a* ***subroutine*** *to calculate* $(A_i, B_i)$, $\forall\ i = 0, ..., I$ *from (5.1) and (5.2).*

4- *Build a* ***subroutine*** *to calculate* $(P_i, Q_i)$, $\forall\ i = 0, ..., I$ *from (8.1).*

5- *Build a* ***subroutine*** *to calculate the cost function* $(J)$ *by calling the subroutine in 3.*

6- *Build a* ***subroutine*** *to calculate the gradient (8.2-8.3) by calling the subroutines in 3 and 4.*

7- ***Call BCONG*** *in subject to find* $v_0 = (v_{0,0}, ..., v_{0,I})$ *by using the subroutines in 5 and 6.*

8- ***Return*** $v_0 = (v_{0,0}, ..., v_{0,I})$.

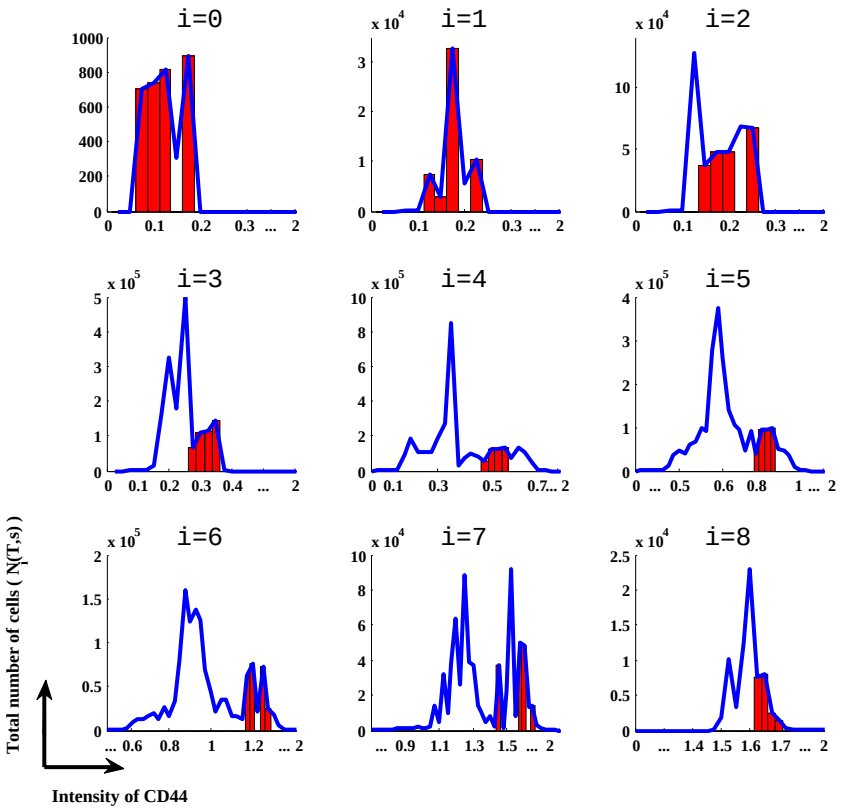


FIGURE 8.2: The vertical axis represent the total number of cells $\left(N_i(T,s) := \Delta s \int_0^{\Delta} B_i(T,\tau,s)d\tau + \Delta s A_i(T,s)\right)$ as a function of the intensity of CD44 (i.e normalised median fluorescence intensity (MFI) of CD44) in each division ($i$). The solid line depicts the predictions of the model and the bar depicts the observed data. Note that the horizontal axis is zoomed in each sub-figure in order to improve the illustration clarity.

## 8.3 Numerical results

In this section, we present the numerical results for the velocity by using our numerical method defined in the previous section. As in Chapter 7, the rate of entry into cell division ($\lambda$) was a function of the size of the T cells compartment. The dependence was chosen as $\lambda = \lambda_0 e^{-\eta N(t)}$. Also, the rate of cells which divided at

age $\tau$, is expressed in the following form

$$\mu(\tau) = \begin{cases} \frac{1}{h} & if \quad \Delta - h \leqslant \tau \leqslant \Delta, \\ \\ 0 & else, \end{cases} \tag{8.4}$$

where $h = 30$ mn is the time division before age $\Delta$.
In addition, the choice of some numerical and optimization parameters $(\lambda_0, \eta, \Delta)$ follows the parameters value estimated in the previous chapter 7. The mortality ($\delta_A$ and $\delta_B$) was considered null because no death was observed [10]. According to Materials and Methods in [10], the initial number of cells is approximately 1.5 million cells per mouse having low intensities of CD44, but their distribution according to the CD44 expression is unknown. In this study, we assume that the cells are distributed homogeneously over an interval of small intensity of CD44. It is expressed in the following form

$$A_0(0, s^k) = \begin{cases} 8 \times 10^4 & if\ 0.075 \leqslant k \leqslant 0.12, \\ \\ 0 & else. \end{cases} \tag{8.5}$$

where $\sum_{k=0}^{N_s} A_0(0, s^k) \simeq 1.5 \times 10^6$ cells.

By using the algorithm in the previous section, we observe in Fig. 8.2 that the model fits well the experimental data. Indeed, the cells are up-regulating CD44 during B-phase. In $A_i$ phase (i.e ith division in A-state), cells inherit the same intensity of CD44 of those that have divided in the previous B-phase ($B_{i-1}$ phase). In Fig. 2, the total cell number $N_i(T, s)$ depends on the number of cells in $B_i$ phase for all ages ($\int_0^\Delta B_i(T, \tau, s)d\tau$), and implicitly on the divided cells that come from $B_{i-1}$ phase (i.e the mothers cells in $B_{i-1}$ phase, give the same intensity of CD44 to the daughter cells that enter immediately in $A_i$ phase). Then, the peaks predicted by the model in Fig. 8.2, are due to this complex relationship between A-state and B-phase over the division number.
To clarify this relationship, we show in Fig. 8.3 the dynamic of cells in $B_i$ phase at day 7 with respect to their intensity of CD44 and their age, for all $i = 0, ..., 8$. "$(j)$" depicts in Fig. 8.3, the peak $j$ in each sub-figure ($j = 0, .., 12$). The dashed arrow shows that there remains cells from peak "$(j)$" (by increasing their age).

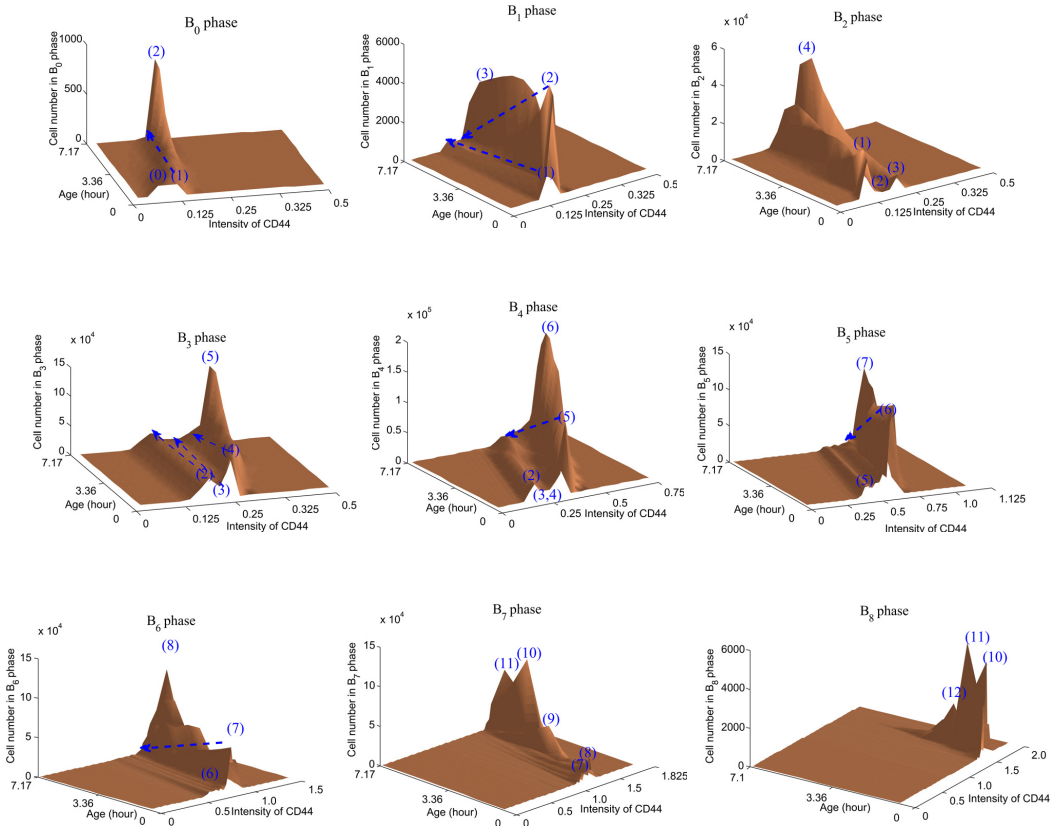


FIGURE 8.3: Dynamic of cells in $B_i$ phase (i.e ith division in B-phase) at day 7. Z-axes depict the number of cells in B-phase ($B_i(T,\tau,s)$) as a function of their intensity of CD44 (x-axes) and their age (Y-axes) in each division ($i$). The intensity of CD44 is the weight of CD44 expression (normalised median fluorescence intensity) on the surface of cells in each division ($s \in [0,m]$ and $m=2$). Note that the scale on the x-axis, is zoomed in each sub-figure in order to improve the illustration clarity. The maximum age of cells ($\Delta$) in B-phase is estimated in the previous chapter 7 by 7.17 hour. "$(j)$" represents the peak $j$ in each sub-figure ($j=0,..,12$). The dashed arrow indicates that there remains cells from peak "$(j)$" (by increasing their age).

In Fig. 8.3 ($B_0$ phase), the number of newborn cells "(0)" and "(1)", decreases over age because they change their level of CD44, which allow to appear new peak "(2)". Note that this new peak has been validated by the experimental data (see last bar in Fig. 8.2 ($i=0$)). Typically, in Fig. 8.3 ($B_1$,..., $B_8$ phases), the peaks in $B_{i-1}$ phase are reproduced in $B_i$ phase in the form of peaks which depict the newborn cells (the mother cells in $B_{i-1}$ phase will divide and give rise to two daughter cells that enter immediately in $A_i$ phase where some of these daughter cells will be recruited in $B_i$ phase, as newborn cells). Moreover, the number of newborn cells, decreases or stabilizes (e.g "(1)" in $B_1$ phase and "(2), (3)" in $B_3$ phase) over age, since it depends on their capacity to change their CD44 expression in each division. In case of decrease, some peaks increases or new peak appears. Taken together Fig. 8.2 and Fig. 8.3, we remark that the appearance of new peaks in some panel (e.g "(3)", "(4)", "(5)", "(7)", "(8)", "(11)", "(12)" in $B_1$, $B_2$, $B_3$, $B_5$,...,$B_8$ phases respectively) is observed by the experimental data (see the last bars in Fig. 8.2 ($i=1,2,3,5,...,8$)). Therefore, the highest peaks predicted by the model where

there was no experimental data to support them ($i = 3, ..., 8$ in Fig. 8.2), return implicitly to those of the previous divisions where they have been observed in some panel by the experimental data.

Before discussing biologically the velocity obtained, we must prove the robustness of our algorithm. For this reason, we modify the initial velocity $v^g$ in order to calculate the cost function and the relative error on the estimated parameters (see Table 11.2). We remark from this table that the error is negligible by changing the

TABLE 8.1: **The algorithm is independent of the initialisation** $(v^{g_0})$**.**

| Cost function | Value |
|---|---|
| $J_\theta(v_0; v^{g_0})$ | 0.5254 |
| $J_\theta(v_1; v^{g_1})$ | 0.5695 |
| $J_\theta(v_2; v^{g_2})$ | 0.5961 |

| $i$ | $\xi_i(v_{0,i}, v_{1,i})$ | $\xi_i(v_{0,i}, v_{2,i})$ |
|---|---|---|
| 0 | $2.0570E-05$ | $3.9715E-05$ |
| 1 | $2.5403E-05$ | $2.5101E-05$ |
| 2 | $7.2569E-05$ | $3.3016E-05$ |
| 3 | $2.7315E-04$ | $4.7416E-07$ |
| 4 | $4.5836E-05$ | $4.0277E-05$ |
| 5 | $1.1171E-04$ | $1.7949E-05$ |
| 6 | $1.4370E-04$ | $1.4737E-04$ |
| 7 | $5.8189E-04$ | $6.6271E-05$ |
| 8 | $3.3944E-04$ | $3.2401E-04$ |

*The notation $(v_m, v^{g_m})$ represents the velocity estimated $v_m = (v_{m,0}, ..., v_{m,I})$ with an initialization $v^{g_m} = (v_0^{g_m}, ..., v_I^{g_m})$, $\forall\ m = 0, 1, 2$. In this test, we suppose an initialization $v_i^{g_0}$. We took $v_i^{g_1}(s) = random \times v_i^{g_0}(s)$ and $v_i^{g_2}(s) = random \times v_i^{g_0}(s)$, for $s \in [0, m]$ and $i = 0, ..., I$ (i is the division number). On the left, the tabular represents the cost functions given by $[P_\theta]$ with a different initialisation $(v^{g_0}, v^{g_1}, v^{g_2})$. On the right, $\xi_i(v_{0,i}, v_{m,i})$ is the calculated error between the velocity $v_{0,i}$ and $v_{m,i}$, $\forall\ m = 1, 2$. This error is equal to $\frac{\|v_{0,i} - v_{m,i}\|_2}{\|v_{0,i}\|_2}$, $\forall\ m = 1, 2$ and for $i = 0, ..., I$.*

initial velocity. Therefore we can conclude that our algorithm is independent of the initial velocity.

In addition, we identified the velocity in each division by using the data available in [10]. The purpose here was to evaluate the reliability of the estimates. Indeed biological datasets usually contain noise and measurement errors, and they are seldom complete. For this reason, we tested our estimated parameters by adding random noise to the experimental data. After repeating the inverse problem to find the new parameters, we calculate the relative error between the estimated parameters obtained by the noisy data and the data without noise. This allows us to evaluate the loss due to random noise and we can see if our algorithm can accommodate the

TABLE 8.2: **The algorithm supports the noisy data.**

| Error ╲ Noise | 1% | 2% | 3% | 4% | 5% | 6% |
|---|---|---|---|---|---|---|
| $\varsigma_0$ | 0.0110 | 0.0148 | 0.0191 | 0.0038 | 0.0051 | 0.0075 |
| $\varsigma_1$ | 0.0180 | 0.0177 | 0.0187 | 0.0165 | 0.0157 | 0.0154 |
| $\varsigma_2$ | 0.0099 | 0.0011 | 0.0359 | 0.0083 | 0.0020 | 0.0355 |
| $\varsigma_3$ | 0.0107 | 0.0076 | 0.0148 | 0.0161 | 0.0189 | 0.0085 |
| $\varsigma_4$ | 0.0025 | 0.0050 | 0.0151 | 0.0103 | 0.0124 | 0.0151 |
| $\varsigma_5$ | 0.0062 | 0.0128 | 0.0154 | 0.0235 | 0.0334 | – |
| $\varsigma_6$ | 0.0063 | 0.0129 | 0.0006 | 0.0118 | 0.0011 | 0.0133 |
| $\varsigma_7$ | 0.0392 | 0.0693 | 0.0372 | 0.0375 | 0.0385 | 0.0390 |
| $\varsigma_8$ | 0.0379 | 0.0392 | 0.0406 | 0.0425 | 0.0446 | 0.0475 |

*$\varsigma_i$ is the relative error on the estimated parameters caused by a random noise in the data.* $\varsigma_i = \frac{\|v_i - v_i^*\|_2}{\|v_i\|_2}$, *where* $v_i^*$ *is the velocity estimated by using the noisy data. Noisy data* $= N_{i,k}^{exp} + \phi_i \times rand_i(k)$, *where % of noise* $= \frac{\phi_i}{\sum_{k\in D} N_{i,k}^{exp}}$ *and* $-1 \leqslant rand_i(k) \leqslant 1$ *for* $k \in D$, $i = 0, ..., I$.

noise. We show in Table 8.2 the relative error $\varsigma_i$ for $i = 0, ..., I$. We remark that the error is very small. This allows us to conclude that the noise slightly affects the identified velocity.

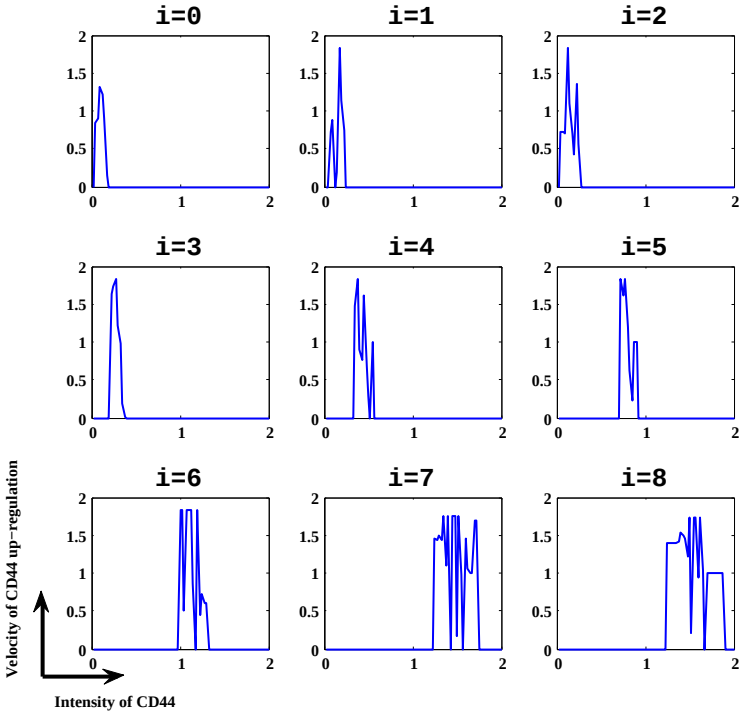


FIGURE 8.4: The velocity (vertical axis) as a function of the observed intensity of CD44 (i.e intensity of fluorescence CD44) in each division ($i$) by using the parameters $(\Delta, \lambda_0, \eta)$ estimated in the previous chapter.

Fig. 8.4 shows the numerical result of the identified velocity according to the observed intensity of CD44 in each division.

Naive cells in A-state are recruited to enter the B-phase, and the evolution of CD44 on the surface of these cells is undergone during the proliferative B-phase. From Fig. 8.3 and 8.4, we observe that some cells may divide without increasing CD44 expression, and other cells increase CD44 by dividing. In cells with few divisions, the cells with the lowest CD44 expression were those with the highest velocity of CD44 expression whereas, amongst cells that have experienced numerous divisions, cells with the highest level of CD44 also had the highest velocity.

To compare the extent of up-regulation of CD44 expression between the divisions,

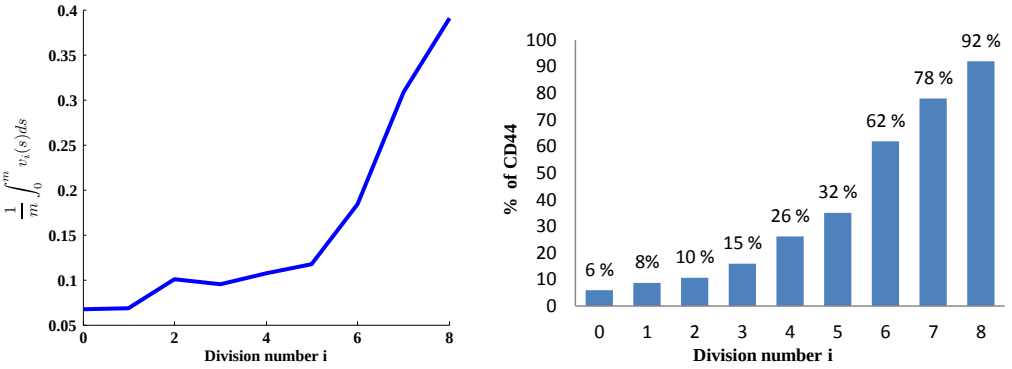


(8.5a) (8.5b)

FIGURE 8.5: (8.5a) represents the intrinsic average of CD44 upregulation as a function of division number $i$. (8.5b) depicts the percentage of CD44 measured on the surface of cells having undergone $i$ divisions. According to Materials and Methods in [10], the intensity of CD44 (MFI of CD44) was measured on the surface of T cells for each mouse analysed (between three and five host mice were analysed at each day of the experiment), and separated according to the number of divisions performed as assessed by CFSE labelling. Fig. (8.5b) is drawn by calculating the average percentage of CD44 at division $i$, relative to the different mice analysed in the experiment.

we show in Fig. 8.5a the intrinsic average velocity as a function to the division number. We note that the average velocity stabilizes between the division 0 and 5. After division 5, it appears that this average velocity of CD44 plummets. Furthermore, we show in Fig. 8.5b, the percentage of the average median fluorescence intensity (MFI) of CD44 measured in each division. We remark that this percentage of CD44 is 32% at division 5, which next is hugely increased at division 6-8 (62%, 78%, 92%). This validates the large increase in the average velocity after division 5 (Fig. 8.5a). Then, we conclude that the cells from the division 6, increase hugely the CD44 expression on their surface (CD44+) (this is consistent with Figs. 8.2 and 8.3). Therefore, these cells are probably switching to memory phenotype [32, 89].

In Fig. 8.6, the number of cells that have changed their CD44 in $B_i$ phase (solid

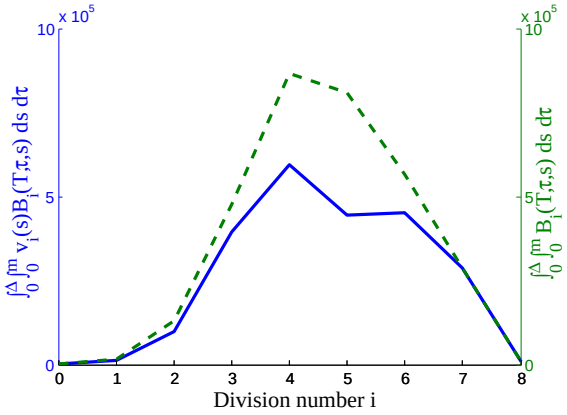


FIGURE 8.6: Number of cells that have changed their CD44 expression (solid line) as a function of the total cell number in $B_i$ phase (dashed line) at day 7.

line) and the total number of cells in $B_i$ phase (dashed line) are presented. We remark that the number of cells being able to change their level of CD44 (solid line), increases over division 0-4. Thereafter ($i > 4$), the total cell number in B-phase (dashed line) decreases due to the limited cell number that can reach the maximum division number ('8') observed by the experimental data. This implies the decrease of the number of cells that have changed their CD44.

Furthermore, the majority of cells changing their CD44 expression level is at the number of divisions where the dashed and the solid line overlay each other. In the series of first divisions (0-5), the number of cells that have changed their level of CD44 (solid line), decreases according to the total cell number (dashed line) in each division (i.e the difference between the solid line and the dashed line, becomes thicker with respect to division number 0-5). Later on, it appears that the majority of cells that enter $B_6$,...,$B_8$ phases, have a large capacity to modify their level of CD44 with a maximum at division 7-8 (this is consistent with Fig. 8.3). Precisely, 54% of cells modifies their level of CD44 expression at division 5. In contrast, at division 6-8, a large number of cells change their CD44 expression (80% for division 6 and 100% for divisions 7 and 8). Taken together Fig. 8.5a and Fig. 8.6, we conclude that the majority of cells with a memory phenotype undergo a change in their CD44 expression.

## 8.4 Discussion and Conclusion

T cell division depends on TCR signalling but results in distinct patterns of proliferation and differences in development of effector function for many cells. Several

studies have successfully used mathematical modelling to describe the proliferative response of F5 and OT-1 T cells to lymphopenia ([7, 10]) and greatly facilitated our understanding of the cell cycle control involved. Moreover, these studies have not taken into account the concept of phenotype that characterizes the memory-like phenotype during the homeostatic process. Indeed, the CD44 is an established marker that identifies the transition of T cells from naive to memory phenotype through LIP [18]. In this chapter, we use the mathematical model $SM_{CD44}$ to better understand the program of cell division through LIP of OT-1 T cells. A velocity is introduced in $SM_{CD44}$ model to describe the up-regulation of CD44 expression during the T cell division. In general, the CD44 expression is approximately increased on the surface of cells during B-phase before the mitosis is complete. Then, this velocity can depend on the level of CD44 presented on the surface of cells and the division number undergone by these cells.

An important modification in the manner of identifying T cells at a specific stage of cell cycle (CFSE label with 7AAD) allows us to obtain information about the intensity of CD44 on the surface of T cells in each division [10]. By applying this new type of data on our model, we find that we can identify the velocity of CD44 expression. The fit of our model to the observed data of CD44 is simplified by using the other parameters $(\Delta, \lambda_0, \eta)$ from the previous chapter 7. The identified velocity (Fig. 8.4) allows to derive the average growth of CD44 (Fig. 8.5a), which indicates the large increase in the intensity of CD44 after division 5.

Furthermore, this average velocity (Fig. 8.5a) and the frequency of cells that have changed their CD44 expression profile with respect to the total number of cells (Fig. 8.6), are the keys to explain the transition of cells from naive to memory phenotype. However, these important keys enable us to deduce that the cells which are the most likely switching to memory phenotype, are those that have divided 6 times or more. These numerical results are very close to the observations stated in the introduction of this chapter. This means that the $SM_{CD44}$ model gives a good prediction of the number of divisions needed by the cells to acquire memory-like phenotype. In conclusion, $SM_{CD44}$ model not only provides some remarkably description of lymphopenia induced proliferation by T cells but also may be a new path to better explain the complex relationship between LIP and naive to memory transition.

# Chapter 9

# Identification of the recruitment rate and the rate of division

## 9.1 Introduction

Despite great advances in immunological research during the last decades, relatively little is known about the quantitative characteristics of lymphocyte population kinetics. For example in the literature, the rate of entry into the proliferative phase and the division rate are considered to be independent of the level of CD44 on the surface of cells. Otherwise, it is well known that the CD44 is not only a marker that identifies the transition of cells from naive to memory phenotype, it also participates in a wide variety of cellular functions including lymphocyte activation, recirculation and homing. Hence, the proliferation and the division of T cells can depend on the CD44 expression located on their surface (i.e. the resting cells enter the proliferative phase and divide according to their level of CD44). For these reasons, we are interested in this chapter to connect the CD44 expression with the quantitative characteristics (i.e. proliferation and division of T cell) of T cell population.
This chapter is divided in two sections. In the first one, we assume that the rate of entry into division is dependent on the intensity of CD44 located on the surface of cells. Then, we identify together this rate of entry into division and the velocity of CD44. In the second one, we assume that the rate of division is dependent on the intensity of CD44 and then we identify only this rate of division by using the other estimated parameters from the previous Chapters 7 and 8 .

## 9.2 Estimating the recruitment rate and the velocity of CD44

As a consequence of the numerical results of the previous chapter, the cells which are the most likely to switch to memory phenotype, are those that have divided 6 times or more. This means that there exists a link between the naive/memory cells (CD44 low/high), and their number of divisions. Thus, by combining this interpretation with the introduction of this chapter, one may assume that the recruitment rate ($\lambda$) is dependent on the total population ($N$), on the CD44 expression ($s$) and on the number of divisions ($i$) undergone by cells. Precisely, it can be expressed in the following form

$$\lambda^i(s,N) = \lambda_0^i(s)e^{-\eta N}, \quad \forall\ s \in [0,m] \ and\ i \in \mathbb{N}_I. \tag{9.1}$$

where $\lambda_0^i(s)$ can be described as the ability of cells to respond to an unlimited resource according to their level of CD44 ($s$) and their division number ($i$).
In what follows, we denote by $SM_{CD44}^{\lambda_0^i}$, the model $SM_{CD44}$ when we consider the recruitment rate as the previous form (9.1).

In this section, we identify together the velocity of CD44 up-regulation ($v_i$) and the parameters ($\lambda_0^i(s)$) by using the other parameters estimated and assumed ($\Delta$, $\eta$, $\mu$, $A_{0,0}(.)$) in the previous chapter.

### 9.2.1 Parameter identification problem

The identification of the parameters $\lambda_0^i$ and $v_i$, $\forall\ i \in \mathbb{N}_I := \{0,...,I\}$ together consists in minimizing the following cost function

$$[P^1] \quad \left\{ \min_{(v,\lambda_0)\in K\times K} \sum_{i\in\mathbb{N}_I}\sum_{s\in D}\left[\Delta s\left(\int_0^\Delta B_i(T,\tau,s)d\tau + A_i(T,s)\right) - N_{i,s}^{exp}\right]^2,\right.$$

where the constant $\Delta s$ is the mesh size of the CD44 expression, $B_i(T,\tau,s)$ and $A_i(T,s)$ are given by $SM_{CD44}^{\lambda_0^i}$ model, and $\{N_{i,s}^{exp}\}$ are the observed data at day $T=7$ described in Chapter 8. The parameters $v=(v_0,...,v_I)$ and $\lambda_0=(\lambda_0^0,...,\lambda_0^I)$

are defined in the space $K = (\tilde{C}_+^{\bar{u}})^I$ where

$$\tilde{C}_+^{\bar{u}} = \{u \in C^0([0,m]),\ u(0) = 0,\ 0 \leq u(s) \leqslant \bar{u}\ ,\ \forall\ s \in ]0,m]\}.$$

In what follows in this section, we use the same strategy of the previous chapter 8.

### 9.2.2 The discrete parameter identification problem

The approximation of $\lambda$ is

$$\lambda_i(s^k, N(t^n)) := \lambda_{0,k}^i\, f^n \quad \forall\ k = 0,...,N_s,\ n = 0,...,N_T \text{ and } i \in \mathbb{N}_I,$$

where $f^n := e^{-\eta N^n}$.
The approximate problem of $[P^1]$ is defined by

$$[P_d^1] \quad \left\{ \min_{\Theta \in K_{N_s} \times K_{N_s}} J(\Theta) := \min_{\Theta \in K_{N_s} \times K_{N_s}} \sum_{i \in \mathbb{N}_I} \sum_{k \in D} \left[ \Delta s \left( \Delta\tau \sum_{j=0}^{N_\tau} B_{j,k}^{i,N_T} + A_k^{i,N_T} \right) - N_{i,k}^{exp} \right]^2,$$

where $\Theta := (v_{N_s}, \lambda_{0,N_s})$. The discrete vectors $v_{N_s}$ and $\lambda_{0,N_s}$ are the set of unknown parameters defined by $v_{N_s} = (v_{0,N_s}, ..., v_{I,N_s})$ and $\lambda_{0,N_s} = (\lambda_{0,N_s}^0, ..., \lambda_{0,N_s}^I)$, they belong to the space $K_{N_s} = (\tilde{C}_+^{\bar{u},N_s})^I$ where

$$\tilde{C}_+^{\bar{u},N_s} = \{u(s^k) = u^k,\quad u^0 = 0,\quad 0 < u^k \leqslant \bar{u},\quad k = 1,..,N_s\}.$$

Now, we consider the following Lagrangian formulation of $[P_d^1]$

$$\begin{aligned}
L^1(W) \quad &= \sum_{i=0}^{I} \sum_{k=0}^{N_s} \gamma_D^k \left[ \Delta s \left( \Delta\tau \sum_{j=0}^{N_\tau} B_{j,k}^{i,N_T} + A_k^{i,N_T} \right) - N_{i,k}^{exp} \right]^2 \\
&+ \sum_{n=1}^{N_T} \sum_{k=0}^{N_s} \left[ A_k^{0,n} - \frac{A_k^{0,n-1}}{1 + \Delta t\delta_A + \Delta t \lambda_{0,k}^0 f^n} \right] P_k^{0,n} \\
&+ \sum_{i=1}^{I} \sum_{n=1}^{N_T} \sum_{k=0}^{N_s} \left[ A_k^{i,n} - \frac{A_k^{i,n-1} + 2\Delta t\Delta\tau \sum_{j=1}^{N_\tau} \mu^{j-1} B_{j-1,k}^{i-1,n-1}}{1 + \Delta t\delta_A + \Delta t \lambda_{0,k}^i f^n} \right] P_k^{i,n} \\
&+ \sum_{i=0}^{I} \sum_{n=1}^{N_T} \sum_{j=1}^{N_\tau} \sum_{k=1}^{N_s} \left[ B_{j,k}^{i,n} - \frac{(1 - \frac{\Delta t}{\Delta s} v_i^k) B_{j-1,k}^{i,n-1} + \frac{\Delta t}{\Delta s} v_i^{k-1} B_{j-1,k-1}^{i,n-1}}{1 + \Delta t\delta_B + \Delta t\mu^j} \right] Q_{j,k}^{i,n} \\
&+ \sum_{i=0}^{I} \sum_{n=1}^{N_T} \sum_{k=0}^{N_s} \left[ B_{0,k}^{i,n} - \lambda_{0,k}^i f^{n-1} A_k^{i,n-1} \right] Q_{0,k}^{i,n},
\end{aligned} \tag{9.2}$$

where the vector $W = (W_0, ..., W_I)$, with $W_i = (v_i, \lambda_0^i, A^i, B^i, P^i, Q^i)$ for all $i \in \mathbb{N}_I$. The variable $(P^i, Q^i)$ corresponds to the dual variables. $\gamma_D^k$ is a function in the following form

$$\gamma_D^k := \begin{cases} 1 & \text{if } k \in D, \\ \\ 0 & \text{else.} \end{cases}$$

The first derivative of the Lagrangian with respect to $A_k^{i,n}$ and $B_{j,k}^{i,n}$ gives us the adjoint equations. For $i = I, ..., 0$; $n = N_T - 1, ..., 0$; $j = N_\tau - 1, ..., 0$ and $k = 0, ..., N_s - 1$, one has

$$\begin{cases} Q_{j,k}^{i,n} = \frac{(1-\frac{\Delta t}{\Delta s}v_i^k)Q_{j+1,k}^{i,n+1} + \frac{\Delta t}{\Delta s}v_i^k Q_{j+1,k+1}^{i,n+1}}{1+\Delta t\delta_B+\Delta t\mu^{j+1}} + \gamma_{[0,I-1]}^i \frac{2\Delta t\Delta\tau\mu^j P_k^{i+1,n+1}}{1+\Delta t\delta_A+\Delta t\lambda_{0,k}^i f^{n+1}\lambda^{n+1}} \\ \\ P_k^{i,n} = \frac{P_k^{i,n+1}}{1+\Delta t\delta_A+\Delta t\lambda_{0,k}^i f^{n+1}} + \lambda_{0,k}^i f^n Q_{0,k}^{i,n+1} \\ \\ Q_{j,k}^{i,N_T} = 2\gamma_D^k \Delta s\Delta\tau \left[ N_{i,k}^{exp} - \Delta s A_k^{i,N_T} - \Delta s\Delta\tau \sum_{j=0}^{N_\tau} B_{j,k}^{i,N_T} \right] \\ \\ P_k^{i,N_T} = 2\gamma_D^k \Delta s \left[ N_{i,k}^{exp} - \Delta s A_k^{i,N_T} - \Delta s\Delta\tau \sum_{j=0}^{N_\tau} B_{j,k}^{i,N_T} \right] \\ \\ Q_{N_\tau,k}^{i,n} = Q_{j,N_s}^{i,n} = 0 \end{cases} \tag{9.3}$$

where $[0, I-1] := \{0, ..., I-1\}$.

The first derivative of the Lagrangian (9.2) with respect to $v_{i_0}^{k_0}$ and $\lambda_{0,k_0}^{i_0}$ are $\forall\ i_0 \in \mathbb{N}_I$

$$\frac{\partial L}{\partial v_{i_0}^{k_0}} = \sum_{n=1}^{N_T}\sum_{j=1}^{N_\tau} \frac{\frac{\Delta t}{\Delta s} B_{j-1,k_0}^{i_0,n-1}\left[Q_{j,k_0}^{i_0,n} - Q_{j,k_0+1}^{i_0,n}\right]}{1+\Delta t\delta_B+\Delta t\mu^{j-1}}, \quad \forall\ k_0 = 0, ..., N_s - 1,$$

$$\frac{\partial L}{\partial v_{i_0}^{N_s}} = \sum_{n=1}^{N_T}\sum_{j=1}^{N_\tau} \frac{\frac{\Delta t}{\Delta s} B_{j-1,N_s}^{i_0,n-1} Q_{j,N_s}^{i_0,n}}{1+\Delta t\delta_B+\Delta t\mu^{j-1}},$$

and $\forall\ k_0 = 0, ..., N_s - 1$

$$\frac{\partial L}{\partial \lambda_{0,k_0}^{i_0}} = \sum_{n=1}^{N_T} \left[ \Delta t f^n \left( \frac{A_{k_0}^{i_0,n-1} + 2\Delta t\Delta\tau \sum_{j=1}^{N_\tau} \mu^{j-1} B_{j-1,k_0}^{i_0-1,n-1}}{\left(1+\Delta t\delta_A+\Delta t\lambda_{0,k_0}^{i_0} f^n\right)^2} \right) P_{k_0}^{i_0,n} - f^{n-1} A_{k_0}^{i_0,n-1} Q_{0,k_0}^{i_0,n} \right].$$

where $B^{i-l} := 0$ if $l > i$.

### 9.2.3 Numerical results

In this subsection, we present the numerical results of the identified parameters ($v_i$ and $\lambda_0^i$) by using the same algorithm 8.2.1.1 of the previous chapter. The division rate ($\mu$) and the initial conditions ($A_{0,0}$) are given in 8.4 and 8.5 respectively. Also, the mortalities, $\delta_A$ and $\delta_B$ are considered zeros because no death was observed in the experimental data [10]. In addition, we use the parameters ($\Delta$, $\eta$) estimated in Chapter 7.

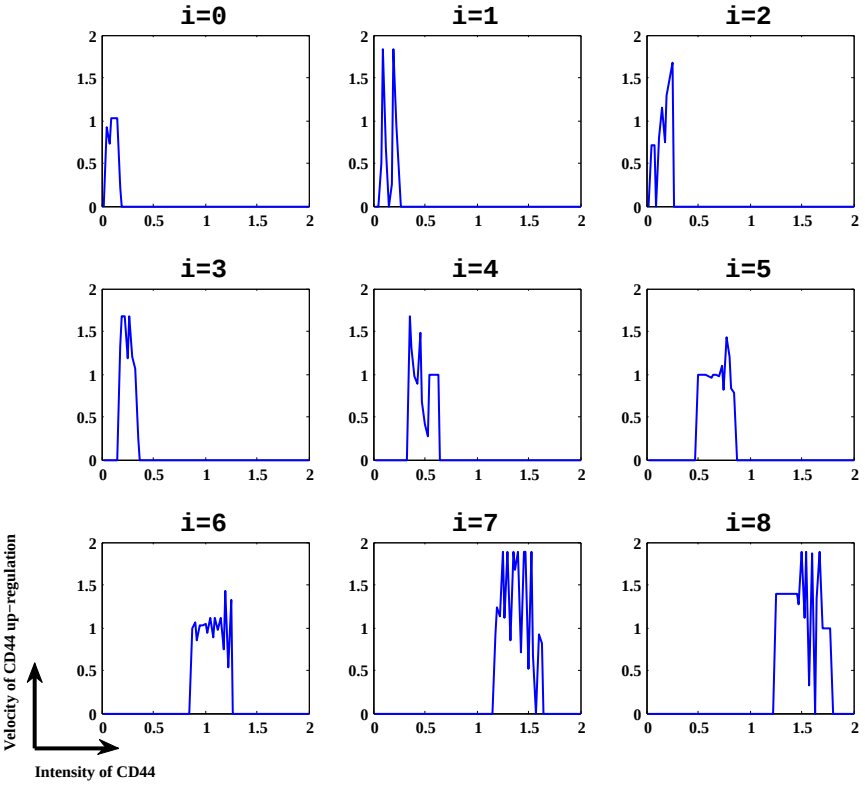


FIGURE 9.1: The velocity estimated (vertical axis) as a function of the observed intensity of CD44 (the weight of CD44 expression on the surface of cells) in each division ($i$) by using $SM_{CD44}^{\lambda_0^i}$ model.

Figs. 9.1 and 9.2 show the numerical results of the identified parameters ($v_i$ and $\lambda_0^i$) through the $SM_{CD44}^{\lambda_0^i}$ model. It seems that the velocity of CD44 (Fig. 9.1) is slightly changed, with respect to what has been identified in the previous chapter (Fig. 8.4). In addition, we remark in each subfigure of Fig. 9.2 that the peaks are shifted to higher intensity of CD44 when the division number increases. This is consistent with Fig. 9.1.

In Fig. 9.3a, we present the average velocity of CD44 estimated by using $SM_{CD44}$ model (dashed line) and $SM_{CD44}^{\lambda_0^i}$ model (solid line). The average velocity (solid line)

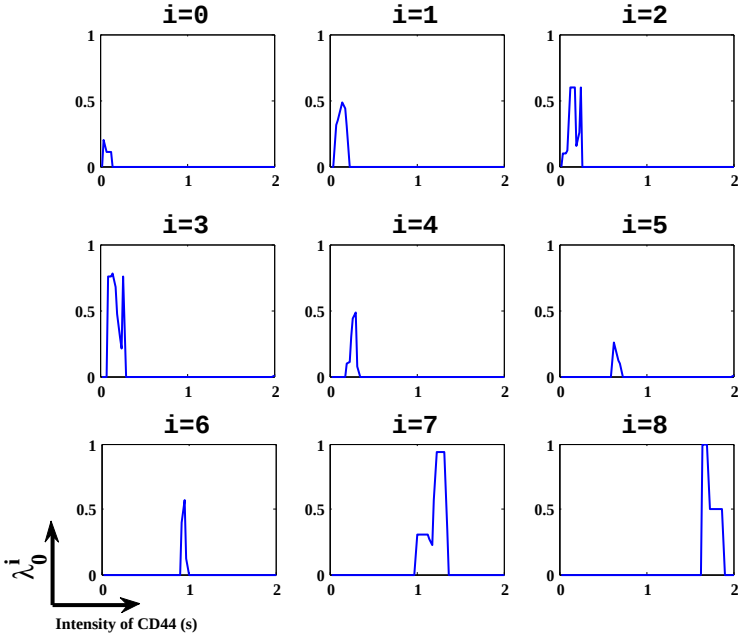


FIGURE 9.2: The parameters $\lambda_0^i$ estimated by using $SM_{CD44}^{\lambda_0^i}$ model. The vertical axis depicts $\lambda_0^i$ as a function of the observed intensity of CD44( horizontal axis) in each division ($i$).

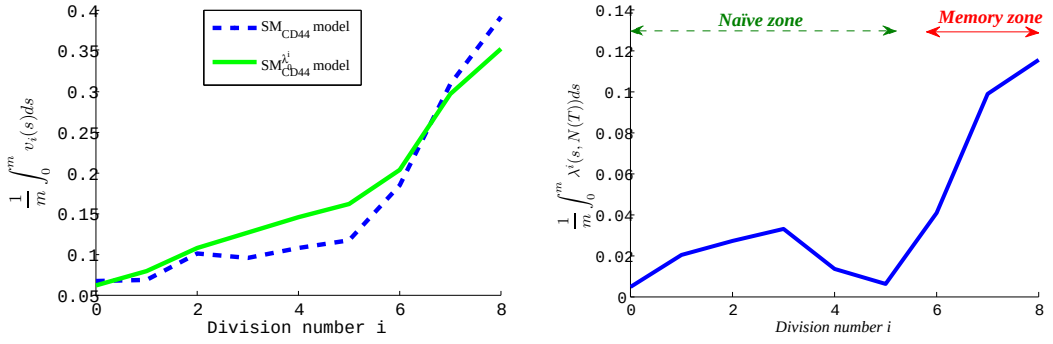


(9.3a) (9.3b)

FIGURE 9.3: Fig. 9.3a (solid line) represents the average velocity estimated as a function of division number ($i$) through $SM_{CD44}^{\lambda_0^i}$ model. The dashed line in this figure is reproduced from Fig. 8.5a in order to evaluate the difference between the average velocities estimated by using $SM_{CD44}^{\lambda_0^i}$ and $SM_{CD44}$ models. Fig. 9.3b depicts the average rate of entry into division at day 7 versus the division number ($i$). The variations of the average velocity in Fig. 9.3a allow to conclude the naive and memory zones (Fig. 9.3b) according to the number of divisions undergone by cells.

related to $SM_{CD44}^{\lambda_0^i}$, slightly increases in the first divisions (division 0 to 5), and the other one (dashed line) related to $SM_{CD44}$ model stabilizes in the first divisions. Therefore, the up-regulation of CD44 in the first divisions, is more significant by taking into account the CD44 expression and the division number in the rate of entry into division. Next (from division 6), it appears that these average velocities of CD44 (dashed and solid lines) plummet. This means that the cells change slightly their level of CD44 in the first divisions, that is why it can be qualified as naive. In addition, these cells transits to a memory phenotype when they undergo more than

6 divisions.

In Fig. 9.3b, the average rate of entry into division at day 7 is presented. We remark that the cells having undergone few divisions, enter the proliferative phase with a slow rate, but this rate is higher when the cells undergo more than six divisions. Taken together the subfigures in Fig. 9.3, we deduce that the naive T cells undergo cell divisions with a slow rate, while the others memory cells undergo more rapid divisions.

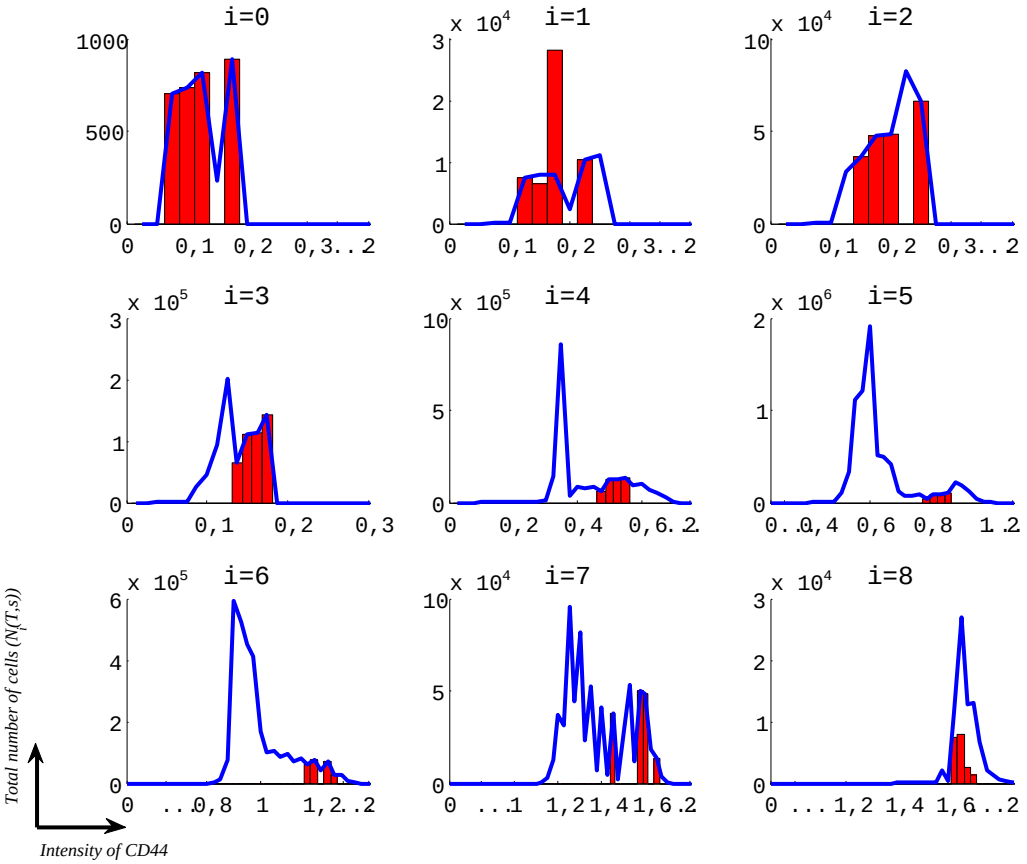


FIGURE 9.4: The vertical axis represent the total number of cells $N_i(T,s) := \left(\Delta s \int_0^{\Delta} B_i(T,\tau,s)ds + \Delta s A_i(T,s)\right)$ versus the intensity of CD44 (i.e. normalised median fluorescence intensity (MFI) of CD44) in each division (i). Here, $A_i$ and $B_i$ is the solution related to $SM^{\lambda_0^i}_{CD44}$ model. The solid line depicts the predictions of the model and the bar depicts the observed data. Note that the horizontal axis is zoomed in each subfigure in order to improve the illustration clarity.

Finally, we present in Fig. 9.4 the fit of $SM^{\lambda_0^i}_{CD44}$ model to the observed OT-1 T cell. As the explanation of Fig. 8.2, the highest peaks predicted by $SM^{\lambda_0^i}_{CD44}$ model where there was no experimental data to support them, return implicitly to those of the previous divisions where they have been observed in some panel by the experimental data. Taken together Figs. 8.2 and 9.4, we remark that $SM_{CD44}$ model fits the experimental data better than $SM^{\lambda_0^i}_{CD44}$ model.

## 9.3 Estimating the rate of division

In lymphopenia conditions, naive T cells undergo cell divisions, accompanied with a change in the cell surface phenotype, including increased CD44 expression. Furthermore, an important functional of the up-regulation of CD44 is the differentiation and proliferation of cells. Therefore, there exists a link between the cell division and their CD44 expression. To explore this link, we suppose in this section that the cells divide according to their level of CD44 and their age in the proliferative phase (B-phase). Then, we assume the division rate ($\mu$) in the following form

$$\mu(\tau, s) = \begin{cases} \frac{a(\tau)}{b(\tau)+e^{-c(\tau)s}} & if \quad \frac{\Delta}{2} \leqslant \tau \leqslant \Delta, \quad s \in [0, m], \\ \\ 0 & else. \end{cases} \tag{9.4}$$

where $a(.)$, $b(.)$ and $c(.)$ are functions that depend on the age $\tau$. We denote by $SM^{\mu}_{CD44}$ , the model $SM_{CD44}$ when we consider the division rate ($\mu$) as the previous form (9.4).

In this section, we identify the division rate $\mu$ by using the other parameters ($\Delta$, $\lambda_0$, $\eta$, $A_{0,0}(.)$) estimated and assumed in Chapter 7. Note that in this section, we fix the parameters ($v_i$) (by using the estimated parameters (Fig. 8.4) in Chapter 8) in order to prevent the compensations of CD44 between the velocity ($v_i(s)$) and the division rate $\mu(\tau, s)$ when they are estimated together.

### 9.3.1 Parameter identification problem.

To identify the division rate $\mu$, we estimate the coefficients $a(.)$, $b(.)$ and $c(.)$. The same strategy of the previous section and previous chapter can be used to estimate the above coefficients. Thus, we want to minimize the following cost function

$$[P^2] \quad \left\{ \min_{(a,b,c)\in(C_+)^3} \sum_{i\in\mathbb{N}_I} \sum_{s\in D} \left[ \Delta s \left( \int_0^{\Delta} B_i(T, \tau, s) d\tau + A_i(T, s) \right) - N^{exp}_{i,s} \right]^2 .$$

where the constant $\Delta s$ is the mesh size of the CD44 expression, $B_i(T, \tau, s)$, $A_i(T, s)$ are given by $SM^{\mu}_{CD44}$ model and $\{N^{exp}_{i,s}\}$ are the observed data at day 7. The

parameters $a$, $b$ and $c$ are defined in the space $C_+$ where

$$C_+ := \{u \in C^0([0,\Delta]),\quad 0 \leq u(\tau) \leq \bar{u},\quad \forall\, u \in [0,\Delta]\}. \tag{9.5}$$

We define the approximation of $\mu$ by

$$\mu(\tau^j, s^k) = \begin{cases} \frac{a^j}{b^j + e^{-c^j\, k}} & \text{for } j = \frac{N_\tau}{2}, ..., N_\tau \quad \textit{and} \quad k = 0, ..., N_s, \\ \\ 0 & \text{else.} \end{cases}$$

The discrete parameter identification problem of $[P^2]$ is

$$[P_d^2] \quad \left\{ \min_{\omega \in (C_+^{N_\tau})^3} \tilde{J}(\omega) := \min_{\omega \in (C_+^{N_\tau})^3} \sum_{i \in \mathbb{N}_I} \sum_{k \in D} \left[ \Delta s \left( \Delta\tau \sum_{j=0}^{N_\tau} B_{j,k}^{i,N_T} + A_k^{i,N_T} \right) - N_{i,k}^{exp} \right]^2.$$

where $\omega = (a_{N_\tau}, b_{N_\tau}, c_{N_\tau})$. The discrete vectors $a_{N_\tau}$, $b_{N_\tau}$ and $c_{N_\tau}$ are the set of unknown parameters, they belong to the space $C_+^{N_\tau}$ where

$$C_+^{N_\tau} = \{u(\tau^j) = u^j,\quad 0 \leqslant u^j \leqslant \bar{u},\quad j = 0, .., N_\tau\}.$$

As the previous section, a similar calculus gives us the ingredients (Lagrangian formulation, adjoint equations and the gradient of the cost function) that we needed to apply our algorithm 8.2.1.1.

TABLE 9.1: **Best-fit parameter estimations for $SM_{SM^{\mu}_{CD44}}$ model.**

| age (h)╲ parameters | $a(\tau)$ | $b(\tau)$ | $c(\tau)$ |
|---|---|---|---|
| $\tau = \frac{\Delta}{2}$ | 1.1921E-007 | 1.5162 | 1.0000E-004 |
| $\tau = \frac{3\Delta}{5}$ | 5.0664E-007 | 1.5046 | 1.0000E-004 |
| $\tau = \frac{7\Delta}{10}$ | 1.0000E-006 | 1.5192 | 1.0000E-004 |
| $\tau = \frac{4\Delta}{5}$ | 0.0037 | 1.1815 | 1.0000E-004 |
| $\tau = \frac{9\Delta}{10}$ | 1.5544 | 0.5583 | 8.3440E-005 |
| $\tau = \Delta$ | 1.8285 | 1.8248 | 1.4445 |

*$\Delta$ is the duration of the proliferative phase (B-phase). From Chapter 7, the parameter value $\Delta$ has been estimated by 7.17 hours. In this table, we present the estimated parameters $(a, b, c)$ for different age points between $\frac{\Delta}{2}$ and $\Delta$.*

### 9.3.2 Numerical results

In this subsection, we present the numerical results of the identified parameters $(a, b, c)$ by using the others parameters $(\lambda_0, \eta, \Delta,\ A_{0,0},\ v_i)$ from Chapters 7 and 8. The mortalities, $\delta_A$ and $\delta_B$ are considered zeros because no death was observed in the experiment of Hogan et al. [10].

In Table 9.1, we show the identified parameters for different age points. Fig. 9.5 is devoted to present the division rate $(\mu)$ according to the intensity of CD44 in different age points. We remark in Fig. 9.5 that the division rate is negligible when

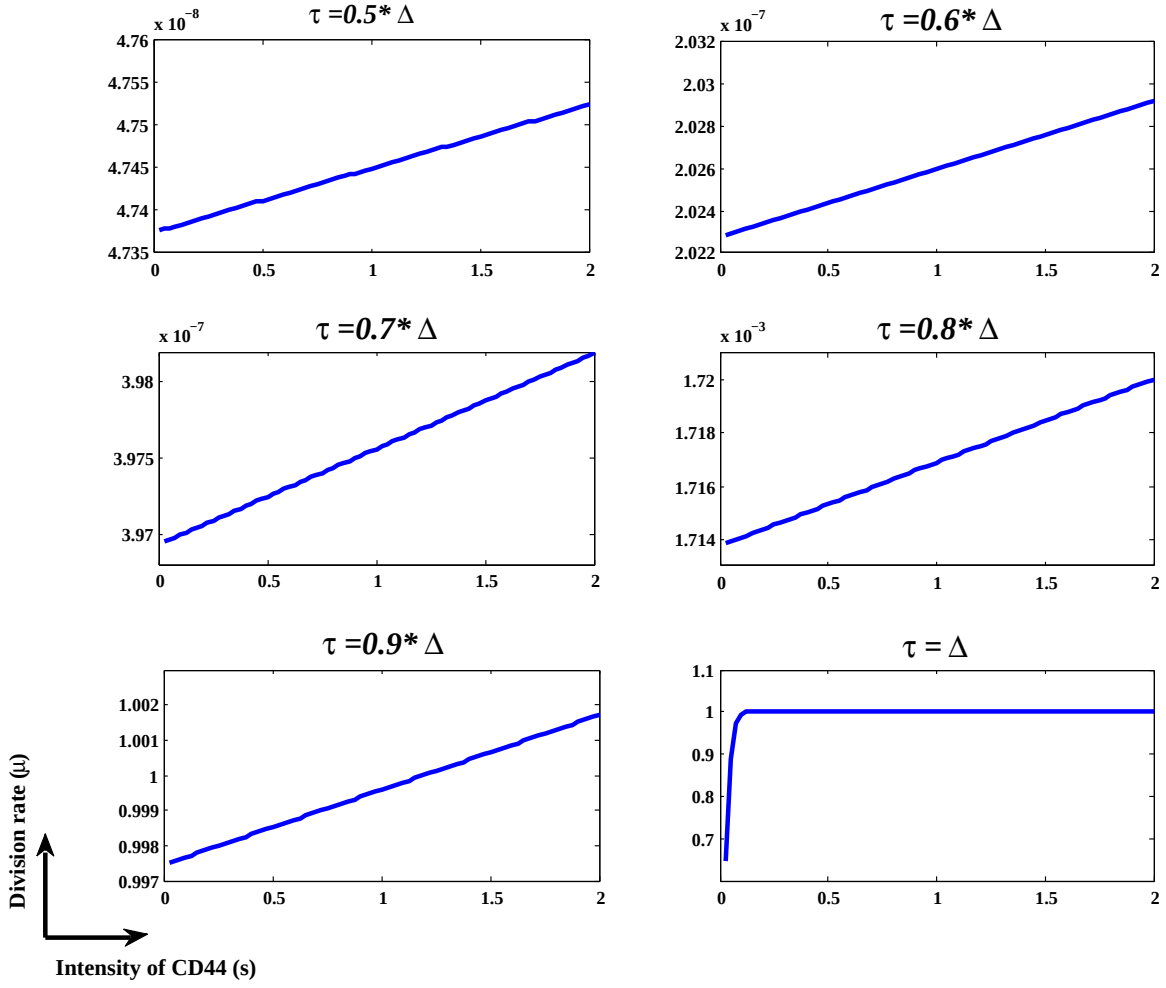


FIGURE 9.5: Division rate as a function of the intensity of CD44 in different age points.

the age of cells in B-phase is below to $\frac{4\Delta}{5}$ (hour), and becomes more important when their age is near to $\Delta$. In addition, the division rate at age less than $\Delta$, is slightly large when the cells have more CD44 expression on their surface, but at age $\Delta$, the

cells are compelled to divide independently of their level of CD44 because $\Delta$ is the maximum age in the proliferative phase (B-phase).
Furthermore, the figure that depicts the comparison of observed and $SM^{\mu}_{CD44}$ model-predicted OT-1 T cells, is omitted in this section because it is approximatively the same as in Fig. 8.2. Therefore, the prediction of $SM_{CD44}$ model is similar to this of $SM^{\mu}_{CD44}$ model, but this latter (i.e $SM^{\mu}_{CD44}$ model) provides more details about the link between the division rate and the CD44 expression.

## 9.4 Discussion and Conclusion

The number of T lymphocytes in the body is under homeostatic control. At equilibrium, the majority of naive T cells are non-dividing and express low levels of the surface protein CD44. In contrast, lymphopenia induces naive T cells to undergo cell divisions that depend on TCR signaling [18]. Interestingly, lymphopenia-induced homeostatic proliferation can also be associated with acquisition of a memory phenotype, and such cells share both functional and molecular characteristics of conventional memory cells [102, 103]. The CD44 antigen plays an important role in lymphopenia induced proliferation. It is a multistructural and multifunctional cell surface molecule involved in cell proliferation, cell differentiation and cell migration from naive to memory phenotype. These biological properties are an important motivation to explore the link between the different multifunctions of CD44 using a mathematical model like the $SM_{CD44}$ model. In this chapter, we have addressed the question, how the dynamic of CD44 expression can be linked to the proliferation, division and migration of cells. In the first section 9.2, a recruitment rate ($\lambda^i(s, N(t))$) which depends on the CD44 expression, division number and the total cell number, is considered in $SM_{CD44}$ model. By using CFSE data with CD44 (see [10] or Chapter 6), we estimate together the rate of entry into division and the velocity of CD44 up-regulation. The numerical results show that the rate of entry into division by the naive cells is much less than that of memory cells. Therefore, this interpretation represents the relationship between the cell proliferation and migration from naive (CD44 low) to memory (CD44 high) phenotype. In the second section 9.3, we estimate the division rate ($\mu$) which depends on the CD44 expression and the maturity of cells in the proliferative phase. This estimate allows to deduce that the cells having an important CD44 expression on their surface, have also a large possibility to divide when their ages are near to $\Delta$. In contrast at age $\Delta$, these

cells divide independently of their level of CD44.

In conclusion, this chapter gives some interpretations about the link between the multifunctional of CD44 through different mathematical models ($SM^{\lambda_0^i}_{CD44}$ and $SM^{\mu}_{CD44}$ models). In fact, a question remains in this study which is determination of the best model among the $SM_{CD44}$, $SM^{\lambda_0^i}_{CD44}$ and $SM^{\mu}_{CD44}$ models. Indeed, the comparison between the different models needs supplementary data in order to apply a cross validation approach as in Chapter 7.

# Part IV

# Models of T Cell Homeostasis in Vivo: Mathematical analysis and Optimal Control

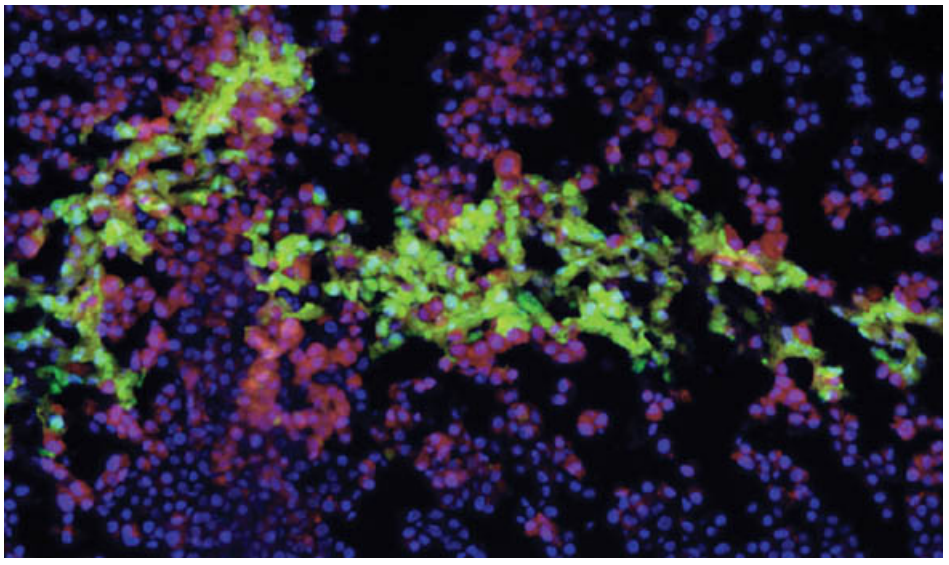

# Chapter 10

# Well-posedness of a model of T cell homeostasis in vivo

## 10.1 Introduction

The size and composition of the T lymphocyte compartment is subject to strict homeostatic regulation and is remarkably stable throughout life, despite variable dynamics in cell production and death during T cell development and immune responses [40, 104]. Homeostasis is achieved by careful orchestration of lymphocyte survival and cell division. T cells that have yet to encounter the antigen they recognise are termed naive as they have not been activated to respond. In normal case, the majority of naive T cells are non dividing and express low level of the surface phenotype (CD44 low). Under such conditions of T cell deficiency (eg. AIDS), naive T cells undergo cell division, termed homeostasic proliferation or lymphopenia induced proliferation (LIP). This regularization process can also be associated with acquisition of a memory phenotype (CD44 hight), and such cells share both functional and molecular characteristics of conventional memory cells [102, 103]. In vivo, the homeostatic cell division plays a more important role in maintaining naive T cell homeostasis in humans, even in replete conditions, as cell division is evident in the naive pool [44, 105], whereas recent thymic emigrants and naive T cells from cord blood have an enhanced ability to divide in response to IL-7 (Interleukin 7) signaling [106, 107].

In this context, a standard realistic mathematical model for analysing the kinetics of the cell cycle in vitro is proposed by Smith and Martin [69]. As it is described

in the previous chapters, this model consists to separate the phase of the cell cycle into two phases. Cells in the resting phase (G0, G1) are in the so-called A-state and B-phase is the state where the cells are in a proliferative phase (S, G2, M). B-phase has a fixed duration ($\Delta$). Cells involve a stochastic recruitment from A-state into B-phase. After completing the 'deterministic' B-phase a cell delivers two daughter cells in the 'stochastic' A-state from which the cells can be recruited for another round of division.

Most of the earlier work on modelling the dynamics of T cell has been done with models resembling the Smith and Martin model with an explicit time delay for the proliferative phases of the cell cycle [3, 4, 6, 51, 70, 78]. Specially, Bernard et al. [3], Yates et al. [7] and Hogan et al. [10] have formulated this model in terms of partial differential equations in order to take into account the continuous age of cells in the proliferative phase. Next, Ayoub et al [80] (or see Part II and III) have improved this new version of Smith-Martin model by including a new criteria (CD44 expression) that represents the transition of T cells from naive to memory phenotype during the homoeostatic mechanism in vitro (noted $SM_{CD44}$ model). In this chapter, we extend the $SM_{CD44}$ model to an in vivo model by implementing a rate $\Lambda$ of export of cells from the thymus (Fig. 10.1). In addition, we consider a large number of division ($I >> 0$) in the extended model with a rate of entry into division depending on the number of division ($i$) and the total cell number ($N$).

## 10.2 The model

The model with an export ($\Lambda$) of cells from the thymus is

$$\begin{cases} \dfrac{dA_0(t,s)}{dt} = \Lambda - \delta_A A_0(t,s) - \lambda^0(N) A_0(t,s), \\ \\ \begin{cases} for \quad i \in \mathbb{N}^* \\ \\ \dfrac{dA_i(t,s)}{dt} = 2\displaystyle\int_0^{\Delta} \mu(\tau) B_{i-1}(t,\tau,s)\, d\tau - \delta_A A_i(t,s) - \lambda^i(N) A_i(t,s), \end{cases} \\ \\ \begin{cases} for \quad i \in \mathbb{N} \\ \\ \frac{\partial}{\partial t} B_i(t,\tau,s) + \frac{\partial}{\partial \tau} B_i(t,\tau,s) + \frac{\partial}{\partial s}[v_i(s)\, B_i(t,\tau,s)] = -\left(\delta_B + \mu(\tau)\right) B_i(t,\tau,s), \end{cases} \end{cases} \tag{10.1}$$

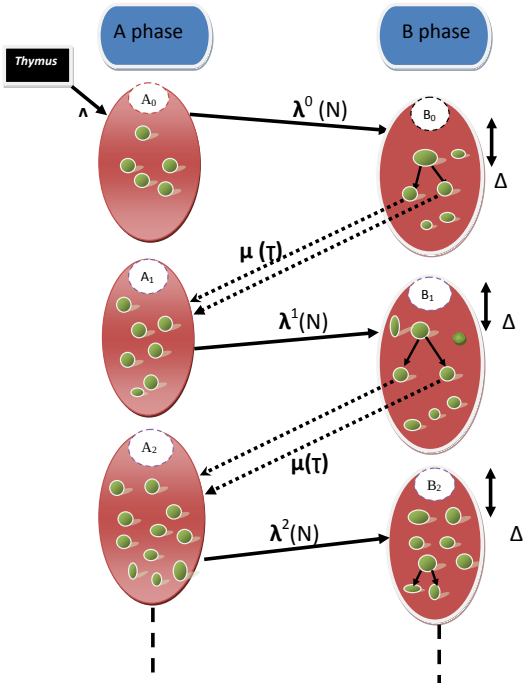


FIGURE 10.1: Dynamic of T cells in vivo during the homoeostatic process. $A_i$ and $B_i$ are the number of T cells, having undergone $i$ divisions in A phase and B phase respectively. $\Lambda$ is the rate of export of cells from the thymus. $\Delta$ is the duration of B phase. The rate of entry into division ($\lambda^i$) is described by a function of the total cell number ($N$) and division number $i$, which is linked to all phases and all divisions [10]. $\mu(\tau)$ represents the rate of cells which are divided at age $\tau$ and have given rise to two daughter cells in the resting phase [80].

for all $s \in [0, m]$ and $\tau \in [0, \Delta]$, where $m$ is the maximum intensity of CD44. The total number of cells is defined by

$$N := N(t) = \sum_{i \in \mathbb{N}} \left( \int_0^{\Delta} \int_0^{m} B_i(t, \tau, s) ds \, d\tau + \int_0^{m} A_i(t, s) ds \right). \tag{10.2}$$

System (10.1) includes natural mortality rates $\delta_A$ and $\delta_B$ of cells in A-state and B-phase respectively. Function, $\mu(\tau)$, denotes the rate of cells which divided at age $\tau$ and have given rise to two daughter cells in the resting phase.

The up-regulation of the CD44 expression on the surface of T cells is represented in (10.1) by a velocity $v_i$ in each division that depends on variable $s$.

The recruitment rate from A-state into B-phase is denoted by $\lambda^i$. It depends on the total number of cells $N := N(t)$ and the number of division ($i$) undergone by cells.

*Remark* 10.1. According to Yates et al. [7] and Hogan et al [10], T cells can undergo a finite number of division ($I$) (8 or 9 division with CFSE labelling). We assume a

recruitment rate from A-state into B-phase, for all $i \in \mathbb{N}$

$$\lambda^i(N) = \begin{cases} \lambda(N) & if \quad i \in \mathbb{N}_{I-1} := \{0, ..., I-1\} \\ \\ 0 & else. \end{cases}$$

where $N := N(t)$. Therefore, there are no cells after $A_I$ phase (i.e Ith division in A-state).

Boundary conditions and initial conditions of Eqs. (10.1) are defined by, $\forall\ i \in \mathbb{N}$,

$$\begin{cases} B_i(t,0,s) = \lambda^i(N) A_i(t,s), \\ \\ v_i(0) B_i(t,\tau,0) = 0, \end{cases} \qquad \begin{cases} A_0(0,s) = A_{0,0}(s) \geqslant 0, \\ \\ B_{i\in\mathbb{N}}(0,\tau,s) = 0 \ and \ A_{i\in\mathbb{N}^*}(0,s) = 0. \end{cases} \tag{10.3}$$

The structure of this chapter is organized as follows. At first, Sec. 10.3 is devoted to derive the integral formulation of System (10.1-10.3). Next, we prove in Sec. 10.4 the local existence and uniqueness of the solution of System (10.1-10.3) by using the fixed point method. Finally in Sec. 10.5, we conclude the global existence by using the maximal interval of existence.

## 10.3 Integral formulation

In this section, we are looking for the well-posedness of the mathematical model (10.1-10.3). We first state some notion of solution.

Let $L^1((0,\Delta),(0,m);\mathbb{R}^n)$ be the Banach space of equivalence classes of Lebesgue integrable functions, from $(0,\Delta)\times(0,m)$ in $\mathbb{R}^n$ with norm:

$$\|u\|_{L^1((0,\Delta)\times(0,m))} = \int_0^\Delta \int_0^m |u(\tau,s)| d\tau ds.$$

Let $T > 0$. We define two spaces $L_T$ and $H_T$ respectively by setting

$$\begin{aligned} L_T &:= L^\infty(0,T,L^1((0,\Delta)\times(0,m))) \\ &= \{u(t,.,.) \in L^1((0,\Delta)\times(0,m)) \ , \quad \sup_{0\leqslant t\leqslant T} \|u(t,.,.)\|_{L^1((0,\Delta)\times(0,m))} < +\infty\}, \\ H_T &:= L^\infty(0,T,L^1((0,m))) = \{q(t,.) \in L^1((0,m)) \ , \quad \sup_{0\leqslant t\leqslant T} \|q(t,.)\|_{L^1((0,m))} < +\infty\}. \end{aligned}$$

By using Lagrange method and Remark. 10.1, one obtains an implicit solution of $A_i$

$$\begin{aligned} A_0(t,s) &= A_{0,0}(s)\ e^{-\int_0^t(\delta_A+\lambda(N(u)))du} + \Lambda\int_0^t e^{-\int_r^t(\delta_A+\lambda(N(q)))dq}dr, \\ for\ \ i\in\mathbb{N}_I^*,\ \ A_i(t,s) &= 2\int_0^t\int_0^\Delta e^{-\int_r^t(\delta_A+\lambda^i(N(q)))dq}\mu(\tau)B_{i-1}(r,\tau,s)d\tau\ dr, \\ for\ \ i>I\ \ A_i(t,s) &\equiv 0. \end{aligned} \tag{10.4}$$

Now, we consider the following differential equations:

$$\begin{cases} \frac{ds_i^1(t)}{dt} = v_i(s_i^1(t)) \\ \\ s_i^1(t_0) = s_{i,0}^1 \geqslant 0 \end{cases}, \quad \begin{cases} \frac{ds_i^2(\tau)}{d\tau} = v_i(s_i^2(\tau)) \\ \\ s_i^2(\tau_0) = s_{i,0}^2 \geqslant 0. \end{cases} \tag{10.5}$$

where $s_i^1(t;t_0;s_{i,0}^1)$ and $s_i^2(\tau;\tau_0;s_{i,0}^2)$ are the curves witch goes through $(t_0,s_{i,0}^1)$ and $(\tau_0,s_{i,0}^2)$ respectively. The curves, $Z_i^1(t) := s_i^1(t;0;0)$ and $Z_i^2(\tau) := s_i^2(\tau;0;0)$ are the characteristic through the origin. The solution of (10.5) is given by the following equations

$$s_i^1(t) = s_{i,0}^1 + \int_{t_0}^t v_i(s_i^1(z))dz, \quad s_i^2(\tau) = s_{i,0}^2 + \int_{\tau_0}^\tau v_i(s_i^2(r))dr.$$

Using Remark 10.1 and integrating along the characteristic curve the PDE of System (10.1), one obtains

$$\begin{cases} B_{i\in\mathbb{N}_{I-1}}(t,\tau,s) = \begin{cases} 0 & t\leq\tau,\ Z_i^1(t)<s \\ \\ \frac{\lambda(N(t-\tau))\,A_i(t-\tau,\zeta_i)\,v_i(\zeta_i)}{v_i(s)}f(\tau) & 0\leq\tau<t,\ Z_i^2(\tau)<s \\ \\ 0 & Z_i^1(t)\geqslant s,\ Z_i^2(\tau)\geqslant s \end{cases} \\ \\ B_{i\geqslant I}(t,\tau,s)\equiv 0 \end{cases} \tag{10.6}$$

where $\zeta_i := s - Z_i^2(\tau)$ and $f(\tau) := e^{-\int_0^\tau(\delta_B+\mu(r))dr}$.

**Definition 10.2.** For all $T>0$. $(A_i,B_i)$ is called a global solution of (10.1-10.3) (in the sense of the expressions (10.4) and (10.6)), if it belongs to $L^\infty(0,T,L^1(0,m))$

and $L^\infty(0,T,L^1((0,\Delta)\times(0,m)))$ respectively and it satisfies System (10.4)-(10.6) respectively.

## 10.4 Local existence and uniqueness of solution

In this section we shall discuss the local existence of the solution of System (10.4)-(10.6) and we will make use the following assumption.

*Assumption* 10.4.1.

- Natural mortalities $\delta_A$ and $\delta_B$ are non-negative constants.
- Rate of export of cells from the thymus $\Lambda$ is non-negative constant.
- Function $\mu(.)$ is bounded, non-negative and satisfies the following inequality

$$0 \leq \underline{\mu} \leq \mu(\tau) \leq \bar{\mu}, \quad \forall\, \tau \in (0,\Delta).$$

- Function $\lambda(N)$ is non-negative, bounded and Lipschitz continuous with constant $k$

$$|\lambda(N) - \lambda(N^*)| \leqslant k|N - N^*|, \qquad N \geqslant 0, \quad N^* \geqslant 0.$$

- The velocity $v_i$ is bounded, non-negative for all $i \in \mathbb{N}_{I-1}$, satisfies the condition

$$v_i(0) = 0, \quad and \quad 0 < \underline{v_i} \leq v_i(s) \leq \bar{v_i}, \ \forall s \in ]0,m],$$

and continuously differentiable with respect to the variable $s$. In addition, there exists a positive constant $d_{v_i}$ such that

$$|\frac{\partial v_i}{\partial s}| \leqslant d_{v_i}, \quad \forall \ \ s \in [0,m].$$

- Initial condition $A_{0,0}(.)$ are non-negative and belongs to the space $L^1_+((0,m))$.

*Remark* 10.3.

The integral formulation (10.6) rewrites as

$$B_i(t,\tau,s) = \lambda(N(t-\tau))A_i(t-\tau,\zeta_i)\, f(\tau)\, e^{-\int_{\zeta_i}^{s} \frac{\partial v_i(\sigma)}{\partial \sigma}\frac{1}{v_i(\sigma)}d\sigma}, \quad \forall\ 0 \leq \tau < t \ \ and \ \ Z_i^2(\tau) < s.$$

for all $i \in \mathbb{N}_{I-1} := \{0, ..., I-1\}$. Using (10.6) and Assumption 10.4.1, one obtains

$$\|B_i(t,.,.)\|_{L^1((0,\Delta)\times(0,m))} \leq \int_0^t \int_{Z_i^2(\tau)}^m \lambda(N(t-\tau))|A_i(t-\tau, s-Z_i^2(\tau))| e^{\frac{d_{v_i} Z_i^2(\tau)}{\underline{v_i}}} ds\, d\tau.$$

Using $Z_i^2(\tau) := \int_0^\tau v_i(s_i^2(r))dr$, one deduces the following estimate

$$\|B_i(t,.,.)\|_{L^1((0,\Delta)\times(0,m))} \leq \int_0^t \int_{Z_i^2(\tau)}^m \lambda(N(t-\tau))|A_i(t-\tau, s-Z_i^2(\tau))| e^{C_{v_i}\tau} ds\, d\tau, \tag{10.7}$$

where $C_{v_i} := \frac{d_{v_i}\bar{v_i}}{\underline{v_i}}$.

In what follows in this section, we shall use the following convention

$$\sum_j^i = 0, \quad \prod_j^i = 1 \quad \textit{and} \quad \|.\|_\infty^{i-j} = 1 \qquad \textit{if } j > i.$$

Before studying local existence of a solution, we give the following preliminary results.

**Lemma 10.4.** *Let Assumption 10.4.1 be satisfied. For $T > 0$ and $t \in [0,T]$, any solution $((A_0,B_0),...,(A_{I-1},B_{I-1}),A_I)$ of (10.4)-(10.6) in the sense of Definition 10.2, satisfies $\forall\ \ i \in \mathbb{N}_I$*

$$\|A_i\|_{H_T} \ \leqslant\ \frac{2^i \bar{\mu}^i \|\lambda\|_\infty^i R_{A_0}}{\delta_A^i \left(\prod_{j=0}^{i-1} C_{v_j}\right)} \left(1 - e^{-\delta_A T}\right)^i \left[\prod_{j=0}^{i-1} \left(e^{C_{v_j} T} - 1\right)\right] := R_{A_i}, \tag{10.8}$$

*and $\forall\ i \in \mathbb{N}_{I-1}$,*

$$\|B_i\|_{L_T} \leqslant \frac{2^i \bar{\mu}^i \|\lambda\|_\infty^{i+1} R_{A_0}}{\delta_A^i \left(\prod_{j=0}^{i} C_{v_j}\right)} \left(1 - e^{-\delta_A T}\right)^i \left[\prod_{j=0}^{i} \left(e^{C_{v_j} T} - 1\right)\right] := R_{B_i}. \tag{10.9}$$

*where $R_{A_0} = e^{-\delta_A T}\|A_{0,0}\|_{L^1((0,m))} + \frac{\Lambda}{\delta_A}\left(1 - e^{-\delta_A T}\right)$.*

*Proof.* We proceed by induction.

**For $i = 0$**

Let $T > 0$ and $t \in [0, T]$. By using (10.4), let us integrate $A_0$ from 0 to $m$

$$\begin{aligned}\|A_0(t,.)\|_{L^1((0,m))} &= \int_0^m \left[ |A_{0,0}(s)|\ e^{-\int_0^t (\delta_A + \lambda(N(u)))du} + \Lambda \int_0^t e^{-\int_r^t (\delta_A+\lambda(N(u)))du} dr \right] ds \\ &\leqslant e^{-\delta_A t}\|A_{0,0}\|_{L^1((0,m))} + \frac{\Lambda}{\delta_A}(1 - e^{-\delta_A t}),\end{aligned}$$

that implies $\|A_0\|_{H_T} \leqslant R_{A_0}$. Using (10.7), one has

$$\begin{aligned}\|B_0(t,.,.)\|_{L^1((0,\Delta)\times(0,m))} &\leq \int_0^t \int_{Z_0^2(\tau)}^m \lambda(N(t-\tau))|A_0(t-\tau,\zeta_0)|\ e^{C_{v_0}\tau} ds\ d\tau \\ &\leq \int_0^t \int_{Z_0^2(\tau)}^m \lambda(N(t-\tau))|A_0(t-\tau, s - Z_0^2(\tau))|\ e^{C_{v_0}\tau} ds\ d\tau.\end{aligned}$$

Performing the change of variables $\sigma = s - Z_0^2(\tau)$ and $a = t - \tau$, one obtains

$$\|B_0(t,.,.)\|_{L^1((0,\Delta)\times(0,m))} \leq \int_0^t \int_0^m \lambda(N(a))|A_0(a,\sigma)|\ e^{C_{v_0}(t-a)} d\sigma\ da,$$

and one gets

$$\|B_0\|_{L_T} \leq \frac{\|\lambda\|_\infty}{C_{v_0}} \left(e^{C_{v_0}T} - 1\right) \|A_0\|_{H_T},$$

that implies $\|B_0\|_{L_T} \leq \frac{\|\lambda\|_\infty R_{A_0}}{C_{v_0}} \left(e^{C_{v_0}T} - 1\right)$. Then, inequalities (10.8) and (10.9) hold for $i = 0$.

**For** $i \in \mathbb{N}^*_{I-1}$

Assuming that inequalities (10.8) and (10.9) hold for $i$, let us show they still hold for $i + 1$. Integrating $A_{i+1}$ over (0, m), one has

$$\|A_{i+1}(t,.)\|_{L^1((0,m))} \leqslant 2\bar{\mu} \int_0^m \int_0^t \int_0^\Delta e^{-\int_r^t (\delta_A + \lambda^i(N(q)))dq} |B_i(r,\tau,s)| d\tau\ dr\ ds.$$

Inequality (10.9) holds for i. Therefore, by using Fubini's theorem, one can write

$$\begin{aligned}\|A_{i+1}\|_{H_T} &\leqslant \frac{2\bar{\mu}}{\delta_A}\left(1 - e^{-\delta_A T}\right)\|B_i\|_{L_T} \qquad (10.10)\\ &\leqslant \frac{2^{i+1}\bar{\mu}^{i+1}\|\lambda\|_\infty^{i+1} R_{A_0}}{\delta_A^{i+1}\left(\prod_{j=0}^i C_{v_j}\right)}\left(1 - e^{-\delta_A T}\right)^{i+1}\left[\prod_{j=0}^i \left(e^{C_{v_j}T} - 1\right)\right].\end{aligned}$$

Now, let us integrate the solution $B_{i+1}$ along the characteristic. Then one finds

$$\|B_{i+1}\|_{L_T} \leqslant \frac{\|\lambda\|_\infty}{C_{v_{i+1}}} \left(e^{C_{v_{i+1}}T} - 1\right) \|A_{i+1}\|_{H_T}.$$

By using the inequality in (10.10), one eventually gets

$$\|B_{i+1}\|_{L_T} \leqslant \frac{2^{i+1}\bar{\mu}^{i+1}\|\lambda\|_\infty^{i+2} R_{A_0}}{\delta_A^{i+1}\left(\prod_{j=0}^{i+1} C_{v_j}\right)} \left(1 - e^{-\delta_A T}\right)^{i+1} \left[\prod_{j=0}^{i+1} \left(e^{C_{v_j}T} - 1\right)\right].$$

Then, inequalities (10.8) and (10.9) holds for $i+1$. Finally, the proof of (10.8) for $I$ is rather straightforward by using (10.9) for $I-1$. □

Notation $(A_i, B_i; A_{0,0})$ stands for a solution $(A_i, B_i)$ with initial condition $A_{0,0}$.

**Lemma 10.5.** *Let Assumption (10.4.1) be satisfied. Let $T > 0$ and $t \in [0,T]$. For any two solutions $(A_i, B_i; A_{0,0})$ and $(A_i^*, B_i^*; A_{0,0}^*)$ of (10.4)-(10.6) in the sense of Definition 10.2, the following set of inequalities hold $\forall\ i \in \mathbb{N}_{I-1}$,*

$$\begin{aligned}
\|A_i - A_i^*\|_{H_T} &\leq \alpha^i e^{-\delta_A T}\|A_{0,0} - A_{0,0}^*\|_{L^1((0,m))} + k\beta_A^i \sup_{0\leqslant t\leqslant T} |N(t) - N^*(t)|,\\
\|B_i - B_i^*\|_{L_T} &\leq \frac{\alpha^i\|\lambda\|_\infty\left(e^{C_{v_i}T} - 1\right)}{C_{v_i}} e^{-\delta_A T}\|A_{0,0} - A_{0,0}^*\|_{L^1((0,m))} + k\beta_B^i \sup_{0\leqslant t\leqslant T} |N(t) - N^*(t)|,
\end{aligned}$$

*and*

$$\|A_I - A_I^*\|_{H_T} \leq \alpha^I e^{-\delta_A T}\|A_{0,0} - A_{0,0}^*\|_{L^1((0,m))} + 2\bar{\mu}k\beta_B^{I-1}\frac{\left(1 - e^{-\delta_A T}\right)}{\delta_A} \sup_{0\leqslant t\leqslant T} |N(t) - N^*(t)|,$$

*where*

$$\begin{aligned}
\alpha^i &= \left[\frac{2\bar{\mu}\left(1 - e^{-\delta_A T}\right)}{\delta_A}\right]^i \|\lambda\|_\infty^{i-1} \prod_{j=0}^{i-1} \frac{e^{C_{v_j}T} - 1}{C_{v_j}},\\
\beta_A^i &= \sum_{j=0}^{i-1} \left[\frac{2\bar{\mu}\left(1 - e^{-\delta_A T}\right)}{\delta_A}\right]^{i-j} \|\lambda\|_\infty^{i-j-1} \left[\prod_{k=j+1}^{i-1} \frac{\left(e^{C_{v_k}T} - 1\right)}{C_{v_k}}\right] \left(R_{A_j^*} \frac{\left(e^{C_{v_0}T} - 1\right)}{C_{v_0}} + TR_{B_j}\right)\\
&\quad + \left[\frac{2\bar{\mu}\|\lambda\|_\infty\left(1 - e^{-\delta_A T}\right)}{\delta_A}\right]^i \left[\prod_{j=0}^{i-1} \frac{\left(e^{C_{v_j}T} - 1\right)}{C_{v_j}}\right] L,
\end{aligned} \tag{10.11}$$

*with* $L = T\left(e^{-\delta_A T}\|A_{0,0}\|_{L^1((0,m))} + \frac{\Lambda}{\delta_A}\left(1-e^{-\delta_A T}\right)\right)$, *and*

$$\begin{aligned}\beta_B^i &= \sum_{j=0}^{i-1}\left[\frac{2\bar{\mu}\|\lambda\|_\infty\left(1-e^{-\delta_A T}\right)}{\delta_A}\right]^{i-j}\left[\prod_{k=j+1}^{i}\frac{\left(e^{C_{v_k}T}-1\right)}{C_{v_k}}\right]TR_{B_j}\\ &+\sum_{j=0}^{i}\left[\frac{2\bar{\mu}\|\lambda\|_\infty\left(1-e^{-\delta_A T}\right)}{\delta_A}\right]^{i-j}\left[\prod_{k=j}^{i}\frac{\left(e^{C_{v_k}T}-1\right)}{C_{v_k}}\right]R_{A_j^*}\\ &+\|\lambda\|_\infty\left[\frac{2\bar{\mu}\|\lambda\|_\infty\left(1-e^{-\delta_A T}\right)}{\delta_A}\right]^{i}\left[\prod_{j=0}^{i}\frac{\left(e^{C_{v_j}T}-1\right)}{C_{v_j}}\right]L. \qquad (10.12)\end{aligned}$$

$R_{A_i}$ *and* $R_{B_i}$ *are given in the previous Lemma 10.4.*

*Proof.* As in the previous proof, we proceed by induction.

**For** $i = 0$

Let us integrate the difference between $A_0$ and $A_0^*$ over $(0,m)$

$$\begin{aligned}\|A_0(t,.)-A_0^*(t,.)\|_{L^1((0,m))} &\leqslant e^{-\delta_A t}\int_0^m |A_{0,0}^*(s)||e^{-\int_0^t\lambda(N(u))du}-e^{-\int_0^t\lambda(N^*(u))du}|\,ds\\ &+e^{-\delta_A t}\int_0^m |A_{0,0}(s)-A_{0,0}^*(s)|e^{-\int_0^t\lambda(N(u))du}\,ds\\ &+\int_0^t \Lambda e^{-(t-r)\delta_A}|e^{-\int_r^t\lambda(N(u))du}-e^{-\int_r^t\lambda(N^*(u))du}|dr.\end{aligned}$$

Note that function $x \longrightarrow e^{-x}$ is Lipschitz continuous on $[0,+\infty)$ with constant 1. Then by using Assumption (10.4.1), one obtains

$$\begin{aligned}\|A_0-A_0^*\|_{H_T} &\leqslant e^{-\delta_A T}\|A_{0,0}-A_{0,0}^*\|_{L^1((0,m))}\\ &+kT\left[e^{-\delta_A T}\|A_{0,0}^*\|_{L^1((0,m))}+\frac{\Lambda}{\delta_A}\left(1-e^{-\delta_A T}\right)\right]\sup_{0\leqslant t\leqslant T}|N(t)-N^*(t)|.\end{aligned}$$

On the other hand, integrating the difference between $B_0$ and $B_0^*$ on $(0,\Delta)\times(0,m)$ one finds

$$\begin{aligned}\|B_0(t,.,.) &- B_0^*(t,.,.)\|_{L^1((0,\Delta)\times(0,m))}\\ &\leqslant \int_0^t\int_{Z_0^2(\tau)}^m e^{C_{v_0}\tau}\left[\lambda(N(t-\tau))\;|A_0(t-\tau,\zeta_0)-A_0^*(t-\tau,\zeta_0)|\right.\\ &\qquad\left.+|\lambda(N(t-\tau))-\lambda(N^*(t-\tau))|\;|A_0^*(t-\tau,\zeta_0)|\right]\,ds\,d\tau.\end{aligned}$$

By using Lemma 10.4 and Assumption (10.4.1), one gets

$$\begin{aligned}\|B_0 - B_0^*\|_{L_T} &\leqslant \|\lambda\|_\infty \frac{\left(e^{C_{v_0}T}-1\right)}{C_{v_0}} e^{-\delta_A T}\|A_{0,0} - A_{0,0}^*\|_{L^1((0,m))} \\ &\quad + k\frac{\left(e^{C_{v_0}T}-1\right)}{C_{v_0}}\left(\|\lambda\|_\infty L + R_{A_0^*}\right) \sup_{0\leqslant t\leqslant T}|N(t)-N^*(t)|.\end{aligned}$$

Then, the inequalities in the statement of Lemma 10.5 are satisfied for $i = 0$.

**For** $i \in \mathbb{N}^*_{I-1}$

Assuming that the inequalities in the statement of Lemma 10.5 hold for i. Let us show they still hold for i+1.

$$\begin{aligned}\|A_{i+1}(t,.) &- A_{i+1}^*(t,.)\|_{L^1((0,m))} \\ &\leqslant 2\bar{\mu}\int_0^m\int_0^t\int_0^\Delta e^{-\delta_A(t-r)}\Big[\left|e^{-\int_r^t\lambda(N(q))dq} - e^{-\int_r^t\lambda(N^*(q))dq}\right| |B_i(r,\tau,s)| \\ &\qquad + e^{-\int_r^t\lambda(N^*(q))dq}\,|B_i(r,\tau,s) - B_i^*(r,\tau,s)|\Big]\, d\tau\, dr\, ds.\end{aligned}$$

Therefore

$$\begin{aligned}\|A_{i+1} - \bar{A}_{i+1}\|_{H_T} &\leqslant 2\bar{\mu}\frac{\left(1-e^{-\delta_A T}\right)}{\delta_A}\|B_i - B_i^*\|_{L_T} \\ &\quad + 2\bar{\mu}kTR_{B_i}\frac{\left(1-e^{-\delta_A T}\right)}{\delta_A}\sup_{0\leqslant t\leqslant T}|N(t)-N^*(t)|.\end{aligned}$$

By recalling Lemma 10.4, one obtains

$$\|A_{i+1} - \bar{A}_{i+1}\|_{H_T} \leqslant \alpha^{i+1}e^{-\delta_A T}\|A_{0,0} - A_{0,0}^*\|_{L^1((0,m))} + k\beta_A^{i+1}\sup_{0\leqslant t\leqslant T}|N(t)-N^*(t)|,$$

where $\alpha^{i+1}$ and $\beta_A^{i+1}$ are given in the statement of lemma 10.5.

Also, one has

$$\begin{aligned}\|B_{i+1}(t,.,.) &- B_{i+1}^*(t,.,.)\|_{L^1((0,\Delta)\times(0,m))} \\ &\leqslant \int_0^t\int_{Z_{i+1}^2(\tau)}^m e^{C_{v_{i+1}}\tau}\big[|\lambda(N(t-\tau))|\,|A_{i+1}(t-\tau,\zeta_{i+1}) - A_{i+1}^*(t-\tau,\zeta_{i+1})| \\ &\qquad + |\lambda(N(t-\tau)) - \lambda(N^*(t-\tau))|\,|A_{i+1}^*(t-\tau,\zeta_{i+1})|\big]\, ds\, d\tau.\end{aligned}$$

Furthermore

$$\begin{aligned}\|B_{i+1}-B^*_{i+1}\|_{L^T} &\leqslant \|\lambda\|_\infty \frac{\left(e^{C_{v_{i+1}}T}-1\right)}{C_{v_{i+1}}} e^{-\delta_A T}\|A_{0,0}-A^*_{0,0}\|_{L^1((0,m))} \\ &\quad + k\frac{\left(e^{C_{v_{i+1}}T}-1\right)}{C_{v_{i+1}}}\left(\|\lambda\|_\infty L + R_{A^*_{i+1}}\right)\sup_{0\leqslant t\leqslant T}|N(t)-N^*(t)|.\end{aligned}$$

Finally, using Lemma 10.4

$$\begin{aligned}\|B_{i+1}-B^*_{i+1}\|_{L^T} &\leqslant \frac{\alpha^{i+1}\|\lambda\|_\infty\left(e^{C_{v_{i+1}}T}-1\right)}{C_{v_{i+1}}} e^{-\delta_A T}\|A_{0,0}-A^*_{0,0}\|_{L^1((0,m))} \\ &\quad + k\beta_B^{i+1}\sup_{0\leqslant t\leqslant T}|N(t)-N^*(t)|,\end{aligned}$$

This ends the proof of the Lemma 10.5. □

Now, we will state the main result of this section.

**Theorem 10.6.** *Under Assumption 10.4.1, System (10.4)-(10.6) admits a unique local solution in* $[0,T^*]$.

*Proof.* We set up a fixed point method.

At first, define an operator

$$\bigwedge : \quad ((A_0,B_0),...,(A_{I-1},B_{I-1}),A_I) \longmapsto \left((\hat{A}_0,\hat{B}_0),...,(\hat{A}_{I-1},\hat{B}_{I-1}),\hat{A}_I\right)$$

wherein

$$\begin{aligned}\hat{A}_0(t,s) &= A_{0,0}(s)\; e^{-\int_0^t(\delta_A+\lambda(N(u)))du} + \Lambda\int_0^t e^{-\int_r^t(\delta_A+\lambda(N(q)))dq}dr, \\ \hat{A}_{i\in\mathbb{N}^*_I}(t,s) &= 2\int_0^t\int_0^\Delta e^{-\int_r^t(\delta_A+\lambda(N(q)))dq}\mu(\tau)\hat{B}_{i-1}(r,\tau,s)d\tau\; dr, \\ \hat{B}_{i\in\mathbb{N}_{I-1}}(t,\tau,s) &= \begin{cases} 0 & t\leq\tau,\ Z^1_i(t)<s \\ \frac{\lambda(N(t-\tau))\,\hat{A}_i(t-\tau,\zeta_i)\,v_i(\zeta_i)}{v_i(s)}f(\tau) & 0\leq\tau<t,\ Z^2_i(\tau)<s \\ 0 & Z^1_i(t)\geqslant s,\ Z^2_i(\tau)\geqslant s \end{cases}\end{aligned}$$

where $\zeta_i := s - Z_i^2(\tau)$ and $f(\tau) := e^{-\int_0^\tau (\delta_B + \mu(r))dr}$, and

$$N(t) = \left( \sum_{i=0}^{I} \int_0^m A_i(t,s)ds \right) + \left( \sum_{i=0}^{I-1} \int_0^\Delta \int_0^m B_i(t,\tau,s)d\tau ds \right),$$

where $(A_i,\ B_i)$ is given by System (10.4)-(10.6).

Let $M := (H_T \times L_T)^{I-1} \times H_T$ and define a norm on M as follows

$$\|u\|_M = \sum_{i=0}^{I-1} \sup_{0\leqslant t\leqslant T} \int_0^\Delta \int_0^m |B_i(t,\tau,s)|\ ds\ d\tau + \sum_{i=0}^{I} \sup_{0\leqslant t\leqslant T} \int_0^m |A_i(t,s)|\ ds, \quad (10.13)$$

for all $u := ((A_0, B_0), ..., (A_{I-1}, B_{I-1}), A_I) \in M$.

We shall show that the operator $\bigwedge$ is a map from M into M and it is strict contraction for T small enough.

(1) $\bigwedge : M \longmapsto M$

Let $u$ and $\hat{u} := \left((\hat{A}_0, \hat{B}_0), ..., (\hat{A}_{I-1}, \hat{B}_{I-1}), \hat{A}_I\right)$ lie in $M$ and satisfy (10.4)-(10.6). By using (10.13), one can write

$$\|\hat{u}\|_M = \sum_{i=0}^{I-1} \|\hat{B}_i\|_{L_T} + \sum_{i=0}^{I} \|\hat{A}_i\|_{H_T}.$$

Substituting (10.8) and (10.9) in the previous equality, one obtains

$$\|\hat{u}\|_M \leq \left( \sum_{i=0}^{I-1} R_{\hat{B}_i} \right) + \left( \sum_{i=0}^{I} R_{\hat{A}_i} \right).$$

Then for $T < +\infty$, one gets $\bigwedge$ maps M into M.

(2) It remains to show that $\bigwedge$ is a contraction for T small enough
Let $u, \hat{u}, \bar{u} := \left((\bar{A}_0, \bar{B}_0), ..., (\bar{A}_{I-1}, \bar{B}_{I-1}), \bar{A}_I\right)$ and $\bar{\hat{u}} := \left((\bar{\hat{A}}_0, \bar{\hat{B}}_0), ..., (\bar{\hat{A}}_{I-1}, \bar{\hat{B}}_{I-1}), \bar{\hat{A}}_I\right)$ in $M$ and satisfies (10.1-10.3).

Then, the norm in $M$ of the difference between $\hat{u}$ and $\bar{\hat{u}}$ is

$$\|\hat{u} - \bar{\hat{u}}\|_M = \sum_{i=0}^{I-1} \|\hat{B}_i - \bar{\hat{B}}_i\|_{L_T} + \sum_{i=0}^{I} \|\hat{A}_i - \bar{\hat{A}}_i\|_{H_T}.$$

Solutions, $\hat{u}$ and $\bar{\hat{u}}$ having the same initial condition ($\hat{A}_{0,0} \equiv \bar{\hat{A}}_{0,0}$). Lemma 10.5 allows us to estimate the previous equality by

$$\begin{aligned} \|\hat{u} - \bar{\hat{u}}\|_M &\leqslant \Theta \sup_{0 \leqslant t \leqslant T} |N(t) - \bar{N}(t)| \\ &\leqslant \Theta \|u - \bar{u}\|_M, \end{aligned}$$

where

$$\Theta = \Theta(T) = k \left[ 2\bar{\mu}\beta_B^{I-1} \frac{\left(1 - e^{-\delta_A T}\right)}{\delta_A} + \sum_{i=0}^{I-1} \left(\beta_A^i + \beta_B^i\right) \right].$$

Note that $\lim_{T \to 0} \Theta(T) = 0$ (see (10.11-10.12) for $\beta_A^i$ and $\beta_B^i$). Then, there exists at least $T^* > 0$ where $\Theta(T^*) < 1$, which implies that $\bigwedge$ is a strict contraction.

This complete the local existence and uniqueness proof. □

## 10.5 Global existence

*Remark* 10.7. If $u$ is a solution of (10.1-10.3) in $[0, T]$ and $\hat{u}$ is a continuous extension of $u$ in $[T, T + \hat{T}]$ such that

$$A_i(t, s) = \hat{A}_i(t - T, s), \quad \forall i \in \mathbb{N}_I, \quad \textit{and} \quad B_i(t, \tau, s) = \hat{B}_i(t - T, \tau, s), \quad \forall i \in \mathbb{N}_{I-1},$$

then $u$ is a solution in $[0, T + \hat{T}]$.

In the next, we introduce the maximum interval of existence of a solution.

**Definition 10.8.** The maximal interval of existence of a solution, denoted by $[0, T_{max}]$ is the interval with the property that there exists $u \in (H_T \times L_T)^{I-1} \times H_T$, solution of (10.1-10.3) for each $T \in (0, T_{max})$.

**Lemma 10.9.** *Let Assumption 10.4.1 be satisfied and let $u$ be a solution of System (10.1-10.3) in $[0, T_{max})$. If $T_{max} < \infty$, then*

$$\lim_{t \to T_{max}} \|A_i(t, .)\|_{L^1((0,m))} = \infty, \quad \forall i \in \mathbb{N}_I. \tag{10.14}$$

$$\lim_{t \to T_{max}} \|B_i(t, ., .)\|_{L^1((0,\Delta)\times(0,m))} = \infty, \quad \forall i \in \mathbb{N}_{I-1}. \tag{10.15}$$

*Proof.* Assume there exists $r_1 > 0$ and $r_2 > 0$ such that $\|B_i(t,.,.)\|_{L^1((0,\Delta)\times(0,m))} \leqslant r_1$ and $\|A_i(t,.)\|_{L^1((0,m))} \leqslant r_2$ for all $t \in [0, T_{max})$, it suggests that there exists a sequence $(t_n)_{n\in\mathbb{N}}$ satisfying $\lim_{n\to\infty} t_n = T_{max}$. Then, one has

$$\begin{aligned} \sup_{n\in\mathbb{N}} \|B_i(t_n,.,.)\|_{L^1((0,\Delta)\times(0,m))} &\leqslant r_1, \\ \sup_{n\in\mathbb{N}} \|A_i(t_n,.)\|_{L^1((0,m))} &\leqslant r_2. \end{aligned}$$

Such that $u$ is a solution of (10.1-10.3) in $[0, t_n]$. From Remark (10.7), let $u^{t_n}$ be a solution in $[t_n, t_n + \epsilon]$, $\forall\ \epsilon > 0$. According to local uniqueness, one gets a solution $u$ on the larger interval $[0, T_{max} + \epsilon)$. It leads to a contradiction with the maximal interval $[0, T_{max})$. Therefore, (10.14) and (10.15) are hold. □

Obviously, we can state the global existence of the solution as follows

**Theorem 10.10.** *Let Assumption 10.4.1 be satisfied, there exists a unique solution of System (10.4-10.6) for all $T \in (0, \infty)$.*

*Proof.* Suppose that there exists a maximal interval $[0, T_{max})$ of the solution $u$. By the above lemma, $\lim_{t\longrightarrow T_{max}} \|A_i(t,.)\|_{L^1((0,m))} = \infty$ and $\lim_{t\to T_{max}} \|B_i(t,.,.)\|_{L^1((0,\Delta)\times(0,m))} = \infty$. In contrast, one has from Lemma 10.4 for $i = 0$

$$\begin{aligned} \|A_0(t,.)\|_{L^1((0,m))} &\leqslant e^{-\delta_A t}\|A_{0,0}\|_{L^1((0,m))} + \frac{\Lambda}{\delta_A}\left(1 - e^{-\delta_A t}\right), \\ \|B_0(t,.,.)\|_{L^1((0,\Delta)\times(0,m))} &\leqslant \frac{\|\lambda\|_\infty \left(e^{C_{v_0}} - 1\right)}{C_{v_0} t}\left[e^{-\delta_A t}\|A_{0,0}\|_{L^1((0,m))} + \frac{\Lambda}{\delta_A}\left(1 - e^{-\delta_A t}\right)\right]. \end{aligned}$$

That's mean for $t \longrightarrow T_{max}$:

$$\lim_t \|A_0(t,.)\|_{L^1((0,m))} < \infty \quad \textit{and} \quad \lim_t \|B_0(t,.,.)\|_{L^1((0,\Delta)\times(0,m))} < \infty.$$

It is a contradiction. Then the conclusion $T_{max} = \infty$ holds. □

**Corollary 10.11.** *Let Assumption 10.4.1 be satisfied and let $\Lambda = 0$, there exists a unique solution of System (4.4)-(4.6) for all $T \in (0, \infty)$.*

*Proof.* By using Theorem 10.10, one deduces directly the global existence of a solution for System (4.4)-(4.6). □

# Chapter 11

# Asymptotic behaviour for an age-structured model describing the T cell homeostasis in vivo

**This chapter is based on the article [81].**

***Abstract.*** *In this study, we consider a model of T cell proliferation in vivo which is structured by age and CD44 expression. This model is rewritten as an age-structured model system without the CD44 structure, and we investigate its asymptotic behaviour. We find that there exists one or three stationary solutions when cells undergo at least five divisions and only one stationary solution when cells undergo at most three divisions, the limiting case with four divisions is numerically handled. By applying the Lyapunov method, we prove in some cases of uniqueness that the stationary solution is globally asymptotically stable.*

## 11.1 Introduction

Despite great advances in immunological research during the last decades, many questions remain in the modeling of T cell proliferation in condition of cell deficiency. Indeed, understanding the process of T cell homoeostasis in vivo stays a very important subject to address. For example, the asymptotic behaviour of T cells is one of the important keys to analyse the homoeostatic process in vivo. In this

chapter, we rewrite System (10.1-10.3) as an age-structured model system (without CD44 expression), and we investigate its asymptotic behaviour.

## 11.2 Reduced in vivo model

Integrating System (10.1-10.3) with respect to the variable $s$ (CD44 expression), we derive an age-structured system characterized by cascade. It reads

$$\begin{cases} \dfrac{dA_0(t)}{dt} = \Lambda - \delta_A A_0(t) - \lambda^0(N)A_0(t), \\ \dfrac{dA_i(t)}{dt} = 2\displaystyle\int_0^{\Delta} \mu(\tau)B_{i-1}(t,\tau)\, d\tau - \delta_A A_i(t) - \lambda^i(N)A_i(t) \qquad for \quad i \in \mathbb{N}^*, \\ \frac{\partial}{\partial t}B_i(t,\tau) + \frac{\partial}{\partial \tau}B_i(t,\tau) = -(\delta_B + \mu(\tau))B_i(t,\tau) \qquad for \quad i \in \mathbb{N}, \\ B_i(t,0) = \lambda^i(N)A_i(t), \\ B_{i\in\mathbb{N}}(0,\tau) = 0 \quad and \quad A_{i\in\mathbb{N}^*}(0) = 0, \\ A_0(0) = \int_0^m \tilde{A}_{0,0}(s)\, ds := A_{0,0} \geqslant 0. \end{cases} \tag{11.1}$$

where $A_{0,0}$ is a positive constant, $A_i(t) := \int_0^m \tilde{A}_i(t,s)ds$, $B_i(t,\tau) := \int_0^m \tilde{B}_i(t,\tau,s)ds$ and $(\tilde{A}_i, \tilde{B}_i)$, $\forall\ i \in \mathbb{N}$ are the state variables of (10.1-10.3).

*Remark* 11.1. According to Yates et al [7] and Hogan et al [10], T cells can undergo a finite number of division ($I$) (8 or 9 division with CFSE labelling). We assume a recruitment rate from A-state into B-phase, for all $i \in \mathbb{N}$

$$\lambda^i(N) = \begin{cases} \lambda_0 N & if \quad i \in \mathbb{N}_{I-1} := \{0, ..., I-1\} \\ 0 & else. \end{cases}$$

where $\lambda_0 > 0$. Therefore, there are no cells after $A_I$ phase (i.e Ith division in A-state).

In Table 11.1, we describe the parameters used in System (11.1).

TABLE 11.1: Parameters for (11.1).

| Parameters | Description |
|---|---|
| $\Delta$ | Duration of the proliferative phase (B-phase) |
| $\mu(\tau)$ | Division rate at age $\tau$ |
| $\lambda_0$ | Weight rate of entry into division |
| $\Lambda$ | Rate of export of cells from the thymus |
| $I$ | Maximum division number undergone by cells |
| $\delta_A$, $\delta_B$ | Natural mortality rates of cells in A-state and B-phase respectively |

The total cell number is

$$N := N(t) = \sum_{i\in\mathbb{N}} \left( A_i(t) + \int_0^\Delta B_i(t,\tau)d\tau \right). \tag{11.2}$$

*Remark* 11.2. If $\Lambda$ is equal to 0, one gets an in vitro model defined in Part II and III (or see [80]). Then, the total number of cells decreases to zero and the unique stationary solution is the trivial one. Therefore, to study the asymptotic behaviour in case of non trivial equilibrium, the rate of export of cells $\Lambda$ from the thymus must be a strictly positive constant.

In what follows, we shall make use of the following assumption.

*Assumption* 11.2.1. - $\delta_A = \delta_B = \delta > 0$, $\Lambda > 0$.

- Function $\mu(.)$ is bounded, non-negative and satisfies the following inequality

$$0 \leq \underline{\mu} \leq \mu(\tau) \leq \bar{\mu}, \quad \forall\ \tau \in (0,\Delta).$$

- Function $\lambda^i(N)$ is non-negative and satisfies Remark 11.1.

- Initial condition $\tilde{A}_{0,0}(.)$ is non-negative and belongs to $L^1_+(0,m)$.

By integrating the PDEs in (11.1) with respect to $\tau$ and using (11.2), the ODEs in (11.1) and Assumption (11.2.1), one obtains an ordinary differential equation related to the total number of cells ($N$). Hence, it reads as following

$$\frac{dN(t)}{dt} = \Lambda + \sum_{i\in\mathbb{N}^*} \int_0^\Delta \mu(\tau)B_{i-1}(t,\tau)d\tau - \delta N(t). \tag{11.3}$$

In this chapter, we are interested in the asymptotic behaviour of the dynamic of T cells in vivo without CD44 expression (i.e the reduced System (11.1)). This

work is organised as follows. Section 11.3 is devoted to prove the existence of a global attractor and to give some properties which are used in the asymptotic study of System (11.1). Next, we look in Section 11.4 for the existence and uniqueness of stationary solution for System (11.1). Finally, Section 11.5 is divided in two subsections. In the first one, we prove the global stability of the stationary solution in some cases of uniqueness by using the Lyapunov method. Next, we illustrate in the second subsection some numerical simulations of the dynamic of System (11.1) in order to complete the analytical results of the first subsection.

## 11.3 Global attractor for System (11.1)

The aim of this section is to prove the existence of a unique bounded dissipative semiflow associated to System (11.1). Let

$$W_I = \left\{ (A,B) \in \mathbb{R}^{\mathbb{N}} \times L^1_+((0,\Delta),\mathbb{R}^{\mathbb{N}}); \begin{pmatrix} N_0 \\ N_1 \\ : \\ : \\ N_I \end{pmatrix} \leq \begin{pmatrix} \frac{\Lambda}{\delta} \\ \\ \frac{2\Lambda\bar{\mu}}{\delta^2} \\ : \\ : \\ \frac{2^I\Lambda\bar{\mu}^I}{\delta^{I+1}} \end{pmatrix} \right\},$$

where $A = \{A_i,\ i \in \mathbb{N}\},\ B = \{B_i,\ i \in \mathbb{N}\}$ *and* $N_i := A_i + \int_0^\Delta B_i(\tau)d\tau,\ \forall\ i \in \mathbb{N}_I$.

**Lemma 11.3.** *Let Assumption 11.2.1 be satisfied. The set $W_I$ is positively invariant with respect to System (11.1).*

*Proof.* Let $b_i(t) := \int_0^\Delta B_i(t,\tau)d\tau,\ \forall\ i \in \mathbb{N}_I$. By integrating the PDE of System (11.1) with respect to the age $\tau$, one obtains for $i \in \mathbb{N}_I$

$$\frac{db_i}{dt} = \lambda^i(N)A_i(t) - \delta b_i(t) - \int_0^\Delta \mu(\tau)B_i(t,\tau)d\tau.$$

Then, one deduces that $N_i(t)$ satisfies

$$\frac{dN_0(t)}{dt} = \Lambda - \delta N_0(t) - \int_0^\Delta \mu(\tau)B_0(t,\tau)d\tau \leq \Lambda - \delta N_0(t),$$

and for all $i \in \mathbb{N}_I^*$,

$$\begin{aligned}\frac{dN_i(t)}{dt} &= 2\int_0^\Delta \mu(\tau)B_{i-1}(t,\tau)d\tau - \delta N_i(t) - \int_0^\Delta \mu(\tau)B_i(t,\tau)d\tau \\ &\leq 2\int_0^\Delta \mu(\tau)B_{i-1}(t,\tau)d\tau - \delta N_i(t). \end{aligned} \tag{11.4}$$

Therefore $\limsup_{t\to+\infty} N_0(t) \leq \frac{\Lambda}{\delta}$. If $N_0(t) \leq \frac{\Lambda}{\delta}$ is satisfied for some $t = t_0 \in \mathbb{R}$, than it is satisfied for all $t \geqslant t_0$. Hence, one obtains the following estimate

$$\int_0^\Delta B_0(t,\tau)d\tau \leq \frac{\Lambda}{\delta}.$$

Replacing the above estimate in (11.4), one has for $i = 1$

$$\frac{dN_1(t)}{dt} \leq \frac{2\Lambda\bar{\mu}}{\delta} - \delta N_1(t),$$

and therefore $\limsup_{t\to+\infty} N_1(t) \leq \frac{2\Lambda\bar{\mu}}{\delta^2}$. As in the case $i = 0$, if $N_1(t) \leq \frac{2\Lambda\bar{\mu}}{\delta^2}$ is satisfied for some $t = t_1 \geqslant t_0$, then it holds for all $t \geqslant t_1$. By induction, one gets $N_i(t) \leq \frac{2^i\Lambda\bar{\mu}^i}{\delta^{i+1}}$, for all $t \geqslant t^*$, with $t^* = \max_{i\in\mathbb{N}_I} t_i$. □

To prove the existence of a global attractor which is used in the asymptotic study, we shall deal with (11.1) using an integrated semi group approach.

**Integrated semigroup formulation**. This approach has been introduced by Thieme [108] in the context of age structured equations. We also refer to [109–115].

Let us introduce the Banach space

$$\chi = \mathbb{R}^{\mathbb{N}} \times \mathbb{R}^{\mathbb{N}} \times L^1\left((0,\Delta),\mathbb{R}^{\mathbb{N}}\right),$$

endowed with the usual product norm, and set

$$\begin{aligned}\chi_0 &:= \mathbb{R}^{\mathbb{N}} \times \{0_{\mathbb{R}^{\mathbb{N}}}\} \times L^1\left((0,\Delta),\mathbb{R}^{\mathbb{N}}\right), \\ \chi_+ &:= \mathbb{R}_+^{\mathbb{N}} \times \mathbb{R}_+^{\mathbb{N}} \times L_+^1\left((0,\Delta),\mathbb{R}^{\mathbb{N}}\right), \\ \chi_{0+} &:= \chi_0 \cap \chi_+.\end{aligned}$$

Let the following operators be defined by

$$\begin{array}{lccc} \phi: & \mathbb{R}^{\mathbb{N}} & \longmapsto & \mathbb{R}^{\mathbb{N}} \\ & A & \longmapsto & \delta\phi A \end{array}, \quad \begin{array}{lccc} \psi: & \mathbb{R}^{\mathbb{N}} & \longmapsto & \mathbb{R}^{\mathbb{N}} \\ & A & \longmapsto & \lambda(N)\psi A \end{array}, \quad \begin{array}{lccc} \varpi: & L^1\left((0,\Delta),\mathbb{R}^{\mathbb{N}}\right) & \longmapsto & L^1\left((0,\Delta),\mathbb{R}^{\mathbb{N}}\right) \\ & B & \longmapsto & (\delta+\mu(.))\varpi B \end{array}$$

with $(\delta\phi A)_i = \delta A_i$, $(\lambda(N)\psi A)_i = \lambda_0^i N A_i$ and $((\delta+\mu(.))\varpi B)_i = (\delta+\mu(.))B_i$, $\forall$ $i \in \mathbb{N}$.

Now, one considers the linear operator $E : D(E) \subset \chi \longmapsto \chi$ defined by

$$E\begin{pmatrix} A \\ \begin{pmatrix} 0_{\mathbb{R}^{\mathbb{N}}} \\ \\ B \end{pmatrix} \end{pmatrix} = \begin{pmatrix} -\delta\phi A \\ \begin{pmatrix} -B(0,.) \\ \\ -B' - (\delta+\mu(.))\varpi B \end{pmatrix} \end{pmatrix},$$

where

$$D(E) = \mathbb{R}^{\mathbb{N}} \times \{0_{\mathbb{R}^{\mathbb{N}}}\} \times W^{1,1}\left((0,\Delta),\mathbb{R}^{\mathbb{N}}\right),$$

and $W^{1,1}$ is a Sobolev space. Note that the domain of operator $E$ is not dense in $\chi$ because of the identify

$$\bar{D}(E) = \mathbb{R}^{\mathbb{N}} \times \{0_{\mathbb{R}^{\mathbb{N}}}\} \times L^1\left((0,\Delta),\mathbb{R}^{\mathbb{N}}\right) \neq \chi.$$

Finally let us introduce the non-linear map $F : \bar{D}(E) \longmapsto \chi$ defined by

$$F\begin{pmatrix} A \\ \begin{pmatrix} 0_{\mathbb{R}^{\mathbb{N}}} \\ \\ B \end{pmatrix} \end{pmatrix} = \begin{pmatrix} \tilde{\Lambda} - \lambda(N(t))\psi A(t) \\ \begin{pmatrix} \lambda(N(t))\psi A(t) \\ \\ 0_{L^1} \end{pmatrix} \end{pmatrix} \qquad with \quad \tilde{\Lambda} = \begin{pmatrix} \Lambda \\ \\ 2\int_0^\Delta \mu(\tau)B_0(t,\tau)d\tau \\ \\ 2\int_0^\Delta \mu(\tau)B_1(t,\tau)d\tau \\ \vdots \end{pmatrix}.$$

Let $u(t) = \begin{pmatrix} A(t) \\ \begin{pmatrix} 0_{\mathbb{R}^{\mathbb{N}}} \\ B(t,.) \end{pmatrix} \end{pmatrix}$ and $u_0 = \begin{pmatrix} A(0) \\ \begin{pmatrix} 0_{\mathbb{R}^{\mathbb{N}}} \\ B(0,.) \end{pmatrix} \end{pmatrix}$. Then we can reformulated System (11.1) as the following abstract Cauchy problem

$$\frac{du(t)}{dt} = Eu(t) + F(u(t)), \quad t > 0 \ \text{ and } \ u(0) = u_0 \in \chi_{0+}. \tag{11.5}$$

From results in Thieme [108], Magal [110] (see Magal and Ruan [111] for more results), we derive that the above abstract Cauchy problem generates a unique globally defined and positive semiflow.

**Theorem 11.4.** *Let Assumption 11.2.1 be satisfied. Then there exists a unique strongly continuous semiflow* $\{U(t) : \chi_{0+} \longmapsto \chi_{0+}\}_{t\geqslant 0}$ *such that for each* $u_0 \in \chi_{0+}$, *the map* $u \in C([0,\infty) : \chi_{0+})$ *defined by* $u = U(.)u_0$ *is a mild solution of (11.5). Furthermore* $\{U(t)\}_{t\geqslant 0}$ *satisfies the following properties:*

*(i) Let* $U(t)u_0 = (A(t), (0_{\mathbb{R}^{\mathbb{N}}}, B(t,.)))^T$, *then the following Volterra integral formulation holds true for all* $i \in \mathbb{N}_{I-1}$

$$B_i(t,\tau) = \begin{cases} 0 & t < \tau \\ \\ \lambda_0 N(t-\tau) A_i(t-\tau)\ e^{-\int_0^\tau (\delta+\mu(r))dr} & \tau \leqslant t \end{cases}$$

*coupled with the* $A_i$ *equations of (11.1).*

*(ii)* $A_i \equiv 0$, $\forall\ i > I$ *and* $B_i \equiv 0$, $\forall\ i \geqslant I$.

*(iii) There exist* $t^* > 0$ *such that for all* $t \geqslant t^*$, $N_i(t) \leq \frac{2^i \Lambda \bar{\mu}^i}{\delta^{i+1}}$, $\forall\ i \in \mathbb{N}_I$.

*Proof.* The proof of this result is standard. Indeed, one may check that operator $E$ satisfies the Hille-Yosida property. Then standard methodologies apply to provide the existence and uniqueness of mild solution for System (11.1). (see [110–113] for more details). Next, the Volterra integral formulation $(i)$ is also standard in the context of age structured equation. By using Remark 11.1, one deduces $(ii)$. Also from Lemma 11.3, one deduces the estimates in $(iii)$. □

From Lemma 11.3, one deduces that the set

$$M = \left\{ \begin{pmatrix} A \\ \begin{pmatrix} 0_{\mathbb{R}^{\mathbb{N}}} \\ B \end{pmatrix} \end{pmatrix} \in \mathbb{X}_{0+}; \quad \begin{pmatrix} N_0 \\ N_1 \\ \vdots \\ \vdots \\ N_I \end{pmatrix} \leq \begin{pmatrix} \frac{\Lambda}{\delta} \\ \frac{2\Lambda\bar{\mu}}{\delta^2} \\ \vdots \\ \vdots \\ \frac{2^I\Lambda\bar{\mu}^I}{\delta^{I+1}} \end{pmatrix} \right\}$$

is positively invariant absorbing set under $U$ ; in other words

$$U(t)M \subseteq M.$$

By using the result of Hale [116], one concludes that $\{U(t)\}_{t\geqslant 0}$ is bounded dissipative on $\chi_{0+}$. Furthermore, the semiflow is asymptotically smooth (see Webb [117], Magal and Thieme [118], Thieme and Vrabie [119]). Also from Hale [116], we obtain the following theorem of the existence of global attractors.

**Theorem 11.5.** *There exists a non-empty set $\mathcal{A} \subset \chi_{0+}$ such that*

*(i) $\mathcal{A}$ is invariant under the semiflow $\{U(t)\}_{t\geqslant 0}$.*

*(ii) The subset $\mathcal{A}$ attracts the bounded set of $\chi_{0+}$ under the semiflow $U$.*

The attractor $\mathcal{A}$ consists of complete orbits of $U$, meaning that for any point $(A(0), 0_{\mathbb{R}^{\mathbb{N}}}, B(0,.)) \in \mathcal{A}$, there is a solution $\{(A(t), 0_{\mathbb{R}^{\mathbb{N}}}, B(t,.)), \quad t \in \mathbb{R}\}$ of equation (11.5) which passes through $(A(0), 0_{\mathbb{R}^{\mathbb{N}}}, B(0,.))$ at time $t = 0$.

**Further estimate**: Without loss of generality, one may restrict ourselves to the subdomain $M$. Hence one may assume that

$$N(t) = \sum_{i=0}^{I} N_i(t) \leq \sum_{i=0}^{I} \frac{2^i\Lambda\bar{\mu}^i}{\delta^{i+1}} := N^+. \tag{11.6}$$

**Lemma 11.6.** *Let Assumption 11.2.1 be satisfied. The domain*

$$M_0 = \left\{ \begin{pmatrix} A \\ \begin{pmatrix} 0_{\mathbb{R}^{\mathbb{N}}} \\ B \end{pmatrix} \end{pmatrix} \in \chi_{0+}; \quad A_0 \geqslant \frac{\Lambda}{\delta + \lambda_0 N^+} \quad \text{and} \quad \begin{pmatrix} N_0 \\ N_1 \\ : \\ : \\ N_I \end{pmatrix} \leq \begin{pmatrix} \frac{\Lambda}{\delta} \\ \frac{2\Lambda\bar{\mu}}{\delta^2} \\ : \\ : \\ \frac{2^I \Lambda \bar{\mu}^I}{\delta^{I+1}} \end{pmatrix} \right\}$$

*is positively invariant and is an absorbing set for $U$ restricted to $M$. Furthermore, $\mathcal{A} \subseteq M_0$.*

*Proof.* Let $u_0 = \begin{pmatrix} A(0) \\ \begin{pmatrix} 0_{\mathbb{R}^{\mathbb{N}}} \\ B(0,.) \end{pmatrix} \end{pmatrix} \in M_0$ be given and let us denote for each $t \geqslant 0$, $U(t)u_0 := (A(t), 0_{\mathbb{R}^{\mathbb{N}}}, B(t,.))^T$ the orbit passing through $u_0$.

By using (11.6) and the $A_0$ equation in (11.1), one obtains

$$\frac{dA_0(t)}{dt} \geqslant \Lambda - (\delta_A + \lambda_0 N^+) A_0(t). \tag{11.7}$$

Since $u_0 \in M_0$, then $A_0(0) \geqslant \frac{\Lambda}{\delta + \lambda_0 N^+}$, and therefore, one has

$$A_0(t) \geqslant \frac{\Lambda}{\delta + \lambda_0 N^+}.$$

This completes the proof of Lemma 11.6. □

Finally in this section, we give a result that will be used to prove our stability result.

**Lemma 11.7.** *For each $(A, 0_{\mathbb{R}^{\mathbb{N}}}, B) \in \mathcal{A}$, there exists $A_i^- > 0$ for all $i \in \mathbb{N}_I$ and $B_i^- > 0$ for all $i \in \mathbb{N}_{I-1}$ such that*

$$A_i > A_i^- \quad \text{and} \quad \int_0^{\Delta} B_i(\tau) d\tau > B_i^- \ .$$

*Proof.* Let $(A, 0_{\mathbb{R}^{\mathbb{N}}}, B)$ be the solution of equation (11.5) with initial condition $(A(0,.), 0_{\mathbb{R}^{\mathbb{N}}}, B(0,.,.)) \in \mathcal{A}$. Since the solution is in the attractor, the previous lemma implies

$$A_0(t) \geqslant \frac{\Lambda}{\delta + \lambda_0 N^+} > 0,$$

for all $t \geqslant 0$. Thus, for sufficiently small $A_0^- > 0$, one has $A_0(t) \geqslant A_0^-$, for all $t \geqslant 0$. Equation (11.3) can be written as

$$\frac{dN}{dt} \geqslant \Lambda - \delta N(t).$$

Then, for a given large $t^*$, one has

$$N(t) \geqslant N^- := \min\{\frac{\Lambda}{\delta}, N(t^*)\}. \tag{11.8}$$

Thus, by (11.8) and (i) of Theorem 11.4, one obtains for all $t \geqslant t^*$

$$\int_0^\Delta B_0(t,\tau)d\tau \geqslant \lambda_0 N^- A_0^- \beta, \quad where \quad \beta := \int_0^\Delta e^{-\int_0^\tau (\delta+\mu(r))dr} d\tau.$$

Therefore for sufficiently small $B_0^- > 0$, one has $\int_0^\Delta B_0(t,\tau)d\tau > B_0^-$.

From (11.6), one has

$$\frac{dA_1(t)}{dt} \geqslant 2\underline{\mu}\int_0^\Delta B_0(t,\tau)d\tau - (\delta + \lambda_0 N^+)A_1(t) \quad \Longrightarrow \quad A_1(t) \geqslant \frac{2\underline{\mu}B_0^-}{(\delta+\lambda_0 N^+)} := A_1^-.$$

By induction, one may check

$$A_i(t) \geqslant \frac{2\underline{\mu}B_{i-1}^-}{(\delta+\lambda_0 N^+)} > A_i^-, \quad \int_0^\Delta B_i(t,\tau)d\tau \geqslant \lambda_0 \Lambda N^- A_i^- \beta > B_i^-,$$

$\forall\ i = 2, ..., I-1$, and for $i = I$

$$A_I(t) \geqslant \frac{2\underline{\mu}B_{I-1}^-}{\delta} > A_I^-.$$

where $A_i^-$ and $B_i^-$ are sufficiently small. This completes the proof of Lemma 11.7. □

## 11.4 Stationary solution for System (11.1)

In what follows,

$$I, \quad d := \int_0^\Delta \mu(\tau) e^{-\int_0^\tau (\delta+\mu(r))dr} \quad and \quad \rho := \frac{2\delta^2}{\lambda_0 \Lambda}, \tag{11.9}$$

are the key parameters to study the asymptotic behaviour of System (11.1). Parameter $d$ can be described by the cumulative rate of cells that will divide in B-phase. $\frac{1}{\rho} = \frac{1}{2\delta^2}\lambda_0\Lambda$ is an aggregated parameter related to $\lambda_0\Lambda$, the recruitment rate of exported cells coming from the thymus and passing from A-state to B-phase, see Remark 11.1, whose dimension is *cell* $\times$ *hour*.

Let $\bar{A}_i$ for all $i \in \mathbb{N}_I$ and $\bar{B}_i(.)$ for all $i \in \mathbb{N}_{I-1}$ be a stationary solution of System (11.1)

$$\begin{cases} \Lambda - \delta\bar{A}_0 - \lambda_0\bar{N}\bar{A}_0 = 0, \\ 2\int_0^\Delta \mu(\tau)\bar{B}_{i-1}(\tau)d\tau - \delta\bar{A}_i - \lambda_{0,i}\bar{N}\bar{A}_i = 0, \qquad \forall\ i \in \mathbb{N}_I^* := \{1, ...I\} \\ \\ \frac{d\bar{B}_i(\tau)}{d\tau} + (\delta + \mu(\tau))\bar{B}_i(\tau) = 0, \qquad \forall\ i \in \mathbb{N}_{I-1} := \{0, ..., I-1\} \\ \bar{B}_i(0) - \lambda_0\bar{N}\bar{A}_i = 0. \end{cases} \tag{11.10}$$

Then, one has

$$\begin{aligned} \bar{A}_0 &= \frac{\Lambda}{\delta + \lambda_0\bar{N}}, \quad \bar{A}_i = \frac{2\int_0^\Delta \mu(\tau)\bar{B}_{i-1}(\tau)}{\delta + \lambda_0\bar{N}}, \qquad \forall\ i \in \mathbb{N}_I^*, \\ \bar{B}_i(\tau) &= \lambda_0\bar{N}\bar{A}_i\ e^{-\int_0^\tau(\delta+\mu(r))dr}, \qquad \forall\ i \in \mathbb{N}_{I-1} \end{aligned}$$

wherein

$$\bar{N} = \sum_{i=0}^{I-1}\left(\int_0^\Delta \bar{B}_i(\tau)d\tau\right) + \sum_{i=0}^{I}\bar{A}_i. \tag{11.11}$$

A recursive argument yields

$$\bar{A}_i = \frac{2^i\Lambda\lambda_0^i\bar{N}^i d^i}{\left(\delta + \lambda_0\bar{N}\right)^{i+1}},\ \bar{B}_i(\tau) = \frac{2^i\Lambda\lambda_0^{i+1}\bar{N}^{i+1}d^i c(\tau)}{\left(\delta + \lambda_0\bar{N}\right)^{i+1}},\ \forall\ i \in \mathbb{N}_{I-1}\ \textit{and}\ \bar{A}_I = \frac{2^I\Lambda\lambda_0^I\bar{N}^I d^I}{\delta\left(\delta + \lambda_0\bar{N}\right)^I}, \tag{11.12}$$

where $c(\tau) := e^{-\int_0^\tau(\delta+\mu(r))dr}$ and $d$ is given in (11.9). Note that

$$0 < d \leq 1 - e^{-\int_0^\Delta \mu(r)dr} < 1. \tag{11.13}$$

Constant $d$ is much smaller than $\frac{1}{2}$ when using realistic parameters from [4, 6, 7, 10, 80].

**Theorem 11.8.** *Let Assumption 11.2.1 be satisfied. System (11.1) admits one or three stationary solutions for all $I \in \mathbb{N}^*$. Uniqueness holds when one of the following conditions is fulfilled*

*1-)* $I = 1, 2$ *or* $3$ *for all* $d \in (0, 1)$ *and* $\rho > 0$.

*2-)* $0 < d \leq \frac{1}{2}$ *for all* $I \in \mathbb{N}^*$ *and* $\rho > 0$.

*3-)* $I \geq 4$, $\rho \geq \rho(I)$ *for a suitably large* $\rho(I) > 0$ *given in (11.18) below and all* $d \in (\frac{1}{2}, 1)$.

*4-)* $I \geq 4$, $\rho > 0$ *and* $d \in (\frac{1}{2}, 1)$ *satisfying*

$$\frac{2d}{(1-2d)^2}\left[1 + (2d)^I\ (2Id - I - 1)\right] < \frac{(\rho+2)^2}{\rho} \quad cf.\ (11.9)\ for\ (d,\ \rho). \tag{11.14}$$

*Proof.* According to (11.12), it is sufficient to prove the existence of one or three stationary solutions for $\bar{N}$. At equilibrium, $\frac{d\bar{N}}{dt} = 0$, then (11.3) leads to the following equality

$$\bar{N} = \frac{\Lambda}{\delta} + \sum_{i=1}^{I} \frac{2^{i-1}\lambda_0^i \bar{N}^i d^i \Lambda}{\delta\left(\delta + \lambda_0 \bar{N}\right)^i}. \tag{11.15}$$

The mean value theorem applied to $[0, +\infty)$ ensures that (11.15) admits at least one positive root. Next, performing a change of variable ($\omega := \frac{\lambda_0}{\delta}\bar{N}$ and $\rho := \frac{2\delta^2}{\lambda_0 \Lambda}$), one obtains

$$\rho\omega = 2 + \sum_{i=1}^{I} \frac{2^i \omega^i d^i}{(1+\omega)^i} \tag{11.16}$$

**Proof of 1-)**

**For $I = 1$:** (11.16) reduces to a quadratic polynomial equation, $\rho\omega^2 + a_1\omega + a_2 = 0$, with $a_2 = -2$ yielding a unique positive root.

**For $I = 2$:** (11.16) reduces to a cubic polynomial equation $P_3(\omega) = \rho\omega^3 + a_1\omega^2 + a_2\omega + a_3 = 0$, with $a_3 = -2 < 0$ so that $P_3$ has 1 or 3 positive roots. Descartes's rule of signs requires three sign changes to get three positive solutions, that is $a_1 < 0$ and $a_2 > 0$. Elementary algebra shows that $a_1 = 2\left[\rho - (1 + d + 2d^2)\right] < 0$ and $a_2 = [\rho - 2(2 + d)] > 0$ imply $2d^2 - d - 3 > 0$ that is impossible because $0 < d < 1$. This shows uniqueness for $I = 2$.

**For $I = 3$:** (11.16) reduces to a 4th order polynomial equation $P_4(\omega) = \rho\omega^4 + a_1\omega^3 + a_2\omega^2 + a_3\omega + a_4 = 0$, with $a_4 = -2 < 0$ so that $P_4$ has 1 or 3 positive roots.

• When $a_1 > 0$, Descartes's rule of signs requires three sign changes to get three positive solutions, that is $a_2 < 0$ and $a_3 > 0$. Elementary algebra shows that $a_2 = 3\rho - 6 - 4d - 4d^2 < 0$ and $a_3 = \rho - 6 - 2d > 0$ imply $12 + 2d - 4d^2 < 0$ that is impossible because $0 < d < 1$.

• When $a_1 = 3\rho - 2 - 2d - 4d^2 - d^3 < 0$ then one also has $a_3 = \rho - 6 - 2d <$

0. Assuming $P_4$ possesses three positive roots then Rolle's Theorem asserts its derivative polynomial $P_4'$ has at least two positive roots.
Now $P_4'(\omega) = 4\rho\omega^3 + 3a_1\omega^2 + 2a_2\omega + a_3$ and $a_3 < 0$ implies $P_4'$ has 1 or 3 positive roots. As a consequence when $a_1 < 0$ if $P_4$ has 3 positive roots then $P_4'$ also has 3 positive roots.
Setting $Q_4(\omega) = -\frac{1}{4}P_4'(-\omega) = \omega^3 + \alpha_1\omega^2 + \alpha_2\omega + \alpha_3$, one may use Routh-Hurwitz criterion to check whether $Q_4$ has 3 negative roots.
First $\alpha_1 = -\frac{3}{4\rho}a_1 > 0$, $\alpha_3 = -\frac{1}{4\rho}a_3 > 0$. Elementary but lengthy algebra yields $\alpha_1 \times \alpha_2 - \alpha_3 < 0$ because $0 < d < 1$. Indeed

$$\alpha_1 \times \alpha_2 - \alpha_3 := R(\rho) = 25\rho^2 + \beta_1\rho + \beta_2,$$

where

$$\begin{aligned} \beta_1 &:= 60 + 50\,d + 72\,d^2 + 72\,d^3, \\ \beta_2 &:= -36 - 60\,d - 120\,d^2 - 216\,d^3 - 144\,d^4 - 96\,d^5. \end{aligned}$$

Polynomial $R(\rho)$ reaches its maximum value at $\rho = \frac{\beta_1}{50}$.

$$R(\rho) \leq R(\frac{\beta_1}{50}) \leq H(d) := \frac{d^2}{25}\left(-215 - 1440\,d - 504\,d^2 + 192\,d^3 + 1296\,d^4\right)$$

Finally, one remarks that $0 < d < 1 \;\Rightarrow\; R(\frac{\beta_1}{50}) < 0$. Then, $Q_4$ cannot have three negative roots. As a consequence uniqueness holds for $I = 3$.

**Proof of 2-)** Assume $I \geq 4$. Performing a change of variable in (11.16), $u := \frac{2\omega d}{1+\omega}$, one gets

$$P_{I+1}(u) := u^{I+1} + (1-2d)u^I + ... + (1-2d)u^2 + (2-2d+\rho)u - 4d = 0. \quad (11.17)$$

Using Descartes's rule of signs and (11.13), polynomial $P_{I+1}$ for all $I \in \mathbb{N}^*$ admits one or three positive roots (see Fig. 11.1) that satisfies $0 < u < 2d$ ($u = \frac{2\omega d}{1+\omega} \;\Leftrightarrow\; \omega = \frac{u}{2d-u}$).
If $1 - 2d > 0$, $P_{I+1}$ has only one sign change in its coefficients and admits only one positive root.

**Proof of 3-) (Estimating the sign of the derivative of (11.17))** The first derivative of (11.17) is $P_{I+1}'(u) = (I+1)u^I + (1-2d)\sum_{j=2}^{I} ju^{j-1} + (2-2d+\rho)$.

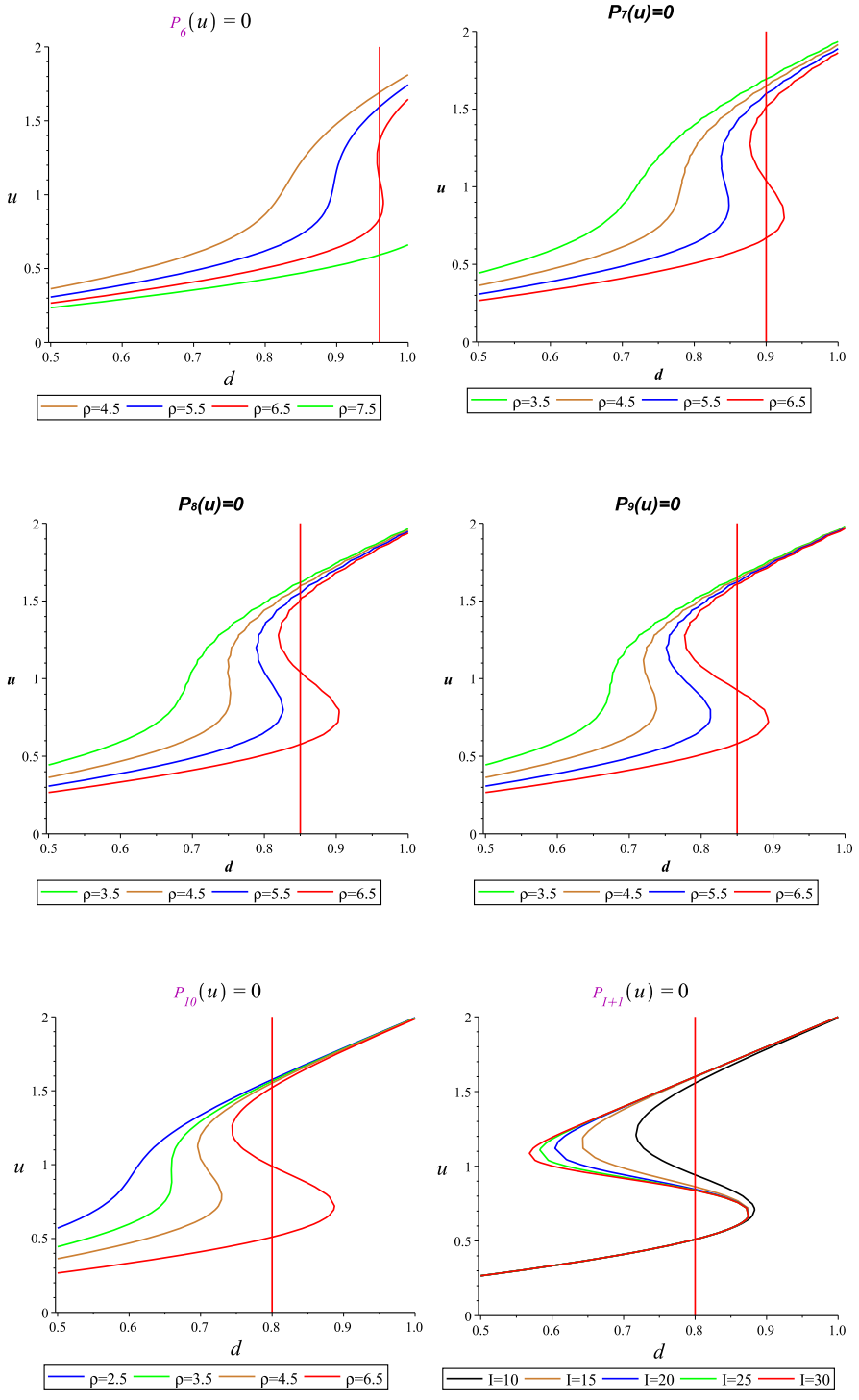


FIGURE 11.1: The first five subfigures represent the implicit plot of the level set $P_{I+1}(u) = 0$ as a function of $(d, u)$ when $I = 5, 6, 7, 8, 9$ and $\rho$ constant. The last one $(P_{I+1})$ is drawn for a large $I = 10, 15, 20, 25, 30$ and $\rho = 6.5$. The vertical lines (red lines) show the existence of three stationary solutions for some values of $d$.

Since $u > 0$ and $0 < d < \frac{1}{2}$, one has

$$P'_{I+1}(u) \geq H_I(u) + \rho, \quad H_I(u) := (I+1)u^I - \sum_{j=2}^{I} j u^{j-1}.$$

Polynomial $H_I(u)$ reaches its minimum value in the range $u > 0$ at some $u_I^{min}$, so does $H_I(u) + \rho$. Therefore if the following condition is fulfilled

$$\rho \geq \rho(I) := -H_I(u_I^{min}), \tag{11.18}$$

polynomial $P_{I+1}$ is strictly increasing and has a unique positive root.

**Proof of 4-) (Fixed point method)** From (11.16), let

$$f(\omega) := \frac{1}{\rho}\left(2 + \sum_{i=1}^{I} \frac{2^i \omega^i d^i}{(1+\omega)^i}\right), \quad \omega > 0$$

Stationary solutions correspond to solutions of $\omega = f(\omega)$. We shall prove that

(i) $f$ is a map from $[0, H]$ to $[\frac{2}{\rho}, H]$ where

$$H := \frac{2}{\rho}\left[1 + \frac{d(1 - 2^I d^I)}{1 - 2d}\right]. \tag{11.19}$$

(ii) If (11.14) is fulfilled then $f$ is a strict contraction i.e $0 < |Df(\omega)| < 1$ for $\frac{2}{\rho} \leq \omega \leq H$.

The proof of (i) is rather straightforward, using $0 \leq \frac{\omega}{1+\omega} \leq 1$. This implies that any positive fixed point of $f$ belongs to $[\frac{2}{\rho}, H]$.
Proof of (ii): The derivative of $f$ is

$$f'(\omega) = \frac{1}{\rho}\sum_{i=1}^{I} i 2^i d^i \left[\frac{\omega^{i-1}}{(1+\omega)^{i+1}}\right] > 0. \tag{11.20}$$

Since $\omega \in [\frac{2}{\rho}, H]$ and $d \in (\frac{1}{2}, 1)$, one has

$$f'(\omega) \leq \frac{1}{\rho(1+\frac{2}{\rho})^2} \sum_{i=1}^{I} 2^i d^i i = \frac{2d\rho}{(2+\rho)^2} \left( \sum_{i=1}^{I} (2d)^i \right)'_{2d}$$
$$= \frac{2d\rho}{(2+\rho)^2(1-2d)^2} \left[ 1 + (2d)^I \ (2Id - I - 1) \right] := \varphi(d, I, \rho),$$

where $(\vartheta(x))'_x = \frac{d\vartheta(x)}{dx}$. From condition (11.14), one gets (ii). Therefore, one deduces the existence and uniqueness of $\omega$ by referring to Picard's fixed point theorem. □

*Remark* 11.9. **Case $I = 4$.** According to (11.18) in the proof of item 3-) of Theorem 11.8, $H_4(u)$ reaches its minimum value at $u = 1$. Then if $\rho \geq \rho(4) := -H_4(1) = 4$, polynomial $P_5$ has a unique positive root. For $\frac{1}{2} < d < 1$ the left hand side of (3.6) is larger than 10 so that (11.14) is fulfilled uniformly in $d$ when $0 < \rho < 0.763932022$ in which case uniqueness holds according item 4-). Furthermore graphical analysis suggests that $P_5$ has a unique positive root when $0 < \rho < 4$ and $\frac{1}{2} < d < 1$ (Fig. 11.2), and System (11.1) has a unique stationary solution for $I = 4$.

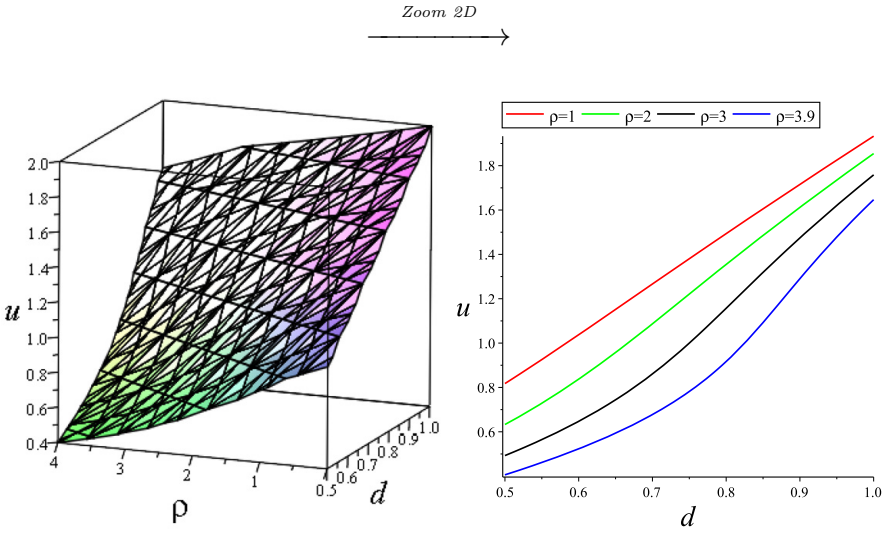


FIGURE 11.2: Implicit plot of the level set $P_5(u) = 0$ as a function of $0 < d < \frac{1}{2}$, $0 < \rho < 4$ and $0 < u < 2$. These figures ensure that graphically System (11.1) admits a unique stationary solution when $I = 4$.

*Remark* 11.10. According to item 2-) in Theorem 11.8 and Remark 11.9, the parameter condition (11.14) for uniqueness, is relevant only when $I \geqslant 5$ and $d \in (\frac{1}{2}, 1)$. Furthermore, if $d$ tends to $\frac{1}{2}$ or 1, then the contraction in item (ii) of the previous

proof, depends on the values of $\rho$ and $I \geqslant 5$. Indeed, one has

$$\begin{aligned} \lim_{d\to\frac{1}{2}} f'(\omega) &\leq \lim_{d\to\frac{1}{2}} \varphi(d, I, \rho) = \frac{\rho I(I+1)}{2(\rho+2)^2}, \\ \lim_{d\to 1} f'(\omega) &\leq \lim_{d\to 1} \varphi(d, I, \rho) = \frac{2\rho}{(\rho+2)^2}\left[1 + 2^I(I-1)\right]. \end{aligned}$$

In Fig. 11.1, graphical analysis shows that uniqueness of a stationary solution is dependent on the values of $d \in (\frac{1}{2}, 1)$, $I \geqslant 5$ and $\rho > 0$. On the other hand, the sufficient conditions (11.14) and (11.18) which depend on $(d, I, \rho)$, allow to conclude algebraically to two different uniqueness results.

Now, we provide graphical examples of the analytical uniqueness results given by items 3-) and 4-) in Theorem 11.8 with respect to numerical results of uniqueness, for $I \geqslant 5$ and $d \in (\frac{1}{2}, 1)$.

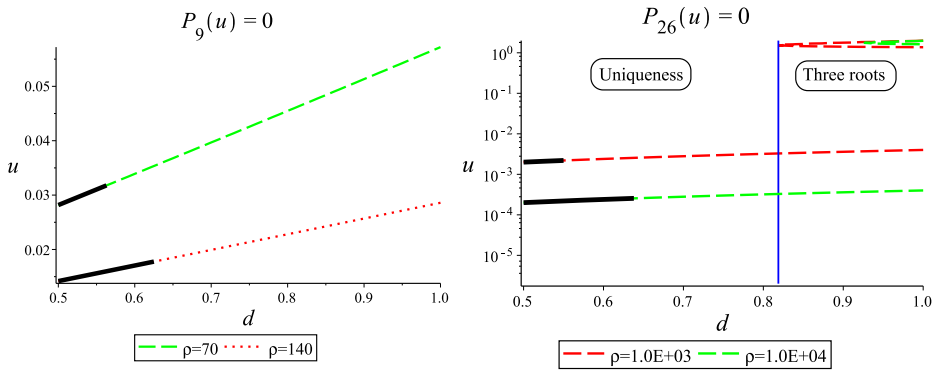


FIGURE 11.3: Implicit plot of the level set $P_{I+1}(u) = 0$ (dashed line) as a function of $(d, u)$ for $I = 8$ (left) and $I = 25$ (right) and various values of $\rho$. In both subfigures bold solid lines depict the subset of $d \in (\frac{1}{2}, 1)$ where uniqueness follows from item 4-). In left subfigure $I = 8$; item 3-) yields $\rho(8) \simeq 80$ and uniqueness holds for $\rho = 140$ and for all $d \in (\frac{1}{2}, 1)$ (dotted line), while it does not apply for $\rho = 70$. In right subfigure $I = 25$ then $\rho(25) \simeq 9.0E + 06$ so that item 3-) does not apply for the data set used; note that multiple stationary solutions are possible for a larger $d$. Log-scale is used in y-axis on the right subfigure.

In Fig. 11.3, we present the implicit plot of the level set $P_{I+1}(u) = 0$ (dashed line) as a function of $\frac{1}{2} < d < 1$, $0 < u < 2$ when $I = 8$ and 25 and various values of $\rho$.
For $I = 8$, bold solid lines depicts the subset of $d \in (\frac{1}{2}, 1)$ where uniqueness follows from item 4-). Item 3-) yields $\rho(8) \simeq 80$ and uniqueness holds for $\rho = 140$ and for all $d \in (\frac{1}{2}, 1)$ (dotted line), while item 3-) does not apply for $\rho = 70$.
For $I = 25$ then $\rho(25) \simeq 9.0E + 06$ and item 3-) does not apply for the data set used. In contrast, bold solid lines depicts the subset of $d \in (\frac{1}{2}, 1)$ where uniqueness follows from item 4-). Note that multiple stationary solutions are possible for a larger $d$.

## 11.5 Global stability of the stationary solution when $d \in (0, \frac{1}{2})$

Through this section, we use normalised variables $x_i \ \forall \ i \in \mathbb{N}_I$ and $y$ defined by

$$x_i := x_i(t) = \frac{A_i(t)}{\bar{A}_i}; \quad y := y(t) = \frac{N(t)}{\bar{N}}.$$

### 11.5.1 Main analytical result

**Theorem 11.11.** *Let Assumption 11.2.1 be satisfied and fix $d \in (0, \frac{1}{2})$. Then, the unique stationary solution noted $E_q$ is globally asymptotically stable if the parameters satisfy the following condition*

$$\rho \geqslant \frac{2d}{1-2d}\left(1 + d\sum_{i=0}^{I-1}(2d)^i\right). \tag{11.21}$$

*Proof.* Let $(A_{i\in\mathbb{N}_I}(t), B_{i\in\mathbb{N}_{I-1}}(t,.))$ be a complete solution to (11.1) that lies in the attractor $\mathcal{A} \subseteq M_0$. From Lemma 11.7, one knows there exits $\delta_i^1$, $\delta'_{1,i}$, $\delta_i^2$, $\delta'_{2,i}$, $\delta_3$ and $\delta'_3$ such that

$$\delta_i^1 < \frac{A_i(t)}{\bar{A}_i} < \delta'_{1,i}, \qquad \delta_i^2 < \frac{B_i(t,\tau)}{\bar{B}_i(\tau)} < \delta'_{2,i}, \qquad \delta_3 < \frac{N(t)}{\bar{N}} < \delta'_3 \tag{11.22}$$

for $t \in \mathbb{R}$ and $\tau \in (0, \Delta)$.
Let $g(x) := x - 1 - \ln(x)$. Then $g : (0,\infty) \to \mathbb{R}_+$ has global minimum at $x = 1$, $g(1) = 0$. It follows from (11.22) that $g(x_i)$, $g(y)$ and $g(\frac{B_i(t,\tau)}{\bar{B}_i(\tau)})$ are bounded. Let

$$V_{A_i}(t) := g\left(x_i\right), \quad \forall \ i \in \mathbb{N}_I, \quad V_N(t) := g\left(y\right)$$

and

$$V_{B_{i-1}}(t) := \int_0^\Delta \alpha_{i-1}(\tau) g\left(\frac{B_{i-1}(t,\tau)}{\bar{B}_{i-1}(\tau)}\right) d\tau, \quad \forall \ i \in \mathbb{N}_I^*$$

where $c(r) := e^{-\int_0^r (\delta+\mu(x))dx}$, $\omega = \frac{\lambda_0}{\delta}\bar{N}$,

$$\alpha_{i-1}(\tau) = \int_\tau^\Delta (2+\omega)\psi_{i-1}\mu(r)c(r)dr, \quad \psi_{i-1} = \frac{\Lambda\lambda_0}{\delta}\left(\frac{2^{i-1}d^{i-1}\omega^{i-1}}{(1+\omega)^i}\right). \tag{11.23}$$

Since $g(\frac{B_i(t,\tau)}{\bar{B}_i(\tau)})$ and $\alpha_i(\tau)$ are bounded. Then, $V_{B_i}$ is finite for each $t$, $i \in \mathbb{N}_I^*$.
For $u = (A_0, ..., A_I, B_0, ..., B_{I-1})$, let

$$V[u](t) = \sum_{i=0}^{I} \frac{\bar{A}_i}{\bar{N}} V_{A_i}(t) + \sum_{i=1}^{I} V_{B_{i-1}}(t) + \frac{\lambda_0 \bar{N}}{\delta} V_N(t) \tag{11.24}$$

One notes that, when restricted to $\mathcal{A}$, function $V$ is bounded. Furthermore, $V$ reaches its minimum value at the stationary solution $E_q$.
In the following calculations, one uses the substitutions from (11.10). For clarity of presentation, one computes separately the derivatives of $V_{A_0}$, $V_{A_i}$ for all $i \in \mathbb{N}_{I-1}^*$, $V_{A_I}$, $V_N$ and $V_{B_i}$ for all $i \in \mathbb{N}_I^*$. Using the first equality in (11.10) to replace $\Lambda$, one obtains

$$\begin{aligned}
\frac{dV_{A_0}}{dt} &= \left(1 - \frac{\bar{A}_0}{A_0(t)}\right) \frac{1}{\bar{A}_0} \frac{dA_0}{dt} \\
&= \left(1 - \frac{\bar{A}_0}{A_0(t)}\right) \frac{1}{\bar{A}_0} \left[\delta \bar{A}_0 \left(1 - \frac{A_0(t)}{\bar{A}_0}\right) + \lambda_0 \bar{N} \bar{A}_0 \left(1 - \frac{A_0(t)N(t)}{\bar{A}_0 \bar{N}}\right)\right] \\
&= \delta \left[2 - \frac{A_0(t)}{\bar{A}_0} - \frac{\bar{A}_0}{A_0(t)}\right] + \lambda_0 \bar{N} \left[1 - \frac{\bar{A}_0}{A_0(t)} - \frac{A_0(t)N(t)}{\bar{A}_0 \bar{N}} + \frac{N(t)}{\bar{N}}\right] \\
&= -\delta g(x_0) - (\delta + \lambda_0 \bar{N}) g(\frac{1}{x_0}) - \lambda_0 \bar{N} g(x_0 y) + \lambda_0 \bar{N} g(y).
\end{aligned}$$

Using (11.10), one obtains, $\forall\ i \in \mathbb{N}_{I-1}^*$

$$\begin{aligned}
\frac{dV_{A_i}}{dt} &= -\delta g(x_i) - (\delta + \lambda_0 \bar{N}) g(\frac{1}{x_i}) - \lambda_0 \bar{N} g(x_i y) + \lambda_0 \bar{N} g(y) \\
&\quad -2 \int_0^{\Delta} \frac{\mu(\tau) \bar{B}_{i-1}(\tau)}{\bar{A}_i} \left(1 - \frac{\bar{A}_i}{A_i(t)}\right) \left(1 - \frac{B_{i-1}(t,\tau)}{\bar{B}_{i-1}(\tau)}\right) d\tau
\end{aligned}$$

One notes the last term of the above equation by $P_i(t)$. It can be written as

$$P_i(t) = -2 \int_0^{\Delta} \frac{\mu(\tau) \bar{B}_{i-1}(\tau)}{\bar{A}_i} \left(1 - \frac{\bar{A}_i}{A_i(t)}\right) \left(1 - \frac{B_{i-1}(t-\tau, 0)}{\bar{B}_{i-1}(0)}\right) d\tau$$

Using $\sigma = t - \tau$ to replace $\tau$, one gets

$$\begin{aligned} P_i(t) &= -2\int_{t-\Delta}^{t} \frac{\mu(t-\sigma)\bar{B}_{i-1}(t-\sigma)}{\bar{A}_i}\left(1-\frac{\bar{A}_i}{A_i(t)}\right)\left(1-\frac{N(\sigma)A_{i-1}(\sigma)}{\bar{N}\bar{A}_{i-1}}\right)d\sigma \\ &= -2\int_{t-\Delta}^{t} \frac{\mu(t-\sigma)\bar{B}_{i-1}(t-\sigma)}{\bar{A}_i}\left(1-\frac{1}{x_i(t)}-x_{i-1}(\sigma)y(\sigma)+\frac{x_{i-1}(\sigma)y(\sigma)}{x_i(t)}\right)d\sigma \\ &= -2\int_{0}^{\Delta} \frac{\mu(\tau)\bar{B}_{i-1}(\tau)}{\bar{A}_i} g\left(\frac{x_{i-1}(t-\tau)y(t-\tau)}{x_i(t)}\right)d\tau \\ &\quad +(\delta+\lambda_0\bar{N})g(\frac{1}{x_i})+2\int_{0}^{\Delta} \frac{\mu(\tau)\bar{B}_{i-1}(\tau)}{\bar{A}_i} g\left(x_{i-1}(t-\tau)y(t-\tau)\right)d\tau \end{aligned}$$

Then the derivative of $V_{A_i}$, $\forall\ i \in \mathbb{N}^*_{I-1}$ becomes

$$\begin{aligned} \frac{dV_{A_i}}{dt} &= -\delta g(x_i)-\lambda_0\bar{N}g(x_iy)+\lambda_0\bar{N}g(y)+2\int_{0}^{\Delta} \frac{\mu(\tau)\bar{B}_{i-1}(\tau)}{\bar{A}_i} g\left(x_{i-1}(t-\tau)y(t-\tau)\right)d\tau \\ &\quad -2\int_{0}^{\Delta} \frac{\mu(\tau)\bar{B}_{i-1}(\tau)}{\bar{A}_i} g\left(\frac{x_{i-1}(t-\tau)y(t-\tau)}{x_i(t)}\right)d\tau \end{aligned}$$

Also the derivative of $V_{A_I}$ is

$$\begin{aligned} \frac{dV_{A_I}}{dt} &= -\delta g(x_I)+2\int_{0}^{\Delta} \frac{\mu(\tau)\bar{B}_{I-1}(\tau)}{\bar{A}_I} g\left(x_{I-1}(t-\tau)y(t-\tau)\right)d\tau \\ &\quad -2\int_{0}^{\Delta} \frac{\mu(\tau)\bar{B}_{I-1}(\tau)}{\bar{A}_I} g\left(\frac{x_{I-1}(t-\tau)y(t-\tau)}{x_I(t)}\right)d\tau \end{aligned}$$

Next, one calculates the derivative of $V_{B_{i-1}}$, $\forall\ i \in \mathbb{N}^*_I$

$$\frac{dV_{B_{i-1}}}{dt} = \frac{d}{dt}\int_{0}^{\Delta} \alpha_{i-1}(\tau) g\left(\frac{B_{i-1}(t,\tau)}{\bar{B}_{i-1}(\tau)}\right)d\tau = \frac{d}{dt}\int_{0}^{\Delta} \alpha_{i-1}(\tau) g\left(\frac{B_{i-1}(t-\tau,0)}{\bar{B}_{i-1}(0)}\right)d\tau.$$

Using $\sigma = t - \tau$ to replace $\tau$, one obtains

$$\begin{aligned} \frac{dV_{B_{i-1}}}{dt} &= \frac{d}{dt}\int_{t-\Delta}^{t} \alpha_{i-1}(t-\sigma) g\left(\frac{B_{i-1}(\sigma,0)}{\bar{B}_{i-1}(0)}\right)d\tau \\ &= -\alpha_{i-1}(\Delta) g\left(x_{i-1}(t-\Delta)y(t-\Delta)\right)+\alpha_{i-1}(0) g\left(x_{i-1}y\right) \\ &\quad +\int_{0}^{\Delta} \alpha'_{i-1}(\tau) g\left(\frac{B_{i-1}(t,\tau)}{\bar{B}_{i-1}(\tau)}\right)d\tau \end{aligned}$$

Now, using equations (11.23) to replace $\alpha_i(0)$ and $\alpha'_i(\tau)$, one finds

$$\begin{aligned} \frac{dV_{B_{i-1}}}{dt} &= -\alpha_{i-1}(\Delta) g\left(x_{i-1}(t-\Delta)y(t-\Delta)\right)+\psi_{i-1}(2+\omega)d\ g(x_{i-1}y) \\ &\quad -\int_{0}^{\Delta} (2+\omega)\mu(\tau)c(\tau)\ \psi_{i-1}\ g\left(x_{i-1}(t-\tau)y(t-\tau)\right)\ d\tau. \end{aligned}$$

Finally, one calculates the derivative of $V_N$. Using $\Lambda = \delta\bar{N} - \sum_{i=1}^{I}\int_0^\Delta \mu(\tau)\bar{B}_{i-1}(\tau)d\tau$, one obtains

$$\begin{aligned}
\frac{dV_N}{dt} &= \left(1-\frac{\bar{N}}{N(t)}\right)\frac{1}{\bar{N}}\frac{dN}{dt} \\
&= \left(1-\frac{\bar{N}}{N(t)}\right)\frac{1}{\bar{N}}\left[\delta\bar{N}\left(1-\frac{N(t)}{\bar{N}}\right)-\sum_{i=1}^{I}\int_0^\Delta \mu(\tau)\bar{B}_{i-1}(\tau)\left(1-\frac{B_{i-1}(t,\tau)}{\bar{B}_{i-1}(\tau)}\right)d\tau\right] \\
&= -\sum_{i=1}^{I}\int_0^\Delta \frac{\mu(\tau)\bar{B}_{i-1}(\tau)}{\bar{N}}\left(1-\frac{1}{y(t)}-x_{i-1}(t-\tau)y(t-\tau)-\frac{x_{i-1}(t-\tau)y(t-\tau)}{y(t)}\right)d\tau \\
&\quad +\delta\left[2-\frac{N(t)}{\bar{N}}-\frac{\bar{N}}{N(t)}\right].
\end{aligned}$$

Then,

$$\begin{aligned}
\frac{dV_N}{dt} &= -\delta g(y)-\delta g\left(\frac{1}{y}\right)+\left(\sum_{i=1}^{I}\int_0^\Delta \frac{\mu(\tau)\bar{B}_{i-1}(\tau)}{\bar{N}}\,d\tau\right)\; g\left(\frac{1}{y}\right) \\
&\quad +\sum_{i=1}^{I}\int_0^\Delta \frac{\mu(\tau)\bar{B}_{i-1}(\tau)}{\bar{N}}g\left(x_{i-1}(t-\tau)y(t-\tau)\right)d\tau \\
&\quad -\sum_{i=1}^{I}\int_0^\Delta \frac{\mu(\tau)\bar{B}_{i-1}(\tau)}{\bar{N}}g\left(\frac{x_{i-1}(t-\tau)y(t-\tau)}{y(t)}\right)d\tau
\end{aligned}$$

From (11.3), one gets

$$\begin{aligned}
\frac{dV_N}{dt} &= -\delta g(y)-\frac{\Lambda}{\bar{N}}\,g\left(\frac{1}{y}\right)+\sum_{i=1}^{I}\int_0^\Delta \frac{\mu(\tau)\bar{B}_{i-1}(\tau)}{\bar{N}}g\left(x_{i-1}(t-\tau)y(t-\tau)\right)d\tau \\
&\quad -\sum_{i=1}^{I}\int_0^\Delta \frac{\mu(\tau)\bar{B}_{i-1}(\tau)}{\bar{N}}g\left(\frac{x_{i-1}(t-\tau)y(t-\tau)}{y(t)}\right)d\tau
\end{aligned}$$

Next, one calculates $W_1 := \frac{\lambda_0\bar{N}}{\delta}\frac{dV_N}{dt}+\sum_{i=0}^{I}\frac{\bar{A}_i}{\bar{N}}\frac{dV_{A_i}}{dt}$

$$\begin{aligned}
W_1 &= -\sum_{i=1}^{I}\int_0^\Delta \mu(\tau)\bar{B}_{i-1}(\tau)\left[\frac{\lambda_0}{\delta}g\left(\frac{x_{i-1}(t-\tau)y(t-\tau)}{y(t)}\right)+\frac{2}{\bar{N}}g\left(\frac{x_{i-1}(t-\tau)y(t-\tau)}{x_i(t)}\right)\right]\,d\tau \\
&\quad -\frac{\bar{A}_0(\delta+\lambda_0\bar{N})}{\bar{N}}g\left(\frac{1}{x_0}\right)-\frac{\delta}{\bar{N}}\sum_{i=0}^{I}\bar{A}_i g(x_i)-\sum_{i=1}^{I}\lambda_0\bar{A}_{i-1}g\left(x_{i-1}y\right)-\lambda_0\left(\bar{N}-\sum_{i=0}^{I-1}\bar{A}_i\right)g(y) \\
&\quad -\frac{\Lambda\lambda_0}{\delta}g\left(\frac{1}{y}\right)+\sum_{i=1}^{I}\int_0^\Delta (2+\omega)\;\psi_{i-1}\;\mu(\tau)c(\tau)\;g\left(x_{i-1}(t-\tau)y(t-\tau)\right)\;d\tau.
\end{aligned}$$

From equation (11.12), one remarks that $\lambda_0\bar{A}_{i-1}=\psi_{i-1}$, $\forall\ i\in\mathbb{N}_I^*$. Finally, we

combine $W_1$ with $\sum_{i=1}^{I} \frac{dV_{B_{i-1}}}{dt}$ to get $\frac{dV[u](t)}{dt}$.

$$\begin{aligned}\frac{dV[u](t)}{dt} &= -\sum_{i=1}^{I}\int_0^{\Delta}\mu(\tau)\bar{B}_{i-1}(\tau)\left[\frac{\lambda_0}{\delta}g\left(\frac{x_{i-1}(t-\tau)y(t-\tau)}{y(t)}\right)+\frac{2}{\bar{N}}g\left(\frac{x_{i-1}(t-\tau)y(t-\tau)}{x_i(t)}\right)\right]d\tau\\ &\quad -\frac{\bar{A}_0(\delta+\lambda_0\bar{N})}{\bar{N}}g\left(\frac{1}{x_0}\right)-\frac{\delta}{\bar{N}}\sum_{i=0}^{I}\bar{A}_i g(x_i)-\sum_{i=1}^{I}\psi_{i-1}\ [1-d(2+\omega)]\,g\left(x_{i-1}y\right)\\ &\quad -\lambda_0\left(\bar{N}-\sum_{i=0}^{I-1}\bar{A}_i\right)g(y)-\frac{\Lambda\lambda_0}{\delta}g\left(\frac{1}{y}\right)-\alpha_{i-1}(\Delta)g\left(x_{i-1}(t-\Delta)y(t-\Delta)\right).\end{aligned}$$

From (11.19), one has $-1+d(2+\omega)\leq -1+d(2+H)$ and from condition (11.21), one has

$$\rho \geqslant \frac{2d\left(1+d\sum_{i=0}^{I-1}(2d)^i\right)}{1-2d} \quad \Leftrightarrow \quad d\leq \frac{1}{2+H}.$$

Then, one gets $-1+d(2+H)\leq 0$. Therefore $\frac{dV[u](t)}{dt}\leq 0$ and $V$ is a Lyapunov functional on $\mathcal{A}$.

Hence, we infer that $t\mapsto V[u](t)$ is decreasing along the entire solutions of $U$. To conclude our proof, let $\{t_n\}_{n\geqslant 0}$ be an increasing sequence tending to $-\infty$ as $n\to\infty$ and consider the sequence of map $u_n(t)=u(t+t_n)$. Note that one has $V[u_n](t)=V[u](t+t_n)$. Then we may assume that $u_n(t)\to\hat{u}(t)$ as $n\to\infty$ locally uniformly for $t\in\mathbb{R}$ where $\{\hat{u}(t)\}_{t\in\mathbb{R}}\subset\mathcal{A}$ is an entire solution of $U$. Since $V$ is decreasing, one obtains that

$$V[\hat{u}](t)\equiv\lim_{t\to-\infty}V[u](t)=\sup_{t\in\mathbb{R}}V[u](t). \tag{11.25}$$

Let $\hat{u}=(\hat{A},0,\hat{B})^T$. Since $V[u]$ is bounded, then from (11.25), we deduce that $V[\hat{u}](t)\equiv 0$ and $\hat{u}\equiv E_q$. Hence $0\leq V[u](t)\leq 0$ for $t\in\mathbb{R}$ and $u(t)\equiv E_q$. □

Finally, we illustrate condition (11.21) by a graphical analysis (Fig. 11.4) of the level set $F(d,\rho):=\rho-\frac{2d}{1-2d}\left(1+d\sum_{i=0}^{I-1}(2d)^i\right)=0$. Dark (green) depicts $F(d,\rho)\geqslant 0$ and the light (orange) represents $F(d,\rho)<0$. Furthermore, these figures show the zone where condition (11.21) is satisfied (i.e the zone where the Lyapunov functional proposed in the previous proof, leads to obtain the global stability of $E_q$). We remark that this condition covers a larger interval of $d$ when $\rho$ is large.

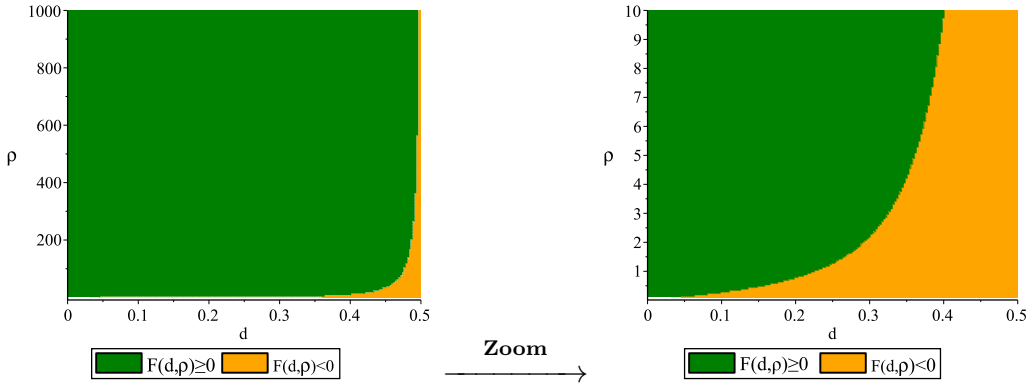


FIGURE 11.4: Implicit plot of the level set $F(d,\rho) := \rho - \frac{2d}{1-2d}\left(1 + d\sum_{i=0}^{I-1}(2d)^i\right)$ as a function $(d,\rho)$ for $I = 9$. Condition (11.21) is satisfied in the green region, i.e, it is the zone where the derivative of the Lyapunov functional ($\frac{dV[u](t)}{dt}$) is guaranteed to be negative. Note that these subfigures do not qualitatively change for all $I \in \mathbb{N}^*$.

### 11.5.2 Additional numerical results

In this subsection, we present some numerical simulations in order to complete the analytical results of the previous subsection ($d \in (0, \frac{1}{2})$), and next we give some simulations for System (11.1) when there are three stationary solutions.

According to [7, 10, 80], it is assumed that the cells take a time approximatively $\Delta$ to complete the process in B-phase. Then, the mother cells divide in B-phase when their age around $\Delta$. Therefore, the rate of cells that divided at age $\tau$ can be defined as follows

$$\mu(\tau) = \frac{\Psi(\tau)}{1 - \int_0^\tau \Psi(r)dr},$$

where $\Psi(\tau) := \frac{1}{\sigma\sqrt{2\pi}} e^{-\frac{1}{2}\left(\frac{\tau-\Delta}{\sigma}\right)^2}$ is a normal distribution with a mean $\Delta$ and variance $\sigma^2$.

*Remark* 11.12. The parameter condition (11.21) seems to be only a technical condition that we cannot overcome. Apparently from numerical computations, the unique equilibrium $E_q$ for all $d \in (0, \frac{1}{2})$ continue to be globally stable even if condition (11.21) is not fulfilled.

First, we provide numerical simulations to illustrate the dynamic of System (11.1) when $d \in (0, \frac{1}{2})$. The choice of numerical and optimization parameters follows the second column in Table 11.2 (Value 1), where $d = 0.470254$ and $\rho = 3.24$. In this

case, uniqueness of stationary solution is guaranteed by Theorem 11.8, and according to Fig. 11.4, the point $(d, \rho)$ is in the light region. Then, condition (11.21) is not fulfilled with this choice of parameters (Table 11.2 - Value 1).

TABLE 11.2: Default values of the parameters used for simulations.

| Parameters | Value 1 | Value 2 | Unit |
|---|---|---|---|
| $I$ | 9 | 17 | - |
| $\Delta$ | 10 | 10 | hour |
| $\sigma^2$ | 2 | 2 | - |
| $\Lambda$ | 42.06 | 42.06 | cell/hour |
| $\delta$ | $2.0 \times 10^{-2}$ | $7.0 \times 10^{-4}$ | 1/hour |
| $\lambda_0$ | $10^{-8}$ | $5.87 \times 10^{-6}$ | - |

*Note. Values indicated in the second column (Value 1) lead to a unique stationary solution ($d = 0.470254$ and $\rho = 3.24$). Moreover these values in the second column do not fulfil condition (11.21). In the third column (Value 2), parameters values lead to three stationary solutions ($d = 0.56007$ and $\rho = 2.33$).*

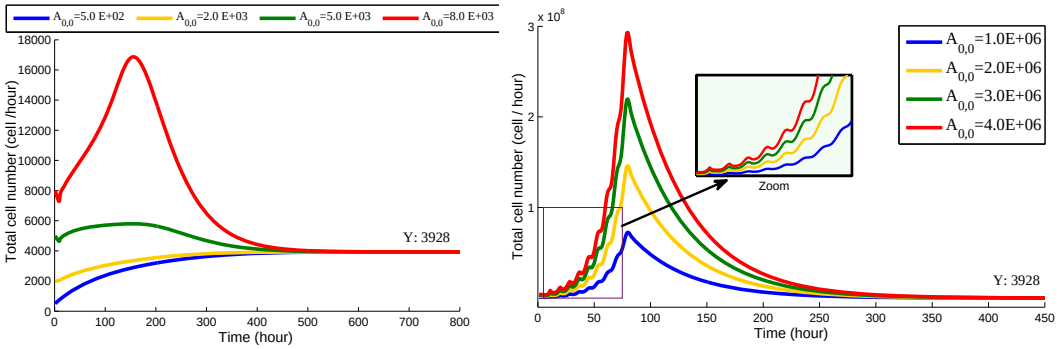


FIGURE 11.5: Solution $N(t)$ converges to the unique stationary solution ($\bar{N} = 3928$) for different initialisation ($A_{0,0}$). Damped oscillations (right subfigure) can be observed when the initialisation $A_{0,0}$ is larger than $\bar{N}$. Parameter values are given by Table 11.2 (Value 1).

In Fig. 11.5, we represent the total number of cells as a function of time. We remark that $N(t)$ converges to the unique stationary solution for several initialisations $(A_{0,0})$. This numerical result illustrates Remark 11.12: System (11.1) has a unique stationary solution and it is numerically asymptotically stable when $d \in (0, \frac{1}{2})$. Moreover when the initialisation $A_{0,0}$ is greater than $\bar{N}$, damped oscillations (right subfigure in Fig. 11.5) can be observed in the first 3 days. This phenomenon probably needs further analysis.

Second, we provide numerical simulations to illustrate the dynamic of System (11.1) when $d \in (\frac{1}{2}, 1)$. Parameter values are given by the third column in Table 11.2

(Value 2), where $d = 0.56007$, $\rho = 2.33$ and $I = 17$. By solving (11.17), one may check the existence of three stationary solutions ($\bar{N}_1 = 6403785$, $\bar{N}_2 = 6404499$, $\bar{N}_3 = 6417034$) for this choice of parameters (Table 11.2 - Value 2). In Fig. 11.6, we numerically show that each of these three stationary solutions has a non-empty basin of attraction. Convergence is slow compared to the case $0 < d < \frac{1}{2}$ (see Fig. 11.5), and reached for carefully selected initial conditions. The stability or instability of each stationary solution will be studied in a forthcoming work.

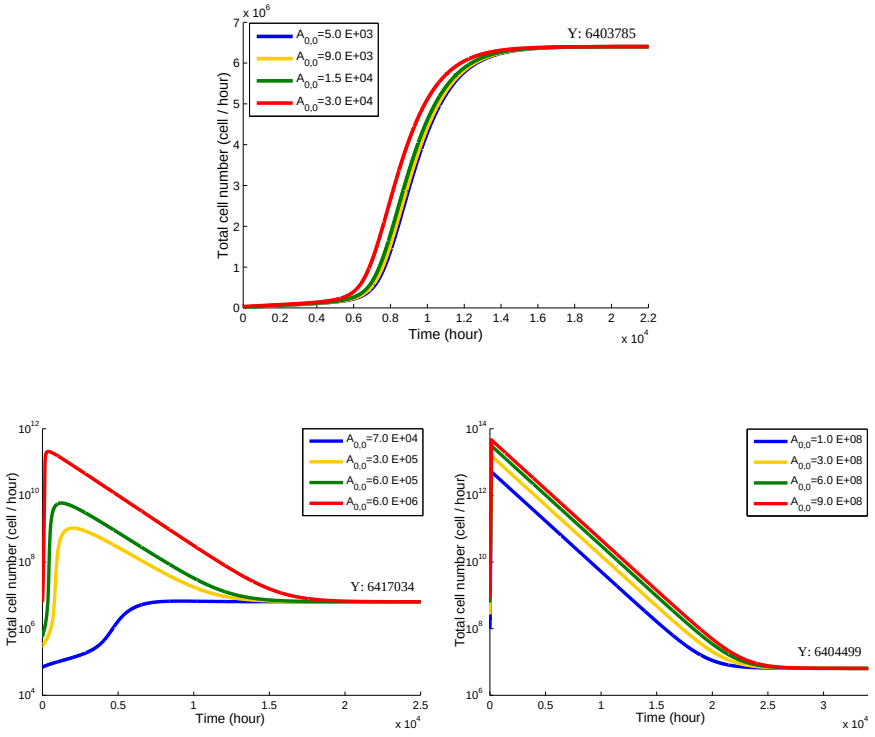


FIGURE 11.6: Numerical simulations for System (11.1) when $d = 0.56007$, $\rho = 2.33$ and $I = 17$. Parameter values are given by Table 11.2 (Value 2). Solution $N(t)$ converges to one of the three stationary solutions depending on the choice of the initial condition ($A_{0,0}$). Numerical simulations are tested until time $10^6$ (hour), and are presented here until $2.2 \times 10^4$ - $3.5 \times 10^4$ hour, where the convergence is numerically reached. Note that the y-axis in the two bottom subfigures is presented in log-scale for sake of clarity.

## 11.6 Conclusions and future work

In this study, we extend the in vitro model proposed by [80] to an in vivo model. Next, we derive an age-structured system (11.1) and we study its asymptotic behaviour. An analysis of System (11.1) shows that there exists one or three stationary solutions when the cells undergo more than five divisions. Precisely, uniqueness of a stationary solution is guaranteed in this case (i.e $I \geqslant 5$) when the parameter conditions (11.14) or (11.18) are satisfied. Also uniqueness is obtained when the

cells undergo at most four divisions or if the parameter $d$ is less than $\frac{1}{2}$. To study the large time behaviour when $0 < d < \frac{1}{2}$, a key tool was a Volterra-type Lyapunov functional that included an integral over all maturity of cells in B phase, similar to the functionals used in [114, 115]. Note that the Lyapounov functional used in this study is not defined on the entire state space. One may observe that similar difficulty also arise in [120–122]. To circumvent this difficulty, we only use the Lyapunov functional on the global attractor. Then, we deduce that the unique stationary solution is globally asymptotically stable if the parameter condition (11.21) is satisfied. A numerical computational suggests that the unique stationary solution in case of $0 < d < \frac{1}{2}$, continues to be stable even if condition (11.21) is not fulfilled (a similar technical problem arises also in [114]). In addition, we remark from Fig. 11.3 and Fig. 11.4 that the algebraic results presented in this chapter, cover a large region of the numerical results when the parameter $\rho$ is large.

Furthermore, Fig. 11.1 shows that there exists three stationary solutions for a specific set of parameters $(\rho, d)$ (when the cells undergo several divisions $(I \geqslant 5)$). This means that if with a few cell divisions, the size of T cells returns to the normal level, the immune system has a unique steady state, else it has three steady state. This phenomenon can provide an interesting biological signification of the homeostasis of T cells in some cases. This will be studied in a forthcoming work. Finally, inspired by the analysis of System (11.1), a further work is to study the asymptotic behaviour of System (10.1-10.3) which includes the concept of phenotype (CD44) in the homeostasis process.

# Chapter 12

# An optimal strategy for rebuilding immunity in conditions of T lymphopenia

## 12.1 Introduction

Throughout adult life, the size and composition of the peripheral lymphocyte pool is tightly regulated and, in the absence of disease, is maintained at relatively constant levels [40, 79]. The correct representation of the T-cell pool is essential to maintain adequate immune competence against pathogens, since it has to maintain a sufficiently diverse repertoire of naive T cells to recognize a broad range of antigens, while efficient immune responses against previously encountered pathogens depend on the memory T-cell pool. For these demanding tasks, homeostatic mechanisms have evolved to maintain distinct populations of naive and memory cells and to retain an appropriate mixture of CD4+ helper T cells and CD8+ cytotoxic T cells. A few general principles govern the physiologic response to perturbation of the balance of T cell. For example, viral infection (e.g. HIV), or drugs used in peritransplant induction therapy or cancer chemotherapy, are the main factors that disrupt the balance of T cell. This perturbation result in Lymphocytopenia or lymphopenia (i.e. it is the condition of having an abnormally low level of lymphocytes in the blood) which induces a rapid proliferation in vivo of T cells with a recruitment of naive T cells from the thymus.
Rapoport et al. [123] have developed a strategy that rebuild the immunity in

lymphopenic individuals with cancer by vaccination and adoptive T-cell transfer. In their study, they offers a platform to help restore impaired adaptive immunity in cancer patients. After high-dose chemotherapy, innate immunity, composed of granulocytes, natural killer cells, and monocytes, is generally restored within a few weeks. Adaptive immunity, however, acquired over the individual's lifetime exposure to infections and vaccines, is lost as a result of the high-dose preparative regimen and is not overcome by the infusion of the memory B and T cells contained in the "autologous graft"[1]. Rapoport et al. [123] show that mature T cells in cancer patients can be ex vivo (in vitro) expanded, and that their infusions in the early post-transplant period accelerate the numerical recovery of T cells with a broad repertoire. The combination of antigen-primed T cells and early post-transplantation booster vaccinations led to enhanced immunity to the specific pathogen. In this context, the optimal memory T cells (i.e. T cells with CD44 high) transferred in vivo by vaccination which support the homeostatic in vivo expansion of T cells and led to enhanced immunity to the specific pathogen, stay unclear.
As proved in the last decades, the use of mathematical models in immunology has allowed great advances, not only on the theoretical side, but also on the side of the management of actual public health policies. In this study, we consider a model of T cell homeostasis in lymphopenia conditions (like the model proposed in Chapter 10 (see also [81])) but with a more realistic parameter) in order to address the problem of determining an optimal strategy that lead to enhanced immunity during the homeostatic process. Next section is devoted to reformulate the model proposed in Chapter 10 to a more realistic version. In Section 12.3 we discuss the cost function and we derive the optimality conditions. Finally, in Section 12.4, we perform some simulations to compute the optimal vaccination.

## 12.2 The model

In condition of T cell deficiency (e.g. viral infection, or drugs used in peritransplant induction therapy or cancer chemotherapy), naive T cells (CD44 low) are delivered from the thymus in order to undergo division. In this study, the modeling of T cell homeostasis in vivo is based on the Smith-Martin model. The model equations used, considered an A-state (resting) and a B-phase (proliferative) where cells undergo division. The number of times cells transfer between the A-state to the B-phase

[1]the transfer of tissue from one site to another on the same body

is indexed by $i$ which reflects the number of times a cell has undergone division. The time since entering the B-phase (either the first time or any subsequent time) is measured by $\tau$ which reflects the maturity of the cells at this stage and has a maximum value of $\Delta$. Since we are interested in this study to enhanced immunity to the specific pathogen (or in another word by "memory T cells"), we take into account the level of CD44 on the surface of cells which is the natural marker that indicates the naive (CD44 low) and memory (CD44 high) cells. Then, both the cells in A-state and B-phase are indexed by $s \in [0, m]$, the intensity of CD44 expression ($m$ is the maximum intensity of CD44). In this work, the model of T cell proliferation in vivo, including a rebuilding strategy of immunity is governed by the following system

$$\begin{cases} \dfrac{dA_0(t,s)}{dt} = \Lambda(s) - \delta A_0(t,s) - \lambda(N)A_0(t,s) + \chi_0(s)u_0(t), \\ \\ \begin{cases} for \quad i \in \mathbb{N}_I^* := \{1, ..., I\} \\ \\ \dfrac{dA_i(t,s)}{dt} = 2\displaystyle\int_0^{\Delta} \mu(\tau)B_{i-1}(t,\tau,s)\, d\tau - \delta A_i(t,s) - \lambda(N)A_i(t,s) + \chi_i(s)u_i(t), \end{cases} \\ \\ \begin{cases} for \quad i \in \mathbb{N}_I := \{0, ..., I\} \\ \\ \frac{\partial}{\partial t}B_i(t,\tau,s) + \frac{\partial}{\partial \tau}B_i(t,\tau,s) + \frac{\partial}{\partial s}[v_i(s).B_i(t,\tau,s)] = -\left(\delta + \mu(\tau)\right) B_i(t,\tau,s), \end{cases} \end{cases} \tag{12.1}$$

where $A_i$ and $B_i$ are the number of cells in $A_i$ phase and $B_i$ phase respectively. $I$ stands to the maximum division number undergone by cells.

Boundary conditions and initial conditions of Eqs. (12.1) are defined by, $\forall\ i \in \mathbb{N}_I := \{0, 1, ..., I\}$,

$$\begin{cases} B_i(t,0,s) = \lambda(N)A_i(t,s), \\ \\ v_i(0)B_i(t,\tau,0) = 0, \end{cases} \quad \begin{cases} A_0(0,s) = A_{0,0}(s) \geqslant 0, \\ \\ B_{i\in\mathbb{N}_I}(0,\tau,s) = 0 \quad and \quad A_{i\in\mathbb{N}_I^*}(0,s) = 0. \end{cases} \tag{12.2}$$

The A-state is described by an ODE equation with source terms from the B-phase. The different A-state components are given by $A_i(t,s)$ for $i = 0, 1, ...$ (depending on how many times the cells have undergone division). For $i = 0$ the growth of the $A_0$ component comes from an export rate of cells $\Lambda$ from the thymus. For $i > 0$

the growth of the $A_i$ components comes from the doubling of the cells in the $B_{i-1}$ component (with the same $s$ value, integrated over $\tau \in [0, \Delta]$) as they undergo cell division. The equations for the B-phase is given by PDE structured by the intensity of CD44 ($s$) and the age ($\tau$). In contrast to the model proposed in the previous chapter, we consider in (12.1) that the rate of export of cells from thymus ($\Lambda$) is depend on the CD44 expression since the cells exported from the thymus have low level of CD44 (naive cells).

In (12.1), the different parameters have the following meaning

- Constant $\delta$ is the natural mortality rate in A-state and B-phase.
- Function $\mu(\tau)$ is the division rate at age $\tau$.
- Function $\lambda(N)$ is the recruitment rate from A-state into B-phase that depend on the total population $N$

$$N := N(t) = \sum_{i=0}^{I} \left( \int_0^m A_i(t,s)ds + \int_0^\Delta \int_0^m B_i(t,\tau,s)ds\, d\tau \right).$$

- Function $v_i(s)$ is the velocity of CD44 upregulation.
- Function $\chi_i$ represents the distribution of CD44 on the surface of cells in $A_i$ phase.
- Function $u_i(t)$ represents the vaccination strategy to rebuild the immunity during the T cell homeostasis, i.e, the number of T cells (having undergone $i$ divisions), transferred in vivo per unit time.

Recruitment of cells from A-state into the B-phase occurs at a rate $\lambda$. As the cellular population increases, the amount of resources per cell is decreasing and the recruitment rate is reduced. A smaller division rate corresponds to the smaller transfer rate $\lambda$ of the model [10]. Recruitment rate is then defined by

$$\lambda = \lambda(N) = \lambda_0 e^{-\eta N},$$

where the parameter $\eta$ determining the size of the reduction caused by increasing number of competing cells ($N$). In addition, $\lambda_0$ is considered to represent the ability of each clonotype to respond to an unlimited resource.

According to [7, 10, 80], the cells take a time approximatively $\Delta$ to complete the process in B-phase. Then, the mother cells divide in B-phase when their age is close to $\Delta$. Then, the function $\mu$ can be approximated by a non-negative rectangular function with a mean value 1.

$$\mu(\tau) = \begin{cases} \frac{1}{h} & \text{if } \tau \in [\Delta - h, \Delta], \\ \\ 0 & \text{else,} \end{cases}$$

where $0 < h << \Delta$.

In (12.1), the cells are up-regulating CD44 during B-phase. In $A_i$ phase (i.e. ith division in A-state), cells inherit the same intensity of CD44 of those that are divided in the previous B-phase ($B_{i-1}$ phase). Then, the cells in $A_i$ phase increase their level of CD44 according to the division number $i$. This is due to the velocity of CD44 upregulation. Then according to the upregulation of CD44 in the experimental data [10], the distribution of CD44 on the surface of cells in $A_i$ phase can be approximated by

$$\chi_i(s) = \frac{1}{\sqrt{2\pi}} e^{-\frac{1}{2}\left(\frac{s-(i+1)c}{i+1}\right)^2}.$$

Furthermore, this function can be written as

$$\chi_i(s) = (i+1)\, g_i(s),$$

where $g_i$ is a Gaussian function which can be described by the probability density function of a normally distributed random variable with expected value $\mu_i = (i+1)c$ ($c$ is a positive constant) and variance $\sigma_i^2 = (i+1)^2$. In other words, the function $\chi_i(s)$ can be interpreted as the levels of CD44 that can be detected on the surface of $A_i$ cells (i.e. Cells in $A_i$ phase) in each division.

We note that in System (12.1), the term $\chi_i(s)u_i(t)$ can be described by the number of T cells, transferred in vivo per unit time which have undergone $i$ divisions and have a level $s$ of CD44 on their surface.

By using Lagrange method, one obtains an implicit solution of $A_i$

$$A_0(t,s) = A_{0,0}(s)\ e^{-\int_0^t(\delta+\lambda(N(u)))du} + \int_0^t (\Lambda + \chi_0(s)u_0(r))\, e^{-\int_r^t(\delta+\lambda(N(q)))dq} dr, \quad (12.3)$$

and for $i \in \mathbb{N}_I^*$,

$$A_i(t,s) = 2\int_0^t \int_0^\Delta e^{-\int_r^t(\delta+\lambda^i(N(q)))dq} (\mu(\tau)B_{i-1}(r,\tau,s) + \chi_i(s)u_i(r))\, d\tau\ dr.$$

Now, we consider the following differential equations:

$$\begin{cases} \frac{ds_i^1(t)}{dt} = v_i(s_i^1(t)) \\ \\ s_i^1(t_0) = s_{i,0}^1 \geqslant 0 \end{cases}, \quad \begin{cases} \frac{ds_i^2(\tau)}{d\tau} = v_i(s_i^2(\tau)) \\ \\ s_i^2(\tau_0) = s_{i,0}^2 \geqslant 0. \end{cases} \quad (12.4)$$

where $s_i^1(t;t_0;s_{i,0}^1)$ and $s_i^2(\tau;\tau_0;s_{i,0}^2)$ are the curves witch goes through $(t_0, s_{i,0}^1)$ and $(\tau_0, s_{i,0}^2)$ respectively. The curves, $Z_i^1(t) := s_i^1(t;0;0)$ and $Z_i^2(\tau) := s_i^2(\tau;0;0)$ are the characteristic through the origin. The solution of (12.4) is given by the following equations

$$s_i^1(t) = s_{i,0}^1 + \int_{t_0}^t v_i(s_i^1(z))dz, \quad s_i^2(\tau) = s_{i,0}^2 + \int_{\tau_0}^\tau v_i(s_i^2(r))dr.$$

Integrating along the characteristic curve the PDE of System (12.1-12.2), one obtains

$$B_{i\in\mathbb{N}_{I-1}}(t,\tau,s) = \begin{cases} 0 & t \leq \tau,\ Z_i^1(t) < s \\ \\ \frac{\lambda(N(t-\tau))\, A_i(t-\tau,\zeta_i)\, v_i(\zeta_i)}{v_i(s)} f(\tau) & 0 \leq \tau < t,\ Z_i^2(\tau) < s \\ \\ 0 & Z_i^1(t) \geqslant s,\ Z_i^2(\tau) \geqslant s \end{cases} \quad (12.5)$$

where $\zeta_i := s - Z_i^2(\tau)$ and $f(\tau) := e^{-\int_0^\tau(\delta+\mu(r))dr}$.

## 12.3 Strategy to enhance immunity

As we have already discussed in the previous Section, in our model (12.1) the strategy to rebuild the immunity during the T cell homeostasis, is quantified by

$u_i(t)$. The purpose of this strategy of transferred cells in vivo, is to maximize the memory T cells (CD44 high) during the homeostasis process in order to acquire an excellent memory against pathogens. To reach this goal with an optimal strategy, we should maximize the number of cells in B-phase having an important level of CD44, and minimize the number of T cells transferred in vivo. Specifically, we consider the following functional

$$\Phi(u_i^*) = \max_{u_i \in \mathbb{K}_i} \Phi(u_i), \tag{12.6}$$

with,

$$\Phi(u_i) := \sum_{i=0}^{I} \phi_i(u_i) := \sum_{i=0}^{I} \left[ \int_0^T \int_0^{\Delta} \int_{s_{high}}^{m} B_i(t,\tau,s) ds d\tau - \int_0^T u_i^2(t) dt \right],$$

where $s_{high}$ is the minimum intensity of CD44 required by cells to be qualified as CD44 high (memory phenotype), and

$$\mathbb{K}_i = \{u_i \in L^{\infty}(0,T) \mid 0 \leq u_i(t) \leq u_i^{max}\}.$$

### 12.3.1 The optimality system

For the optimal vaccination strategy (12.6), we introduce the formal Lagrange function

$$\mathcal{L}(A_i, B_i, P_i, Q_i, u_i) = \Phi(u_i)$$

$$+\int_0^T \int_0^m \left( \frac{dA_0(t,s)}{dt} - \Lambda(s) + (\delta + \lambda(N))A_0(t,s) - \chi_0(s)u_0(t) \right) P_0(t,s)ds\,dt$$

$$+\sum_{i=1}^{I} \int_0^T \int_0^m [\frac{dA_i(t,s)}{dt} - 2\int_0^\Delta \mu(\tau)B_{i-1}(t,\tau,s)\ d\tau + (\delta + \lambda(N))A_i(t,s)$$
$$-\chi_i(s)u_i(t)]P_i(t,s)ds\,dt$$

$$+\sum_{i=0}^{I} \int_0^T \int_0^\Delta \int_0^m [\frac{\partial}{\partial t}B_i(t,\tau,s) + \frac{\partial}{\partial \tau}B_i(t,\tau,s) + \frac{\partial}{\partial s}[v_i(s).B_i(t,\tau,s)]$$
$$+ (\delta + \mu(\tau))\ B_i(t,\tau,s)]Q_i(t,\tau,s)ds\,d\tau\,dt$$

$$+\sum_{i=0}^{I} \int_0^T \int_0^m [B_i(t,0,s) - \lambda(N)A_i(t,s)]Q_i(t,0,s)ds\,dt,$$

with multipliers $P_i \in L^2((0,T)\times(0,m))$ and $Q_i \in L^2((0,T)\times(0,\Delta)\times(0,m))$. Let us now consider the variables $u_i$, $A_i$, $B_i$, $P_i$, $Q_i$ for all $i \in \mathbb{N}_I$, as independent and compute and set equal to zeros the derivatives of $\mathcal{L}$, with respect to the five variables. After some computations, one obtains for all $i \in \mathbb{N}_I$

$$\frac{\partial}{\partial t}Q_i(t,\tau,s) + \frac{\partial}{\partial \tau}Q_i(t,\tau,s) + v_i(s)\frac{\partial}{\partial s}Q_i(t,\tau,s) = (\delta + \mu(\tau))\,Q_i(t,\tau,s) + 1_{[s_{high},m]}(s),$$

$$\frac{dP_i(t,s)}{dt} = -\delta P_i(t,s) + \lambda(N)\left[P_i(t,s) - Q_i(t,0,s)\right],$$

complemented by the transversality conditions

$$P_i(T,s) = 0, \quad Q_i(T,\tau,s) = 0, \quad Q_i(t,\Delta,s) = 0, \quad Q_i(t,\tau,m) = 0,$$

in addition to the state equations (12.1). System (12.7) supplemented by the transversality condition is called the adjoint system of the optimal control problem.

When computing the derivative of the Lagrangian with respect to the first state

variable, one obtains the gradient of $\Phi$.

$$\nabla_{u:=(u_0,\ldots,u_I)}(\Phi) = \sum_{i=0}^{I} \left[ 2u_i(t) + \int_0^m \chi_i(s) P_i(t,s) ds \right]. \tag{12.7}$$

Based on (12.7) and (12.7), one can approximate the optimal vaccination strategy using a discretization of the following algorithm.

1-) Choose a control $u_i(t)$ randomly.

2-) Compute the solution of the state equations (12.1).

3-) Compute the solution of the adjoint equation (12.7).

4-) Compute the gradient of $\Phi$, by (12.7).

5-) Compute the new control using a nonlinear gradient method.

6-) Project the control on the admissible domain (constraints).

7-) If the norm of the gradient of $\phi$ is less than some tolerance then stop; else return to 1-).

## 12.4 Numerical results

Actually, we have used the procedure given in the previous subsection, to run numerical simulations and illustrate the effect of the optimal vaccination on the number of proliferative cells. More specifically, in discretizing the algorithm just described, we used a semi-implicit scheme to solve the state equations; the nonlinear renewal equation ($B_i(t,0,s) = \lambda(N) A_i(t,s)$) was solved explicitly. Besides, the cost function was descretized using the trapezoidal rule and a discret Lagrange function was also obatined by using the trapezoidal rule and the discretized state equation. From this discretized Lagrangien we derive, in the discrete context, a discrete adjoint equation that we use in the computations.

### 12.4.1 Parameters used in the numerical computation

Now, we describe the form of the parameters and their value used in the numerical computation.

According to [124], the thymic emigrants (i.e. Cells exported from the thymus) have slightly lower CD44. Then, we assume that the rate of export of cells from the thymus is

$$\Lambda(s) = \begin{cases} \alpha & if \quad s_0^{low} \leqslant s \leqslant s_1^{low}, \\ \\ 0 & else, \end{cases}$$

where $\alpha$ is a positive constant, $s_0$ and $s_1$ are two low levels of CD44. In the numerical simulations, $\Lambda(s)$ is approximated by

$$\Lambda(s^k) \simeq \Lambda^k = \begin{cases} \alpha & if \quad k_0^{low} \leqslant k \leqslant k_1^{low}, \\ \\ 0 & else, \end{cases} \tag{12.8}$$

In this study, we consider the case of a young patient having a deficiency on T cells which is caused for example by a high-dose of chemotheray. From [125], the median combined production of naive T cells through cell division and thymic export is estimated by $\sim 1.0 \times 10^9$ cells per day ($4.167 \times 10^7$ cells/hour) at the age of 20 years. Thus, we consider that our System (12.1-12.2) starts from age 20 years (i.e the initial time $t = 0$ for System (12.1-12.2) corresponds to age 20).
Moreover, $\sum_{k=0}^{N_s} \Lambda^k \simeq \Lambda := 4.167 \times 10^7$ ($N_s$ is length of discrete vector that depicts the intensity of CD44). Then from (12.8), $\alpha \simeq \frac{\Lambda}{k_1^{low} - k_0^{low}}$.

In addition, the choice of some numerical and optimization parameters follows [10, 125] and Chapters 6 and 7. Indeed, we summarize in the following Table 12.1 the value of the parameters used in the simulations.

### 12.4.2 Results

In Fig. 12.1, we represent the optimal vaccination strategy $u_i$ as a function of time and division number. We remark that the strategy to maximize the memory cells (CD44 high), consists to transfer in vivo (by a vaccination) at the initial time, a high dose of resting cells having undergone 5-7 divisions. Later on, this dose should be reduced over time, which can be realistic.

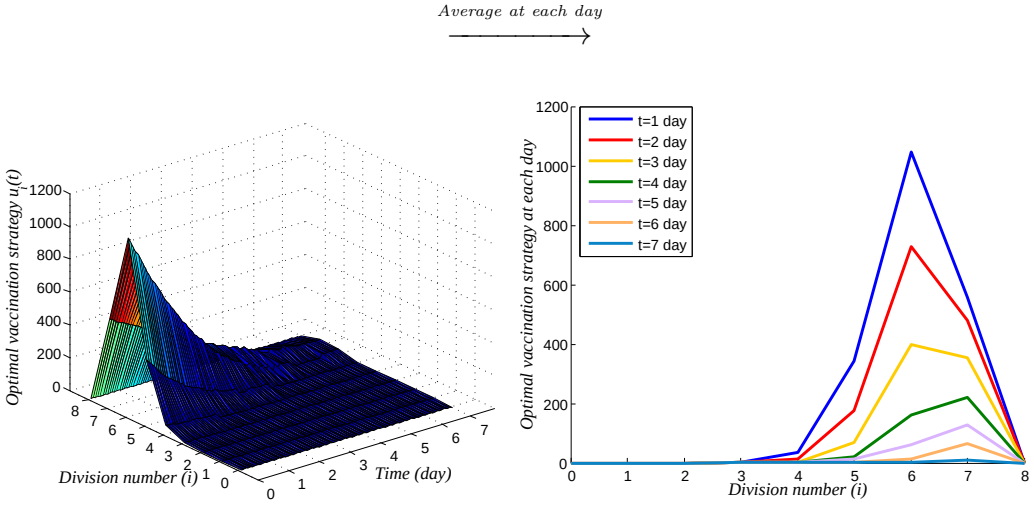


FIGURE 12.1: Left subfigure represents the optimal strategy $u_i$ as a function of the continuous time from 0 to 7 days. The right one depicts the average optimal strategy ($\int_t^{t+1} u_i(r)dr$) during one week. Note that the optimal vaccination given in the right subfigure is more realistic, since for a treatment of one week, one dose in each day is more practical for patients than a continuous dose.

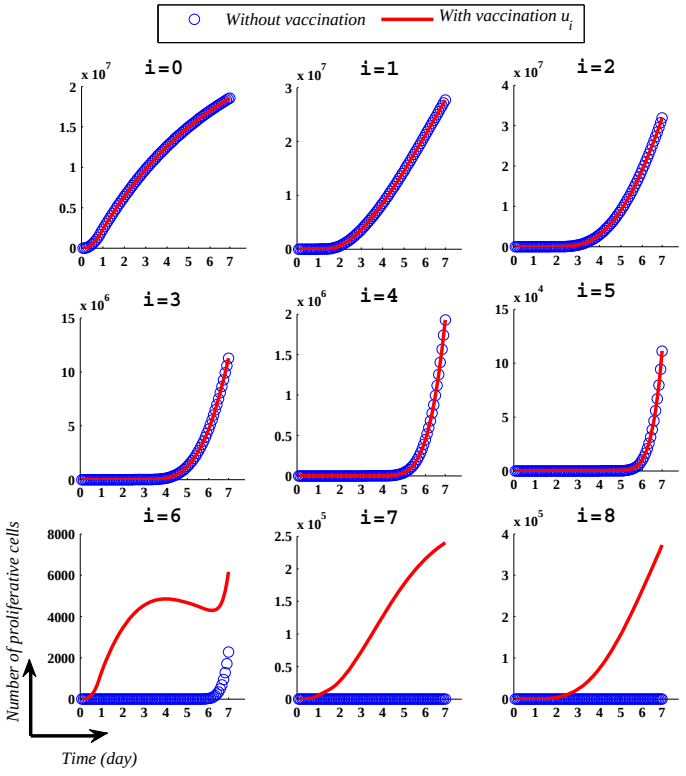


FIGURE 12.2: Comparison of the number of proliferative cells with (solid line) and without (circle) an optimal vaccination (Fig. 12.1) at each division ($i$), as a function of time (days) ($\int_0^{\Delta}\int_0^m B_i(t,\tau,s)ds\,d\tau$).

TABLE 12.1: Table of parameters.

| Parameters | Value | References |
|---|---|---|
| $I$ | 8 | [10] |
| $m$ | 2 | [10] |
| $s_{high}$ | 1.0 | [10] |
| $\Delta$ | 7.12 (hour) | Chapter 7 |
| $h$ | 30 (minute) | Chapter 7 |
| $\delta$ | 0.012 (1/hour) | [51] |
| $\lambda_0$ | $3.768979E-02$ (1/cell/hour) | Chapter 7 |
| $\eta$ | $1.97568E-06$ | Chapter 7 |
| $v_i(s)$ | Fig. 7.4 | Chapter 8 |
| $\Lambda$ | $4.167 \times 10^7$ (cells/hour) | [125] |
| $k_0^{low}$ | 1 | Fixed |
| $k_1^{low}$ | 4 | Fixed |
| $c$ | 2.1 | Fixed |

According to Chapter 8 (see also [80]), the velocity of CD44 upregulation ($v_i$) in (12.1) is the key parameter to identify the component naive and memory during T cell homeostasis. This important key allows to deduce that the cells after 6 divisions are probably switching to memory phenotype. By applying this interpretation to Fig. 12.1, we understand why the optimal strategy consists to transfer in vivo, resting cells having performed 5-7 divisions.

Finally, in Fig. 12.2, we present the simulations of (12.1) with and without the optimal vaccination strategy given in Fig. 12.1. We remark that there are no effect on the number of proliferative cells in the first divisions 0-5 by vaccination. In contrast, it is clear from division 6 that the proliferative cells (memory cells) with the vaccination strategy, are increased with respect to those without vaccination.

## 12.5 Conclusion

In this study, we are interested to analyse the homeostatic mechanism of T cell under lymphopenia conditions, through a mathematical model. Indeed, we have presented in Chapter 10 a model that describes this mechanism in vivo, but with a simple vital parameters defined by constant rates (e.g the rate of exported cells from the thymus $\Lambda$). To give the model a more realistic aspect, we consider in this chapter that the thymic emigrants rate ($\Lambda$) is dependent on the level of CD44, since the cells exported from the thymus have a naive phenotype (i.e. having low level

of CD44). In addition, we applied in this in vivo model, a vaccination strategy (expressed in the model by $\chi_i(s)u_i(t)$) in order to enhanced immunity during the homeostatic process. Furthermore, a cost function is proposed here in order to maximize the memory T cells (CD44 high) and minimize the vaccination strategy. Then, we set up a numerical method to find the optimal control $u_i(t)$ which can be described by the optimal number of resting T cells (having undergone $i$ divisions) transferred in vivo. From Fig. 12.1, we found that the optimal strategy consists to transfer in vivo, resting cells having performed 5-7 divisions. Finally, we presented in Fig. 12.2 the effect of vaccination on the number of proliferative cells.

# Chapter 13

# Discussions, conclusions and future works

## 13.1 Discussions and conclusions

In this thesis, we have developed mathematical models describing the T cell proliferation in vitro and in vivo, under lymphopenic conditions.

**Firstly**, we have started by an in vitro model ($SM_{CD44}$) in order to analyse the experimental data at hand (recent published data [10]). The $SM_{CD44}$ model is based on the Smith-Martin model which is used widely in the literature. This model is composed on ODEs and PDEs that represent the dynamic of cells between the resting and proliferative phases (A-state and B-phase respectively) during LIP (lymphopenia induced proliferation). By using CFSE data with CD44 generated by Hogan et al. [10], we found that the velocity of CD44 upregulation $v_i$, the rate of entry into division $\lambda$ and the duration of B-phase $\Delta$ are identifiable through $SM_{CD44}$ model.
In the literature, one remarks that most mathematical models based on the Smith-Martin model assume that the cells divide in B-phase exactly at age $\Delta$. In contrast, $SM_{CD44}$ model takes into account the small variability in the time of division between cells, and eliminates the assumption of an immediate switch at time $\Delta$. In the present work, we interested to compare these two types of modeling by fitting $SM_1$ (latest version of Smith-Martin model widely used) and $SM_2$ (our $SM_{CD44}$ model without the CD44 structure) models to the data of OT-1 T cells. By taking

into account the small variability in the time of division, we remarked that the duration of B-phase related to $SM_2$ model becomes shorter than the one related to $SM_1$. In contrast, the rate of entry into division is approximately the same in these two models. Finally, we concluded that LIP by OT-1 was better modeled with $SM_2$ than $SM_1$ model, as reflected in the lower $CrV$ for $SM_2$ model fit (Table 7.1), which is a measure of goodness of fit (low is better).

By estimating the velocity $v_i$, we remarked that the average velocity (Fig. 8.5a) and the frequency of cells that have changed their CD44 expression profile (Fig. 8.6), are the keys to explain the transition of cells from naive to memory phenotype through LIP. However, these important keys enabled us to deduce that the cells which are the most likely switching to memory phenotype, are those that have divided 6 times or more. These numerical results are very close to the results observed in the biological experiment of [10]. This may be an important validation to our $SM_{CD44}$ model.

On the other side, we have taken into account the multistructural and multifunctional of CD44 (i.e. CD44 participates in cell proliferation, cell differentiation and cell migration from naive to memory phenotype) in $SM_{CD44}$ model. Indeed, we considered that the recruitment rate $(\lambda^i(s, N(t)))$ and the division rate $\mu(\tau, s)$ are depend on the intensity of CD44 on cells. In this context, numerical results show that the rate of entry into division by naive cells is much less than this of memory cells. In addition, another result allows to deduce that the cells having an important CD44 expression on their surface, have also a large possibility to divide when their age is near to $\Delta$. Otherwise at age $\Delta$, these cells divide independently of their level of CD44. Therefore, these interpretations clarify the relationship between the multifunctional of CD44 during LIP.

In conclusion, $SM_{CD44}$ model not only provides some remarkably description of lymphopenia induced proliferation by T cells but also may be a new path to better explain the complex relationship between LIP and naive to memory transition.

**Secondly**, we extended the $SM_{CD44}$ model to an in vivo model by implementing a rate $\Lambda$ of export of cells from the thymus. In this part of our work, the mathematical analysis of the in vivo model was our interest. Indeed, we proved the global existence of the in vivo model by using Fixed point method.

Next, we derived an age-structured system (11.1) from the in vivo model (10.1-10.3), and we investigated its asymptotic behaviour. An analysis of System (11.1) shows that there exists one or three stationary solutions when the cells undergo more than

five divisions. Precisely, uniqueness of a stationary solution is guaranteed in this case (i.e $I \geqslant 5$) when the parameter conditions (11.14) or (11.18) are satisfied. Also uniqueness is obtained when cells undergo at most four divisions or if the parameter $d$ is less than $\frac{1}{2}$. To study the large time behaviour when $0 < d < \frac{1}{2}$, a key tool was a Volterra-type Lyapunov functional that included an integral over all maturity of cells in B-phase, similar to the functionals used in [114, 115]. Note that the Lyapounov functional used in this study is not defined on the entire state space. One may observe that similar difficulty also arise in [120–122]. To circumvent this difficulty, we only used the Lyapunov functional on the global attractor. Then, we deduced that the unique stationary solution is globally asymptotically stable if the parameter condition (11.21) is satisfied. A numerical computation suggests that the unique stationary solution in the case $0 < d < \frac{1}{2}$ continues to be stable even if condition (11.21) is not fulfilled (a similar technical problem arises also in [114]). In addition, we remarked from Fig. 11.3 and Fig. 11.4 that the algebraic results presented in Chapter 11, cover a large region of the numerical results when the parameter $\rho$ is large.
Then the existence of one or three stationary solutions means that if with a few cell divisions, the size of T cells returns to the normal level, then the immune system has a unique steady state, else it could have three steady state. This phenomenon can provide an interesting biological signification of the proliferation of T cells under conditions of lymphopenia.

**Thirdly**, we reformulated System (10.1-10.3) to a more realistic version which includes a vaccination strategy in order to enhanced immunity during the homeostatic process. We have remarked that the strategy to enhanced immunity (i.e. maximizing memory cells (CD44 high)), consists to transfer in vivo (by vaccination) at the initial time, a high dose of resting cells having undergone 5-7 divisions. Later on, this dose should be reduced over time, which can be realistic.

## 13.2 Future works

T cell homeostasis stays a very important subject in Biology and Medicine, since it is induced in several diseases (e.g HIV, Cancer,...) that are almost without pertinent solutions until now. In our work, we have used a mathematical approach in order to respond to some questions concerning the proliferation of T cells under abnormal

conditions. To improve these responses, some works remain in this study.

**In the context of the in vitro model proposed in Parts II and III:** we have estimated the key parameters ($v_i(s)$, $\lambda_i(s, N(t))$ and $\mu(\tau, s)$) that define the proliferation of T cells in vitro by using the data at day 7 (see Chapter 8 and 9). Indeed, in the experiment of Hogan et al. [10], several mice were sacrificed at each time point. Working with different mice at different time points generated additional variability making the identifiability of parameters more difficult. In our work, we have chosen the data at day 7 because it was a good compromise between early days where there were too few divisions and later time points where CFSE is too much diluted to be very easily measured. In this context, we hope to get another experimental data without large variability between the different time points, in order to improve our estimated parameters. In addition, we interest in a future work to study the theoretical identifiability of the parameters by using only one observation.

**In the context of the in vivo model proposed in Part IV:** we have studied the asymptotic behaviour for a reduced model without the concept of phenotype (CD44). Our analysis show that there exist one or three stationary solutions which may depend on the divisions number undergone by cells ($I$). In some cases of uniqueness ($0 < d < \frac{1}{2}$), we have concluded that the unique stationary solution is asymptotically globally stable. In a future work, we will interest to study the stability of the other uniqueness cases. Moreover in the case of existence of three stationary solutions, the stability or instability of each one of them may be an interesting mathematical and biological subject which it will be treated in a forthcoming work. Finally, inspired by the analysis of the reduced model (11.1), a further work is to study the asymptotic behaviour of the complete in vivo model (10.1-10.3) which includes the concept of phenotype (CD44) in the homeostasis process.

# Bibliography


[1] A. V. Gett and P. D. Hodgkin. A cellular calculus for signal integration by T cells. *Nat Immunol*, 1(3):239–244, 2000.

[2] Sergei S. P., V. V. Ganusov, Kaja M., Rafi A., and Rustom A. The rescaling method for quantifying the turnover of cell populations . *Journal of Theoretical Biology*, 225(2):275 – 283, 2003.

[3] S. Bernard, L. Pujo-Menjouet, and M. C Mackey. Analysis of cell kinetics using a cell division marker: mathematical modeling of experimental data. *Biophysical Journal*, 84(5):3414–24, 2003.

[4] V. V. Ganusov, S. S. Pilyugin, R. J. de Boer, K. Murali-Krishna, R. Ahmed, and R. Antia. Quantifying cell turnover using {CFSE} data . *Journal of Immunological Methods*, 298(12):183 – 200, 2005.

[5] R. J. Boer, V. V. Ganusov, D. Milutinovic, P. D. Hodgkin, and A. S. Perelson. Estimating Lymphocyte Division and Death Rates from CFSE Data. *Bulletin of Mathematical Biology*, 68(5):1011–1031, 2006.

[6] V. V. Ganusov, D. Milutinovi, and R. J. De Boer. IL-2 Regulates Expansion of CD4+ T Cell Populations by Affecting Cell Death: Insights from Modeling CFSE Data. *The Journal of Immunology*, 179(2):950–957, 2007.

[7] A. Yates, M. Saini, A. Mathiot, and B. Seddon. Mathematical modeling reveals the biological program regulating lymphopenia-induced proliferation. *The Journal of Immunology*, 180(3):1414–1422, 2008.

[8] H. Lee and A. S. Perelson. Modeling T Cell Proliferation and Death in Vitro Based on Labeling Data: Generalizations of the SmithMartin Cell Cycle Model. *Bulletin of Mathematical Biology*, 70(1):21–44, 2008.

[9] H. Lee, E. Hawkins, M. S. Zand, T. Mosmann, H. Wu, P. D. Hodgkin, and A. S. Perelson. Interpreting CFSE Obtained Division Histories of B Cells in Vitro with SmithMartin and Cyton Type Models. *Bulletin of Mathematical Biology*, 71(7):1649–1670, 2009.

[10] T. Hogan, A. Shuvaev, D. Commenges, A. Yates, R. Callard, R. Thiebaut, and B. Seddon. Clonally Diverse T Cell Homeostasis Is Maintained by a Common Program of Cell-Cycle Control. *The Journal of Immunology*, 190 (8):3985–3993, 2013.

[11] Chahrazed Benosman. *Contrôle de la Dynamique de la Leucémie Myéloïde Chronique par Imatinib*. PhD thesis, Université Bordeaux 1, 2010.

[12] R. M. Liskay. Absence of a measurable g2 phase in two chinese hamster cell lines. *Proceedings of the National Academy of Sciences*, 74(4):1622–1625, 1977.

[13] J. Sprent and C. D. Surh. T Cell Memory. *Annual Review of Immunology*, 20(1):551–579, 2002.

[14] F. Sallusto, D. Lenig, R. Förster, M. Lipp, and A. Lanzavecchia. Two subsets of memory T lymphocytes with distinct homing potentials and effector functions. *Nature*, 401(6754):708–712, 1999.

[15] K. Murali-Krishna and R. Ahmed. Cutting Edge: Naive T Cells Masquerading as Memory Cells. *The Journal of Immunology*, 165(4):1733–1737, 2000.

[16] S. L. Swain, M. Croft, C. Dubey, L. Haynes, P. Rogers, X. Zhang, and L. M. Bradley. From naive to memory T cells. *Immunological reviews*, 150(1):143–167, 1996.

[17] B. Ernst, D. Lee, J. M. Chang, J. Sprent, and C. D. Surh. The peptide ligands mediating positive selection in the thymus control T cell survival and homeostatic proliferation in the periphery. *Immunity*, 11(2):173–181, 1999.

[18] W. C. Kieper and S. C. Jameson. Homeostatic expansion and phenotypic conversion of nave T cells in response to self peptide/MHC ligands. *Proceedings of the National Academy of Sciences*, 96(23):13306–13311, 1999.

[19] E. C. Butcher and L. J. Picker. Lymphocyte homing and homeostasis. *Science*, 272(5258):60–67, 1996.

[20] L. Bruno, J. Kirberg, and H. V. Boehmer. On the cellular basis of immunological T cell memory . *Immunity*, 2(1):37 – 43, 1995.

[21] R. Ahmed and D. Gray. Immunological memory and protective immunity: understanding their relation. *Science*, 272(5258):54–60, 1996.

[22] S. M. Kaech, E J. Wherry, and R. Ahmed. Effector and memory T-cell differentiation: implications for vaccine development. *Nature Reviews Immunology*, 2(4):251–262, 2002.

[23] T. P. Arstila, A. Casrouge, V. Baron, J. Even, J. Kanellopoulos, and P. Kourilsky. A direct estimate of the human $\alpha\beta$ T cell receptor diversity. *Science*, 286 (5441):958–961, 1999.

[24] R. Ahmed, M. J. Bevan, S. L. Reiner, and D. T. Fearon. The precursors of memory: models and controversies. *Nature Reviews Immunology*, 9(9): 662–668, 2009.

[25] K. Murali-Krishna, J. D. Altman, M. Suresh, D. JD. Sourdive, A. J. Zajac, J. D. Miller, J. Slansky, and R. Ahmed. Counting antigen specific CD8 T cells: a reevaluation of bystander activation during viral infection. *Immunity*, 8(2):177–187, 1998.

[26] W.B. Cannon. *The wisdom of the body*. W.W. Norton & Company, inc., 1932. URL http://books.google.fr/books?id=zdkEAQAAIAAJ.

[27] Stephen C Jameson. Maintaining the norm: T-cell homeostasis. *Nature Reviews Immunology*, 2(8):547–556, 2002.

[28] C. Tanchot, F. A. Lemonnier, B. Pérarnau, A. A. Freitas, and B. Rocha. Differential requirements for survival and proliferation of CD8 naïve or memory T cells. *Science*, 276(5321):2057–62, 1997.

[29] A. Freitas and J. Chen. Introduction: regulation of lymphocyte homeostasis. *Microbes and Infection*, 4(5):529–530, 2002.

[30] Zvi Grossman, Booki Min, Martin Meier-Schellersheim, and William E Paul. Concomitant regulation of t-cell activation and homeostasis. *Nature Reviews Immunology*, 4(5):387–395, 2004.

[31] FA. Spring, R. Dalchau, GL. Daniels, G. Mallinson, PA. Judson, SF. Parsons, JW. Fabre, and DJ. Anstee. The Ina and Inb blood group antigens are located

on a glycoprotein of 80,000 MW (the CDw44 glycoprotein) whose expression is influenced by the In (Lu) gene. *Immunology*, 64(1):37, 1988.

[32] E. Puré and C. A. Cuff. A crucial role for {CD44} in inflammation . *Trends in Molecular Medicine*, 7(5):213 – 221, 2001.

[33] H. Ponta, L. Sherman, and P. A. Herrlich. CD44: from adhesion molecules to signalling regulators. *Nature Reviews Molecular Cell Biology*, 4(1):33–45, 2003.

[34] E. Puré and R. K. Assoian. Rheostatic signaling by CD44 and hyaluronan. *Cellular signalling*, 21(5):651–655, 2009.

[35] Heather C DeGrendele, Maria Kosfiszer, Pila Estess, and Mark H Siegelman. Cd44 activation and associated primary adhesion is inducible via t cell receptor stimulation. *The Journal of Immunology*, 159(6):2549–2553, 1997.

[36] J. Lesley, N. Howes, A. Perschl, and R. Hyman. Hyaluronan binding function of CD44 is transiently activated on T cells during an in vivo immune response. *The Journal of experimental medicine*, 180(1):383–387, 1994.

[37] A. Nandi, P. Estess, and M. Siegelman. Bimolecular complex between rolling and firm adhesion receptors required for cell arrest: Cd44 association with vla-4 in t cell extravasation. *Immunity*, 20(4):455–465, 2004.

[38] A. Berezné, W. Bono, L. Guillevin, and L. Mouthon. Orientation diagnostique devant une lymphopénie. *La Presse Médicale*, 35(5):895–902, 2006.

[39] A. Malaspina, S. Moir, D. G. Chaitt, C. A. Rehm, S. Kottilil, J. Falloon, and A. S. Fauci. Idiopathic CD4+ T lymphocytopenia is associated with increases in immature/transitional B cells and serum levels of IL-7. *Blood*, 109(5):2086–2088, 2007.

[40] A. Freitas and B. Rocha. Population biology of lymphocytes: the flight for survival. *Annual Review of Immunology*, 18:83–111, 2000.

[41] C. D. Surh and J. Sprent. Homeostasis of Naive and Memory T Cells . *Immunity*, 29(6):848 – 862, 2008.

[42] R. J. De Boer and A. S. Perelson. Quantifying T lymphocyte turnover . *Journal of Theoretical Biology*, 327(0):45 – 87, 2013.

[43] J. AM. Borghans and R. J. De Boer. Quantification of T-cell dynamics: from telomeres to DNA labeling. *Immunological reviews*, 216(1):35–47, 2007.

[44] I. Braber, T. Mugwagwa, N. Vrisekoop, L. Westera, and R. Mgling. Maintenance of Peripheral Naive T Cells Is Sustained by Thymus Output in Mice but Not Humans . *Immunity*, 36(2):288 – 297, 2012.

[45] R. J. De Boer and A. S. Perelson. Towards a general function describing T cell proliferation. *Journal of theoretical biology*, 175(4):567–576, 1995.

[46] M. A. Nowak and C. RM. Bangham. Population dynamics of immune responses to persistent viruses. *Science*, 272(5258):74–79, 1996.

[47] R. Antia, C. T. Bergstrom, S. S. Pilyugin, S. M. Kaech, and R. Ahmed. Models of CD8+ responses: 1. What is the antigen-independent proliferation program. *Journal of theoretical biology*, 221(4):585–598, 2003.

[48] R. J. De Boer, M. Oprea, R. Antia, K. Murali-Krishna, R. Ahmed, and A. S. Perelson. Recruitment times, proliferation, and apoptosis rates during the CD8+ T-cell response to lymphocytic choriomeningitis virus. *Journal of virology*, 75(22):10663–10669, 2001.

[49] V. V. Ganusov, D. L. Barber, and R. J. De Boer. Killing of Targets by CD8+ T Cells in the Mouse Spleen Follows the Law of Mass Action. *PloS one*, 6(1): e15959, 2011.

[50] L. E. Jonesa and A. S. Perelson. Opportunistic infection as a cause of transient viremia in chronically infected HIV patients under treatment with HAART. *Bulletin of mathematical biology*, 67(6):1227–1251, 2005.

[51] R. J. De Boer and A. S. Perelson. Estimating division and death rates from {CFSE} data . *Journal of Computational and Applied Mathematics*, 184(1): 140 – 164, 2005.

[52] O. Diekmann, M. Gyllenberg, H. Huang, M. Kirkilionis, J. Metz, and H. R. Thieme. On the formulation and analysis of general deterministic structured population models II. Nonlinear theory. *Journal of Mathematical Biology*, 43 (2):157–189, 2001.

[53] R. J. De Boer and A. J. Noest. T cell renewal rates, telomerase, and telomere length shortening. *The Journal of Immunology*, 160(12):5832–5837, 1998.

[54] K. C. Wolthers, A. J. Noest, S. A. Otto, F. Miedema, and R. J. De Boer. Normal telomere lengths in naive and memory CD4+ T cells in HIV type 1 infection: a mathematical interpretation. *AIDS research and human retroviruses*, 15(12):1053–1062, 1999.

[55] P. Revy, M. Sospedra, B. Barbour, and A. Trautmann. Functional antigen-independent synapses formed between T cells and dendritic cells. *Nature immunology*, 2(10):925–931, 2001.

[56] B. Asquith, C. Debacq, A. Florins, N. Gillet, T. Sanchez-Alcaraz, A. Mosley, and L. Willems. Quantifying lymphocyte kinetics in vivo using carboxyfluorescein diacetate succinimidyl ester. *Proceedings of the Royal Society B: Biological Sciences*, 273(1590):1165–1171, 2006.

[57] V. V. Ganusov and R. J. De Boer. A mechanistic model for bromodeoxyuridine dilution naturally explains labelling data of self-renewing T cell populations. *Journal of The Royal Society Interface*, 10(78), 2013.

[58] A. B. Lyons. Analysing cell division in vivo and in vitro using flow cytometric measurement of CFSE dye dilution. *Journal of immunological methods*, 243 (1):147–154, 2000.

[59] E. D. Hawkins, M. Hommel, M. L. Turner, F. L. Battye, J. F. Markham, and P. D. Hodgkin. Measuring lymphocyte proliferation, survival and differentiation using CFSE time-series data. *Nature protocols*, 2(9):2057–2067, 2007.

[60] C. R. Parish, M. H. Glidden, B. JC. Quah, and H. S. Warren. Use of the intracellular fluorescent dye CFSE to monitor lymphocyte migration and proliferation. *Current protocols in immunology*, pages 4–9, 2009.

[61] T. Luzyanina, D. Roose, T. Schenkel, M. Sester, S. Ehl, A. Meyerhans, and G. Bocharov. Numerical modelling of label-structured cell population growth using CFSE distribution data. *Theoretical Biology and Medical Modelling*, 4 (1):1–15, 2007.

[62] HT. Banks, K. L. Sutton, W. C. Thompson, G. Bocharov, M. Doumic, T. Schenkel, J. Argilaguet, S. Giest, C. Peligero, and A. Meyerhans. A new model for the estimation of cell proliferation dynamics using CFSE data. *Journal of immunological methods*, 373(1):143–160, 2011.

[63] HT. Banks, K. L. Sutton, W. C. Thompson, G. Bocharov, D. Roose, T. Schenkel, and A. Meyerhans. Estimation of cell proliferation dynamics using CFSE data. *Bulletin of mathematical biology*, 73(1):116–150, 2011.

[64] D. Schittler, J. Hasenauer, and F. Allgöwer. A generalized population model for cell proliferation: Integrating division numbers and label dynamics. *TICSP series*, 57:165–168, 2011.

[65] J. Hasenauer, D. Schittler, and F. Allgöwer. Analysis and Simulation of Division-and Label-Structured Population Models. *Bulletin of mathematical biology*, 74(11):2692–2732, 2012.

[66] HT. Banks and W. C. Thompson. A division-dependent compartmental model with cyton and intracellular label dynamics. *Int. J. Pure Appl. Math*, 77:119–147, 2012.

[67] O. Hyrien and M. S. Zand. A Mixture Model With Dependent Observations for the Analysis of CSFE–Labeling Experiments. *Journal of the American Statistical Association*, 103(481):222–239, 2008.

[68] H. Miao, X. Jin, A. S. Perelson, and H. Wu. Evaluation of multitype mathematical models for CFSE-labeling experiment data. *Bulletin of mathematical biology*, 74(2):300–326, 2012.

[69] J. A. Smith and L. Martin. Do Cells Cycle? *Proceedings of the National Academy of Sciences*, 70(4):1263–1267, 1973.

[70] S.S. Pilyugin, V.V. Ganusov, K.Murali-Krishna, R. Ahmed, and R. Antia. The rescaling method for quantifying the turnover of cell populations . *Journal of Theoretical Biology*, 225(2):275 – 283, 2003.

[71] S. Cooper. The continuum model: statistical implications. *Journal of theoretical biology*, 94(4):783–800, 1982.

[72] A. L. Koch. The re-incarnation, re-interpretation and re-demise of the transition probability model. *Journal of biotechnology*, 71(1):143–156, 1999.

[73] J. Tyrcha. Age-dependent cell cycle models. *Journal of Theoretical Biology*, 213(1):89–101, 2001.

[74] J. J. Tyson. Modeling the cell division cycle: cdc2 and cyclin interactions. *Proceedings of the National Academy of Sciences*, 88(16):7328–7332, 1991.

[75] B. Novak and J. J. Tyson. A model for restriction point control of the mammalian cell cycle. *Journal of theoretical biology*, 230(4):563–579, 2004.

[76] R. G. Clyde, J. L. Bown, T. R. Hupp, N. Zhelev, and J. W. Crawford. The role of modelling in identifying drug targets for diseases of the cell cycle. *Journal of The Royal Society Interface*, 3(10):617–627, 2006.

[77] T. Luzyanina, S. Mrusek, J. T. Edwards, D. Roose, S. Ehl, and G. Bocharov. Computational analysis of CFSE proliferation assay. *Journal of Mathematical Biology*, 54(1):57–89, 2007.

[78] E. K Deenick, A. V Gett, and P. D Hodgkin. Stochastic model of T cell proliferation: a calculus revealing IL-2 regulation of precursor frequencies, cell cycle time, and survival. *J Immunol*, 170(10):4963–72, 2003.

[79] Ananda W Goldrath and Michael J Bevan. Selecting and maintaining a diverse T-cell repertoire. *Nature*, 402(6759):255–262, 1999.

[80] H Ayoub, BE Ainseba, M Langlais, T Hogan, R Callard, B Seddon, and R Thiébaut. Parameter identification for model of T cell proliferation in Lymphopenia conditions. *Mathematical Biosciences*, 251:63–71, 2014.

[81] BE. Ainseba, H. Ayoub, and M. Langlais. An age-structured model for T cell homeostasis in vivo. *SIAM Applied Mathematics*, Accepted, 2014.

[82] H. Ayoub, B. Ainseba, and M. Langlais. Parameters identification for a model of T cell homeostasis. *Submitted*, 2014.

[83] C. Ferreira, T. Barthlott, S. Garcia, R. Zamoyska, and B. Stockinger. Differential Survival of Naive CD4 and CD8 T Cells. *The Journal of Immunology*, 165(7):3689–3694, 2000.

[84] B. K. Cho, V. P. Rao, Q. Ge, H. N. Eisen, and J. Chen. Homeostasis-Stimulated Proliferation Drives Naive T Cells to Differentiate Directly into Memory T Cells. *The Journal of Experimental Medicine*, 192(4):549–556, 2000.

[85] Q; Ge, V. P. Rao, Bryan K. Cho, H. N. Eisen, and J. Chen. Dependence of lymphopenia-induced T cell proliferation on the abundance of peptide/ MHC epitopes and strength of their interaction with T cell receptors. *Proceedings of the National Academy of Sciences*, 98(4):1728–1733, 2001.

[86] C. D. Surh, O. Boyman, J. F. Purton, and J. Sprent. Homeostasis of memory T cells. *Immunological Reviews*, 211(1):154–163, 2006.

[87] C. R. Parish. Fluorescent dyes for lymphocyte migration and proliferation studies. *Immunol Cell Biol*, 77(6):499–508, 1999.

[88] Rob J. De B. and Alan S. P. T Cell Repertoires and Competitive Exclusion. *Journal of Theoretical Biology*, 169(4):375 – 390, 1994.

[89] B. J.G. Baaten, C. Li, M. F. Deiro, M. M. Lin, P. J. Linton, and L. M. Bradley. {CD44} Regulates Survival and Memory Development in Th1 Cells . *Immunity*, 32(1):104 – 115, 2010.

[90] J. Douglas and F.A. Milner. Numerical methods for a model of population dynamics. *CALCOLO*, 24(3-4):247–254, 1987.

[91] Y. Kwon and C. Cho. Second-Order Accurate Difference Methods for a One-Sex Model of Population Dynamics. *SIAM Journal on Numerical Analysis*, 30(5):1385–1399, 1993.

[92] D. Sulsky. Numerical solution of structured population models. *Journal of Mathematical Biology*, 31(8):817–839, 1993.

[93] J. W. Sinko and W. Streifer. A New Model For Age-Size Structure of a Population. *Ecology*, 6(48):910–918, 1967.

[94] O. Angulo and J.C. Lpez-Marcos. Numerical integration of nonlinear size-structured population equations . *Ecological Modelling*, 133(12):3 – 14, 2000.

[95] O. Angulo and J. C. López-Marcos. Numerical integration of fully nonlinear size-structured population models. *Appl. Numer. Math.*, 50(3-4):291–327, 2004.

[96] T. Kostova. An explicit third-order numerical method for size-structured population equations. *Numerical Methods for Partial Differential Equations*, 19(1):1–21, 2003.

[97] H. Brézis. *Analyse fonctionelle*. Collection Mathématiques appliquées pour la maîtrise. Masson, 1983. ISBN 9782225771989.

[98] F. J. Burns and I. F. Tannock. On the existence of a go-phase in the cell cycle. *Cell Proliferation*, 3(4):321–334, 1970.

[99] Inc Visual Numerics. *IMSL Fortran 90 Library: User's Guide*. Visual Numerics, 1996.

[100] J. E. Dennis and R. B. Schnabel. *Numerical Methods for Unconstrained Optimization and Nonlinear Equations*. Prentice-Hall, Englewood Cliffs, NJ, 1983.

[101] C-K Cho and YH Kwon. Parameter estimation in nonlinear age-dependent population dynamics. *IMA Journal of Applied Mathematics*, 62(3):227–244, 1999.

[102] S. E. Hamilton, M. C. Wolkers, S. P. Schoenberger, and S. C. Jameson. The generation of protective memory-like CD8+ T cells during homeostatic proliferation requires CD4+ T cells . *Nat Immunol*, 7:1529–2908, 2006.

[103] A. W. Goldrath, C. J. Luckey, R. Park, C. Benoist, and D. Mathis. The molecular program induced in T cells undergoing homeostatic proliferation. *Proceedings of the National Academy of Sciences of the United States of America*, 101(48):16885–16890, 2004.

[104] S. C. Jameson. T cell homeostasis: Keeping useful T cells alive and live T cells useful . *Seminars in Immunology*, 17(3):231 – 237, 2005.

[105] B. Asquith, J. A.M. Borghans, V. V. Ganusov, and D. C. Macallan. Lymphocyte kinetics in health and disease . *Trends in Immunology*, 30(4):182 – 189, 2009.

[106] M. Vieira, D. Soares, N. J. Borthwick, M. K. Maini, G. Janossy, M. Salmon, and A. N. Akbar. IL-7-Dependent Extrathymic Expansion of CD45RA+ T Cells Enables Preservation of a Naive Repertoire. *The Journal of Immunology*, 161(11):5909–5917, 1998.

[107] L. Swainson, S. Kinet, C. Mongellaz, M. Sourisseau, T. Henriques, and N. Taylor. IL-7induced proliferation of recent thymic emigrants requires activation of the PI3K pathway. *Blood*, 109(3):1034–1042, 2007.

[108] H. R. Thieme. Semiflows generated by Lipschitz perturbations of non-densely defined operators. *Differential Integral Equations*, pages 1035–1066, 1990.

[109] H. Kellerman and M. Hieber. Integrated semigroups . *Journal of Functional Analysis*, 84(1):160 – 180, 1989. ISSN 0022-1236.

[110] P. Magal. Compact attractors for time-periodic age-structured population models. *Electronic Journal of Differential Equations (EJDE)*, pages 1 – 35, 2001.

[111] P. Magal and S. Ruan. On Semilinear Cauchy Problems with Non-dense Domain. *Advances in Differential Equations*, 14:1041–1084, 2009.

[112] P. Magal and S. Ruan. Center Manifolds for Semilinear Equations with Non-dense Domain and Applications to Hopf Bifurcation in Age Structured Models. *Memoirs of the American Mathematical Society*, 202:1–80, 2009.

[113] H. R. Thieme. Integrated semigroups and integrated solutions to abstract Cauchy problems . *Journal of Mathematical Analysis and Applications*, 152 (2):416 – 447, 1990.

[114] R. Demasse and A. Ducrot. An Age-Structured Within-Host Model for Multistrain Malaria Infections. *SIAM Journal on Applied Mathematics*, 73(1): 572–593, 2013.

[115] P. Magal and C. McCluskey. Two-Group Infection Age Model Including an Application to Nosocomial Infection. *SIAM Journal on Applied Mathematics*, 73(2):1058–1095, 2013.

[116] J.K. Hale. *Asymptotic Behavior of Dissipative Systems*. Mathematical surveys and monographs. American Mathematical Society, 1988. ISBN 9780821874806. URL http://books.google.fr/books?id=fSzscCu37ygC.

[117] G.F. Webb. *Theory of Nonlinear Age-Dependent Population Dynamics*. Chapman & Hall Pure and Applied Mathematics. Taylor & Francis, 1985. ISBN 9780824772901. URL http://books.google.fr/books?id=TlUI-vSkqKAC.

[118] P. Magal and H. R. Thieme. Eventual compactness for semiflows generated by nonlinear age-structured models. *Communications on Pure and Applied Analysis*, 3:695–727, 2004.

[119] H. R. Thieme and I. Vrabie. Relatively Compact Orbits and Compact Attractors for a Class of Nonlinear Evolution Equations. *Journal of Dynamics and Differential Equations*, 15(4):731–750, 2003.

[120] C.C. McCluskey. Global stability for an SEIR epidemiological model with varying infectivity and infinite delay . *Math Biosci Eng*, 6(3):603–610, 2009.

[121] P. Magal, C.C. McCluskey, and G.F. Webb. Lyapunov functional and global asymptotic stability for an infection-age model. *Applicable Analysis*, 89(7): 1109–1140, 2010.

[122] Horst R. Thieme. Global stability of the endemic equilibrium in infinite dimension: Lyapunov functions and positive operators . *Journal of Differential Equations*, 250(9):3772 – 3801, 2011.

[123] Aaron P Rapoport, Edward A Stadtmauer, Nicole Aqui, Ashraf Badros, Julio Cotte, Lisa Chrisley, Elizabeth Veloso, Zhaohui Zheng, Sandra Westphal, Rebecca Mair, et al. Restoration of immunity in lymphopenic individuals with cancer by vaccination and adoptive t-cell transfer. *Nature medicine*, 11(11): 1230–1237, 2005.

[124] Gugasyan, Coward, OConnor, Shortman, and Scollay. Emigration of mature t cells from the thymus is inhibited by the imidazole-based compound 2-acetyl-4-tetrahydroxybutylimidazole. *Immunology*, 93(3):398–404, 1998.

[125] Iren Bains, Rodolphe Thibaut, Andrew J. Yates, and Robin Callard. Quantifying thymic export: Combining models of naive t cell proliferation and tcr excision circle dynamics gives an explicit measure of thymic output. *The Journal of Immunology*, 2009.